Electronic Thesis and Dissertation Repository

11-20-2017 10:45 AM

Hydrothermal decarboxylation of fatty acids and their derivatives for liquid transportation fuels

Md Zakir Hossain, *The University of Western Ontario*

Follow this and additional works at: https://ir.lib.uwo.ca/etd

Part of the Catalysis and Reaction Engineering Commons

Abstract

Due to the depletion of fossil fuel reserves, renewable resources are required to produce tomorrow's fuel range hydrocarbons. This thesis focuses on the hydrothermal decarboxylation of fatty acids and their derivatives derived from renewable sources. These are required for liquid transportation fuels which have similar properties to conventional fuels. Detailed catalytic studies were performed for the decarboxylation of oleic acid as a model compound and corn distiller's oil (CDO) as a real feedstock. Commercial activated carbon and laboratory prepared $Ni-Al_2O_3$, $MgO-Al_2O_3$, $Mo-Al_2O_3$ catalysts were also examined as catalysts. Fatty acid derivatives such as castor oil, waste cooking oil, and palm oil were explored as potential feedstocks.

Activated carbon was found to be an efficient catalyst for oleic acid decarboxylation in both batch and continuous reactor systems. The results showed that up to 97% degree of decarboxylation was achieved using a batch reactor system under optimized experimental conditions, while up to 91% was obtained in a continuous fixed bed reactor system at comparatively low pressure. Liquid yields in both cases were ~ 62 and 63.5 wt% whereas the selectivity of heptadecane was found to be 81 and 89.3%, respectively. This result is attributed to the difference in the process and reaction dynamics of this experimental system. Although the $Mo-Al_2O_3$ catalyst exhibited 91% decarboxylation and 71wt% liquid yield using the continuous reactor system, the selectivity of heptadecane was comparatively lower compared to that of activated carbon. This indicates that the $Mo-Al_2O_3$ catalyst led to some cracking of the oleic acid feed into lower hydrocarbons instead of heptadecane. On the other hand, decarboxylation of CDO in the batch reactor system provided almost 100% degree of decarboxylation with 65% liquid yield using activated carbon as catalyst under the optimized reaction conditions. It was also found that the fuel properties of the decarboxylated liquid products using activated carbon and $Mo-Al_2O_3$ catalyst had a similar density and high heating value (HHV) compared to commercial fuels such as kerosene, jet fuel and diesel.

Decarboxylation of Castor oil, palm oil and waste cooking oil were examined using the $Mo-Al_2O_3$ catalyst in the continuous reactor system. The results showed that the decarboxylation activities of this feedstocks followed the trend of oleic acid and CDO, indicating high potential

for these feedstocks. This thesis shows that hydrothermal decarboxylation of fatty acids or their derivatives provides an excellent opportunity to produce renewable hydrocarbons which can potentially significantly reduce our dependency on fossil fuels.

Co-authorship

Title: Using Subcritical Water for Decarboxylation of Oleic Acid into Fuel-Range Hydrocarbons

Authors: Md Zakir Hossain, Anil Kumar Jhawar, Muhammad B.I. Chowdhury, William Z. Xu, Wei Wu, David Hiscott, Paul A. Charpentier.

The experimental works, product analysis and catalyst characterizations were performed by Md Zakir Hossain in collaboration with Dr Anil Jhawar and Dr Muhammad B.I. Chowdhury under the guidance of Prof. Paul Charpentier. Dr William Z. Xu Dr Wei Wu and David Hiscott help with some analysis. The draft of this manuscript was written by Md Zakir Hossain and reviewed by Prof. Paul A. Charpentier. The final version of this article was published in Energy and Fuel, 2017, 31(4), 4013-4023.

Title: Continuous low pressure decarboxylation of fatty acids to fuel-range hydrocarbons with *insitu* hydrogen production

Authors: Md Zakir Hossain, Muhammad B.I. Chowdhury, Anil Kumar Jhawar, William Z. Xu, Paul A. Charpentier.

The experimental works and product analysis were performed by Md Zakir Hossain in collaboration with Dr Muhammad B.I. Chowdhury and Dr Anil Kumar Jhawar under supervision of Prof. Paul Charpentier. The draft of this manuscript was written by Md Zakir Hossain and final modification were conducted by Prof. Paul A. Charpentier. The final version of this article is published in Fuel 2018, 212, 470-478.

Title: Deactivation and regeneration studies of activated carbon during continuous decarboxylation of oleic acid in subcritical water

Authors: Md Zakir Hossain, Anil Kumar Jhawar, Muhammad B.I. Chowdhury, William Z. Xu, Paul A. Charpentier.

The experimental works, product analysis and characterizations of catalysts were performed by Md Zakir Hossain. Dr Anil Kumar Jhawar and Dr Muhammad B.I. Chowdhury assisted in the experiments. The manuscript was written by Md Zakir Hossain with close discussion with

Dr Anil Kumar Jhawar and Dr Muhammad B.I. Chowdhury. Dr William Z. Xu reviewed the manuscript. Final modification of the manuscript was conducted by Prof. Paul Charpentier.

Title: Continuous decarboxylation of fatty acids and their derivatives into liquid hydrocarbons using Mo/Al_2O_3 catalysts

Authors: Md Zakir Hossain, Muhammad B.I. Chowdhury, Anil Kumar Jhawar, William Z. Xu, Paul A. Charpentier.

The experiment works and catalyst characterization were performed by Md Zakir Hossain. Catalysts synthesis was done by Dr Muhammad B.I. Chowdhury. Experiments involved with fatty acid derivatives were performed by Dr Anil Kumar Jhawar. The manuscript was written by Md Zakir Hossain with close discussion with Dr Muhammad B.I. Chowdhury, Dr Anil Kumar Jhawar and Dr William Z. Xu. Prof. Paul Charpentier reviewed the manuscript and suggested updates as required.

Title: Green Diesel Production from Corn Distiller's Oil through Hydrothermal Decarboxylation
Authors: Md Zakir Hossain, Anil Kumar Jhawar, Muhammad B.I. Chowdhury, William Z. Xu, Paul A. Charpentier.

The experiments, product analysis and catalyst characterization were done by Md Zakir Hossain in collaboration with Dr Anil Kumar Jhawar and Dr Muhammad B.I. Chowdhury under supervision of Prof. Paul Charpentier. Dr William Z. Xu helped with the proposed reaction mechanism of this manuscript. The manuscript was written by Md Zakir Hossain and finalized by Prof. Paul Charpentier. The manuscript is submitted to Applied Energy which is under review.

Dedication

My wife (Farhana Chowdhoury)

My daughters (Fariha and Farah Hossain)

My parents and my parents in laws

Acknowledgements

Table of Contents

List of Tables

List of Figures

Chapter 1

General Introduction

1.1 Renewable Energy

Every aspect of human activity is dependent on the use of energy, which is defined as the ability to do work. Energy demands are increasing daily due to increasing world's population, increasing affluence of emerging society's and the increasing use of technology in our daily lives. For example, the worlds energy consumption increased by 1% in 2016 (is increasing exponentially) owing to the increased number of industries and transport infrastructures [1]. The major sources of energy which fulfills many of our daily demands use conventional energy resources such as coal, petroleum and natural gas for either electricity or transportation uses. Global warming is a major environmental concern resulting from the use of petroleum based fuels. Although the cause of global warming is under debate, greenhouse gas (GHG) emissions are normally considered the principle anthropogenic cause for global warming. The largest source of GHG emissions are from electrical power plants, whereas the second largest contributor to GHG emissions is from transportation vehicles [2]. According to the US based Environmental Protection Agency (EPA), carbon dioxide (CO_2) emissions from transportation vehicles have increased by 29% between 1990 and 2007 [3]. Approximately 20% of the total CO_2 currently released into the atmosphere is due to human activities, which is expected to further increase in the future [4]. There are several other environmental issues in addition to global warming such as air pollution, acid rain, ozone layer depletion, forest destruction, and the emission of radioactive substances. Necessary steps must be taken to reprieve the world from these issues if humanity wants to achieve a clean energy future with no/less environmental impact. Renewable energy can potentially be an excellent alternative to resolve these environmental issues.

Renewable energies are sources of energy that are continually replaced by nature and originate directly from the sun (such as thermal, photo-chemical, and photo-electric), indirectly from the sun (such as wind, hydropower, and photosynthetic energy stored in biomass), or from other natural movements and mechanisms of the environment (such as geothermal and tidal energy). Renewable energy excludes energy resources obtained from fossil fuels, waste products from

fossil fuels or inorganic sources [5]. Figure 1.1 shows an overview of the various renewable energy sources [6]. Different forms of energy such as electricity, heat and fuels are obtained from these renewable energy resources using various technologies. Renewable energy markets have been growing rapidly, especially electricity, heating and transportation over the last few years. Hydro, wind and solar photovoltaic are also rising quickly, which has increased confidence in the technologies, reduced costs and opened up new opportunities in these areas.
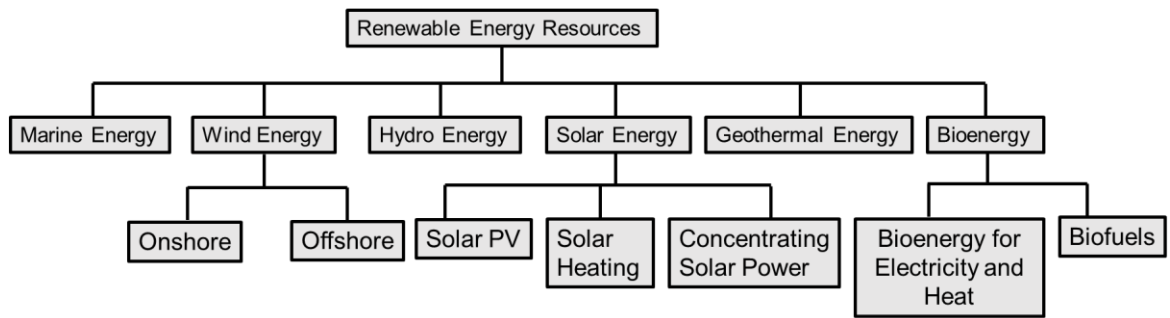
Figure 1.1. Overview of renewable energy sources.

1.2 Liquid Transportation Fuels

The transportation sector is one of the largest energy consuming sectors (around 40% of total energy) which will experience a major challenge in the near future due to a rapid increase of motorized vehicles and depletion of fossil fuel reserves [7]. Coal, petroleum, and natural gas are the principle fossil fuel sources fueling the transportation sector. The worlds liquid fuel demands are expected to increase through 2040, with the US (and Canada) projected to have a slight decrease. However, the demand for diesel fuel is expected to increase for both regions as shown in Figure 1.2. Since the fossil fuels are finite in nature and have significant environmental impacts, new forms for renewable transportation fuel are needed.
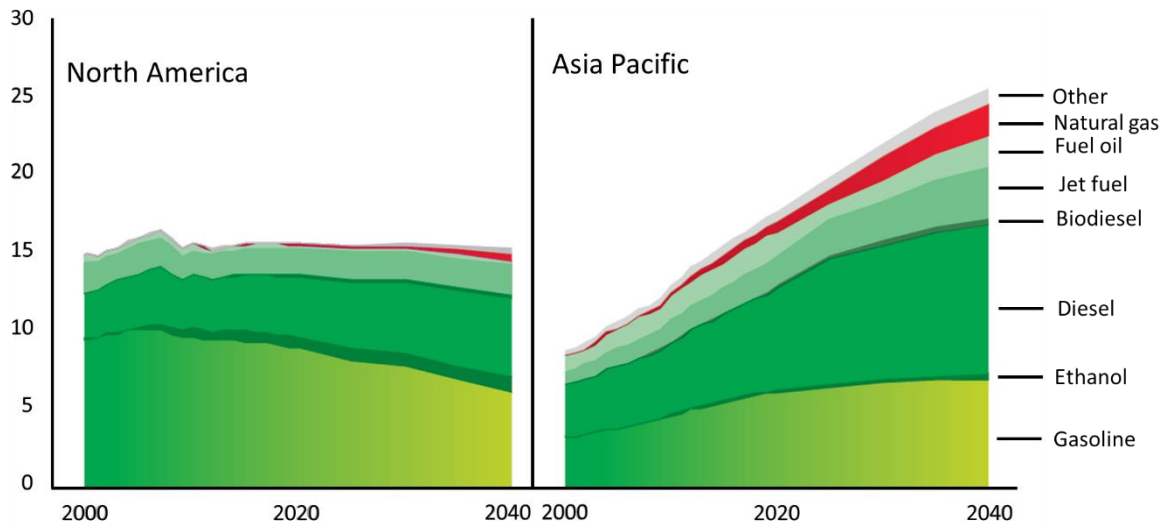
Figure 1.2: Transportation fuel use by type for North America and Asia Pacific (Millions of oil-equivalent barrels per day) [8].

Renewable transportation fuels can be defined as the fuels obtained from the processing and upgrading of different types of biomass or degradable municipal waste feedstocks. Typical examples of renewable transportation fuels are hydrogen, methane, propane, ethanol, butanol, gasoline and diesel. Renewable fuels are categorized into three main subdivisions [9]; (i) from edible feedstocks (e.g., ethanol and biodiesel via fermentation and esterification, respectively) through conventional processing; (ii) obtained from non-edible feedstocks (e.g., waste greases, lignocelluloses, refuse) through advanced processing such as gasification, hydroprocessing, pyrolysis etc. and (iii) from ultra-high yield biomass (e.g., algae) through harvesting and advanced processing. Figure 1.3 shows a schematic for renewable fuel production from biomass. The biomass itself may be broken down into three basic categories, carbohydrates, lignin and fats/oils. Carbohydrates primarily include cellulose and hemicellulose fractions. Fats are mainly comprised of triglycerides and fatty acids.
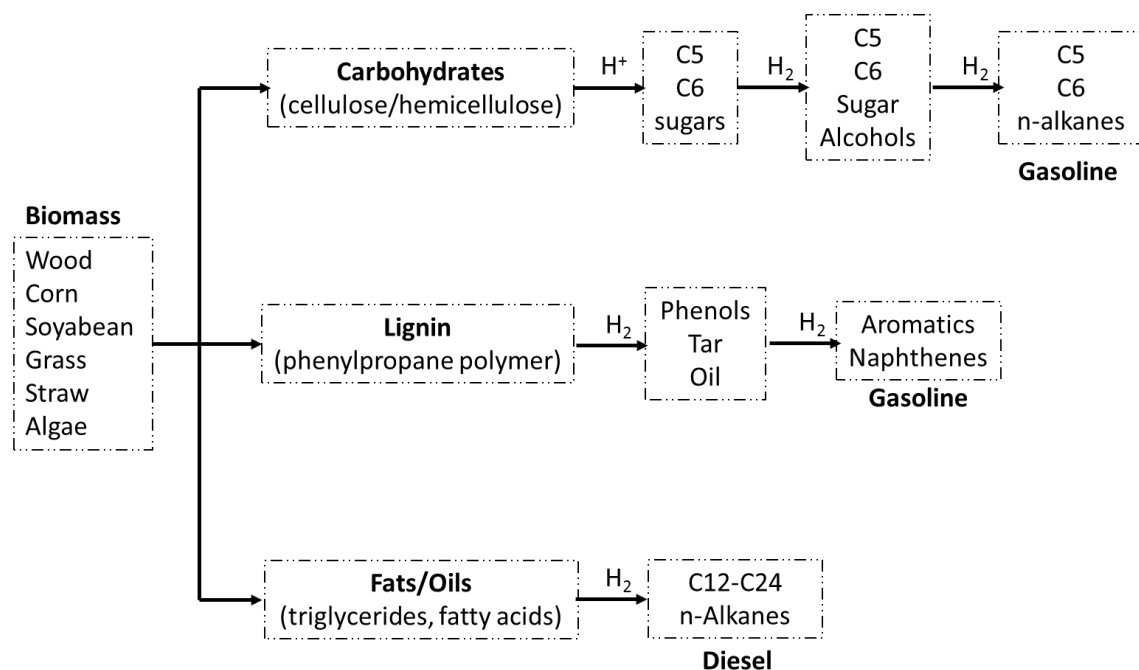
Figure 1.3: Hydrodeoxygenation of the basic building blocks of biomass to renewable hydrocarbon fuels.

1.3 Liquid Fuel Production Processes

Several processes have been used for renewable liquid fuel production. Pyrolysis is a simple process which converts biomass into bio-oils containing a number of fuel-range products. However, pyrolysis products contain mainly oxygenated compounds which normally require an additional processing step for upgrading.

On the other hand, vegetable oils or animal fats can be converted into fatty acid methyl esters (FAMEs) which is called biodiesel through transesterification reactions. Although biodiesel is currently used as a transportation fuel either blended with commercial diesel or used as is, its cold flow properties, poor storage stability and engine compatibility prevent its usage in northern climates such as Canada. Lower heat content and higher oxygen content of bio-oils and biodiesel have garnered considerable attention towards finding alternative routes to produce higher heat content and oxygen free hydrocarbons which have a similar fingerprint as commercial fuels.

As shown by Eqns. 1.1-1.3 below, deoxygenation of esters and fatty acids can occur by 3 primary mechanisms: (1) hydrodeoxygenation, (2) decarbonylation, and (3) decarboxylation. Hydrodeoxygenation as shown in Eqn. (1.1) requires 4 moles of hydrogen per mole of oxygen

4

removed and is expensive because of its high hydrogen requirements. Similarly, decarbonylation also has high hydrogen requirements, i.e. 2 moles of hydrogen per mole of product. Decarboxylation only requires 1 mole of hydrogen per mole of oxygen removed. Also, the thermodynamics of decarboxylation and decarbonylation are favorable at 300°C: ΔG_{rxn} = -83.5 kJ/mol for decarboxylation and -17 kJ/mol for decarbonylation.

$$4H_2 + C_{17}H_{33}COOH \rightarrow n\text{-}C_{18}H_{38} + 2H_2O \qquad\qquad (1.1)$$

$$2H_2 + C_{17}H_{33}COOH \rightarrow n\text{-}C_{17}H_{36} + CO + H_2O \qquad\qquad (1.2)$$

$$1H_2 + C_{17}H_{33}COOH \rightarrow n\text{-}C_{17}H_{36} + CO_2 \qquad\qquad (1.3)$$
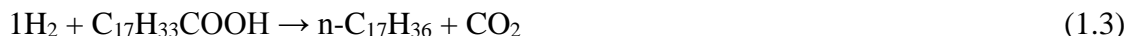
These deoxygenated materials produced from Eqn's 1.1-1.3 have a higher energy density, lower acidity, lower viscosity, higher oxygen stability and are better suited for the existing infrastructure for distribution to vehicles. Deoxygenated products also have a much higher Cetane number (>70) than that of petroleum diesel fuel (~45), while the boiling point range is comparable to typical petroleum based-diesel [10].

Hydrodeoxygenation and decarbonylation technology to produce so-called "green diesel" i.e. diesel produced from renewable sources but with limited O, has been investigated by a number of research groups and companies [11-14]. Currently hydrodeoxygenation to produce green diesel is commercialized by Neste Oil having 4 plants in different countries with a combined capacity of over 2 million tons/year [15]. Another hydrodeoxygenation commercialization effort using vegetable oils is led by UOP LLC and Eni cooperation [16]. Ecofining technology planned to start its renewable diesel fuel production using a catalytic hydroprocessing technology to convert vegetable oils to a green diesel fuel. Kukushkin et al. [17] reported over 85% yield of hydrocarbons during hydrodeoxygenation of free fatty acids esters using a Ni based catalyst at 1 MPa pressure.

However, all these existing technologies for green diesel production use external sources of hydrogen to upgrade oil or fat. Hydrogen prices are increasing, which are expected to further increase due to increased demand for fuel cell vehicles with this year's commercialization by several vehicle companies (Hyundai, Toyota, and Honda).

Decarboxylation is the chemical reaction of removing oxygen as CO_2 from the reactant molecules such as fats or oils as shown in Eqn. 3 with the mechanism shown below (Figure

1.4). Decarboxylation can provide tremendous advantages as it requires less hydrogen, which possibly could be obtained by the reaction solvent (i.e. H_2O) [18]. Complete removal of oxygen remains a current scientific challenge. To our knowledge, there is no process for complete removal of oxygen from free fatty acids or their derivatives in the published literature without significant degradation in fuel values. To help prevent chain breakage at moderate temperatures, elevated pressures and the use of a catalyst are known to help drive the decarboxylation chemistry [19]. Regarding temperature, Na et al. showed that saponification is dominant at temperatures $<350^\circ C$ and decarboxylation is the main reaction occurring at Temps$> 350^\circ C$ [20].

Saponification
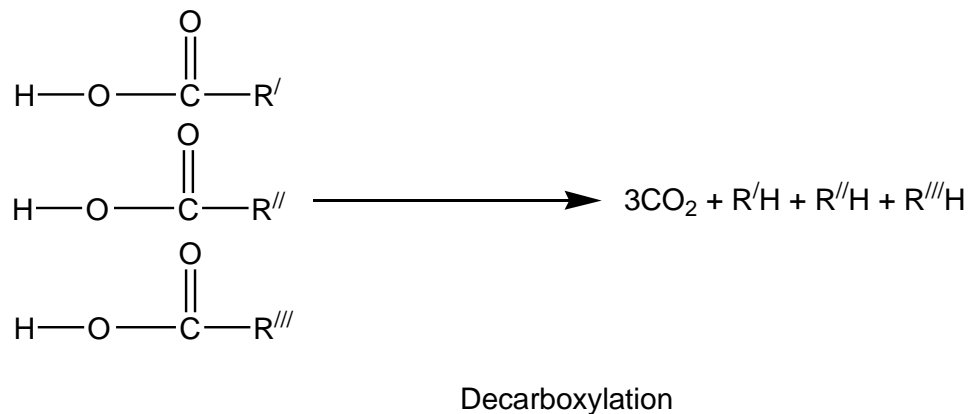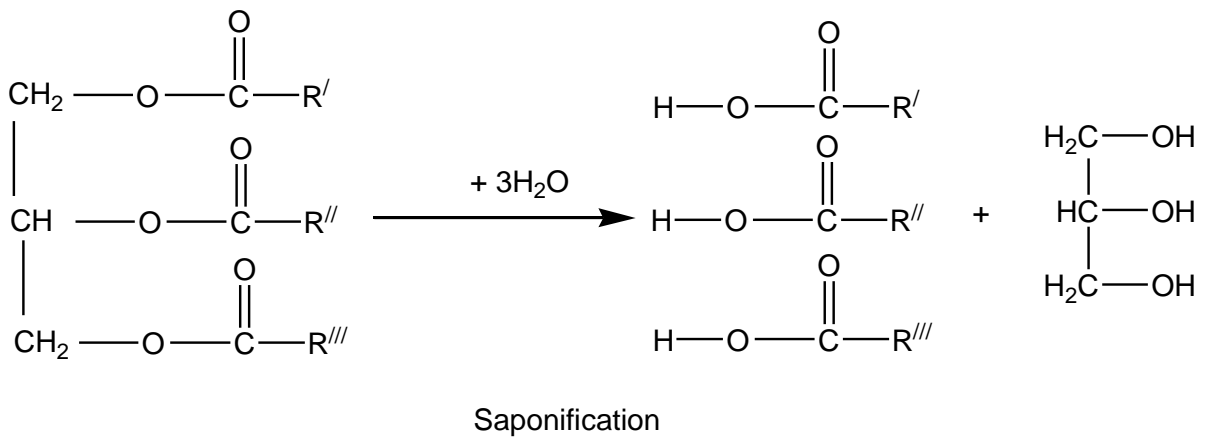
Decarboxylation

Figure 1.4: Saponification and decarboxylation reaction [20].

1.4 Water as a Green Reaction Media

Regarding the proper solvent for decarboxylation chemistry, there is a significant scientific interest for using high-temperature water (HTW) as a green reaction medium for catalytic decarboxylation. The HTW, particularly sub or supercritical water is an environmentally benign solvent, which has intriguing physico-chemical properties making its usage both challenging and potentially useful. For example, water in the supercritical conditions loses its hydrogen bonding ability, becoming more like a non-polar solvent [21-23]. Also its density and dielectric properties vary widely depending on T,P as shown in Figure 1.5.
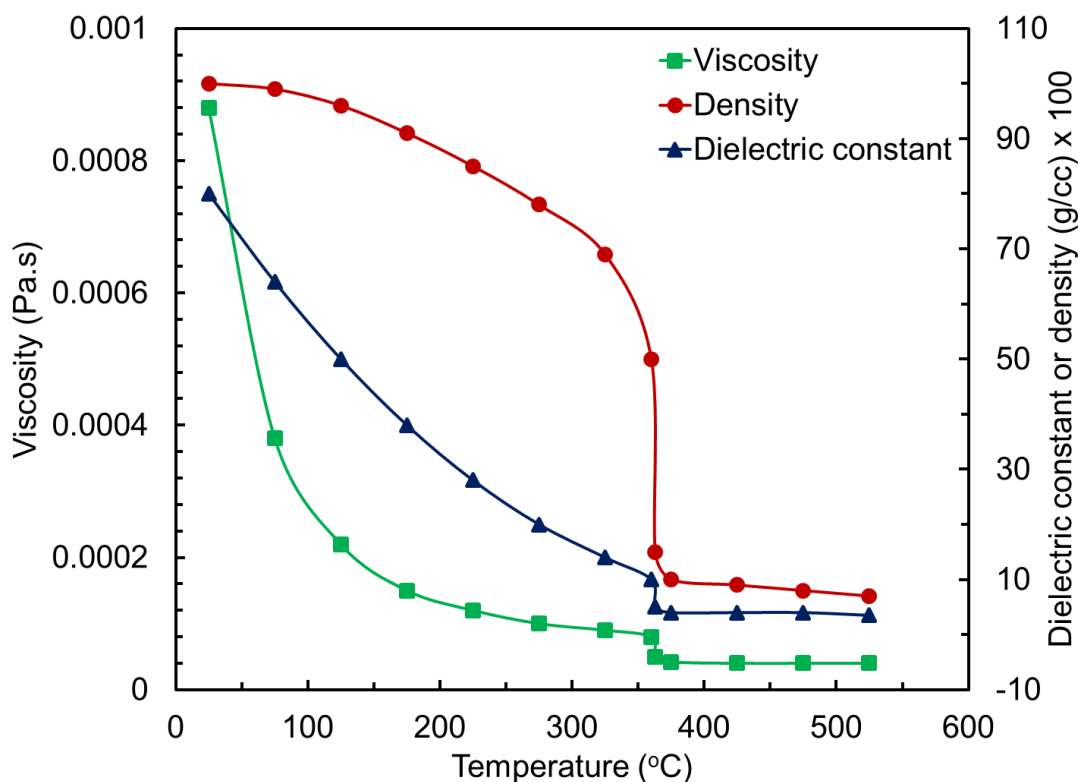
Figure 1.5: Density, static dielectric constant and viscosity of water at 20 MPa as a function of temperature [24].

1.5 Decarboxylation Catalysts

The catalyst is known to greatly enhance the decarboxylation chemistry in sub or supercritical water media. It has been found that thermal decarboxylation of fatty acids and their esters

provide lower hydrocarbon yields at moderate temperatures (<400ºC) without using any catalyst [24, 25]. This clearly indicates the importance of the catalyst for driving the decarboxylation reaction. Snåre *et al*. screened different metal catalysts such as Pd, Pt, Ru, Mo, Ni, Rh, Ir and Os supported either on carbon or different oxides for decarboxylation reactions [24]. Savage et al. [26] demonstrated that activated carbon alone possesses catalytic activity for hydrothermal decarboxylation of oleic acid. Besides this, alkali catalysts were found active for the decarboxylation reaction. Watanabe et al. [27] demonstrated 100% stearic acid conversion was achieved at 400°C using NaOH and KOH as catalysts in supercritical water for a reaction time of 30 min.

1.6 Selection of a Model Compound as Feedstock

Almost all the vegetable oils and animal fats are considered as feedstocks to produce fuel range hydrocarbons. To avoid potential food vs fuel controversial issues, nonedible vegetable oils are widely used as renewable feedstocks for biofuel production. Ultra-high yield biomass such as algae, tall oil fatty acids (TOFA), scrap tallow, yellow grease and brown grease were recently examined as feedstocks. Saturated and unsaturated fatty acids are abundant in the above mentioned feedstocks. Oleic acid, an unsaturated fatty acid was chosen as a model compound for this study. Using a model compound for a feedstock provides several advantages including making it easier to understand the basic chemical pathways occurring during conversion in an unusual reaction medium such as sub or supercritical water.

1.7 Scope of Research

Since biodiesel suffers numerous challenges due to the presence of oxygen contained within its hydrocarbon chains, oxygen free renewable diesel "green diesel" obtained via catalytic hydrothermal decarboxylation (free fatty acids or corn oil) is a desirable option. The decarboxylation process provides oxygen free fuel range hydrocarbons which have similar properties to commercial fuels.

The main objective of this research is to demonstrate fuel range hydrocarbons from oleic acid through hydrothermal decarboxylation using subcritical water as the reaction media. The reaction was first conducted using a stirred tank batch reactor and then examined with a continuous reactor. To understand the reaction chemistry for oleic acid, real feedstocks

including corn distillers oil (CDO) was used for green diesel production. This is very important to use corn oil as a real feedstock, since only real feedstocks have sufficient volumes to be used in a commercial plant.

The objectives of this research can be divided as follows:

❖ Production of fuel range hydrocarbons from both oleic acid (a model compound) and corn oil (lipid based biomass feedstock) using activated carbon as the catalyst
❖ Reactions were conducted in both batch and continuous reactors
❖ The final products were obtained by optimizing the reaction parameters that can be used directly or blended with commercial fuels such as diesel, kerosene or aviation fuel.
❖ In house Mo and Mg based heterogeneous catalysts were synthesized and evaluated for the decarboxylation reaction
❖ Detailed characterization of commercial and in house catalysts (fresh and spent) were performed to understand the stability and reusability of these catalysts

This thesis has eight chapters including the first introductory chapter. Chapter 2 provides a critical review of the hydrothermal decarboxylation process. This chapter presents for the decarboxylation process the types of feedstocks used, the types of products obtained, the role of hydrothermal media, types of catalysts used etc. In Chapter 3, decarboxylation of oleic acid (as a model compound) is presented in subcritical water using a stirred batch reactor system in the presence of activated carbon as catalyst. This chapter shows that complete hydrothermal decarboxylation of oleic acid can be achieved with fuel range hydrocarbons produced. The decarboxylated liquid products can then be directly used as conventional fuels since it has similar properties to conventional fuels. A reaction mechanism of oleic acid decarboxylation in hydrothermal media using activated carbon has also been proposed. The detailed characterization of fresh and spent activated carbon is presented in the chapter to understand the role of catalyst for the decarboxylation of oleic acid.

Chapter 4 presents the continuous hydrothermal decarboxylation of oleic acid in a fixed bed flow reactor using activated carbon as catalyst. Complete decarboxylation was not achieved using the continuous reactor but the process was found to operate at relatively low pressures compared to the stirred batch reactor. A new reaction mechanism is proposed in this chapter

by confirming the in situ hydrogen production experimentally to produce fuel range hydrocarbons.

Catalyst deactivation is a common phenomenon in a high temperature and pressure system. Deactivation and regeneration study of used activated carbon in continuous flow through reactor is presented in Chapter 5. The results show that the spent activated carbon was able to remove less than 50% of –COOH group from oleic acid whereas the regenerated activated carbon shows almost the similar performance as fresh activated carbon for decarboxylation of oleic acid. The detailed characterization of fresh, spent, regenerated and spent regenerated activated carbon is presented in this chapter.

Decarboxylation of oleic acid in hydrothermal media in continuous flow through reactor using a novel Mo-Al$_2$O$_3$ catalyst is presented in Chapter 6. The decarboxylation reaction varies with the type of catalyst used. Decarboxylation of oleic acid using Mo-Al$_2$O$_3$ catalyst was found to require a larger reaction time compared to the activated carbon catalyst but the liquid yield was significantly higher. The detailed characterization of fresh and spent Mo-Al$_2$O$_3$ catalyst is presented in this chapter.

To understand the chemistry of decarboxylation for real feedstocks, decarboxylation of corn distiller's oil (CDO) was performed in a stirred batch reactor using activated carbon as catalyst. Chapter 7 presents the hydrothermal decarboxylation of CDO. Complete decarboxylation of CDO has been achieved in the batch reactor and the formed decarboxylated liquid product has the identical fuel properties as commercial fuels. A reaction mechanism of CDO decarboxylation is proposed in this chapter. Chapter 8 includes the summary of the work performed in this thesis.

1.8 Research Contributions

The main contributions of this research are: (i) developing a new hydrothermal approach for the production of green diesel from fatty acids and their derivatives without adding an external source of hydrogen, (ii) the obtained liquid product has the identical properties as commercial fuels which can be used as is or blended with commercial diesel fuel.

1.9 Thesis Format

This thesis is written in the format of 'Integrated Article thesis' as specified by the Faculty of Graduate Studies of the University of Western Ontario. Individual chapters are presented as research articles. Each chapter has its own conclusions and references with symbols and abbreviations listed at the end of the chapter. Appendix is combined together at the end for all chapters.

References

[1] B. Smith, H.C. Greenwell, A. Whiting, Catalytic upgrading of tri-glycerides and fatty acids to transport biofuels, Energy & Environmental Science, 2 (2009) 262-271.

[2] N.-O. Nylund, P. Aakko-Saksa, K. Sipilä, Status and outlook for biofuels, other alternative fuels and new vehicles, VTT, 2008.

[3] Inventory of U.S. Greenhouse Gas Emissions and Sinks: 1990-2007,EPA (Accessed on 1st May, 2017).

[4] M. Specht, U. Zuberbuhler, A. Bandi, Why biofuels?–An introduction into the topic, RENEW–1st European Summer School on Renewable Motor Fuels, Uwelt-Campus-Birkenfeld, 29th-31st August, (2005).

[5] http://www.treia.org (Accessed on 1st May, 2017).

[6] A. Brown, S. Müller, Z. Dobrotkova, Renewable energy: Markets and prospects by technology, IEA information paper, (2011).

[7] Basic Research Needs: Catalysis for Energy, U.S. Department of Energy, 2007.

[8] "The Outlook for Energy: A View to 2040," ExxonMobil, Tech. Rep., 2014.

[9] S.N. Naik, V.V. Goud, P.K. Rout, A.K. Dalai, Production of first and second generation biofuels: a comprehensive review, Renewable and Sustainable Energy Reviews, 14 (2010) 578-597.

[10] T. Kalnes, T. Marker, D.R. Shonnard, Green diesel: a second generation biofuel, International Journal of Chemical Reactor Engineering, 5 (2007).

[11] B.r. Donnis, R.G. Egeberg, P. Blom, K.G.n. Knudsen, Hydroprocessing of bio-oils and oxygenates to hydrocarbons. Understanding the reaction routes, Topics in Catalysis, 52 (2009) 229-240.

[12] R.O. Idem, S.P.R. Katikaneni, N.N. Bakhshi, Catalytic conversion of canola oil to fuels and chemicals: roles of catalyst acidity, basicity and shape selectivity on product distribution, Fuel Processing Technology, 51 (1997) 101-125.

[13] A. Talebian-Kiakalaieh, N.A.S. Amin, H. Mazaheri, A review on novel processes of biodiesel production from waste cooking oil, Applied Energy, 104 (2013) 683-710.

[14] P. Miller, A. Kumar, Techno-economic assessment of hydrogenation-derived renewable diesel production from canola and camelina, Sustainable Energy Technologies and Assessments, 6 (2014) 105-115.

[15] C. Hodge, Neste Oil. NExBTL diesel, in, 2009.

[16] E. Voegele, Italian refiner to produce green diesel with Ecofining process, in, 2012.

[17] R. Kukushkin, O. Bulavchenko, V. Kaichev, V. Yakovlev, Influence of Mo on catalytic activity of Ni-based catalysts in hydrodeoxygenation of esters, Applied Catalysis B: Environmental, 163 (2015) 531-538.

[18] S. Popov, S. Kumar, Rapid hydrothermal deoxygenation of oleic acid over activated carbon in a continuous flow process, Energy & Fuels, 29 (2015) 3377-3384.

[19] J. Fu, X. Lu, P.E. Savage, Hydrothermal decarboxylation and hydrogenation of fatty acids over Pt/C, ChemSusChem, 4 (2011) 481-486.

[20] J.-G. Na, B.E. Yi, J.N. Kim, K.B. Yi, S.-Y. Park, J.-H. Park, J.-N. Kim, C.H. Ko, Hydrocarbon production from decarboxylation of fatty acid without hydrogen, Catalysis today, 156 (2010) 44-48.

[21] W. Wagner, A. Pruß, The IAPWS formulation 1995 for the thermodynamic properties of ordinary water substance for general and scientific use, Journal of Physical and Chemical Reference Data, 31 (2002) 387-535.

[22] D.G. Archer, P. Wang, The Dielectric Constant of Water and Debye-Hückel Limiting Law Slopes, Journal of physical and chemical reference data, 19 (1990) 371-411.

[23] M. Watanabe, T. Sato, H. Inomata, R.L. Smith, K. Arai, A. Kruse, E. Dinjus, Chemical reactions of C1 compounds in near-critical and supercritical water, Chemical Reviews, 104 (2004) 5803-5822.

[24] M. Snåre, I. Kubickova, P. Mäki-Arvela, K. Eränen, D.Y. Murzin, Heterogeneous catalytic deoxygenation of stearic acid for production of biodiesel, Industrial & engineering chemistry research, 45 (2006) 5708-5715.

[25] P. Mäki-Arvela, I. Kubickova, M. Snåre, K. Eränen, D.Y. Murzin, Catalytic deoxygenation of fatty acids and their derivatives, Energy & Fuels, 21 (2007) 30-41.

[26] J. Fu, F. Shi, L. Thompson Jr, X. Lu, P.E. Savage, Activated carbons for hydrothermal decarboxylation of fatty acids, ACS Catalysis, 1 (2011) 227-231.

[27] M. Watanabe, T. Iida, H. Inomata, Decomposition of a long chain saturated fatty acid with some additives in hot compressed water, Energy conversion and management, 47 (2006) 3344-3350.

Chapter 2

Literature Review

2.1 Introduction

The rapid increase of transportation vehicles worldwide has necessitated the demand for high quality fuel oils. It has been anticipated that the worlds demand for diesel fuel will rapidly increase toward 2035 compared to any other fossil fuels (Figure 2.1) [1]. From 2012 to 2035, diesel fuel and gasoline demand are estimated to increase 10 and 4 million barrels per day, respectively. Meanwhile, the demand for ethane/LPG, naphtha, bitumen, lubricants waxes still gas, coke, direct use of crude oil, etc. will decrease slightly. On the other hand, the demand for residual fuel will globally decrease in the coming years [1].
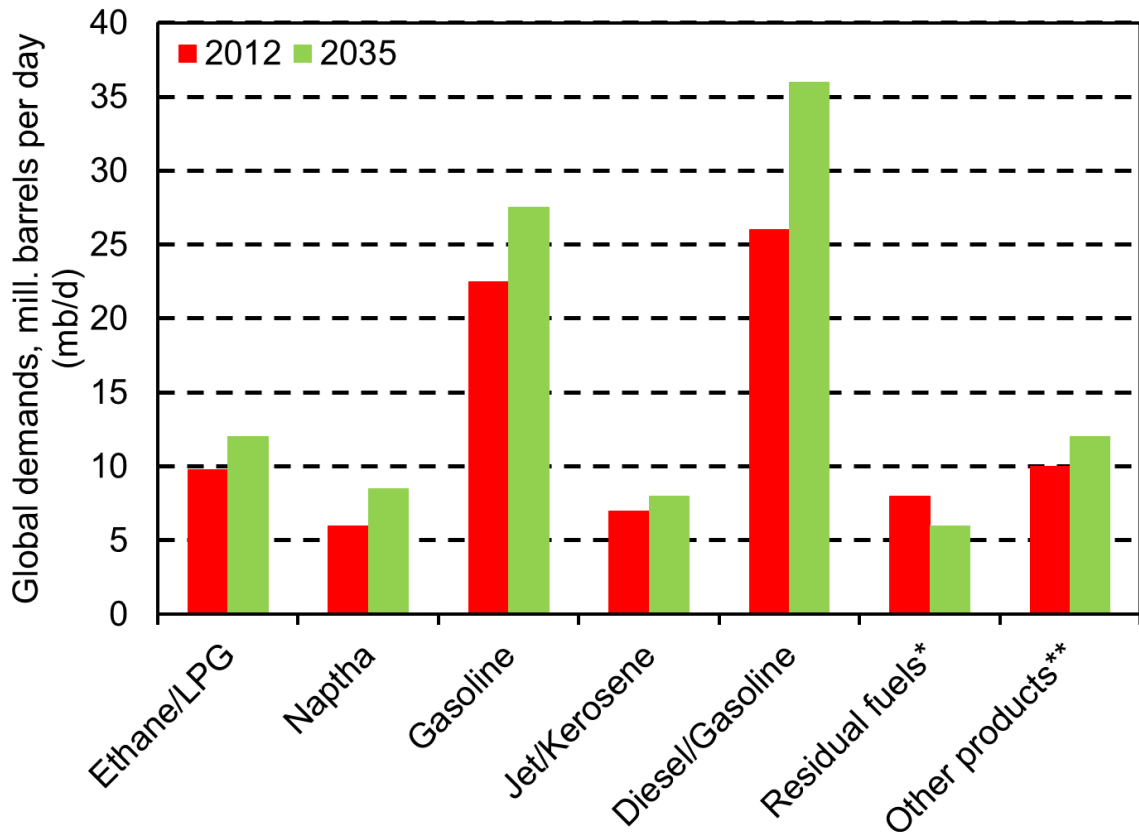
*Includes refinery fuel oil, **Includes bitumen, lubricants, waxes, still gas, coke, sulphur, direct use of crude oil, etc.

Figure 2.1: Global demands for diesel fuel in 2012 and forecast in 2035 compared to other refined oil products [1].

Fossil fuels are going to be depleted in the next few decades due to their rapid consumption. The International Energy Agency (IEA) compares the most probable crude oil supply with the most likely demand requirements, as shown in Figure 2.2 [2]. The conventional crude oil supply surpassed demand from 2009 to 2011, with the demand constantly surpassing supply in 2012 and 2013. Then, from 2014 onwards, the conventional crude oil supply will be in shortage with the demand increasing due to the increasing world population and affluence in emerging markets.
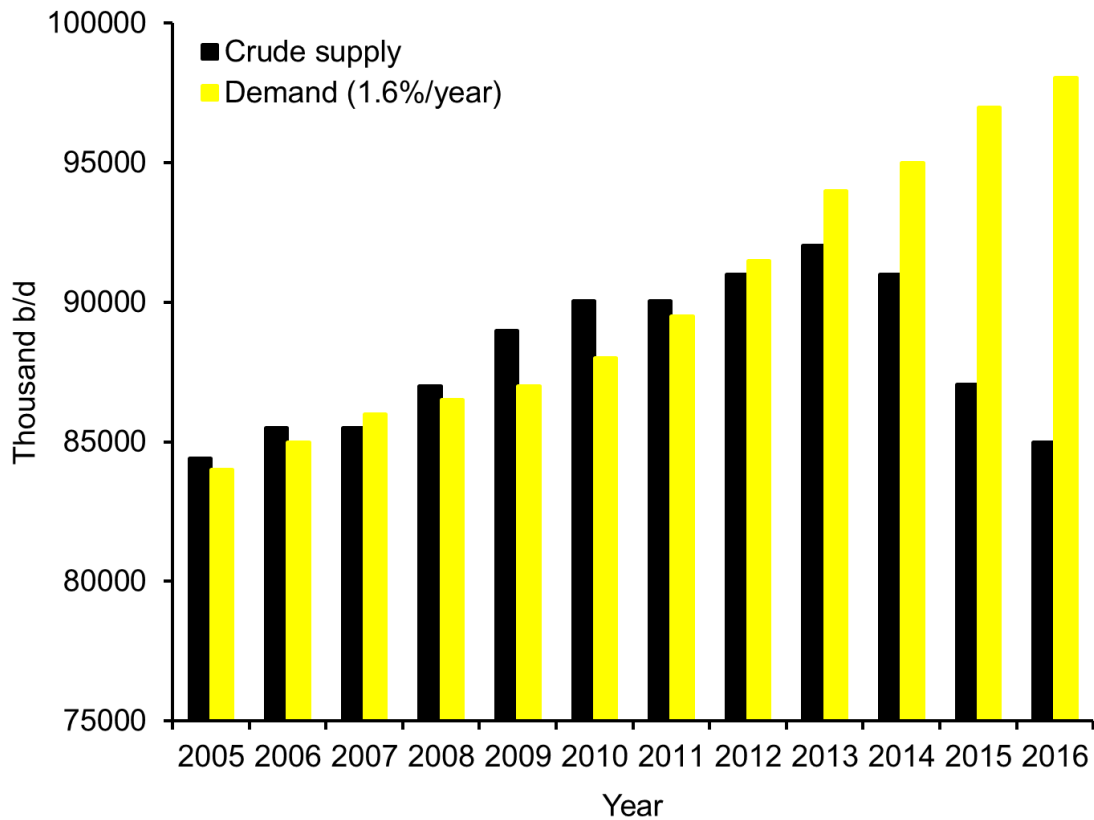
Figure 2.2: Global crude oil supply and projected demand [2].

Therefore, it is necessary to find an alternative energy source to cover this shortage in the next few decades. In this regard, biofuels from various renewable feedstocks and associated technologies have been studied for many years [3-6]. There are numerous advantages of using biofuels including: (a) they are inexhaustible and readily available (b) they represent a carbon dioxide-cycle in combustion, (c) they are biodegradable, environmentally friendly and contribute to sustainability. The benefits include: reducing greenhouse gas emissions at domestic and international level, the diversification of the fuel sector, biodegradability,

15

sustainability, and an additional market for agricultural products. The major benefits of biofuels are listed in Table 2.1 [7].

Table 2.1: Major benefits of biofuels.

Economic Impacts	Sustainability Fuel diversity Increased number of rural manufacturing jobs Increased income taxes Increased investments in plant and equipment Agricultural development International competitiveness Reducing the dependency on imported petroleum
Environmental Impacts	Greenhouse gas reductions Reducing air pollution Biodegradability Higher combustion efficiency Improved land and water use Carbon sequestration
Energy Security	Domestic targets Supply reliability Reducing use of fossil fuels Ready availability Domestic distribution Renewability

2.2 Feedstocks

Feedstocks for liquid biofuels production are divided into three categories such as lignocellulosic, amorphous sugars and triglycerides [8]. Figure 2.3 shows the types of feedstocks used for liquid biofuels.

Biomass Feedstock

Lignocellulosic
Corn stover
Crop residues
Pinaster
Eucalyptus globules
Forage grasses
Wheat straw
Forest residues
Sorghum stalks
Paper mill residues
bamboo
Wood chips
Switchgrass
Spent grains
Waste wood chips

Amorphous Sugars
Starches
Simple sugars

Triglycerides
Vegetable oils
o Soybean
o Cottonseed
o Palm
o Peanut
o Sunflower
o Coconut
o Jatropha
o Algae
Animal Fats (Tallow)
Waste Oils
o Used frying oils
o Brown grease

Figure 2.3: Different types of feedstocks used for liquid biofuel production.

Lignocellulosic biomass has received significant attention by researchers as a renewable feedstock over the past few decades due to its abundance with easy availability [9, 10]. Lignocellulose consists of mainly three components: rigid cellulose fibers (a polymer of glucose molecules), lignin (a polymer constructed of noncarbohydrate and alcohol units) and hemicelluloses (short, highly branched, sugar chains). Figure 2.4 shows the percentages of cellulose, hemicellulouse and lignin in some typical biomass. Lignocellulosic biomass usually contains 35–50% cellulose, 20–35% hemi-cellulose, and 10–25% lignin. Cellulose is the major ingredient of lignocellulosic biomass. It is anticipated that approximately half of the organic carbon in the biosphere exists in the form of cellulose [11]. Therefore, converting lignocellulosic biomass into fuels and value added chemicals is of utmost importance. Although lignocellulosic biomass is cheaper and readily available, transportation fuel obtained from this is an expensive fuel because it is normally a low-energy-density feedstock [12].
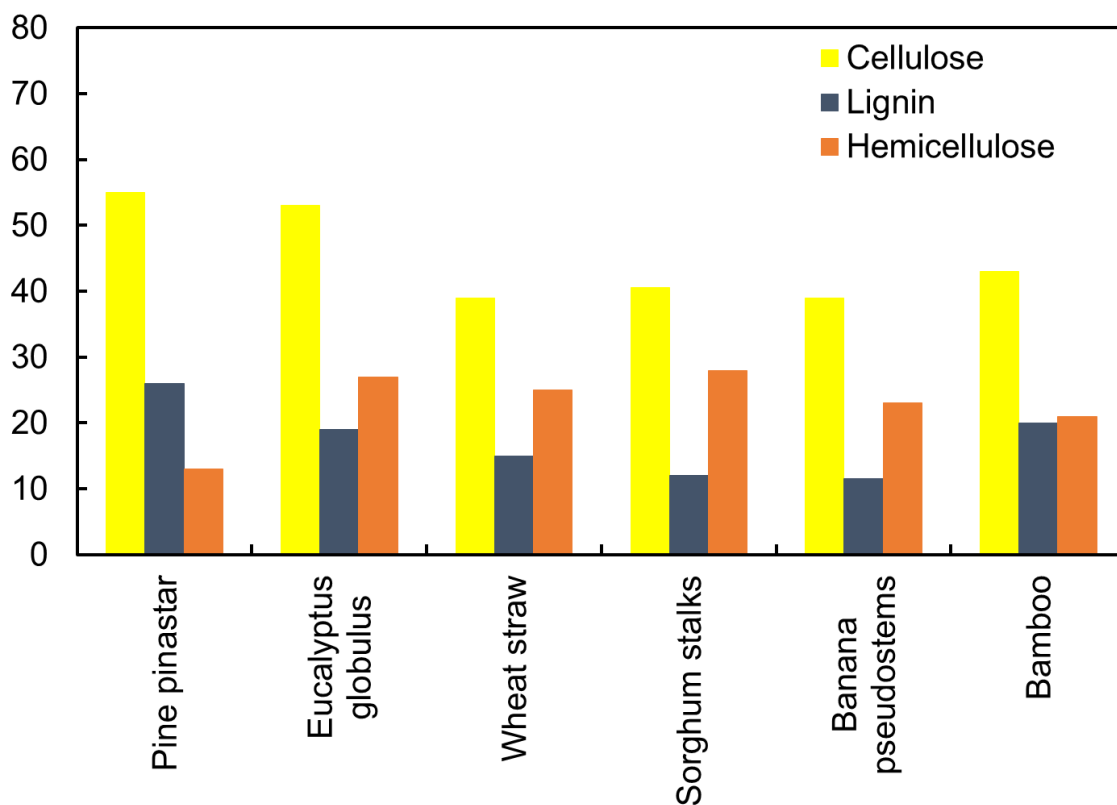
Figure 2.4: The percentages (wt) of cellulose, hemicelluloses and lignin in pine pinaster [13], eucalyptus globules [13], wheat straw [14], sorghum stalks [15], bamboo [16] and banana pseudo-stems [17].

Amorphous sugars (starches or simple sugars) can also be used as a liquid transportation fuel feedstock. But, the food versus fuel debate is the main concern for their usage [18]. Since people or livestock directly consume amorphous sugars as their food source, producing fuel from this crop can have adverse effects. Farmable land will be decreased for harvesting crops for biofuel production instead of food supplies [19]. On the other hand, loss of crops to fuel production will lead to price inflation of food items because of the lack of availability of crops for food consumption [19, 20].

Triglyceride based agricultural fats and oils are another alternative feedstock for liquid biofuels. Triglycerides mainly contain one mole of glycerol and three moles of fatty acids [21] (Figure 2.5). Triglyceride is the main constituent of vegetable oils. Most common vegetable oil sources are soybean, cottonseed, palm, corn, peanut, rapeseed/canola, sunflower, safflower, coconut, rice bran etc. The liquid nature of vegetable oils adds an extra advantage over other

18

feedstocks for their transportation and processing. Products obtained from vegetable oils have a high heat content, which is close to 90% of diesel fuel [22]. Furthermore, vegetable oil fuels are pH neutral, contain no water, and are relatively stable [23].

(a)

(b)
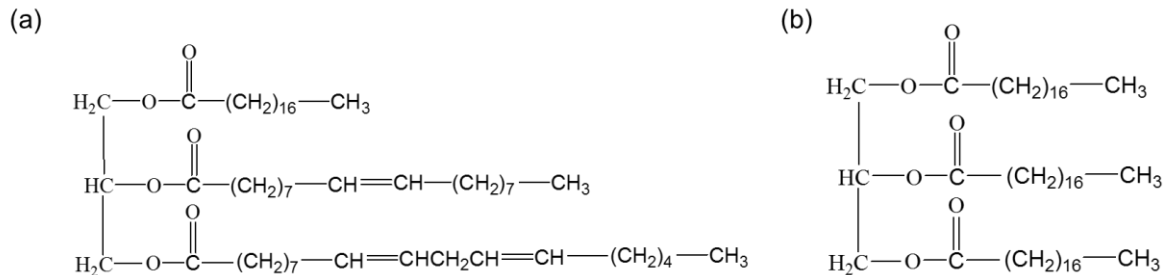
Figure 2.5: (a) Structure of a typical triglyceride molecule (b) triglyceride of stearic acid.

Fatty acids are the simplest monomer of triglycerides. Fatty acids are carboxylic acids with long aliphatic chains, which are either saturated (no carbon-carbon double bond) or unsaturated (one or more carbon-carbon double bond) (Figure 2.6). Palmitic acid, stearic acid, lauric acid etc. are the typical examples of saturated fatty acids. Typical examples of unsaturated fatty acids are oleic acid, myristoleic acid, linoleic acid etc. Soybean oil contains 7% linolenic acid (C18:3) (C18:3 indicates an carboxylic acid with 18 carbon atoms and 3 carbon-carbon double bonds), 51% linoleic acid (C18:2), 23% oleic acid (C18:1), 4% stearic acid (C18:0), and 10% palmitic acid (C16:0) [24]. In addition, two new candidates have emerged as non-food biofuel feedstocks such as jatropha and algae because they can be grown and harvested in non-traditional farming areas [25].

(a)

(b)
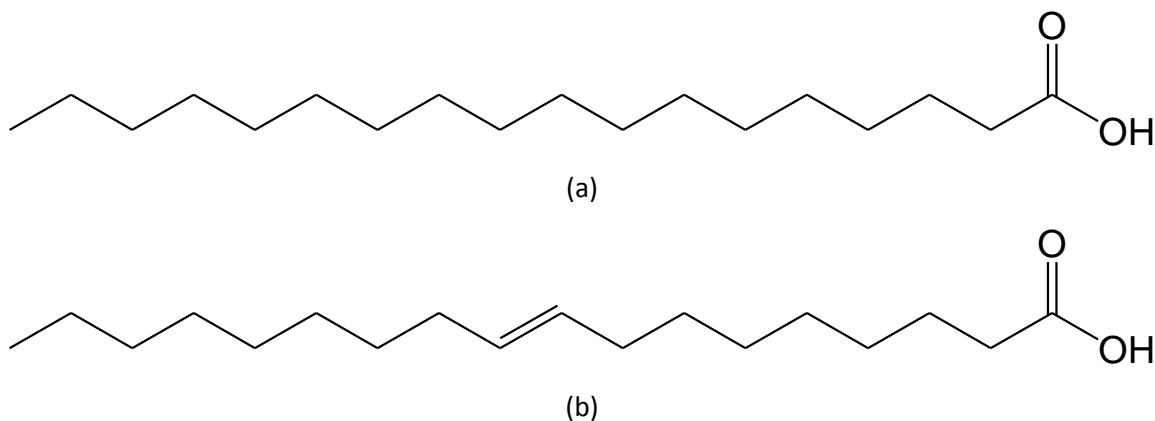
Figure 2.6: (a) Stearic acid (saturated) (b) Oleic acid (unsaturated).

Jatropha (Euphorbiaceae) curcas is a plant which mainly grows in Asia, Africa, Central and South America. This plant can be easily grown in poor soils of tropical and subtropical countries [20]. Its seed kernel contains 40-60% (w/w) oil consisting of 20% saturated fatty acids and 80% unsaturated ones [26]. Oleic acid is the main constituent (44.8%) of Jatropha oil whereas it also contains 34% linoleic acid, 12.8% palmitic acid, and 7.3% stearic acid [27]. Although the compositions are quite similar to other edible oils, the presence of toxic phorbol esters prevents this oil from being used for cooking [28]. Therefore, it is a good candidate for use as a renewable feedstock for liquid biofuel production.

Nowadays, there is a growing interest to exploit algal oils (algae) as a renewable feedstock since algae provides much higher oil production per acre than any other triglycerides feedstocks [29]. Algae produces 7 to 31 time's higher oil than palm oil and 250 times the amount of oil per acre as soybeans [30]. Since it does not conflict with food for land use or water resources, algae oil is a prospective solution due to the concerns regarding the use of agricultural land for energy generation rather than food production [31]. The best algae for liquid biofuel production would be microalgae. Microalgae is an organism capable of photosynthesis that is less than 2 mm in diameter. Microalgae has much more oil than macroalgae and it is much faster and easier to grow.

In addition to vegetable oils, animal fats such as tallow or lard have been also used as renewable feedstocks to produce value added products [32, 33]. Tallow or Lard is a comparatively cheaper feedstock which is obtained from the meat-packing industry as a co-product. However, since it thickens at low temperature, its usage would be limited to the areas where temperature does not fall below 4.5 ℃.

Waste cooking oil would be another renewable feedstock for liquid fuel production. During cooking, especially deep-frying, oils are hydrolyzed and degraded into different products such as polymers, volatiles, FFA, and other degradation products via chemical reactions. Depending on the variations in free fatty acid (FFA) composition, triglycerides, water content, and impurities, the conversion method will have to altered to obtain high grade biodiesel [34]. In fact, quality variability of waste oil is recognized as more problematic than that of vegetable oils [25].

Choosing a biomass for biofuels production is very important as the product quality largely depends on its chemical and physical characteristics. Some other factors such as supply, cost, storage properties, and engine performance are also to be considered. The principle cause of the economic defeat of biofuels against fossil fuels is that triglyceride feedstocks are relatively expensive. Even with the least expensive triglyceride feedstocks, the 70 - 85 % of the total production expense is related to the feedstock cost [35]. Biofuels produced from waste oil and animal grease are comparatively cheaper [20]. With respect to other available biomass feedstocks, generally, the most expensive are triglyceride based followed by amorphous sugars with lignocellulosic feedstocks the least expensive [24].

2.3 Lipid based biofuels

Lipid based biofuels in the form of biodiesel or green diesel are currently being examined for transportation fuels. Researchers are more interested in biodiesel or green diesel as they can be easily integrated with current infrastructure without any engine modifications.

2.3.1 Biodiesel

The plant oils cannot be used as fuel directly as they contain free fatty acids, phospholipids, sterols, water, odorants and other impurities [6]. Chemical modification is required to use them as fuels. Different processes are used to produce biodiesel from plant oils such as transesterification, pyrolysis and emulsification; whereas the transesterification is a popular way to produce biodiesel.

Biodiesel is the fatty acid methyl esters (FAME) which is obtained from the chemical reaction between vegetable oil and an alcohol in the presence of catalyst (Figure 2.7). Triglyceride is the main constituent of vegetable oil which consists of three long chain fatty acid chains esterified to a glycerol backbone. When the triglyceride component reacts with an alcohol such as methanol, the three fatty acid chains are released from the glycerol skeleton and combine with the alcohol to yield fatty acid methyl esters (FAME). Glycerol is produced as a by-product. Methanol, ethanol, propanol and butanol are used for the transesterification reaction. However the yield of esterification is independent of the type of alcohol used [36]. Methanol is the most commonly used alcohol because of its low cost. In general, a large excess of methanol is used to shift the equilibrium to the product side.
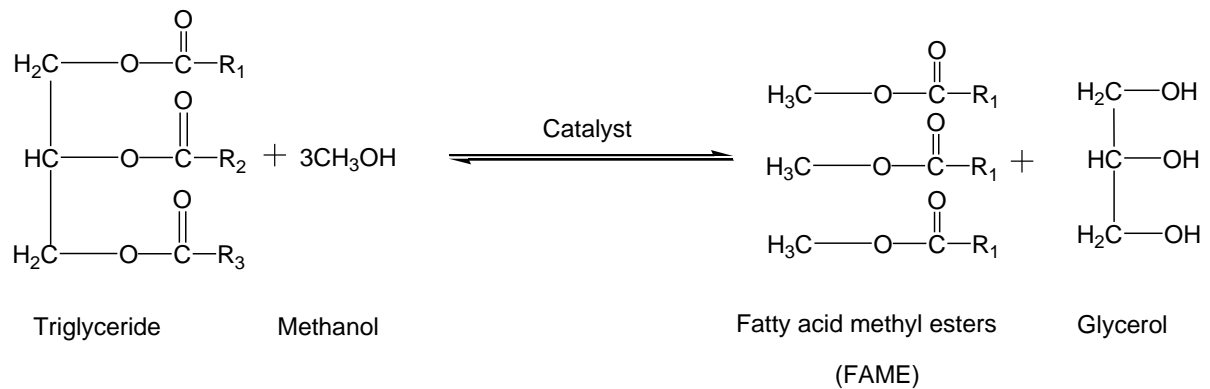
Figure 2.7: A schematic representation of the transesterification of triglycerides (vegetable oil) with methanol to produce fatty acid methyl esters (biodiesel).

Both acid and base catalysts have been examined for the transesterification reaction. However, basic catalysts are found to be effective for higher yield of biodiesel during the transesterification reaction compared to acid catalysts. Potassium hydroxide and sodium hydroxide are the most commonly used alkaline catalysts. Alkaline catalyzed transesterification of vegetable oils is possible only if the acid value of oil is less than 4. A higher percentage of FFA in the oil reduces the yield of the esterification process. Since the alkaline catalyst is a homogeneous catalyst, separating the catalyst after the reaction is challenging, causing material loss while additional production expense related to neutralization and waste reclamation.

Figure 2.8 provides a process flow diagram for biodiesel production using a basic catalyst. The reactor usually operates at ambient pressure and at fixed temperature. Reactants (fat/oil) are fed into the main reactor when heated to 65 °C. An auxiliary reactor containing a mixture of KOH and methanol (molar ratio of 1:6) is also added to the main reactor. The reaction mixture is stirred continuously for 180 min and then the stirrer is turned off. The mixture was left for another 240 min without stirring for aging. The glycerol phase is then separated and the FAME phase is washed with dilute phosphoric acid solution to neutralize residual catalyst, glycerol, methanol and soap. After separation of the water phase, FAME is heated at 105 °C for 30 min to evaporate water and methanol residual, filtered and sent to a storage tank.
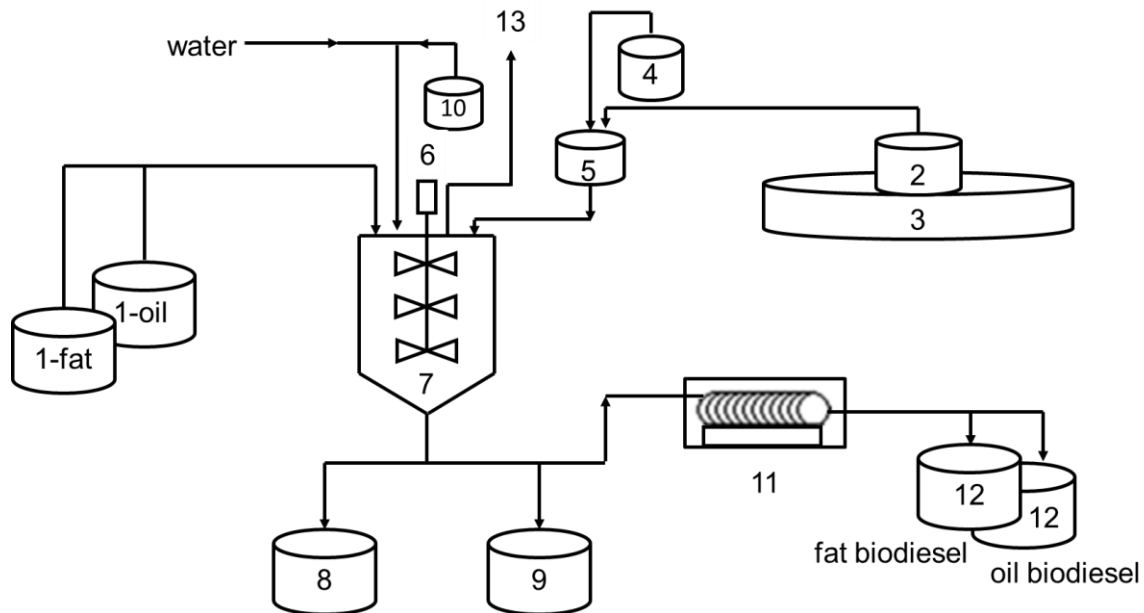
Figure 2.8: Flow sheet of the transesterification process [37]; 1-tank of fat and oil. 2-tank of methanol, 3-containment basin, 4-reservoir of KOH, 5-methoxi reactor, 6-mechanic stirrer, 7-main reactor, 8-tank of glycerol, 9-tank of waste water, 10-reservoir of phosphoric acid, 11-filter, 12-tank of biodiesel, 13-relief valve.

Biodiesel has several advantages as a next-generation fuel. It is derived from a renewable, domestic resource, thereby reducing our dependency on petroleum fuels. It has similar fuel properties as petroleum fuel. It reduces greenhouse gas emissions regardless of its feedstock origin. It provides lubricating properties which can reduce engine wear and extend engine life. It has a much low sulfur content than petroleum diesel which reduces significantly SO_x emissions. Also, the comparatively high flash point (150 °C) of biodiesel provides a lower fire hazard than petroleum diesel and also makes it safer to transport and handle [36].

However, biodiesel also has some major disadvantages. Biodiesel is composed of significant amounts of oxygen containing molecules that have distinctly different chemical identity than conventional petroleum fuel [38]. Higher viscosity, cloud point and acid number of biodiesel cause possible engine problems which prevents their usage in cold areas such as Canada [39]. Biodiesel has 10-20 times higher kinematic viscosity (27.2 to 53.6 mm^2/s) compared to conventional diesel, which adds several problems during combustion of fuel such as low

23

atomisation capacity, coke deposition into the injector and engine, and piston ring sticking [40]. Biodiesel has much higher NO_x emissions, oxidative stability and poor cold flow properties compared to conventional diesel and it has been reported that using various types of biodiesel follows the similar trend which is due to the similar chemical and physicochemical properties [41, 42].

2.3.2 Green diesel

Green diesel is defined as diesel-like hydrocarbons which have a similar combustion properties to commercial fuels. Green diesel is produced via several routes such as hydrodeoxygenation and/or decarboxylation/decarbonylation of triglycerides [43-46]. Hydrodeoxygenation of triglyceride/fatty acid reduces oxygen content and related acidity of fatty acids to obtain saturated hydrocarbons suitable for drop-in diesel fuel. Decarboxylation or decarbonylation removes oxygen as carbon dioxide or carbon monoxide and provides n-paraffin's as the reaction products. This provides a diesel like hydrocarbons product which has identical properties to commercial diesel whereas biodiesel contains oxygenated species that have different properties than commercial diesel [47]. Compared to biodiesel, green diesel has a higher oxidation stability, lower specific gravity, higher Cetane number, and when it is blended with petroleum diesel it has much better cold flow properties. In addition, green diesel is fully compatible with petroleum diesel, thus changes or maintenance to the engine are not required. Green diesel is also environmentally friendly, as its use may produce fewer greenhouse gases than petroleum diesel, biodiesel, and fossil-derived syndiesel (without carbon sequestration) [48]. Furthermore, the high energy density of hydrocarbons makes them a valuable transportation fuel option (Figure 2.9) [49].
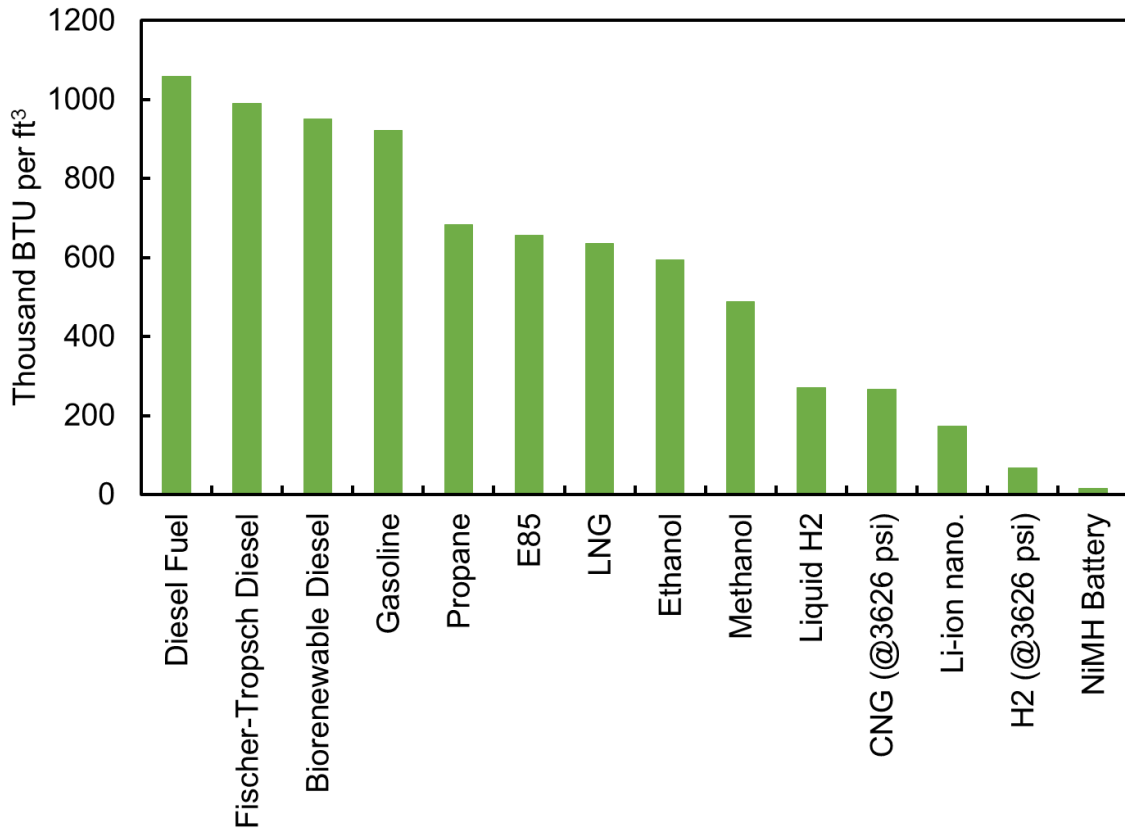
Figure 2.9: Energy density of various fuels [49].

Green diesel had been produced commercially in Finland by Neste oil since 2007 [50]. Neste oil use a hydrodeoxygentaion process to remove oxygen from the feedstock to produce green diesel. Another two companies named UOP and Eni developed hydroprocessing technology which is called the UOP/Eni Green Diesel Process. This process was commercialized in an Eni refinery in Italy since 2009 [51]. Figure 2.10 shows a schematic of the UOP/Eni green diesel process. Vegetable oil (soybean/rapeseed/palm oil) is fed to the reactor with hydrogen at the desired reaction temperature where the vegetable oil is converted into Green diesel using the hydrodeoxygenation reaction. The product is separated from the recycle gas in the separator and the liquid product is sent to a fractionation column. Products such as propane, naphtha, and diesel products are then separated. The recycle gas is treated in an amine system to remove CO_2.
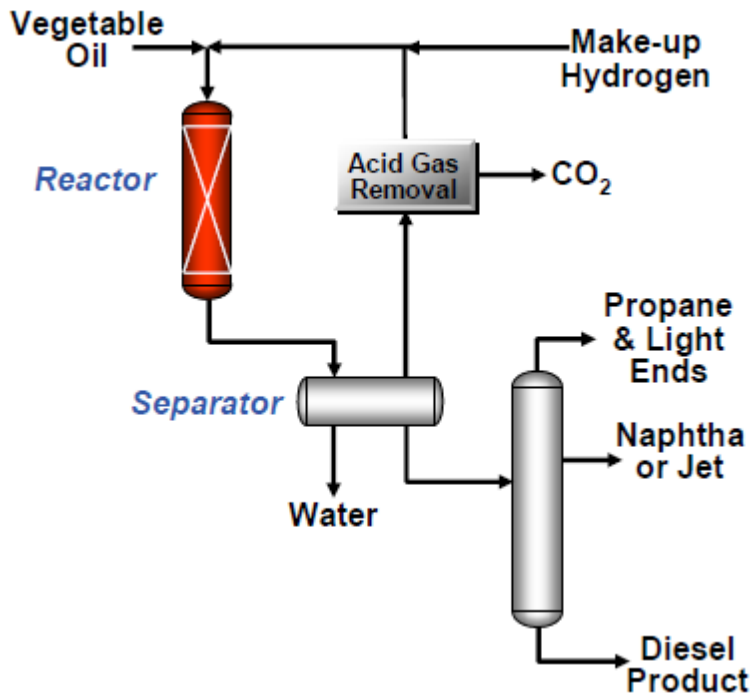
Figure 2.10: A simplified flow diagram for green diesel production [51].

2.3.2.1 Hydrodeoxygenation process

Hydrodeoxygentaion (HDO) is a process which hydrogenates the double bonds of the side chains and removes oxygen on the metal sites of the catalyst. The HDO reaction occurs at moderate temperature ranges from 300-600ºC and under high hydrogen pressure in the presence of heterogeneous catalysts [12]. Figure 2.11 shows a typical HDO reaction of trioleic triglyceride. HDO of most vegetable oils produce C15 to C18 hydrocarbons, which is commonly referred to as "green diesel", "renewable diesel" or "bio-hydrogenated diesel".
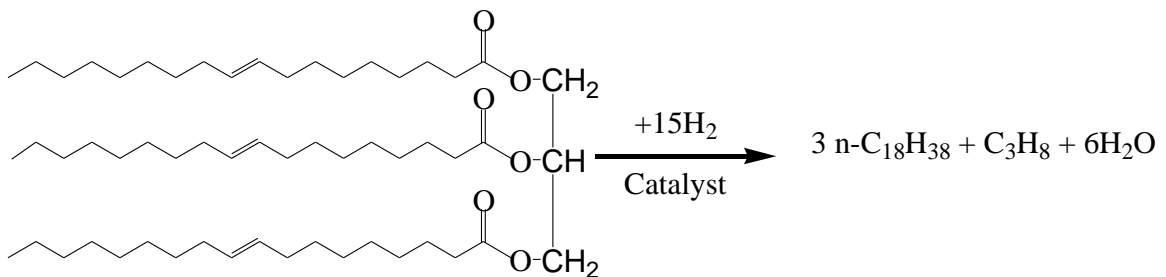
Figure 2.11: Hydrodeoxygenation reaction of trioleic triglyceride.

Compared to biodiesel, green diesel produced during the HDO process has several advantages including: [52]

- ❖ Compatible with the existing infrastructure of petroleum fuels.
- ❖ Flexible feedstock (product quality is independent of free fatty acids content in the).
- ❖ Higher cetane number.
- ❖ Higher energy density.
- ❖ Higher oxidation stability (zero or less O_2 content).
- ❖ Reduces NOx emissions significantly.
- ❖ No by-products like glycerol that require additional treatment.
- ❖ Better performance in excessive cold areas.

On the other hand, requirements of hydrogen is the main drawback of the HDO process. Decarboxylation could be an alternative to HDO as it requires less or no hydrogen.

2.3.2.2 Decarboxylation

Decarboxylation is the chemical reaction where a carboxyl group (-COOH) is removed from a molecule as CO_2 (Figure 2.12). Compared to the HDO process, decarboxylation or decarbonylation ($deCO_x$) requires less or no hydrogen which makes this process more attractive from an economic viewpoint. Less hydrogen consumption provides less operational and capital costs due to the reduced size of hydrogen compressor and hydrogen purchases. Another advantage is the HDO process requires high pressures whereas the decarboxylation reaction can occur at relatively low pressures [24].
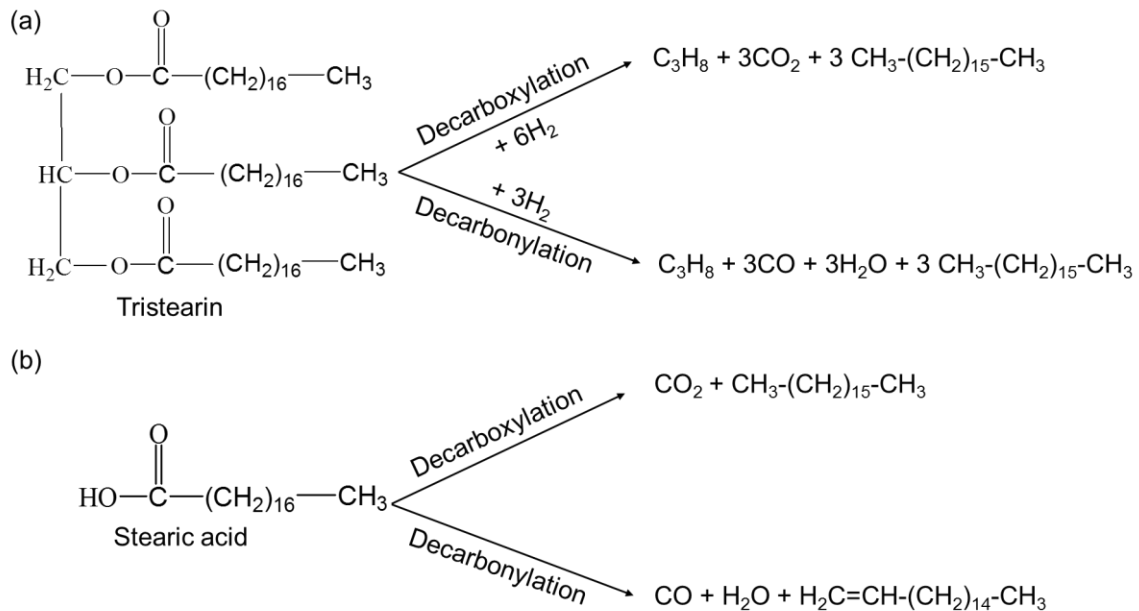
Figure 2.12: Decarboxylation and decarbonylation of tristearin (a) and stearic acid (b).

2.4 Reactor systems and process parameters

Types of the reactor and process parameters are essential factors for obtaining high yield of fuel range hydrocarbons during decarboxylation of fatty acids and their esters in order to meet the fuel quality standard. The reaction parameters which influence the yield and selectivity of hydrocarbons as well as their product compositions are as follows: types of catalyst, feed type, temperature, reaction atmosphere, residence time, catalyst loading, types of solvent, feed to solvent ratio etc.

2.4.1 Reactor types

Three different reactor systems are used to perform the decarboxylation experiments such as batch, semi-batch or semi-continuous and continuous. Since CO_x is the major gas produced during decarboxylation of fatty acid and their derivatives, CO_x may be poisonous to some catalysts used for the reaction. It is possible to remove CO_x gas during the reaction conducted in semi batch and continuous reactors whereas it is not possible in the case of batch experiments until the reaction is complete [53, 54]. From an industrial point of view, continuous reactors are favored.

2.4.2 Catalysts

Thermal decarboxylation of fatty acids and their esters provide lower yields of hydrocarbons at moderate temperatures ($<400^{\circ}C$) [55, 56], which clearly indicates that the process requires a catalyst to increase the rate of reaction. Various supported metal catalysts i.e. Pd, Pt, Ru, Mo, Ni, Rh, Ir and Os have been examined for deoxygenation/decarboxylation of fatty acids and their esters. Supports mainly used for decarboxylation are Al_2O_3, ZrO_2, SiO_2, activated carbon and Zeolites. Madsen et al. [57] demonstrated that Pd/γ-Al_2O_3 catalyst was more active for decarboxylation of stearic acid compared to Pt/γ-Al_2O_3 catalyst due to the higher content of active metal (Pd) in the Pd/γ-Al_2O_3 catalyst. Pd/γ-Al_2O_3 catalyst was also more selective for the production of heptedecane and pentadecane. On the other hand, although Ni/γ-Al_2O_3 catalyst contained the highest active metal (Ni) among the three studied catalysts, it gave the poorest performance for decarboxylation which was ascribed to the largest particle size of Ni in Ni/γ-Al_2O_3 catalyst. The average particle size of Ni, Pd and Pt on γ-Al_2O_3 support was 8.2, 4.6 nm and 5.4 nm, respectively. In the meantime, Morgan et al. showed that Ni decorated on mesoporous carbon (Ni/C) was more active and selective catalyst compared to Pd or Pt supported on mesoporous carbon (Pd/C or Pt/C) for the production of fuel range hydrocarbons using tristearin, triolein and soybean oil as feedstocks under N_2 atmosphere [58]. Higher content of Ni (20 wt%) with small particle size (4 nm) in the Ni/C catalyst was the reason for higher catalytic activity. Pd/C had active metal content of 5 wt% with particle size of 6 nm while Pt/C had metal content of 1 wt% with particle size of 3.7 nm. Hermida et al. [59] studied various Ni functionalized mesostructured cellular foam silica (NiMCF) as catalysts for deoxygentaion of palmitic acid under inert atmosphere and demonstrated that NiMCF catalyst containing highest Ni content (17.57 wt%) with the smallest particle sizes (1 to 3 nm) was more active produce fuel range hydrocarbons.

Snåre et al. [56] reported higher decarboxylation rates when using different metals supported on carbonaceous supports. The reason was ascribed to the ability of the support to enhance the rate of reaction, although its surface functionalities helped prevent coke deposition due to the large surface area of support. The authors investigated 60%Ni/SiO_2, 5%Ru/C, 5%Pd/C, 5%Pt/C, 1%Ir/SiO_2, 5%Os/C and 1%Rh/C catalysts for the decarboxylation of steric acid in a semi-batch reactor at $300^{\circ}C$ for 6h reaction time under He atmosphere. When the performance of these supported catalysts was compared in terms of decarboxylation activity, the order of

performance was found to be Pd>Pt>Ni>Rh>Ir>Ru>Os. This has led to Pd and Pt catalysts and carbon materials as supports being examined for much of the decarboxylation studies in the literature.

Professor Phillip Savage's research group from Univ. of Michigan (now at Pennsylvania State University) have been pioneers on the hydrothermal decarboxylation of fatty acids and their derivatives, showing the utility of using sub and supercritical water to facilitate the decarboxylation process. Fu et al. [60] demonstrated hydrothermal decarboxylation of fatty acids using activated carbon as catalyst and reported the major products from oleic acid decarboxylation were C_{12}-C_{17} alkanes containing 24% stearic acid and some other acids such as nonanoic acid, decanoic acid etc. Fu et al. [46] performed hydrothermal decarboxylation and hydrogenation of saturated and unsaturated fatty acids over Pt/C as catalyst with 90% selectivity of alkanes. Fu et al. [61] showed catalytic hydrothermal decarboxylation of palmitic acid in the presence of metal salts, bases and 5% Pt and Pd on activated carbon. Results showed that 90% selectivity of pentadecane was obtained with no significant loss of catalyst activity. Yeh et al. [62] studied hydrothermal decarboxylation of fatty acids using $PtSn_xC$ catalyst to produce renewable hydrocarbons. Al Alwan et al. [63] reported 97.3% conversion of oleic acid with 5.2% selectivity of heptadecane during hydrothermal decarboxylation (in sub and supercritical water) of oleic acid and soybean oil over Ni based transition metal carbides supported on Al-SBA-15 catalyst but the products were found to contain stearic acid, linoleic acid and unconverted oleic acid. Although Savage and other groups have made significant advances showing the utility of using SCW for decarboxylation, several challenges of this methodology remain including: 1) they have been using primarily expensive platinum-based catalysts; 2) they only use small 2-4 ml SS reactors placed in a sand bath. Hence, both significant challenges in catalyst technology, feedstock utilization (for example, CDO by-product from EtOH production has not yet been examined) and process reaction engineering are required for successful scale-up, which will be addressed in this thesis.

The percentage of metal loading as well as metal dispersion is very important for measuring the catalytic activity for any metal loaded catalyst. Both effects have been studied for the decarboxylation of fatty acids and their esters. Berenblyum et al. [64] studied stearic acid decarboxylation in a batch reactor at $350^\circ C$ under H_2 atmosphere for 3h reaction time, finding 100% selectivity to paraffin's using 5%Pd/Al_2O_3 catalyst whereas 95.1% selectivity was

achieved using 0.5%Pd/Al$_2$O$_3$. The conversion in both cases was 100%. The results showed that increasing the palladium concentration did not have any significant difference in terms of conversion and selectivity of the products. Snare et al. [56] noticed a significant improvement for the deoxygenation of fatty acids using Pd/C when the concentration of Pd was increased from 1 to 5 wt.%. Similarly, Maki-Arvela et al. [65] observed better results for deoxygenation of tall oil fatty acid (TOFA) using 4wt% Pd/C compared to 1wt% Pd/C although both catalysts had identical metal dispersion. This indicates that higher metal loadings are advantageous for deoxygenation of fatty acid as higher loading provides more active sites.

Although Pd and Pt was found to be the most active catalysts for decarboxylation of fatty acids and their derivatives, the high cost of these precious metals prevents the process for commercialization. Less expensive transition metal (Ni, Mo, Co, Cu etc.) based catalysts were also found alternatives of precious metals. Wu et al. [66] demonstrated catalytic decarboxylation of fatty acid to aviation fuel using Ni/C catalyst and achieved 100% stearic acid conversion with 80% selectivity of heptadecane at 370°C for 5 h. Miao et al. [67] found 64.2C% conversion of palmitic acid to liquid paraffin (C8-C15) during hydrothermal deoxygenation using Ni/ZrO$_2$ catalyst. Robin et al. [68] performed hydrothermal processing of lipids into a mixture of alkenes and aromatic compounds which are in the kerosene and gasoline boiling range using HZSM-5 and MoZSM-5. High grade diesel was obtained by Xin et al. [69] from palmitic acid deoxygenation using activated carbon supported sulphided catalysts. Asikin-Mijan et al. [70] obtained green diesel during deoxygenation of jatropha oil using multi-walled carbon nanotube (MWCNTs)-supported catalysts (Co/MWCNT, Ni/MWCNT and NiCo/MWCNT). Itthibenchapong et al. [71] achieved jet fuel like hydrocarbons from deoxygenation of palm karnel oil using Ni-MoS$_2$/γ-Al$_2$O$_3$ catalysts. Although transition metals such as Ni provide good catalytic activity during decarboxylation or deoxygenation reactions, Ni loses its catalytic activity quickly compared to Pd and Pt.

2.4.3 Types of feedstocks

The liquid yield of decarboxylation largely depends on the types of feedstock used as reactant. Different feedstocks behave differently in the decarboxylation media. Yeh et al. [62] performed hydrothermal decarboxylation of saturated and unsaturated fatty acids over PtSn$_x$/C catalyst at 350°C and 2 h of reaction time. Almost 100% conversion of oleic acid was achieved using a

PtSn$_3$/C catalyst with 35% molar yield of heptadecane. For the same reaction conditions, 80% conversion of linoleic acid was obtained with 15% molar yield of heptadecane, whereas 90% conversion of stearic acid was obtained with 60% molar yield of heptadecane. The authors also reported that increasing the degree of unsaturation in the feedstocks i.e more C=C, decreased the catalytic activity and selectivity towards the decarboxylated products.

Maki-Arvela et al. [19] studied the deoxygenation of saturated fatty acids (behenic acid, and stearic acid) and fatty acid esters (stearic acid ethyl ester) using a commercial Pd/C catalyst in dodecane as reaction media at 300°C under 5% H$_2$ balanced with Ar for 6h. It was observed that the initial reaction rate of behnic acid (0.36 mmol/min-gcat) was lower than that of stearic acid (0.63 mmol/min-gcat), while the initial reaction rate of stearic acid ethyl ester was 0.70 mmol/min-gcat, i.e. was slightly higher than stearic acid. The conversion of stearic acid ethyl ester and stearic acid was 38% and 60%, respectively. Lower conversion of stearic acid ethyl ester was observed due to the severe deactivation of Pd/C catalyst which is assigned to higher amounts of unsaturated products that were produced from deoxygenation of stearic acid ethyl ester.

The selectivity of n-alkane was reduced significantly due to the presence of these unsaturated compounds in the product which was mainly aromatics and heptadecenes. Deoxygenation of stearic acid ethyl ester and stearic acid provided 40% and 86% selectivity of n-alkane, respectively at a conversion of 30%. On the other hand, 78% selectivity of n-alkane was obtained from deoxygenation of behenic acid at the same conversion (30%). This result indicates that decarboxylation was the dominant reaction in the case of fatty acids because CO$_2$ was easily removed from the–COOH group rather than from the –COOR group (R group in ester is a nucleophilic group [72]). CO was removed from stearic acid ethyl ester instead of CO$_2$ due to the stability of the ethoxy group in ester. It can be concluded that deoxygenation of behenic and stearic acids was more selective for n-alkane production through decarboxylation compared to stearic acid ethyl ester.

Lestari et al. [73] compared the deoxygenation of palmitic and stearic acids over mesoporous Pd/C catalyst using dodecane as solvent in a semi batch reactor at 300°C under 5% H$_2$ in argon. The authors found the same reaction rate for deoxygenation of palmitic and stearic acids. Pentadecane and heptadecane were the major decarboxylated products from palmitic and stearic acids, respectively.

2.4.4 Reaction atmosphere

To understand the decarboxylation chemistry, the conversion of fatty acids and their derivatives was studied in different reaction media such as inert atmosphere, H_2, organic solvent or water. Yang et al. [74] performed decarboxylation of oleic acid using Pt/ZIF-67membrane/zeolite 5A bead catalyst using two different reaction atmospheres such as hydrogen and nitrogen (inert) with CO_2 (oxidant), respectively. They observed that 90% heptadecane yield was obtained under CO_2 atmosphere, whereas octadecane yield was lower in a CO_2 atmosphere compared to the hydrogen atmosphere (0.26% vs 17.6%). This indicates that the hydrodeoxygenation reaction occurred under hydrogen atmosphere to convert oleic acid into octadecane, while decarboxylation was the dominant reaction to convert oleic acid into heptadecane under CO_2 atmosphere. Rozmysłowicz et al. [75] studied the deoxygenation of lauric acid over mesoporous Pd/C catalyst in a semi batch reactor under hexadecane as solvent using two different reaction atmosphere such as pure Ar and H_2. The authors reported that the yields of desired products (n-undecane and undecene) were higher in the presence of Ar compared to H_2 atmospehre for first 100 min. Lower yields of desired products in the presence of H_2 for the first 100 min were due to the formation of intermediates which were progressively converted into the desired products.

Decarboxylation in hydrogen atmosphere is quite common although stoichiometrically decarboxylation reaction does not require any H_2. Hydrogen sometimes is required to saturate C=C bonds based on both the feedstock and the desired final product. However, it is not necessary to conduct the decarboxylation reaction in a hydrogen atmosphere. Hydrogen can be produced *insitu* depending on the solvent and types of catalyst used. Hossain et al [76] and Fu et al. [60] demonstrated that hydrogenation of oleic acid into heptadecane as a major product in hydrothermal media was accomplished by producing *insitu* hydrogen using activated carbon as catalyst. The *insitu* hydrogen was produced either from the gasification of oleic acid at the desired decarboxylation temperature or from the water gas shift reaction. Na et al [77] demonstrated that 98% oleic acid conversion into saturated hydrocarbons was achieved using MgO loaded hydrotalcites without adding any hydrogen. Aqueous phase reforming of glycerol was found to be a good source for producing H_2 *insitu* [63, 78]. Since decarbonylation is a parallel reaction with decarboxylation, CO may also participate in the water gas shift reaction to produce H_2 [79].

2.4.5 Reaction temperature

Reaction temperature is a critical parameter for the decarboxylation reaction. Higher temperatures favor gasification whereas lower temperature favors the saponification reaction. Na et al. [77] reported that saponification is dominant at T's $<350^{o}$C and decarboxylation is the main reaction occurring at T's $> 350^{o}$C. It was also reported by some other authors that the typical temperature range for decarboxylation of oleic acid into liquid hydrocarbons is 290-380°C [80, 81].

Wu et al. [66] demonstrated that reaction temperature significantly affected conversion and yield/selectivity of aviation fuels from decarboxylation of stearic acid over 20% Nickel supported activated carbon catalyst. Stearic acid conversion was increased with increasing reaction temperature from 330 to 370°C and complete conversion was achieved at 370°C and 5 h of reaction time. Heptadecane selectivity at this temperature and reaction time was found to be 90%. These results indicate that the 20% Ni/C in the decarboxylation of stearic acid has a high selectivity for heptadecane, even at high temperatures. Yang et al. [74] found that the heptadecane yield was increased with increasing temperature from 290 to 320°C for 2h of reaction time during decarboxylation of oleic acid over Pt/ZIF-67membrane/zeolite 5A bead catalysts. The maximum yield was obtained at 320°C. When temperature was further increased from 320 to 335°C, shorter chains of hydrocarbons (C7 –C16) were formed instead of heptadecane due to cracking of the larger hydrocarbon products. As a result, the yield of heptadecane decreased. Bernas et al. [54] conducted decarboxylation of dodecanoic acid to produce diesel like hydrocarbons over 1% Pd/C catalyst in a continuous reactor under inert atmosphere. They found that conversion of dodecanoic acid into undecane and undecene was increased from 10% to 60% with increasing reaction temperature form 300 to 360°C. Lestari et al. [82] performed decarboxylation of stearic acid over 4% Pd/C in a semi-batch reactor under inert atmosphere. They achieved 100% conversion of stearic acid in 20 min by increasing reaction temperature from 270 to 330°C. Kubickova et al. [83] obtained 100% conversion of ethyl stearate during decarboxylation reaction in a semi-batch reactor under the flow of 5% H_2 in argon for 6h by increasing temperature 300 to 360°C. But the selectivity of heptadecane was decreased from 70 to 40%.

2.4.6 Reaction time

The reaction time is known as the contact time of the feed on the catalyst. Product yield or selectivity is a direct function of reaction time for decarboxylation reaction. Reaction time needs to be optimized for higher hydrocarbon yields.

Tian et al. [84] studied the decarboxylation of oleic acid at 350 °C for the direct production of aviation fuel range hydrocarbons using 5% Pt/C catalyst in a micro batch reactor. The yield of 8-heptadecene was decreased from 12% to 0% by increasing the reaction time from 5 min to 90 min. Accordingly, the yield of aromatics increased from 0% to 14% (30 min) very quickly and increased to 19% (80 min) with increasing reaction time and the major product (heptadecane) continued increasing from 6% (5 min) to the peak value of 71% (80 min). Maki-Arvela et al. [85] conducted decarboxylation of lauric acid in a continuous reactor using Pd/C catalyst in the presence of dodecane solvent. They carried out the reactions to study the effect of feed rate for decarboxylation of lauric acid. Chosen feed rates were 0.1 mL/min, 0.25 mL/min, 1 mL/min and 1.5 mL/min, respectively. Lauric acid conversion was increased from 4 to 45% when the feed flow rate was decreased from 1 mL/min to 0.25 mL/min. This indicates that increasing feed rate enhanced to decrease lauric acid conversion due to a shorter residence time that resulted in extensive catalyst deactivation. It can be concluded that, catalyst deactivation during lauric acid deoxygenation was significant when contacting the catalyst with a large quantity of lauric acid. Increasing feed rate increased reaction time, thereby causing extensive catalyst deactivation and consequently lowering the hydrocarbon conversion. Hence, it is necessary to optimize feed flow rate for decarboxylation reaction to minimize the catalyst deactivation with higher conversion rate.

2.4.7 Amount of catalyst

The degree of decarboxylation and the yield or selectivity of the hydrocarbon products largely depend on the amount of catalyst used. Hossain et al. [76] studied the effect of catalyst (activated carbon) amount for the hydrothermal decarboxylation of oleic acid into fuel range hydrocarbons. They demonstrated that increasing the feed to activated carbon ratio from 0.15 to 0.75 significantly improved the degree of decarboxylation of oleic acid in hydrothermal media. Using catalyst to activated carbon ratio of 0.75 achieved complete decarboxylation of oleic acid. Snare et al. [56] reported to increase the decarboxylation activity of stearic acid with

increasing the catalyst loading from 1 to 5 wt%. Maki-Arvela et al. [55] demonstrated the higher degree of decarboxylation and conversion of stearic acid by increasing the amount of Pd/C catalyst from 0.2 to 1 g under He atmosphere. Higher loading of catalyst have less tendency towards catalyst deactivation and better selectivity towards heptadecane as the main decarboxylated product. Kwon et al. [86] reported to increase the conversion and selectivity of linear hydrocarbons from methyl laurate with decreasing intermediates and undesired products under H_2 atmosphere when the amount of $NiMo/Al_2O_3$ catalyst was increased to 0.126 g. They also observed the polymerization of methyl laurate using lower amount of catalyst which may be due to the formation of higher undesired products. During tall oil fatty acid decarboxylation, Maki-Arvela et al. [65] observed higher decarboxylation activity and higher selectivity to heptadecane when the loading of Pd was increased from 1 to 4 wt.% in Pd/C catalyst. The results indicate that increasing the loading of Pd on carbon increased the number of active sites on the catalyst surface. From the above discussion, we can conclude that increased amount of catalyst for decarboxylation reaction avoids catalyst deactivation tendency which ultimately enhance decarboxylation activity On the other hand, lower amount of catalyst sometimes help to polymerization which subsequently increases the formation of aromatics and other undesired products. Thus, higher degree of decarboxylation and higher yield/selectivity of the products require an optimum amount of catalyst.

2.4.8 Use of solvent

Using a solvent for decarboxylation reaction is very essential to produce fuel range hydrocarbons. It was reported that solvent free reaction produced no alkanes [46, 55, 87]. Macromolecules were formed in the absence of solvent on the catalyst surface due to occurrence of coupling reactions between the intermediates [87]. Han et al. [88] conducted palladium catalyzed decarboxylation of higher aliphatic esters without using any solvent and found no alkanes were produced although methyl stearate conversion was 100%. Their results are in good agreement with the results obtained from solvent free decarboxylation of sunflower which was conducted by Li and El-Sayed [89].

Organic solvents such as n-decane, n-dodecane and mesitylene were widely used studying decarboxylation of fatty acids and their derivatives in an inert atmosphere. n-dodecane is reported to show lower decarboxylation activity than n-decane and mesitylene [90]. Mesitylene

acts as a H$_2$ acceptor in the decarboxylation reaction since it is highly unsaturated compared to n-dodecane. On the other hand, n-decane having a lower dehydrogenation capability also showed higher degree of decarboxylation than n-dodecane [90]. Mäki-Arvela et al. [55] observed higher initial reaction rates and higher selectivity to n-heptadecane using dodecane as solvent compared to mesitylene during ethyl stearate decarboxylation over Pd/C catalyst. Mesitylene was favored to form higher intermediate products such as stearic acid. In another study, catalyst deactivation was observed using dodecane as solvent during decarboxylation of lauric acid in presence of Pd/C catalyst [85]. Mesitylene (165°C) and decane (174°C) have lower boiling point compared to dodecane (214 to 218°C). Solvent having lower boiling points are reported to show better decarboxylation activity [85].

Asomaning et al. [91] performed thermal deoxygenation and pyrolysis of oleic acid without any solvent and their results showed that oleic acid mainly decomposed into smaller hydrocarbons ranges from C6 to C10. On the other hand, similar studies were performed by Hossain et al. [76] using subcritical water as a solvent. They showed that decarboxylation was the dominant reaction to produce straight chain hydrocarbons ranges from C12 to C17 whereas the heptadecane selectivity was 81%. Fu et al [60] showed that decarboxylation of palmitic and oleic acid in near and supercritical water produced mainly C8 to C15 and C12 to C17 n-alkanes.

Fu et al. [46] executed hydrothermal decarboxylation of saturated (stearic, palmitic, and lauric acid) and unsaturated fatty acids (oleic and linoleic acid) using near and supercritical water for producing fuel range hydrocarbons over Pt/C catalyst. Their results showed that saturated fatty acids followed decarboxylation pathway for producing straight chain alkanes with higher selectivity. The unsaturated fatty acids followed first hydrogenation into stearic acid and then decarboxylation of stearic acid produced heptadecane as a major product. This is confirmed that H$_2$ participating into the hydrogenation reaction was produced insitu which enhances hydrocarbon selectivity. Fu et al. [61] investigated hydrothermal deoxygenation of palmitic acid using near-critical and supercritical water over Pt/C and Pd/C catalysts in a H$_2$-free atmosphere. They showed higher degree of deoxygenation and higher selectivity of pentadecane with lower catalyst deactivation.

From the above discussion, we can conclude that decarboxylation reaction can occur either in aqueous or organic solvent which implies that the reaction route is not determined by the nature of the solvent used. This is due to the physical properties of solvent such as density, viscosity,

boiling point etc. Immer and Lamb [92] showed that the solvent effect can be attributed to the influence of the vapor pressure of the solvent on the partial pressure of hydrogen. The lower vapor pressure of high boiling point solvents causes the partial pressure of hydrogen to increase, which can inhibit decarboxylation. In addition, using excess amount of solvent may slow down the rate of decarboxylation reaction due to occurrence of volume expansion reactions.

2.5 High temperature water (HTW)

2.5.1 Supercritical Water

There is significant interest to use sub or supercritical water as the reaction media due to several advantages compared to any other solvent [93]. These include water being:

- ❖ Non-toxic, environment friendly, no cost and tunable reaction medium.
- ❖ Ability to serve as a reactant, solvent, and catalyst for both ionic and free radical reactions.
- ❖ Ability to utilize wet feedstocks.
- ❖ High throughputs.
- ❖ High energy and separation efficiency.
- ❖ Lower energy requirements because of avoiding phase changes.
- ❖ Ability to use mixed feedstocks.
- ❖ Ability to produce the direct replacements for petroleum-derived fuels.
- ❖ Can be used as a pre-treatment step in coordination with other biofuel production methods.
- ❖ Can be used as a post-fermentation for processing solid residues.
- ❖ Versatility of chemistry (can produce liquid, gaseous, and solid fuels).
- ❖ No need to maintain specialized microbial cultures/enzymes.
- ❖ Reduced mass transfer resistance.
- ❖ Increased selectivity for the desired products/chemicals (hydrogen, methane, biocrude, carbohydrates, organic acids, etc.).
- ❖ Possibility of efficient energy recovery.
- ❖ Complete sterilization of the products.
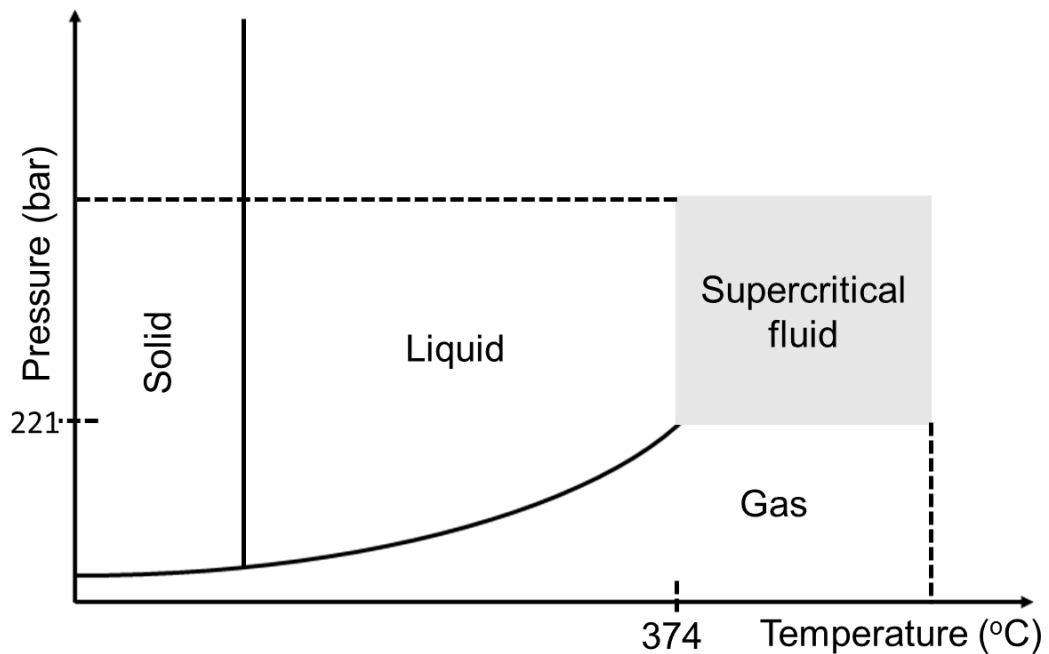
Figure 2.13: Phase diagram of water.

Figure 2.13 shows the phase diagram of water. Water is in a liquid state at room temperature and atmospheric pressure. When the pressure is increased, water stays in the liquid state- even at high temperature. If the pressure is higher than the critical pressure (22.1 MPa), water still stays in its liquid state as long as the temperature is below the critical temperature (374.1°C). Above its critical pressure and critical temperature, a completely new phase is reached, which is called the "supercritical state". Therefore, supercritical water (SCW) is something halfway between a liquid and a gas with its physical characteristics closer to those of a gas while some properties are closer to those of a liquid. Figure 2.14 shows the variation of water density as a function of temperature and pressure. A phase change occurs below the critical pressure (22.1 MPa) which is observed by the straight vertical lines, indicating a sudden drop of density when water passes from the liquid to the vapor phase. This temperature (boiling temperature) increases as the pressure is raised. No straight line can be observed in the supercritical region. Water's density varies continuously and even around the critical point its value diminishes. For example, at 400 °C SCW at 300 bar shows a density 200 times higher than atmospheric water vapor.
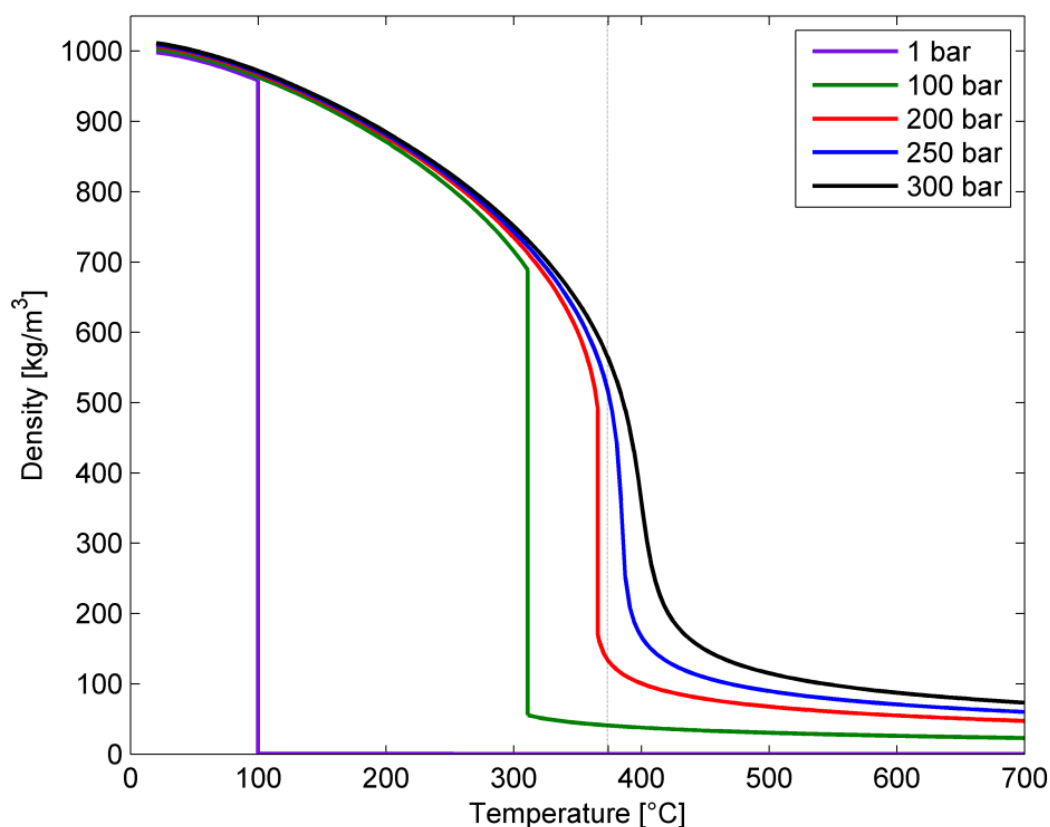
Figure 2.14. Variation of density of water as a function of temperature and pressure [94].

The dielectric constant is also an important property of SCW. This parameter represents the polarity of a solvent i.e whether a substance/solute is dissolved or not in the solvent. Polarity is defined as the ability of a molecule to form a dipole. Polar solutes are dissolved in polar solvents whereas nonpolar solutes dissolve in nonpolar solvents (the so-called "like dissolves like" rule). The dielectric constant for water is around 80 at room temperature, which makes it a strong polar solvent. When water is heated and reaches the supercritical state, the dielectric constant gradually drops to a value closer to a non-polar solvent such as hexane or toluene. Figure 2.15 shows the variation of dielectric constant of water as a function of temperature and pressure. This property becomes very important when dealing with lipid based biomass. Lipid based biomass produces a variety of water insoluble intermediates at high temperature processing which can plug and clog the reactor. During hydrothermal processing of lipid based biomass, those insoluble intermediates are completely solubilized in water to allow the chemical reaction to proceed in a single phase, which enhances reaction rates.

40
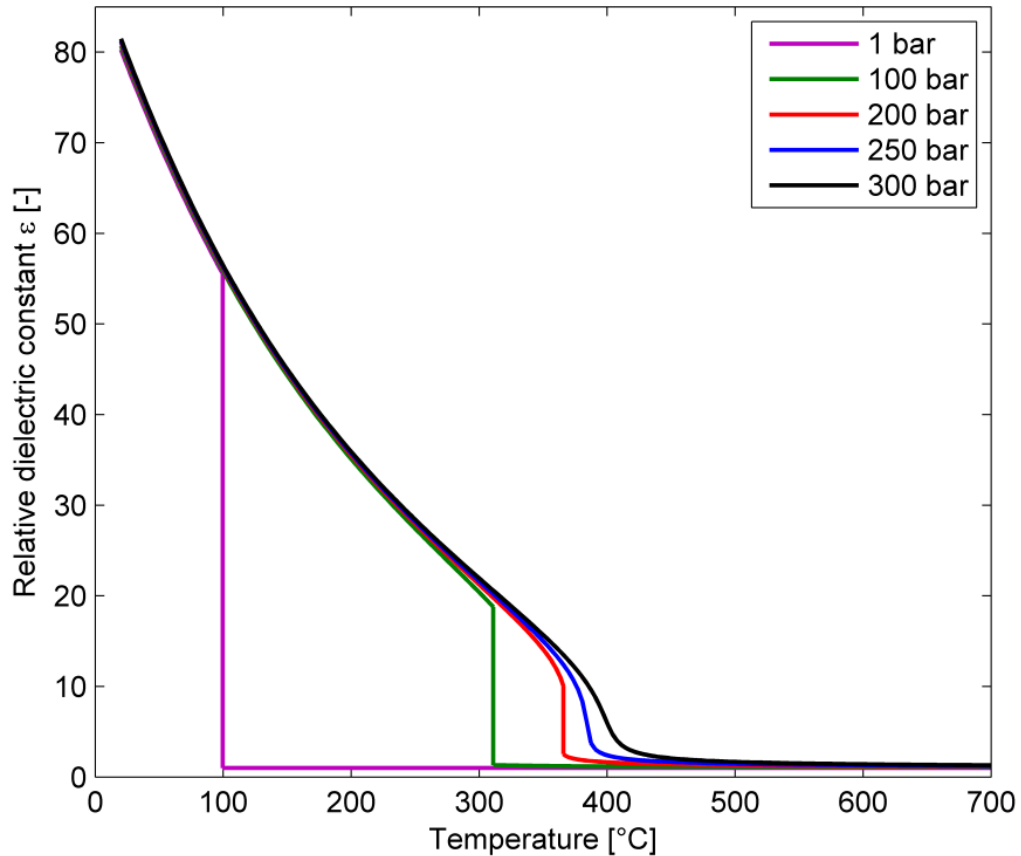
Figure 2.15: Variation of dielectric constant of water as a function of temperature and pressure [94].

Ionic product is another important property of SCW. It is defined as the product between the molar concentration of ions H_3O^+ and OH^- which are in equilibrium with non-dissociated water molecules. The value of the ionic product (K_w) of pure water is $1x10^{-14}$ mole/l or pK_w is 14 which indicates how many ions are present. Figure 2.16 shows the variation of pK_w for water at sub- and supercritical conditions. The value of pK_w is lower at the critical point compared to room temperature which implies that water is more dissociated. On the other hand, water is substantially less dissociated above the critical point compared to room temperature. This causes lower solubility of many substances. Many ionic salts, which are commonly soluble in water, now precipitate and can cause clogging problems to reactors. Moreover, strong acids/bases experience lower dissociations, becoming weak acid/bases. SCW thus provides a unique reaction environment, with many interesting potential applications.
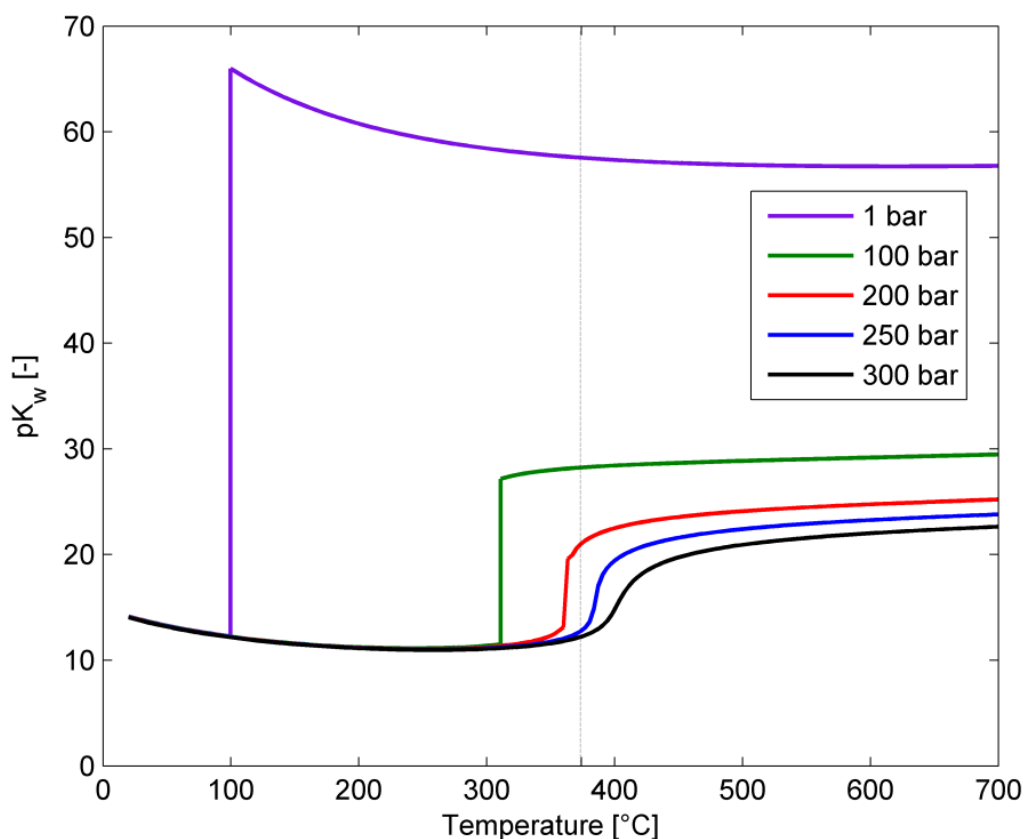
Figure 2.16: Value of pK_w (-$\log K_w$) of water as a function of temperature and pressure.

2.5.2 Subcritical Water

Although SCW is defined as described earlier, no specific definition of subcritical water is found in literature. Yu et al. [95] defined hot compressed water (HCW) as water at temperature above 150°C with varying pressure. Krammer et al. [96], Srokol et al. [97] and Broll et al. [98] reported temperature and pressure ranges for subcritical water such as 150<T<370 °C at 0.4<p<22 MPa, 300≤T≤350 °C at 10≤p≤18 MPa and 250 °C≤T≤450 °C at p>$p_{critical}$. High temperature water (HTW) was defined by Akiya et al. [99] as liquid water above 200°C. All of the above definitions arise from the reaction conditions used for hydrothermal biomass conversion which do not exactly define the term subcritical water. Fundamentally, subcritical water is not a physically defined state, since all water above the triple point and below the critical point is either liquid or gas. Moller et al. [100] introduced subcritical water this way:

water below the critical point but above the boiling point at ambient pressure (>100 $^{\circ}$C and 0.1 MPa).

A comparison of several physical properties of water in the different temperature regions is shown in Table 2.2.

Table 2.2: Physical and chemical properties of water at different temperatures [100].

	Ambient temperature	Subcritical water	Supercritical water
Temperature ($^{\circ}$C)	0-100	100-374	>374
Vapor pressure (MPa)	0.003 (24°C)	0.1 (100°C)-22.1 (374°C)	22.1
Aggregate state	liquid	liquid	no phase separation between gas like and liquid like densities, for example 0.252 (410°C, 30 MPa)
Density (g/cc)	0.997 (25°C)	0.958 (101°C, 0.11 MPa) 0.692 (330°C, 30 MPa)	
Viscosity (μPa.s)	L: 884 G: 9.9 (25°C)	L: 277 G: 12.3 (101°C) L: 50.4 G: 30.7 (371°C)	low
Heat capacity (J/(g.K)	L:4.2 G: 2.0 (25°C)	L:4.2 G: 2.1 (101°C) L:69 G: 145 (371°C)	1300 (400°C, 25 MPa)
Dielectric constant	78.5 (25°C, 0.1 MPa)	27.1 (250°C, 5 MPa) 18.2 (330°C, 30 MPa)	5.9 (400°C, 25 MPa) 10.5 (400°C, 50 MPa)
Compressibility	no	Slightly increased but still a liquid	yes
Ion product (mole/l)	10^{-14} (increasing to 10^{-12} at 100°C)	Increases from 10^{-12} (100°C) to 10^{-11} (300°C)	Strongly decreasing to below 10^{-20} (400°C) and below 10^{-23} (350°C); increases slightly with p

Viscosity is another important parameter of subcritical water. Viscosity of water strongly decreases with increasing temperature, which enhances any mass-transfer-limited chemical reaction. Dielectric constant is another property of subcritical water. The value of dielectric constant decreases with increasing temperature which indicates that the solubility of ionic molecules strongly decreases with temperature, whereas that of hydrophobic molecules such as fatty acids increases [101]. On the other hand the solubility of salts if present in any feedstock decreases significantly in the subcritical water region. When a salt-rich liquid is subjected to subcritical conditions, the low solubility of salts helps to form a fine-crystalline slimy "shock precipitate" when processing any salt-rich feedstock. The precipitated salts have been found to deposit on the walls of heat exchangers or the reactor, causing fouling or even blockage [102, 103]. This scenario can even be worse at supercritical conditions. On-line salt separators have been used to solve this issue [104].

The ion product of water (K_w) increases from 10^{-14} mol/l at 25°C, to 10^{-11} mol/l at 300°C with increasing temperature. The value of K_w started to decrease again at above 300°C and sharply decrease up to the critical point. As for example, the value of K_w at 380°C is below 10^{-20} mol/l [98] clearly indicates that all ionic reactions involving water molecules as reacting agents are generally enhanced in subcritical water. Furthermore, all ionic reactions are prompted due to the stabilization of the charged transition state [105].

The density of subcritical water lies between that of ambient and supercritical conditions. The relatively high density combined with the high dissociation constant of subcritical water, favors ionic reactions.

Corrosion is a vital issue for the subcritical water reaction environment, especially for acidic and oxidizing conditions. Corrosion could even be severe at subcritical conditions compared to supercritical conditions, due to the relatively dense and polar character of subcritical water [106]. Special types of reactor alloys may be required such as Inconel 625 and Hasteloy C-276 to minimize corrosion issues for subcritical applications. Furthermore, titanium alloys also have good resistance, however, their mechanical strength is limited [107].

2.5.3 Conversion of lipids

Fats and oils are non-polar compounds which are mostly insoluble in ambient water. But they are miscible with subcritical/supercritical water as the dielectric constant of water is considerably lower at subcritical/supercritical states. Fats or oils are promptly hydrolyzed in hot compressed water to produce fatty acids without using any catalyst. Fatty acids are very stable in subcritical/supercritical water but they can be partly degraded at hydrothermal conditions to produce n-paraffin, which have excellent fuel properties. Watanabe et al. [108] first showed stearic acid ($C_{17}H_{35}COOH$) conversion into hydrocarbons at supercritical water (400 °C, 25 MPa and 30 min). The yield of hydrocarbon was low for non-catalyzed reaction but 32% yield was achieved using KOH as the catalyst. Heptadecane was the major product which was produced by hydrothermal decarboxylation of stearic acid. The major difference between pyrolysis and hydrothermal decarboxylation is as follows: pyrolysis degrades the feedstocks and produces shorter chain length hydrocarbons whereas hot compressed water actually stabilizes fatty acids, suppresses the degradation and produces longer chain hydrocarbons.

2.6 Reaction mechanism

Watanabe et al. [108] proposed a reaction mechanism of stearic acid conversion both with and without using SCW. In the presence of Ar atmosphere and without SCW, stearic acid was mainly decarbonylated instead of decarboxylation and a lot of carbonyl compounds were formed. Stearic acid was first decomposed into long chain carbonyl free radicals by dissociating carboxylic group and further decomposed into CO or a shorter chain carbonyl compound. Addition of NaOH as catalyst enhanced the CO formation with heptadecane as the main liquid product (Figure 2.17). On the other hand, the carboxyl group was quite stable in SCW and at a slower reaction rate, C17-acid was decomposed into acetic acid and C16 alkene. Addition of KOH as catalyst in SCW enhanced the decarboxylation of steraic acid, producing heptadecane (Figure 2.18).
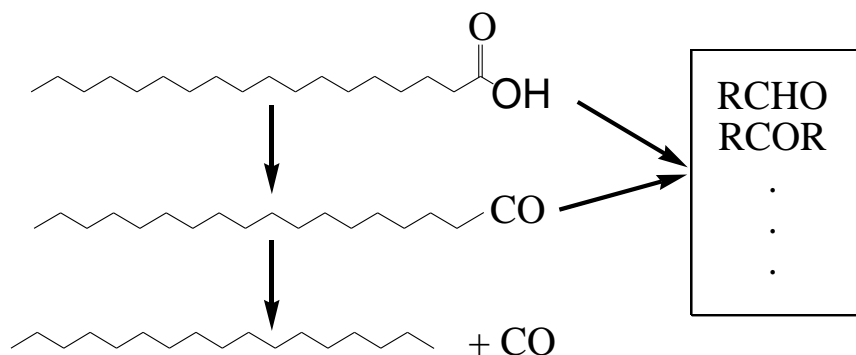
Figure 2.17: Stearic acid conversion under Ar atmosphere [108].

Figure 2.18 also shows stearic acid conversion in the presence of ZrO_2 as catalyst. Addition of ZrO_2 in the system mainly decomposed the stearic acid instead of decarboxylation and produced acetic acid and C16 alkene. In addition, 2-nonadecanone was produced via bimolecular decarboxylation between two molecules of acetic acid and one molecule of stearic acid by adding ZrO_2. On the other hand, C35 ketone was also formed during bimolecular decarboxylation of two molecules of stearic acid. C35 ketone was further decomposed into C16 alkene and 2-nonadecanone.
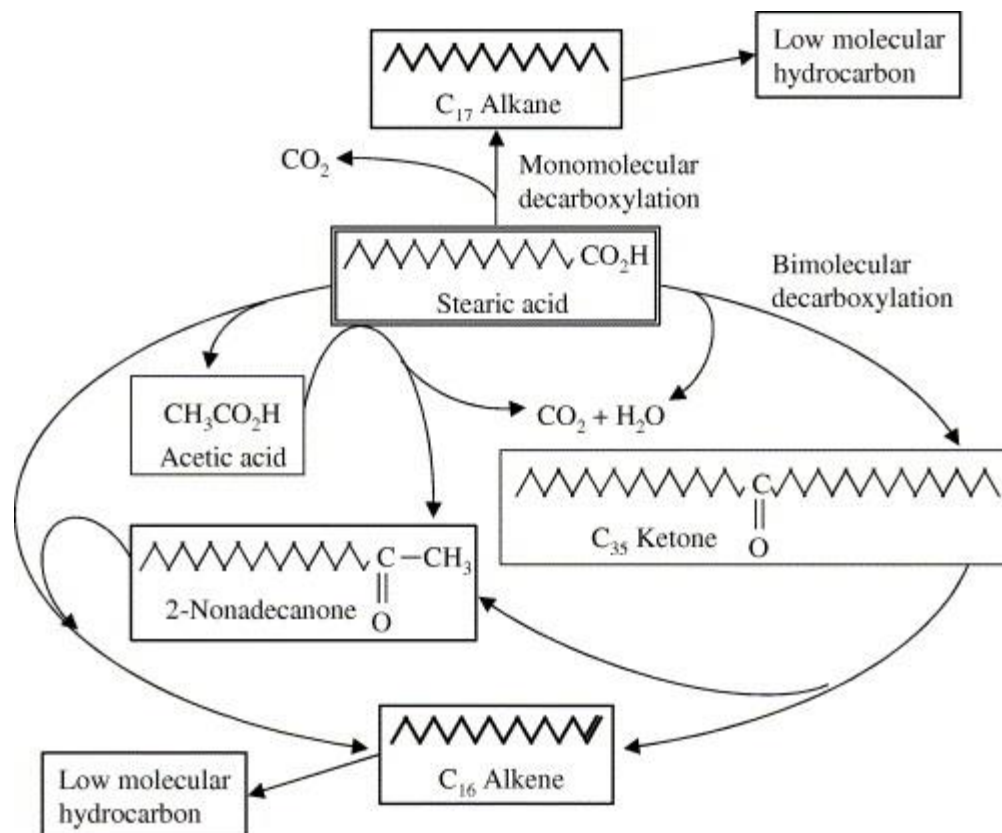
Figure 2.18: Stearic acid conversion in supercritical water with and without additives [108].

Al Alwan et al. [63] proposed a mechanism for the hydrothermal decarboxylation of oleic acid in SCW (Figure 2.19). During the hydrothermal decarboxylation of oleic acid, the carboxylic acid donates protons by the heterolytic cleavage of the O-H bond, generating a carboxylate and hydrogen ions (H^+). Heptadecenes (unsaturated C17) are produced due to the removal of CO_2. The insitu generated hydrogen (as a result of heterolytic cleavage of the O-H bond in oleic acid) is consumed by the hydrogenation of oleic acid or unsaturated C17 to form stearic acid or heptadecane, respectively. The produced stearic acid is then decarboxylated to generate more heptadecane. Moreover, hydrogen molecules can also be generated from the water–gas shift reaction [79].

$$C_{17}H_{33}COOH \xrightarrow[\text{of O-H bond}]{\substack{\text{Heterolytic} \\ \text{cleavage}}} C_{17}H_{33}COO^- + H^+$$

$$+ H_2 \longrightarrow C_{17}H_{33}COOH$$

Hydrogenation

$$C_{17}H_{35}COOH$$

(Decarboxylation) $[C_{17}H_{33}]^- + CO_2$

$[C_{17}H_{33}]^- + H_2O + CO$ (Decarbonylation)

$+ H_2O$

$H_2 + CO_2$ (Water gas shift)

$-H^+$ $+H^+$

$$C_{17}H_{32} \qquad C_{17}H_{34} \xrightarrow{+ H_2} C_{17}H_{36}$$

$- CO_2$
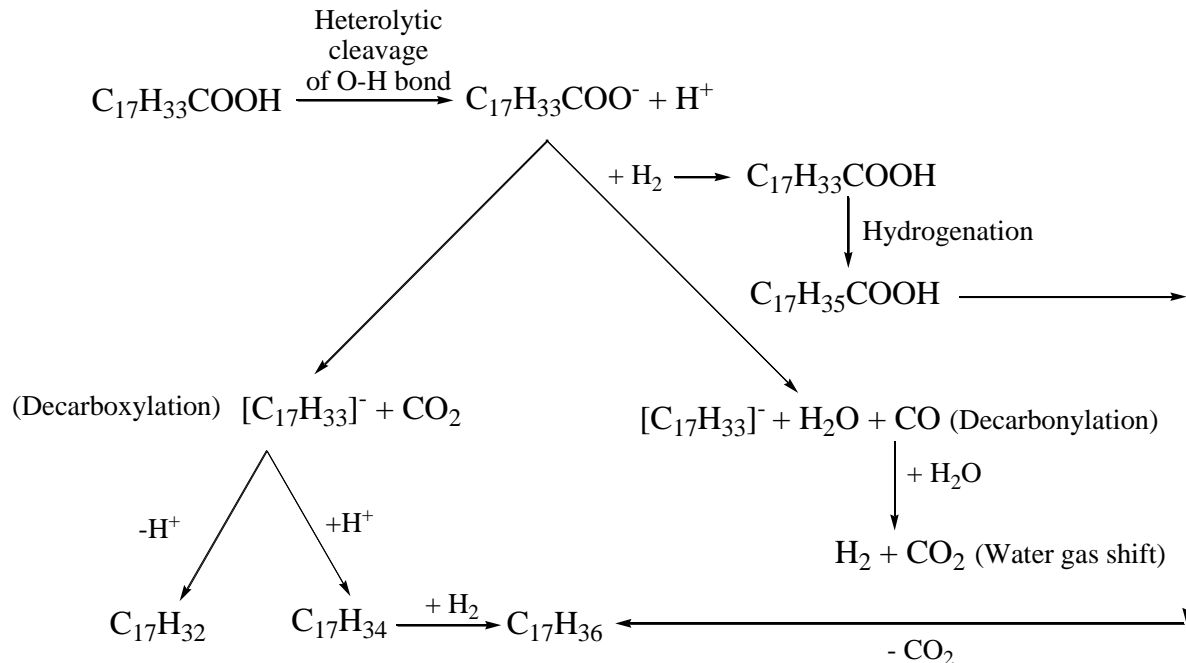
Figure 2.19: Decarboxylation of oleic acid in SCW [63].

2.7 Catalyst deactivation and regeneration

Since decarboxylation reaction is occurred at high temperature and pressure, catalyst deactivation is a common phenomenon. There are several causes reported in the literature for the deactivation of decarboxylated catalysts such as:

- ✓ Presence of chemical poisons in the feed stream
- ✓ Oxidation of the metal
- ✓ Metal leaching from the catalyst surface
- ✓ Reduction of metal specific surface area due to sintering and poisoning
- ✓ Reduction of specific surface area due to pore blockage and coking.

Sulfur is a widely known as catalyst poison. If any feedstock contains sulfur, it can easily bind to metal catalyst which deactivates the catalytic activity of catalyst. To prevent the sulfur poisoning, different methods include developing sulfur-tolerant catalysts, sulfur removal from the feed stream via HDS, or via formation of sulfur salts have been followed. Sulfur-tolerant catalyst such as sulphided catalysts are commonly used for decarboxylation reaction [109, 110].

Several authors reported that metal oxidation [111] and metal leaching [50, 54] are insignificant for supported Pd catalysts. Metal sintering largely depends on the reaction conditions and reaction medium. Metal sintering was found negligible in organic media using Pd/C [65] and Pd/SiO$_2$ [111] catalysts. Although Pt/C and Pd/C catalysts were reported to experience significant sintering in aqueous media during decarboxylation of fatty acids, this does not affect in a loss of catalytic activity [61]. Maki-Arvela et al. [104] reported deactivation of Pd/C catalyst due to poisoning by product gases such as CO/CO$_2$ and coking for continuous decarboxylation of lauric acid. Do et al. [112] observed deactivation of Pt/Al$_2$O$_3$ catalyst for the decarboxylation of methyl-octanoate and methyl-stearate due to site blocking by oligomerization of unsaturated hydrocarbons and heavy compounds (i.e. symmetrical ketone) that leads to coke formation.

The above discussion clearly indicates that there is a need for more work on the long-term stability of decarboxylation catalysts in hydrothermal media. Ping et al. showed that a spent Pd/SiO$_2$ catalyst can be regenerated by a number of organic solvent washes which remove most of the organic deposits from the catalyst surface [111]. However, this regeneration approach is not feasible for commercial applications, whereas simpler approaches such as the burn-off of carbonaceous deposits in hot air can be used. But the second approach cannot be applied for carbon-supported catalysts.

2.8 Thesis Objectives

As biodiesel is not attractive from a commercial point of view as described above, decarboxylation of high lipid feedstocks may provide an innovative solution to providing new routes to green diesel. Although Professor Savage and other groups have made significant advances showing the utility of using high temperature water (HTW) for decarboxylation, several challenges of their methodology remain: 1) they have been using primarily expensive platinum-based catalysts; 2) they only use small 2-4 ml SS reactors placed in a fluidized sand bath. Hence, both significant challenges in catalyst technology, feedstock utilization (for example, CDO by-product from EtOH production has not yet been examined) and process reaction engineering are required for successful scale-up. This dissertation examined

fundamental studies in the catalysis and reaction engineering by conducting experiments in both a stirred 300 mL batch reactor and investigated a small scale continuous system. This dissertation also focused on the development of a cost effective catalyst that can be reused for decarboxylation. Both the decarboxylation mechanism and kinetics in hydrothermal media needs to be investigated to have a better understanding of the reactor conditions and dynamics on how to adopt this technology for potential commercialization.

References

[1] World Oil Outlook. Accessed on May 7, 2017 from 〈http://www.opec.org/opec_web/static_files_project/media/downloads/publications/WOO2015.pdf〉.

[2] Leggett, J. The oil crunch securing the UK's energy future. Accessed on May 7, 2017 from 〈http://peakoiltaskforce.net/wp-content/uploads/2008/10/oil-report-final.pdf〉.

[3] A. Abbas, S. Ansumali, Global potential of rice husk as a renewable feedstock for ethanol biofuel production, Bioenergy Research, 3 (2010) 328-334.

[4] H. Liu, T. Cheng, M. Xian, Y. Cao, F. Fang, H. Zou, Fatty acid from the renewable sources: a promising feedstock for the production of biofuels and biobased chemicals, Biotechnology advances, 32 (2014) 382-389.

[5] A.S. Badday, A.Z. Abdullah, K.-T. Lee, Transesterification of crude Jatropha oil by activated carbon-supported heteropolyacid catalyst in an ultrasound-assisted reactor system, Renewable Energy, 62 (2014) 10-17.

[6] R. Sawangkeaw, S. Ngamprasertsith, A review of lipid-based biomasses as feedstocks for biofuels production, Renewable and Sustainable Energy Reviews, 25 (2013) 97-108.

[7] A. Demirbas, Political, economic and environmental impacts of biofuels: a review, Applied energy, 86 (2009) S108-S117.

[8] BP Statistical Review of World Energy 2016 (Accessed on 1st May, 2017).

[9] C. Somerville, H. Youngs, C. Taylor, S.C. Davis, S.P. Long, Feedstocks for lignocellulosic biofuels, science, 329 (2010) 790-792.

[10] E. Taarning, C.M. Osmundsen, X. Yang, B. Voss, S.I. Andersen, C.H. Christensen, Zeolite-catalyzed biomass conversion to fuels and chemicals, Energy & Environmental Science, 4 (2011) 793-804.

[11] C.-H. Zhou, X. Xia, C.-X. Lin, D.-S. Tong, J. Beltramini, Catalytic conversion of lignocellulosic biomass to fine chemicals and fuels, Chemical Society Reviews, 40 (2011) 5588-5617.

[12] A.T. Bell, B.C. Gates, D. Ray, M.R. Thompson, Basic research needs: catalysis for energy, in, Pacific Northwest National Laboratory (PNNL), Richland, WA (US), 2008.

[13] L. Jiménez, A. Rodríguez, A. Pérez, A. Moral, L. Serrano, Alternative raw materials and pulping process using clean technologies, industrial crops and products, 28 (2008) 11-16.

[14] C.W. Center, Wheat Straw as a Paper Fiber Source, The Clean Washington Center—A Division of the Pacific Northwest Economic Region (PNWER), Seattle, Washington, (1997).

[15] L. Jiménez, F. López, C. Martínez, Paper from sorghum stalks, Holzforschung-International Journal of the Biology, Chemistry, Physics and Technology of Wood, 47 (1993) 529-533.

[16] E. Maekawa, Studies on hemicellulose of bamboo, Wood Research: bulletin of the Wood Research Institute Kyoto University, 59 (1976) 153-179.

[17] N. Cordeiro, M. Belgacem, I. Torres, J. Moura, Chemical composition and pulping of banana pseudo-stems, Industrial Crops and Products, 19 (2004) 147-154.

[18] D. Malloy, K. Mayowski, Biofuels For a Sustainable World.

[19] M. Muller, T. Yelden, H. Schoonover, Food versus fuel in the United States: can both win in the era of ethanol?, Institute for Agriculture and Trade Policy (IATP) Environment and Agriculture Program. Minneapolis, MN, (2007).

[20] J. Pickett, D. Anderson, D. Bowles, T. Bridgwater, P. Jarvis, N. Mortimer, M. Poliakoff, J. Woods, Sustainable biofuels: prospects and challenges, The Royal Society, London, UK, (2008).

[21] N. Sonntag, Fat splitting, Journal of the American Oil Chemists' Society, 56 (1979) 729A-732A.

[22] F. Karaosmanoglu, Vegetable oil fuels: a review, Energy sources, 21 (1999) 221-231.

[23] S.P. Katikaneni, J.D. Adjaye, N.N. Bakhshi, Studies on the catalytic conversion of canola oil to hydrocarbons: influence of hybrid catalysts and steam, Energy & fuels, 9 (1995) 599-609.

[24] Basic Research Needs: Catalysis for Energy, U.S. Department of Energy, 2007.

[25] N.-O. Nylund, P. Aakko-Saksa, K. Sipilä, Status and outlook for biofuels, other alternative fuels and new vehicles, VTT, 2008.

[26] H. Makkar, K. Becker, F. Sporer, M. Wink, Studies on nutritive potential and toxic constituents of different provenances of Jatropha curcas, Journal of Agricultural and Food Chemistry, 45 (1997) 3152-3157.

[27] S. Shah, S. Sharma, M. Gupta, Biodiesel preparation by lipase-catalyzed transesterification of Jatropha oil, Energy & Fuels, 18 (2004) 154-159.

[28] G.M. Gübitz, M. Mittelbach, M. Trabi, Exploitation of the tropical oil seed plant Jatropha curcas L, Bioresource technology, 67 (1999) 73-82.

[29] S. Schwietzke, M. Ladisch, L. Russo, K. Kwant, T. Mäkinen, B. Kavalov, K. Maniatis, R. Zwart, G. Shahanan, K. Sipila, Analysis and identification of gaps in the research for the production of second-generation liquid transportation biofuels, in, Energy research Centre of the Netherlands ECN, 2008.

[30] E.G. Shay, Diesel fuel from vegetable oils: status and opportunities, Biomass and bioenergy, 4 (1993) 227-242.

[31] B. Smith, H.C. Greenwell, A. Whiting, Catalytic upgrading of tri-glycerides and fatty acids to transport biofuels, Energy & Environmental Science, 2 (2009) 262-271.

[32] C. Öner, Ş. Altun, Biodiesel production from inedible animal tallow and an experimental investigation of its use as alternative fuel in a direct injection diesel engine, Applied Energy, 86 (2009) 2114-2120.

[33] K.-T. Lee, T.A. Foglia, K.-S. Chang, Production of alkyl ester as biodiesel from fractionated lard and restaurant grease, Journal of the American Oil Chemists' Society, 79 (2002) 191-195.

[34] G. Knothe, Some aspects of biodiesel oxidative stability, Fuel Processing Technology, 88 (2007) 669-677.

[35] G. Knothe, J.V. Gerpen, J. Krahl, The Biodiesel Handbook; AOCS Press, 2005.

[36] A.S. Ramadhas, S. Jayaraj, C. Muraleedharan, Biodiesel production from high FFA rubber seed oil, Fuel, 84 (2005) 335-340.

[37] M.E. da Cunha, L.C. Krause, M.S.A. Moraes, C.S. Faccini, R.A. Jacques, S.R. Almeida, M.R.A. Rodrigues, E.B. Caramão, Beef tallow biodiesel produced in a pilot scale, Fuel Processing Technology, 90 (2009) 570-575.

[38] G. Knothe, K.R. Steidley, Kinematic viscosity of biodiesel fuel components and related compounds. Influence of compound structure and comparison to petrodiesel fuel components, Fuel, 84 (2005) 1059-1065.

[39] A. Centeno, E. Laurent, B. Delmon, Influence of the support of CoMo sulfide catalysts and of the addition of potassium and platinum on the catalytic performances for the hydrodeoxygenation of carbonyl, carboxyl, and guaiacol-type molecules, Journal of Catalysis, 154 (1995) 288-298.

[40] A. Demirbas, Biodiesel production via non-catalytic SCF method and biodiesel fuel characteristics, Energy conversion and Management, 47 (2006) 2271-2282.

[41] R. Lin, Y. Zhu, L.L. Tavlarides, Effect of thermal decomposition on biodiesel viscosity and cold flow property, Fuel, 117 (2014) 981-988.

[42] K. Anand, R. Sharma, P. Mehta, Experimental investigations on combustion, performance, and emissions characteristics of a neat biodiesel-fuelled, turbocharged, direct injection diesel engine, Proceedings of the Institution of Mechanical Engineers, Part D: Journal of Automobile Engineering, 224 (2010) 661-679.

[43] H. Chen, Q. Wang, X. Zhang, L. Wang, Effect of support on the NiMo phase and its catalytic hydrodeoxygenation of triglycerides, Fuel, 159 (2015) 430-435.

[44] D. Kubička, M. Bejblová, J. Vlk, Conversion of vegetable oils into hydrocarbons over CoMo/MCM-41 catalysts, Topics in Catalysis, 53 (2010) 168-178.

[45] E. Sari, Green diesel production via catalytic hydrogenation/decarboxylation of triglycerides and fatty acids of vegetable oil and brown grease, in, Wayne State University, Detroit, 2013.

[46] J. Fu, X. Lu, P.E. Savage, Hydrothermal decarboxylation and hydrogenation of fatty acids over Pt/C, ChemSusChem, 4 (2011) 481-486.

[47] S.K. Hoekman, Biofuels in the US–challenges and opportunities, Renewable energy, 34 (2009) 14-22.

[48] T.N. Kalnes, K.P. Koers, T. Marker, D.R. Shonnard, A technoeconomic and environmental life cycle comparison of green diesel to biodiesel and syndiesel, Environmental Progress & Sustainable Energy, 28 (2009) 111-120.

[49] S. Goguen, Energy Technology Drivers for Change-U.S. DOE Perspective., Transportation Technologies and Fuels Forum, June 5-7, 2006.

[50] S. Lestari, P. Maki-Arvela, H. Bernas, O. Simakova, R. Sjöholm, J. Beltramini, G.M. Lu, J. Myllyoja, I. Simakova, D.Y. Murzin, Catalytic deoxygenation of stearic acid in a continuous reactor over a mesoporous carbon-supported Pd catalyst, Energy & Fuels, 23 (2009) 3842-3845.

[51] J. Holmgren, C. Gosling, T. Marker, P. Kokayeff, G. Faraci, C. Perego, E.S. Refining, Green diesel production from vegetable oil, in: 2007 Spring AIChE Conference, 2007.

[52] T. Choudhary, C. Phillips, Renewable fuels via catalytic hydrodeoxygenation, Applied Catalysis A: General, 397 (2011) 1-12.

[53] S. Lestari, P. Mäki-Arvela, K. Eränen, J. Beltramini, G.M. Lu, D.Y. Murzin, Diesel-like hydrocarbons from catalytic deoxygenation of stearic acid over supported Pd nanoparticles on SBA-15 catalysts, Catalysis Letters, 134 (2010) 250-257.

[54] H. Bernas, K. Eränen, I. Simakova, A.-R. Leino, K. Kordás, J. Myllyoja, P. Mäki-Arvela, T. Salmi, D.Y. Murzin, Deoxygenation of dodecanoic acid under inert atmosphere, Fuel, 89 (2010) 2033-2039.

[55] P. Mäki-Arvela, I. Kubickova, M. Snåre, K. Eränen, D.Y. Murzin, Catalytic deoxygenation of fatty acids and their derivatives, Energy & Fuels, 21 (2007) 30-41.

[56] M. Snåre, I. Kubickova, P. Mäki-Arvela, K. Eränen, D.Y. Murzin, Heterogeneous catalytic deoxygenation of stearic acid for production of biodiesel, Industrial & engineering chemistry research, 45 (2006) 5708-5715.

[57] A.T. Madsen, B. Rozmysłowicz, I.L. Simakova, T. Kilpiö, A.-R. Leino, K.n. Kordás, K. Eränen, P.i. Mäki-Arvela, D.Y. Murzin, Step changes and deactivation behavior in the continuous decarboxylation of stearic acid, Industrial & Engineering Chemistry Research, 50 (2011) 11049-11058.

[58] T. Morgan, D. Grubb, E. Santillan-Jimenez, M. Crocker, Conversion of triglycerides to hydrocarbons over supported metal catalysts, Topics in Catalysis, 53 (2010) 820-829.

[59] L. Hermida, A.Z. Abdullah, A.R. Mohamed, Nickel functionalized mesostructured cellular foam (MCF) silica as a catalyst for solventless deoxygenation of palmitic acid to produce diesel-like hydrocarbons, Materials and Processes for Energy: Communicatin g Current Research and Technological Developments. Brown Walker Press, Boca Raton, USA, (2013).

[60] J. Fu, F. Shi, L. Thompson Jr, X. Lu, P.E. Savage, Activated carbons for hydrothermal decarboxylation of fatty acids, ACS Catalysis, 1 (2011) 227-231.

[61] J. Fu, X. Lu, P.E. Savage, Catalytic hydrothermal deoxygenation of palmitic acid, Energy & Environmental Science, 3 (2010) 311-317.

[62] T.M. Yeh, R.L. Hockstad, S. Linic, P.E. Savage, Hydrothermal decarboxylation of unsaturated fatty acids over PtSnx/C catalysts, Fuel, 156 (2015) 219-224.

[63] B. Al Alwan, S.O. Salley, K.S. Ng, Biofuels production from hydrothermal decarboxylation of oleic acid and soybean oil over Ni-based transition metal carbides supported on Al-SBA-15, Applied Catalysis A: General, 498 (2015) 32-40.

[64] A. Berenblyum, T. Podoplelova, R. Shamsiev, E. Katsman, V.Y. Danyushevsky, On the mechanism of catalytic conversion of fatty acids into hydrocarbons in the presence of palladium catalysts on alumina, Petroleum Chemistry, 51 (2011) 336.

[65] P.i. Mäki-Arvela, B. Rozmysłowicz, S. Lestari, O. Simakova, K. Eränen, T. Salmi, D.Y. Murzin, Catalytic deoxygenation of tall oil fatty acid over palladium supported on mesoporous carbon, Energy & Fuels, 25 (2011) 2815-2825.

[66] J. Wu, J. Shi, J. Fu, J.A. Leidl, Z. Hou, X. Lu, Catalytic Decarboxylation of Fatty Acids to Aviation Fuels over Nickel Supported on Activated Carbon, Scientific reports, 6 (2016).

[67] C. Miao, O. Marin-Flores, S.D. Davidson, T. Li, T. Dong, D. Gao, Y. Wang, M. Garcia-Pérez, S. Chen, Hydrothermal catalytic deoxygenation of palmitic acid over nickel catalyst, Fuel, 166 (2016) 302-308.

[68] T. Robin, J.M. Jones, A.B. Ross, Catalytic hydrothermal processing of lipids using metal doped zeolites, Biomass and Bioenergy, 98 (2017) 26-36.

[69] H. Xin, K. Guo, D. Li, H. Yang, C. Hu, Production of high-grade diesel from palmitic acid over activated carbon-supported nickel phosphide catalysts, Applied Catalysis B: Environmental, 187 (2016) 375-385.

[70] N. Asikin-Mijan, H. Lee, G. Abdulkareem-Alsultan, A. Afandi, Y. Taufiq-Yap, Production of green diesel via cleaner catalytic deoxygenation of Jatropha curcas oil, Journal of Cleaner Production, (2016).

[71] V. Itthibenchapong, A. Srifa, R. Kaewmeesri, P. Kidkhunthod, K. Faungnawakij, Deoxygenation of palm kernel oil to jet fuel-like hydrocarbons using Ni-MoS 2/γ-Al 2 O 3 catalysts, Energy Conversion and Management, 134 (2017) 188-196.

[72] M.N. Santiago, M. Sanchez-Castillo, R. Cortright, J. Dumesic, Catalytic reduction of acetic acid, methyl acetate, and ethyl acetate over silica-supported copper, Journal of Catalysis, 193 (2000) 16-28.

[73] S. Lestari, P. Mäki-Arvela, I. Simakova, J. Beltramini, G.M. Lu, D.Y. Murzin, Catalytic deoxygenation of stearic acid and palmitic acid in semibatch mode, Catalysis Letters, 130 (2009) 48-51.

[74] L. Yang, M.A. Carreon, Effect of reaction parameters on the decarboxylation of oleic acid over Pt/ZIF-67membrane/zeolite 5A bead catalysts, Journal of Chemical Technology and Biotechnology, 92 (2017) 52-58.

[75] B. Rozmysłowicz, P. Maki-Arvela, A. Tokarev, A.-R. Leino, K. Eränen, D.Y. Murzin, Influence of hydrogen in catalytic deoxygenation of fatty acids and their derivatives over Pd/C, Industrial & Engineering Chemistry Research, 51 (2012) 8922-8927.

[76] M.Z. Hossain, A.K. Jhawar, M.B. Chowdhury, W.Z. Xu, W. Wu, D.V. Hiscott, P.A. Charpentier, Using Subcritical Water for Decarboxylation of Oleic Acid into Fuel-Range Hydrocarbons, Energy & Fuels, 31 (2017) 4013-4023.

[77] J.-G. Na, B.E. Yi, J.N. Kim, K.B. Yi, S.-Y. Park, J.-H. Park, J.-N. Kim, C.H. Ko, Hydrocarbon production from decarboxylation of fatty acid without hydrogen, Catalysis Today, 156 (2010) 44-48.

[78] R.D. Cortright, R. Davda, J.A. Dumesic, Hydrogen from catalytic reforming of biomass-derived hydrocarbons in liquid water, Nature, 418 (2002) 964-967.

[79] R.L. Holliday, J.W. King, G.R. List, Hydrolysis of vegetable oils in sub-and supercritical water, Industrial & Engineering Chemistry Research, 36 (1997) 932-935.

[80] S. Popov, S. Kumar, Rapid hydrothermal deoxygenation of oleic acid over activated carbon in a continuous flow process, Energy & Fuels, 29 (2015) 3377-3384.

[81] H. Zhang, H. Lin, W. Wang, Y. Zheng, P. Hu, Hydroprocessing of waste cooking oil over a dispersed nano catalyst: kinetics study and temperature effect, Applied Catalysis B: Environmental, 150 (2014) 238-248.

[82] S. Lestari, I. Simakova, A. Tokarev, P. Mäki-Arvela, K. Eränen, D.Y. Murzin, Synthesis of biodiesel via deoxygenation of stearic acid over supported Pd/C catalyst, Catalysis Letters, 122 (2008) 247-251.

[83] I. Kubičková, M. Snåre, K. Eränen, P. Mäki-Arvela, D.Y. Murzin, Hydrocarbons for diesel fuel via decarboxylation of vegetable oils, Catalysis Today, 106 (2005) 197-200.

[84] Q. Tian, K. Qiao, F. Zhou, K. Chen, T. Wang, J. Fu, X. Lu, P. Ouyang, Direct Production of Aviation Fuel Range Hydrocarbons and Aromatics from Oleic Acid without an Added Hydrogen Donor, Energy & Fuels, 30 (2016) 7291-7297.

[85] P. Mäki-Arvela, M. Snåre, K. Eränen, J. Myllyoja, D.Y. Murzin, Continuous decarboxylation of lauric acid over Pd/C catalyst, Fuel, 87 (2008) 3543-3549.

[86] K.C. Kwon, H. Mayfield, T. Marolla, B. Nichols, M. Mashburn, Catalytic deoxygenation of liquid biomass for hydrocarbon fuels, Renewable Energy, 36 (2011) 907-915.

[87] L. Hermida, A.Z. Abdullah, A.R. Mohamed, Deoxygenation of fatty acid to produce diesel-like hydrocarbons: a review of process conditions, reaction kinetics and mechanism, Renewable and Sustainable Energy Reviews, 42 (2015) 1223-1233.

[88] J. Han, H. Sun, Y. Ding, H. Lou, X. Zheng, Palladium-catalyzed decarboxylation of higher aliphatic esters: Towards a new protocol to the second generation biodiesel production, Green Chemistry, 12 (2010) 463-467.

[89] Y. Li, M.A. El-Sayed, The effect of stabilizers on the catalytic activity and stability of Pd colloidal nanoparticles in the Suzuki reactions in aqueous solution, The Journal of Physical Chemistry B, 105 (2001) 8938-8943.

[90] R.W. Gosselink, S.A. Hollak, S.W. Chang, J. van Haveren, K.P. de Jong, J.H. Bitter, D.S. van Es, Reaction pathways for the deoxygenation of vegetable oils and related model compounds, ChemSusChem, 6 (2013) 1576-1594.

[91] J. Asomaning, P. Mussone, D.C. Bressler, Thermal deoxygenation and pyrolysis of oleic acid, Journal of Analytical and Applied Pyrolysis, 105 (2014) 1-7.

[92] J.G. Immer, M.J. Kelly, H.H. Lamb, Catalytic reaction pathways in liquid-phase deoxygenation of C18 free fatty acids, Applied Catalysis A: General, 375 (2010) 134-139.

[93] A.A. Peterson, F. Vogel, R.P. Lachance, M. Fröling, M.J. Antal Jr, J.W. Tester, Thermochemical biofuel production in hydrothermal media: a review of sub-and supercritical water technologies, Energy & Environmental Science, 1 (2008) 32-65.

[94] D. Castello, Supercritical Water Gasification of Biomass, in, University of Trento, 2013.

[95] Y. Yu, X. Lou, H. Wu, Some recent advances in hydrolysis of biomass in hot-compressed water and its comparisons with other hydrolysis methods, Energy & Fuels, 22 (2007) 46-60.

[96] P. Krammer, H. Vogel, Hydrolysis of esters in subcritical and supercritical water, The Journal of Supercritical Fluids, 16 (2000) 189-206.

[97] Z. Srokol, A.-G. Bouche, A. van Estrik, R.C. Strik, T. Maschmeyer, J.A. Peters, Hydrothermal upgrading of biomass to biofuel; studies on some monosaccharide model compounds, Carbohydrate Research, 339 (2004) 1717-1726.

[98] D. Bröll, C. Kaul, A. Krämer, P. Krammer, T. Richter, M. Jung, H. Vogel, P. Zehner, Chemistry in supercritical water, Angewandte Chemie International Edition, 38 (1999) 2998-3014.

[99] N. Akiya, P.E. Savage, Roles of water for chemical reactions in high-temperature water, Chemical reviews, 102 (2002) 2725-2750.

[100] M. Möller, P. Nilges, F. Harnisch, U. Schröder, Subcritical water as reaction environment: fundamentals of hydrothermal biomass transformation, ChemSusChem, 4 (2011) 566-579.

[101] H. Weingärtner, E.U. Franck, Supercritical water as a solvent, Angewandte Chemie International Edition, 44 (2005) 2672-2692.

[102] P.A. Marrone, M. Hodes, K.A. Smith, J.W. Tester, Salt precipitation and scale control in supercritical water oxidation—part B: commercial/full-scale applications, The Journal of Supercritical Fluids, 29 (2004) 289-312.

[103] M. Hodes, P.A. Marrone, G.T. Hong, K.A. Smith, J.W. Tester, Salt precipitation and scale control in supercritical water oxidation—Part A: fundamentals and research, The Journal of Supercritical Fluids, 29 (2004) 265-288.

[104] M. Schubert, J.W. Regler, F. Vogel, Continuous salt precipitation and separation from supercritical water. Part 1: Type 1 salts, The Journal of Supercritical Fluids, 52 (2010) 99-112.

[105] R.E. Westacott, K.P. Johnston, P.J. Rossky, Stability of ionic and radical molecular dissociation pathways for reaction in supercritical water, The Journal of Physical Chemistry B, 105 (2001) 6611-6619.

[106] S.S. Toor, L. Rosendahl, A. Rudolf, Hydrothermal liquefaction of biomass: a review of subcritical water technologies, Energy, 36 (2011) 2328-2342.

[107] P. Kritzer, E. Dinjus, An assessment of supercritical water oxidation (SCWO): existing problems, possible solutions and new reactor concepts, Chemical Engineering Journal, 83 (2001) 207-214.

[108] M. Watanabe, T. Iida, H. Inomata, Decomposition of a long chain saturated fatty acid with some additives in hot compressed water, Energy conversion and management, 47 (2006) 3344-3350.

[109] O. Şenol, T.-R. Viljava, A. Krause, Hydrodeoxygenation of methyl esters on sulphided NiMo/γ-Al 2 O 3 and CoMo/γ-Al 2 O 3 catalysts, Catalysis Today, 100 (2005) 331-335.

[110] M. Toba, Y. Abe, H. Kuramochi, M. Osako, T. Mochizuki, Y. Yoshimura, Hydrodeoxygenation of waste vegetable oil over sulfide catalysts, Catalysis Today, 164 (2011) 533-537.

[111] E.W. Ping, J. Pierson, R. Wallace, J.T. Miller, T.F. Fuller, C.W. Jones, On the nature of the deactivation of supported palladium nanoparticle catalysts in the decarboxylation of fatty acids, Applied Catalysis A: General, 396 (2011) 85-90.

[112] P.T. Do, M. Chiappero, L.L. Lobban, D.E. Resasco, Catalytic deoxygenation of methyl-octanoate and methyl-stearate on Pt/Al2O3, Catalysis letters, 130 (2009) 9-18.

Chapter 3

Using Subcritical Water for Decarboxylation of Oleic Acid into Fuel-Range Hydrocarbons[1]

Abstract

Current interest in renewable fuel production is focused on high-performance fuels such as jet fuel because of their premium value in the marketplace. Currently, lower-value fuels such as biodiesel can be obtained using variety of feedstocks, but contain significant amounts of oxygen, hence lowering their fuel value. In this work, we examined a one-pot catalytic hydrothermal process for the decarboxylation of oleic acid as a model compound for free fatty acids with an activated carbon catalyst. Temperature (350-400 ºC), water-to-oleic acid ratio (2:1- 4:1) (v/v), catalyst, catalyst-to-total feed ratio (0.15-0.75) and residence time (1-2 h) were found to be key factors for removing oxygen from oleic acid. The complete removal of the carboxylic group from the upgraded liquid phase was achieved at 400°C with a water-to-oleic acid ratio of 4:1(v/v) and residence time of 2 h as confirmed by FTIR and ^{13}C NMR results. The pseudo-first-order reaction rate constant was found to follow Arrhenius behavior with the activation energy determined to be 90.6±3 kJ/mol. GC-FID results showed a high selectivity to heptadecane conversion, wheareas the GC-TCD results indicated that decarboxylation was the dominating chemical reaction. High heating values and fuel densities in the range of commercial jet fuels were obtained using this approach, without the addition of high-pressure hydrogen or a hydrogen-donor-solvent.

Keywords: Hydrothermal decarboxylation, Subcritical water, Activated carbon, Oleic acid, Fuel like hydrocarbons.

3.1 Introduction

The depletion of fossil-fuel reserves and the increase of greenhouse gas-emissions have encouraged researchers to explore biomass as a renewable feedstock for the production of liquid transportation fuels [1]. Esterification or transesterification of long-chain fatty acids or their derivatives for the production of liquid fuels such as biodiesel is a well-established process [2, 3]. However, the poor cold flow properties of biodiesel, such as high pour and cold filter plugging points are major drawbacks for use of this fuel in Northern climates [4]. Although the esterified products have a lower higher heating value (HHV) than petroleum diesel, the high carbon number long-chain fatty acids can give sufficiently high heating values when properly deoxygenated. The deoxygenated hydrocarbons have higher energy densities, lower nitrogen oxide (NO_x) emissions, lower acidities, lower viscosities, higher oxygen stabilities and are better suited for the existing infrastructure for distribution and vehicles [5]. The deoxygenated products also have much higher cetane numbers (>70) than petroleum diesel fuel (~45), and their boiling-point range is comparable to that of typical petroleum-based diesel [6].

To produce deoxygenated fuels, free fatty acids or their derivatives can be decarboxylated or decarbonylated [7]. Both reactions are thermodynamically favorable at 300 ^{o}C (ΔG_{rxn} = -83.5 and -17 kJ/mol for decarboxylation and decarbonylation, respectively) [8], but complete removal of oxygen can be achieved only through the decarboxylation reaction. Decarboxylation requires less hydrogen than other processes (such as hydrodeoxygenation), thereby reducing production costs. In a previously proposed decarboxylation mechanism of fatty acids, the carboxylic acid group was found to adsorb on the catalyst surface, with the -COOH group removed through a C-C cleavage to release CO_2, thereby forming a hydrocarbon with one fewer carbon atoms than the original fatty acid chain [9]. Heterogeneous catalytic decarboxylation of fatty-acids has previously been performed either in an organic solvent such as dodecane or mesitylene or without any solvent [10-13]. However, the use of sub- or supercritical water has been shown to enhance the decarboxylation mechanism [14]. Water at high temperatures and pressures is an environmentally benign solvent that has intriguing physicochemical properties making its use both challenging and potentially useful. For example, water under supercritical conditions loses its hydrogen-bonding ability, becoming

more like a nonpolar solvent. Also, its density and dielectric properties vary widely depending on the utilized temperature and pressure [15-17].

The decarboxylation of fatty acids or their derivatives provides low hydrocarbon yields at moderate temperatures (<400 $^{\circ}$C), which clearly shows the need for a catalyst for the reaction [12]. Noble-metal catalysts such as Pd [18-20] and Pt [5, 21-24] are mostly reported in the literature to be effective catalysts for the decarboxylation reactions. However, the use of noble metals as catalysts is an economic shortcoming for commercializing the process. Popov and Kumar [25] found that activated carbon is an effective catalyst converting saturated/unsaturated fatty acids into alkanes/alkenes in sub- and supercritical water using dilute formic acid as the hydrogen donor within a short residence time. Fu et al. [26] conducted the hydrothermal decarboxylation of palmitic and oleic acids to fuel-range hydrocarbons using activated carbon in sub- and supercritical water with no added H_2. Although the decarboxylation reactions were accomplished in hydrothermal media in the two cases mentioned above, as only nonstirred reactors were used, mass transfer might have been a limitation as fuel values were not provided. Also the mechanism of this reaction is still poorly understood.

The objective of this study was to demonstrate the hydrothermal decarboxylation of oleic acid (OA) in the presence of activated carbon as catalyst without the addition of high-pressure hydrogen or a hydrogen-donor solvent in a stirred reactor and to examine the effects of temperature, water-to-oleic acid ratio and reaction time. This work also focused on examining the liquid and gaseous products and the fresh and used catalysts.

3.2 Experimental Section

3.2.1 Materials

Technical-grade OA (purity 90%), powdered activated carbon (DARCO G-60, 100-325 mesh particle size), and hexane (ACS grade) were purchased from Sigma-Aldrich, Oakville, ON, Canada, and used as received. Deionized water (18 MΩ) was obtained from a compact ultrapure water system (EASY pure LF, Mandel Scientific Co. model BDI-D7381).

3.2.2 Catalyst Characterization

The Brunauer-Emmett-Teller (BET) surface areas, pore diameters and pore volumes of both the fresh and spent activated carbons were determined from nitrogen adsorption and desorption isotherm data obtained at -193 °C in a constant-volume adsorption apparatus (Tristar II 3020, Micromeritics Instrument Corporation) using 99.995% pure N_2 gas obtained from Praxair (Oakville, ON, Canada). The total pore volume and pore size distribution were determined using the Barret-Joyner-Halenda (BJH) method. In a typical experiment, a minimum of 80 mg of sample was degassed at 150 °C for 12 h before measurements to remove the moisture and other adsorbed gases from the catalyst surface.

X-ray diffraction (XRD) was used to study the crystal structures of the fresh and spent activated carbon catalysts. The analysis was done in a Bruker D2 Phaser powder diffractometer using Cu Kα radiation (λ for Kα is equal to 1.54059 Å) over $2\theta = 10$ - 80 using a scan rate 0.2 º per min.

Scanning electron microscopy (SEM) (model LEO1530) was used to obtain the surface morphologies of the catalysts.

Infrared spectra of the fresh and spent samples were analyzed using an attenuated-total-reflection Fourier transform infrared (ATR-FTIR) spectrometer (Nicolet 6700 FTIR), connected to a computer, and supported by Thermo Scientific OMNIC^{TM} software. After the crystal area had been cleaned and the background collected, a small amount of the sample was loaded onto the ATR probe positioned over the crystal/sample area and force was applied to the sample for collection. X-ray photoelectron spectroscopy (XPS) analysis was carried out with a Kratos Axis Ultra spectrometer using a monochromatic Al Kα source (15 mA, 14 kV). Raman spectroscopy measurements of fresh and spent catalysts were done using a Kaiser Optical Systems RXNI-785 instrument with at an excitation wavelength of 785 nm.

Thermogravimetric analysis of the fresh and spent activated carbons was performed on a TGA/SDT A851 model gravimetric analyzer at a heating rate of 10 ºC/min from ambient temperature to 1000 ºC. The sample (ca. 10 mg) was loaded onto an alumina crucible, with an empty alumina crucible as a reference, and heated from room temperature to 1000 ºC at a rate of 10 ºC/min in N_2 with a flow rate of 50 mL/min.

3.2.3 Reaction Procedure

The catalytic hydrothermal decarboxylation of OA was conducted in a continuous stirred tank 300 mL stainless steel batch reactor (Autoclave Engineers, Erie, PA) with an operating pressure of 5500 psi rating at 340 ^{o}C. The reactor was heated with a 1.2 kW electric furnace that surrounded its main body manufactured by Industrial Heater Corp., (Cheshire, CT). The detailed reactor system is shown in Figure 3.1. Prior to use in any experiments, the reactor was washed with hexane and then water. In a typical experiment, 5 g of catalyst and the required amount of H_2O were loaded into the reactor to maintain the proper volume ratio of H_2O to OA. The reactor was sealed and purged with N_2 for 10-15 min to remove air from the system. After this step, the outlet valve was closed and the reactor was then heated to the desired reaction temperature and autogenous pressure (2000-2500 psi) of H_2O (subcritical conditions), which depended on the volume of water used. After the desired reaction temperature had been reached, the reactor was left for 5 min to stabilize. Subsequently, the OA feed was injected into the reactor with a syringe pump (Isco 100 DM, Lincoln, NE) (constant volume). As soon as the feed injection was complete, the reaction time was started. After the desired reaction time was completed, the electric furnace was turned off. The furnace was then immediately removed from the reactor body, and an ice bath was used to quench the reaction. When the reactor temperature reached room temperature, the gas was collected into a Tedlar gas bag obtained from SKC Inc. (Pittsburgh, PA) and the volume of gas produced was measured using a mass flow meter with totalizer (Omega Engineering Inc.). The liquid product was collected by opening the reactor and transferring the liquid contents into a volumetric flask, after which the reactor was rinsed with known amount of hexane washes until all of the products plus catalyst were separated from the reactor wall. The recovered product was then filtered under a vacuum to separate the catalyst from the product mixture. Hexane was then evaporated to obtain the pure product for further analysis and the used catalyst was dried in a vacuum oven at 90 ^{o}C overnight to obtain dry powder. The dry used catalyst (spent) was further evaluated for decarboxylation under the optimum reaction conditions.
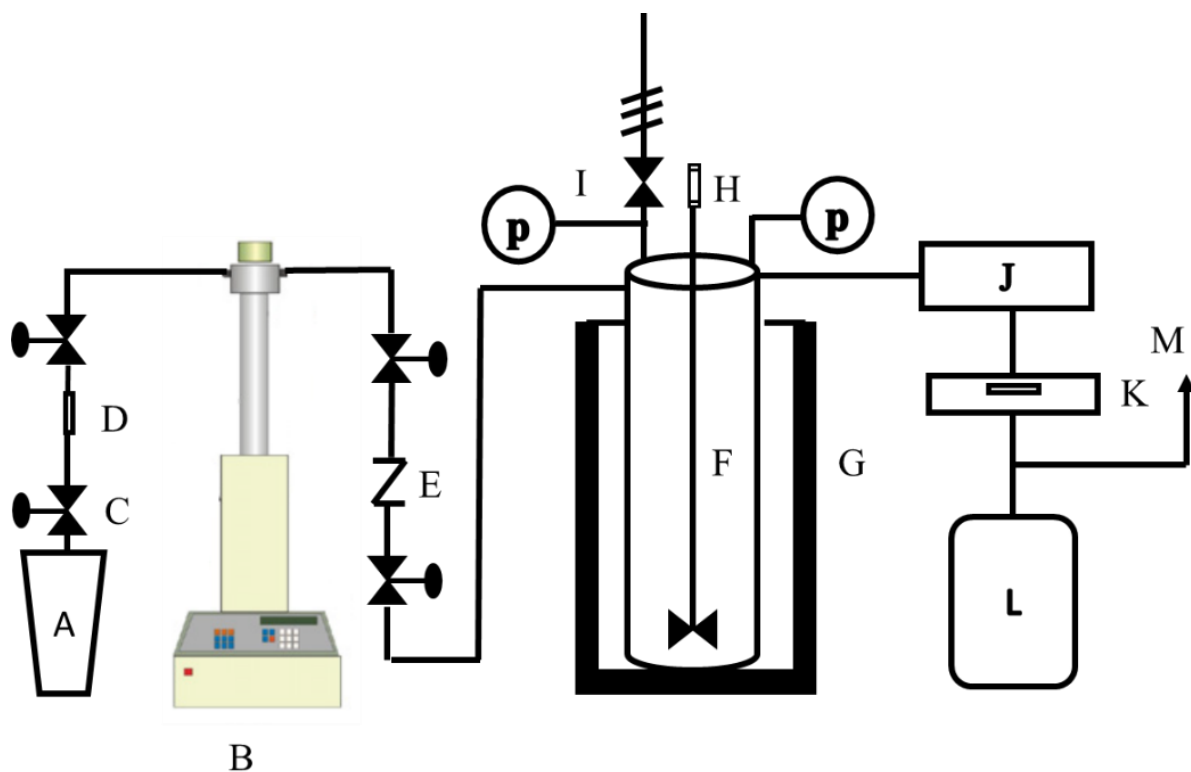
Figure 3.1. Hydrothermal batch reactor system: (A) feed tank, (B) Isco 100DM syringe pump, (C) gate valve, (D & J) filters, (E) check valve, (F) reactor, (G) electric furnace, (H) Stirrer, (I) safety valve, (K) mass flow controller, (L) gas bag, (M) vent.

3.2.4 Product Analysis

The liquid products were analyzed using a gas chromatograph (Shimadzu, GC-2014) equipped with a flame ionization detector and a capillary DB WAX column (Agilent Technologies, Santa Clara, CA) (dimensions, 30m x 0.250mm x 0.25μm, temperature limit, 20 to 260 °C). The oven temperature of the gas chromatograph was programmed as follows: 3 min hold at 50 °C, 10 °C/min ramp to 250 °C. The injector and detector temperatures were maintained at 200 and 250 °C, respectively. Samples (1 μL) were injected manually into the column with a 10:1 split ratio. The injection of liquid sample into the gas chromatograph was repeated at least three times and the results were averaged to minimize analytical error. Helium, hydrogen and helium/air were used as the carrier gas, flame gas, and make-up gas, respectively. The reaction products were determined by matching gas chromatograph retention times with known standards (C8-C20 saturated hydrocarbons, heptadecene and oleic acid) obtained from Sigma-Aldrich, Oakville, ON. Quantitative measurements (calculating product selectivity's) were

performed as follows: The total areas of the detected peaks combined were counted as 100%, with the relative percentage (area of peak/total area of peaks) determined for each individual product of interest.

Infrared analysis of reactant and product samples was performed using an ATR-FTIR spectroscope (Nicolet 6700 FTIR, Thermo Scientific). The spectra were recorded in the range of 600-4000 cm^{-1} with a resolution of 4 cm^{-1} over 32 scans.

^1H and ^{13}C nuclear magnetic resonance (NMR) spectra of reactant and product samples were recorded using a Varian Inova 400 spectrometer. Samples were dissolved in $CDCl_3$ and the chemical shifts were referenced to tetramethylsilane (0.0 ppm).

The densities of the products were measured using an Eagle Eye SG-Ultra Max Hydrometer (density meter) [dimensions 5.5in. W x 5.5 in. D x 1 in. H (outside)]. Liquid-product higher heating values (HHVs), also called gross calorific values, were measured using an IKA C2000 bomb calorimeter. Test samples were sealed in a decomposition vessel, sometimes referred to as a bomb, and were then automatically pressurized with oxygen and ignited. The resulting heat of decomposition was then quantified and used to calculate the sample's energy content and is reported as the calorific value.

The gaseous products were analyzed using the same gas chromatograph (Shimadzu, GC-2014) equipped with a thermal conductivity detector and a different nickel-packed column (120/80 Hayesep D stainless steel 3.18-mm i.d., 6.2 m). The oven temperature of the gas chromatograph was programmed as follows: 6 min hold at 35 ^{o}C, 25 ^{o}C/min ramp to 200 ^{o}C, 1 min hold at 200 ^{o}C. The injector and detector temperatures were maintained at 200 and 250 ^{o}C, respectively with He used as the carrier gas. The gas chromatograph was calibrated using a standard gas mixture of known composition. The analysis was performed manually using a 1 mL SGE gastight syringe (model number 008100, Reno, NV) by collecting the sample from the gas bag. The injection of sample gas into the gas chromatograph was repeated a minimum three times, and the results were averaged to minimize analytical error.

3.3 Results and Discussion

3.3.1 Gas Chromatography (GC)-Flame Ionization Detection (FID) Analysis of Decarboxylated Liquid Product

Three blank experiments (without catalyst) were conducted with water only at 350 to 400 ℃ to compare the oleic acid (OA) conversion and selectivities of products with catalytic decarboxylation reactions. Figure 3.2 shows the conversions of OA and selectivities of the formed hydrocarbons during decarboxylation at different temperatures (350-400 ℃), water/OA ratios (2:1 - 4:1) and reaction times (0-2 h). Figure 3.2(a) and (b) shows the importance of using a catalyst for the hydrothermal decarboxylation of oleic acid. Decarboxylation of OA without catalyst gave a relatively low conversion (61% at 400 ℃), and higher selectivity to heptadecene (46% at 400 ℃) compared to heptadecane (9% at 400 ℃) along with some other lower hydrocarbons (C8 to C16). In comparison, the catalyzed samples gave greatly enhanced decarboxylation, resulting in 97% conversion of OA and increasing the selectivity to heptadecane from 9 to 81% for the same operating conditions. Catalytic decarboxylation was found to produce more heptadecane than heptadecene. This provides a further advantage of this technology, as heptadecane is more stable than heptadecene, which is prone to polymerization or oxidation during storage. The water-to-OA ratio and reaction time were found to be important factors for the decarboxylation reaction in a batch reactor. Figure 3.2(c) shows the effect of water-to-OA ratio at 400 ℃, reaction time of 2 h and stirring speed of 800, whereas Figure 3.2(d) shows the effect of reaction time in the presence of 5 g of activated carbon catalyst at 400 ℃, water/OA of 4:1, and stirring speed of 800 on the decarboxylation reaction of OA. Water/OA of 4:1 and a reaction time of 2 h were found to be optimal for higher heptadecane selectivity.
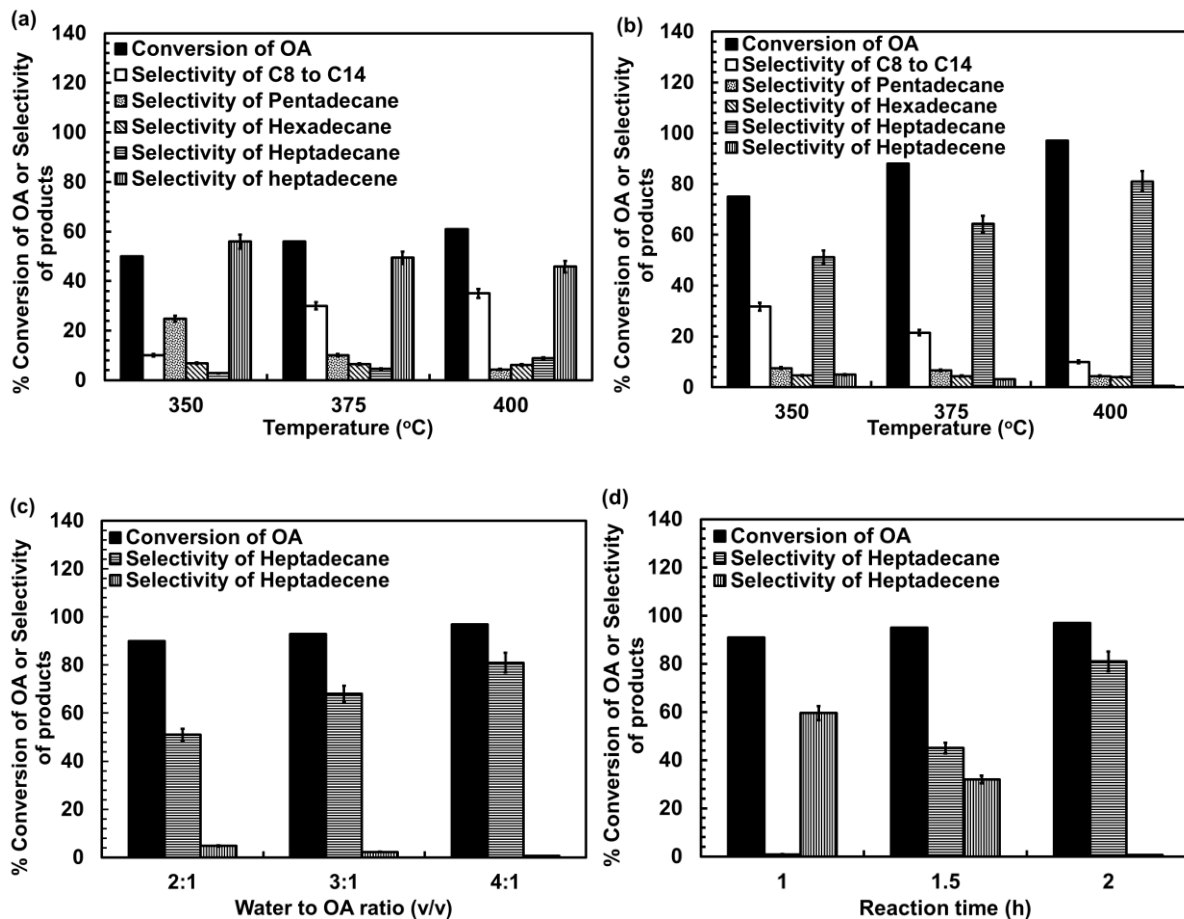
Figure 3.2: Oleic acid conversions and product distributions (a) without and (b) with 5 g of catalyst at different temperatures, (c) for different water-to-OA ratios at 400 $^{\circ}$C, and (d) for different reaction times at 400 $^{\circ}$C.

Popov & Kumar [27] reported 80.6% selectivity to heptadecane during the hydrothermal deoxygenation of fatty acids in a packed-bed tubular reactor with the addition of formic acid as a hydrogen donor between 370 and 380 $^{\circ}$C using a ratio of oil to water to formic acid of 1:5:0.5 by volume. Fu et al. reported yields of (5.8±1.1)% heptadecane and (24±1%) for stearic acid in the product mixture during the decarboxylation of oleic acid in sub-/supercritical water after 3 h reaction time at 370 $^{\circ}$C in the presence of activated carbon [26]. In comparison with the above literature data, we achieved 81% selectivity to heptadecane at 400 $^{\circ}$C without adding any external source of hydrogen or hydrogen-donor solvent at a reaction time of 2 h using an oleic acid-to-water ratio of 1:4. Hydrothermal decarboxylation of OA in the presence of catalyst for a reaction time of 2 h and a water/OA ratio of 4:1 without added H$_2$ led to the

production of heptadecane rather than heptadecene. This indicates that hydrogen was produced *in situ* during the reaction and contributed to the hydrogenation of the products. Youssef et al. and Fu et al. showed that hydrogen was produced by a gasification reaction at the chosen temperature [21, 28]. Because the decarbonylation reaction is occurring with decarboxylation, CO can react with water to form hydrogen through the water-gas shift reaction [29]. The Thermal cracking of oleic acid at high temperature also produces hydrogen [30]. A liquid yield of 62% was obtained under these optimum conditions (see Figure A1). The mass balance was > 95% for this experiment, ranging from 90 to 95% for all of the experiments performed in this study.

Table 3.1 reports the typical selectivity's or percentage compositions of the products at 400 ^{o}C, reaction time of 2 h and water-to-OA ratio of 4:1, and a stirring speed of 800 rpm in the presence of 5 g of activated carbon catalyst. As shown in this table, the formed product can be used as aviation fuel, which consists of C8 to C17 alkanes, alkenes, and aromatic hydrocarbons [25, 31].

Table 3.1: Product Distribution of Oleic Acid Decarboxylation at 400 ^{o}C, a Reaction Time of 2 h, a water-to-OA Ratio of 4:1, and a Stirring Speed of 800 rpm.

compounds	percentage selectivity (composition)
octane (C_8H_{18})	0
nonane (C_9H_{20})	0
decane ($C_{10}H_{22}$)	0
undecane ($C_{11}H_{24}$)	0
dodecane ($C_{12}H_{26}$)	2.2
tridecane ($C_{13}H_{28}$)	5.1
tetradecane ($C_{14}H_{30}$)	2.8
pentadecane ($C_{15}H_{32}$)	4.4
hexadecane ($C_{16}H_{34}$)	4.0
n-heptadecane ($C_{17}H_{36}$)	81
heptadecene ($C_{17}H_{34}$)	0.6
octadecane ($C_{18}H_{38}$)	0
nonadecane ($C_{19}H_{40}$)	0
icosane ($C_{20}H_{42}$)	0
oleic acid	0

3.3.2 Fuel Quality

Specific gravity is an important parameter for any liquid because it helps to determine the usability of the fuel product. The values of the specific gravity of the decarboxylated product at different temperatures and of some commercial fuels listed in Table 3.2. A comparison of the experimental data with the values for conventional fuels indicates that our experimental decarboxylated product falls within the typical diesel range.

Table 3.2: Specific Gravity Data for the Decarboxylated Product at 400 ºC, a Reaction Time of 2 h and a Water-to-OA Ratio of 4:1, and a Stirring Speed of 800 rpm (in the Presence of 5 g of catalyst) and Commercial Fuels.

Compounds	Temperature (ºC)	specific gravity
decarboxylated product	15.6	0.798
	21.6	0.798
	25	0.792
	40	0.780
kerosene [32]	15.6	0.78-0.82
jet fuel [33]	15	0.78-0.84
diesel [32]	15.6	0.80-0.96

The heating value of a fuel is the amount of heat released during the combustion of a specified amount, which is characteristic for each fuel. Table 3.3 reports the HHVs values of the feed, decarboxylated product, and some commercial fuels, respectively. The HHV of our decarboxylated product is slightly higher than those of jet fuel and diesel but slightly lower than that of kerosene, which means that the product quality lies within the ranges of jet fuel, kerosene, and diesel.

Table 3.3: High Heating Values of Feed, Product and Commercial Fuels

compounds	HHV (MJ/kg)
oleic acid	39.22
decarboxylated product[*]	45.73
jet fuel [34]	43.54
kerosene [32]	46.20
diesel [32]	44.80

*product obtained under optimum conditions

3.3.3 Mechanism of Decarboxylation

3.3.3.1 ATR-FTIR Analysis of Decarboxylated Liquid Products

To examine the degree of decarboxylation of oleic acid under different reaction conditions, ATR-FTIR spectra of oleic acid and the formed products were measured and are compared in Figure 3.3. The spectrum of oleic acid (Figure 3.3a) shows several major peaks at 3004, 2921, 2852, 1707, 1463, 1412, 1284, 934, and 722 cm^{-1}. The peak at 3004 cm^{-1} is ascribed to the alkene CH stretching mode. The peaks at 2921, 2852, and 722 cm^{-1} are attributed to asymmetric stretching, symmetric stretching, and rocking modes of CH_2, respectively. The peak at 1463 cm^{-1} is assigned to CH_2 scissoring and CH_3 asymmetric bending modes. The peak at 1707, 1412, 1284, and 934 cm^{-1} are attributable to C=O stretching, combination of C-O stretching and O-H deformation, C-O stretching, and OH out of plane bending modes, respectively. After the decarboxylation reactions in the presence of 5 g of activated carbon, all the peaks related to the C=O, C-O, O-H, and alkene C-H vibrations decrease (Figure 3.3b-e and g-h) or completely disappear (Figure 3.3f).

By comparing panels b, c, and f of Figure 3.3, one can see that the degree of decarboxylation increased when the ratio of H_2O to oleic acid was increased from 2:1 to 4:1 in the reaction for 2 h at 400 $^{\circ}C$. A comparison of panels d-f of Figure 3.3 shows that the degree of decarboxylation increased when the reaction time was increased from 1 h to 2 h at 400 $^{\circ}C$ with the ratio of H_2O to oleic acid was held constant at 4:1. By comparing panels f-h of Figure 3.3, one can observe that the degree of decarboxylation increased when the reaction temperature was increased from 350 $^{\circ}C$ to 400 $^{\circ}C$ at a constant reaction time of 2 h and a constant ratio of H_2O to oleic acid of 4:1. By varying reaction conditions, we achieved complete decarboxylation and conversion of alkenyl group of oleic acid by running the reaction at 400 $^{\circ}C$ for 2 h with a ratio of H_2O to oleic acid of 4:1, as evidenced by the absence of the peaks of C=O, C-O, O-H and the alkene C-H peak in Figure 3.3f.
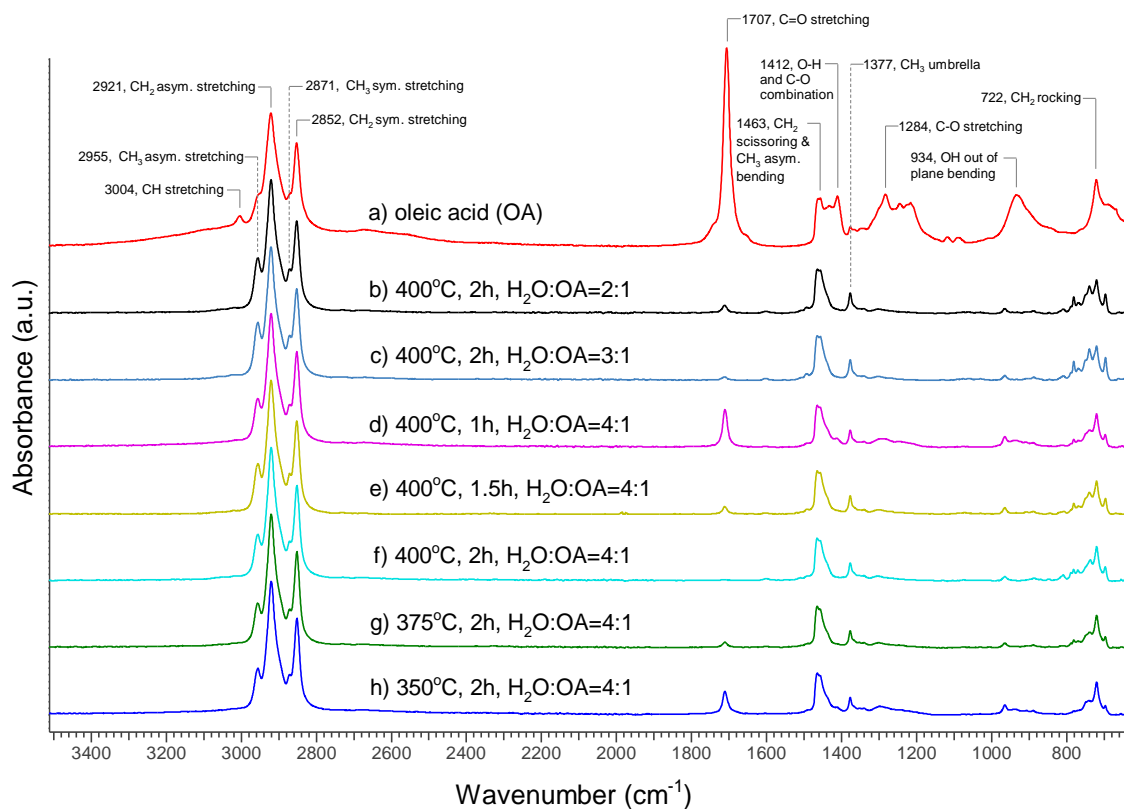
Figure 3.3: ATR-FTIR spectra of (a) oleic acid and (b-h) products formed under different reaction conditions for a catalyst loading of 5 g.

To study the effect of the catalyst on decarboxylation, the reaction was then conducted at 350, 375, and 400 °C for 2 h with a ratio of H_2O to oleic acid of 4:1 but without any catalyst. The FTIR results showed that the peaks of the formed products were almost identical to those of oleic acid (see Figure A2), indicating that no reaction took place without a catalyst under the tested conditions. To study the effect of catalyst on the decarboxylation of oleic acid, reactions were performed with varying ratio of catalyst to feed in the range from 0.15 to 0.75 (w/w). As shown in Figure 3.4, increasing the ratio of catalyst to the feed from 0.15 to 0.75 resulted in the gradual decrease and eventual disappearance of the peaks correspond to C=O, C-O, and O-H suggesting that the catalyst played a key role in the decarboxylation of oleic acid.
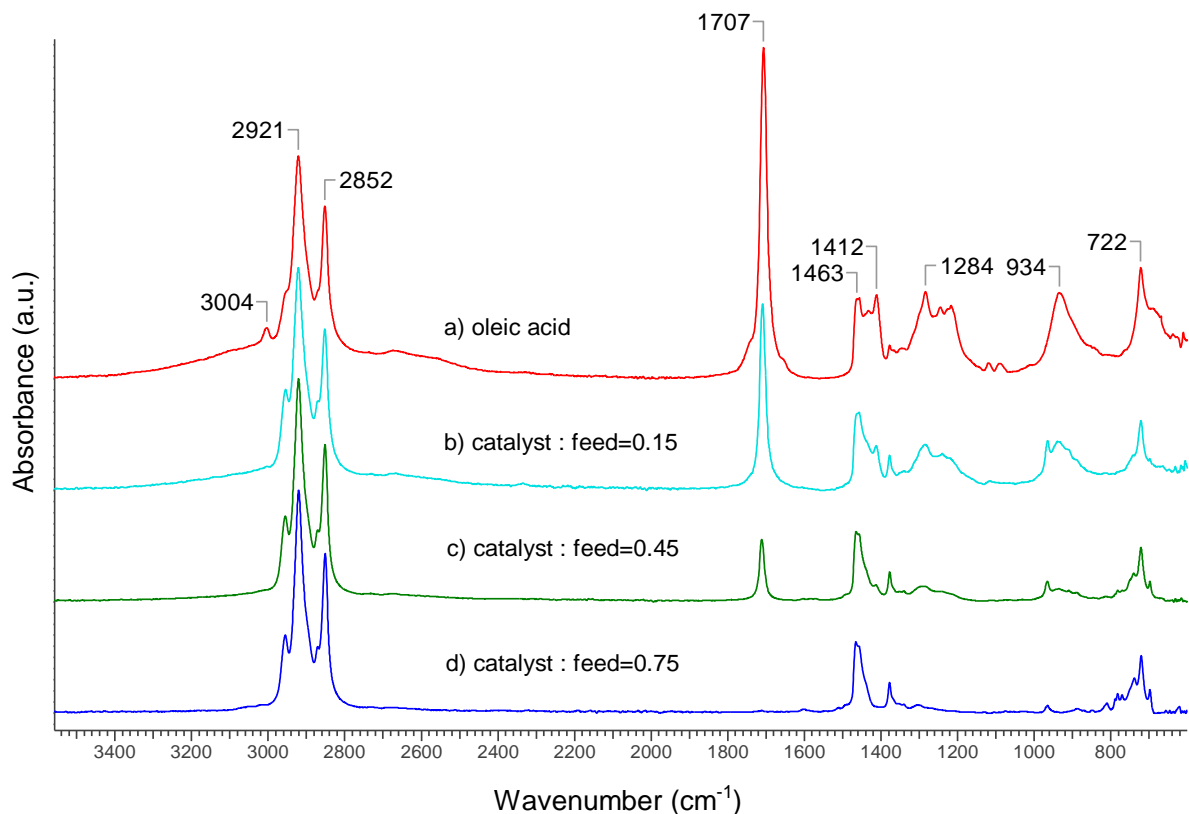
Figure 3.4: Comparison of ATR-FTIR spectra of (a) oleic acid and (b) products formed after reaction at 400 °C for 2 h using different ratios (w/w) of catalyst to feed.

To observe the catalytic activity of the spent catalyst for decarboxylation, a sample of the used catalyst was examined under the optimum reaction conditions, namely, 400 °C, reaction time of 2 h, a water/OA ratio of 4:1 and a stirring speed of 800. Figure A3 compares the FTIR results for the decarboxylation of oleic acid using both the fresh and spent catalysts. In comparison to the almost-complete removal of the carboxylic groups using the fresh catalyst, only about 70% of the carboxylic group was removed using the spent one. To obtain a higher decarboxylation efficiency using spent catalyst, regeneration of the catalyst will be required. This will be presented in Chapter 5.

3.3.3.2 NMR Analysis of Decarboxylated Liquid Products

To better understand the conversion of alkenyl group and decarboxylation of oleic acid, the decarboxylated liquid products were further characterized by ^{1}H and ^{13}C NMR spectroscopies. Figure 3.5 compares the ^{1}H NMR spectra of oleic acid and the formed liquid products. In the

72

spectrum of oleic acid (Figure 3.5a), there are several proton peaks located at 10.74 (a broad peak, not shown), 5.35, 2.36, 2.04, 1.64, 1.30, and 0.89 ppm that can be attributed to carboxylic acid (1), alkenyl (10 and 11), methylene (3), methylene (9 and 12), methylene (4), methylene (5-8 and 13-18), and methyl (19) protons, respectively. In the spectrum of the formed products (Figure 3.5b), all of the peaks related to the carboxylic group (1, 3, and 4) and the alkenyl group (9-12) disappear, suggesting complete decarboxylation and conversion of the alkenyl group.
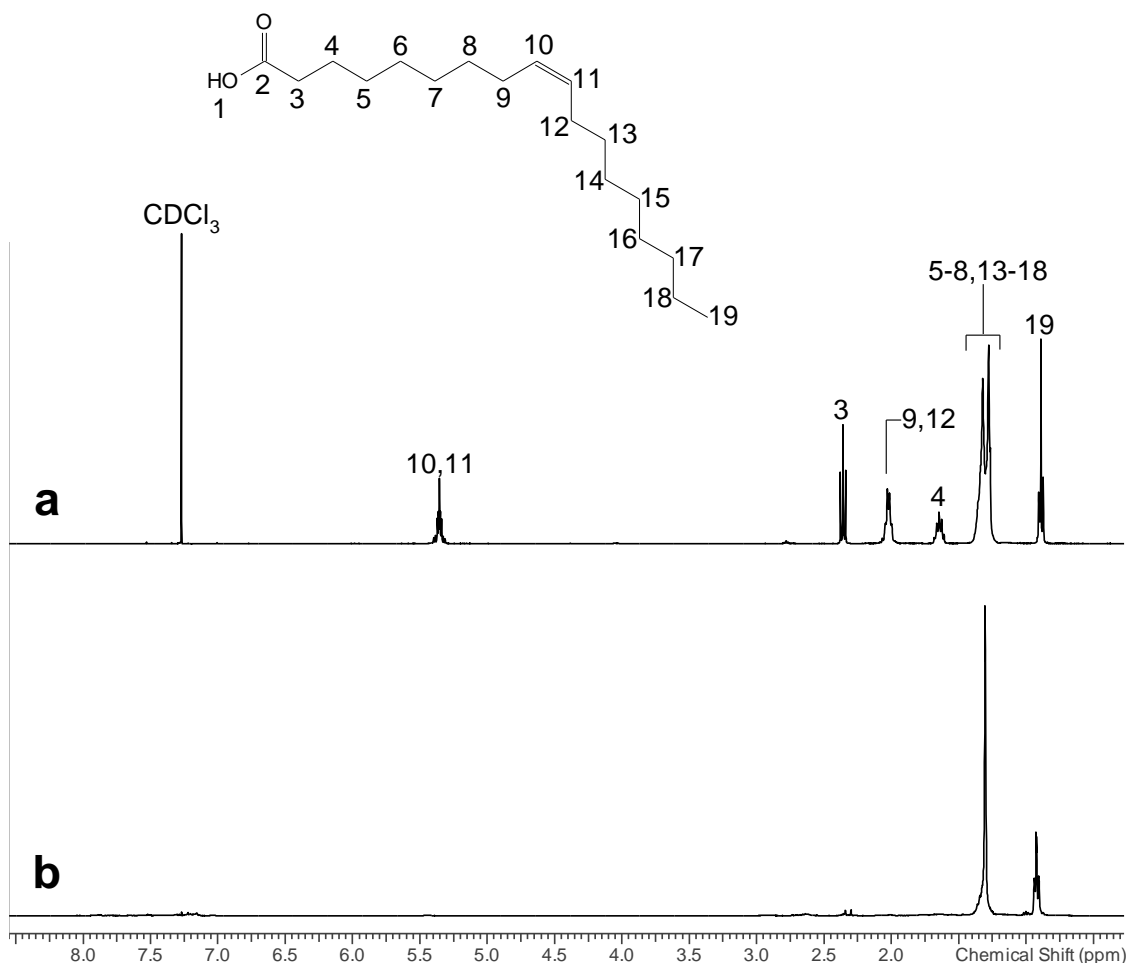
Figure 3.5: ^{1}H NMR spectra of (a) oleic acid and (b) the formed products.

Similarly, in the ^{13}C NMR spectrum of oleic acid (Figure 3.6a), there are several peaks located at 180.6, 129.7-130.0, 34.1, 31.9, 29.0-29.8, 27.2, 24.6, 22.7 and 14.1 ppm that are attributed to the carboxylic (2), alkenyl (10 and 11), methylene (3), methylene (18), methylene (5-8 and

13-16), methylene (9 and 12), methylene (4), methylene (17), and methyl (19) carbons, respectively. After the decarboxylation reaction, the peaks related to the carboxylic group (2-4) and the alkenyl group (9-12) disappear, indicating complete decarboxylation and conversion of the alkenyl group. Therefore, all of these NMR results confirm the complete conversion of the carboxylic and alkenyl groups after the decarboxylation reaction under the selected reaction conditions, in good agreement with the FTIR results discussed above.
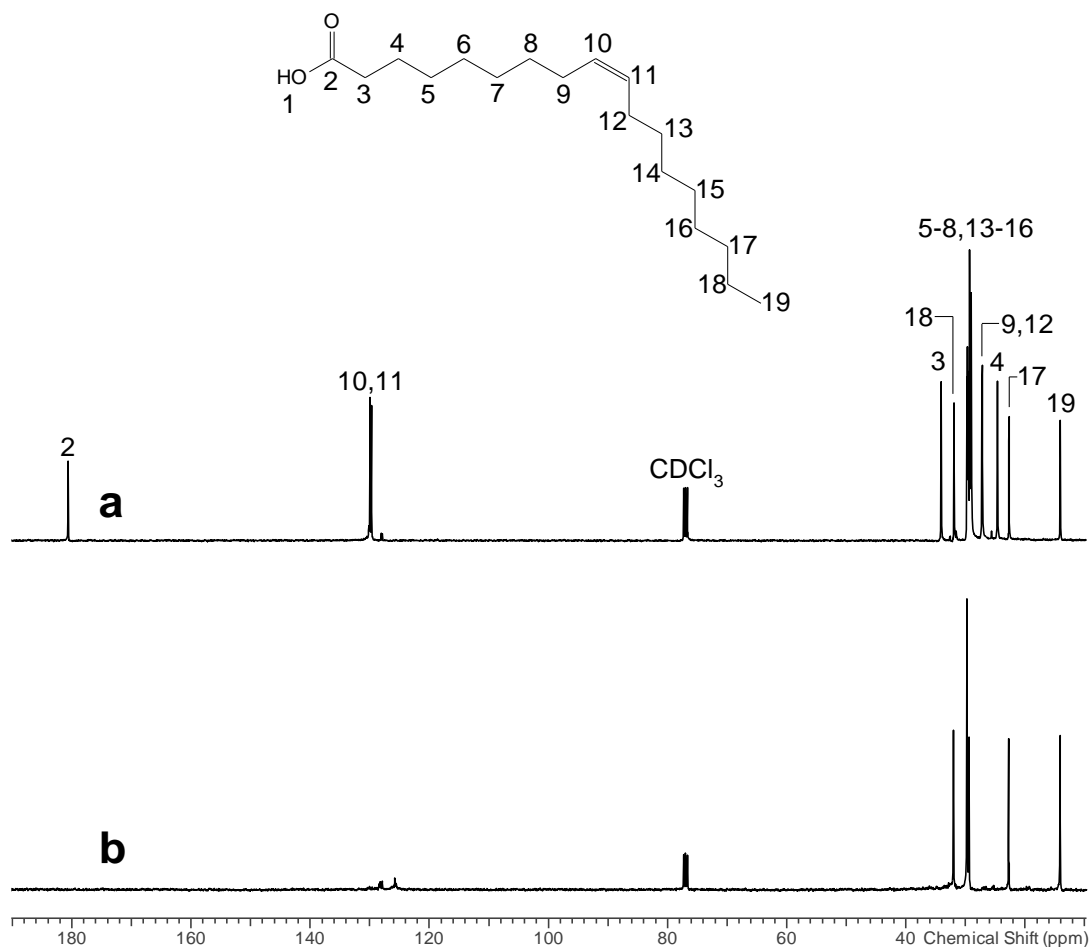
Figure 3.6: ^{13}C NMR spectra of (a) oleic acid and (b) the formed products.

3.3.3.3 Gas Chromatography (GC)-Thermal Conductivity Detection (TCD) Analysis of Gaseous Products

The decarboxylation of oleic acid under all of the experimental conditions tested in the presence of catalyst resulted in the formation of gaseous products. Carbon dioxide and carbon monoxide were mainly detected in the gaseous products under the reaction conditions

investigated. Figure 3.7 shows the mole percentages of CO and CO_2 in the gas fraction of oleic acid decarboxylated products at 400 ºC, reaction time of 2 h and a stirring speed of 800 rpm in the presence of 5 g catalyst. The results follow the general trends under the reaction conditions investigated. Previous studies have suggested the formation of these carbonaceous species through the decarboxylation/decarbonylation of free fatty acids. [35, 36] Several researchers have also reported the presence of both CO and CO_2 in the gas fraction resulting from the thermal and catalytic pyrolysis of fats and oils as well as model triglycerols [36, 37]. In our case, at 400 ºC, the amount of CO_2 is much higher than the amount of CO in the gas mixture. It was shown by Akgul and Kruse [29] that the water-gas shift reaction is still possible in the presence of less CO and excess water in the reaction mixture. The GC-TCD results are consistent with the ATR-FTIR and NMR results. Some other compounds such as methane and some other lighter fractions of hydrocarbons were also confirmed by GC-TCD (data not shown).
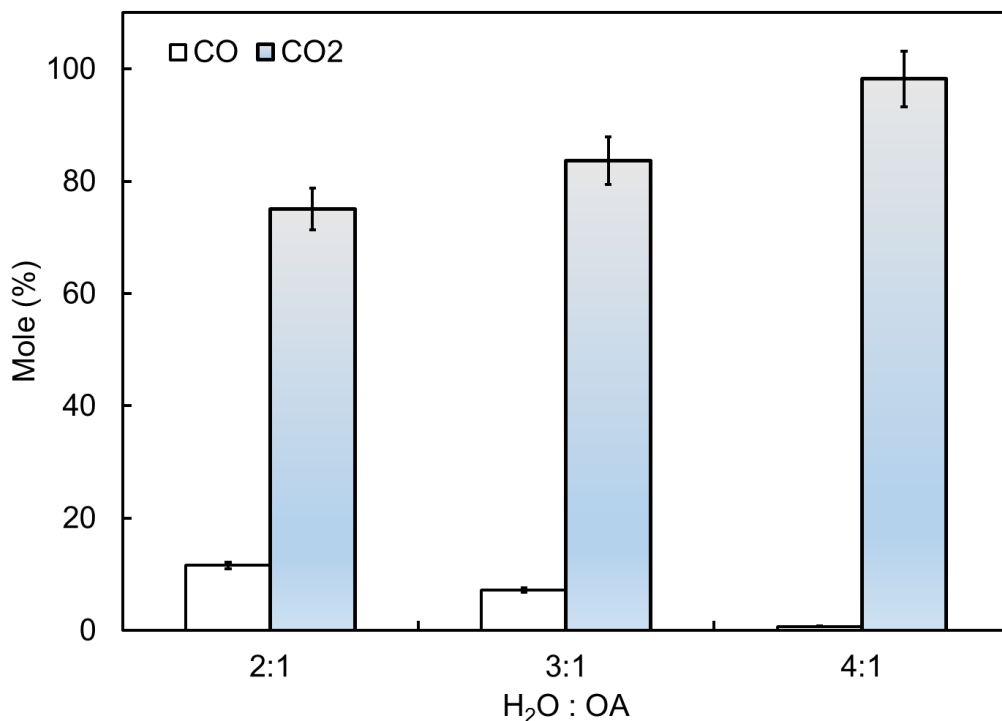
Figure 3.7: Percentages of CO and CO_2 in the gas fraction of oleic acid decarboxylated products.

3.3.3.4 Proposed Reaction Mechanism

A proposed reaction mechanism for the hydrothermal decarboxylation of oleic acid in subcritical water based on our experimental and catalyst characterization results is shown in Scheme 3.1. The hydrogen produced in situ during the thermal cracking of oleic acid [30] and/or the water-gas shift reaction [29] will hydrogenate the feedstock oleic acid ($C_{17}H_{33}COOH$) into stearic acid ($C_{17}H_{35}COOH$) [26]. Higher temperatures such as $400^{o}C$ were found to promote the thermal cracking reaction, which produced larger amounts of hydrogen, leading to complete hydrogenation even in the blank experiment without activated carbon (see Figure A2). The formed stearic acid was finally decarboxylated in the presence of activated carbon to form heptadecane ($C_{17}H_{36}$). It was found by ATR-FTIR that the catalytic performance of the fresh activated carbon was higher than that of the spent one (Figure A3), and the XPS results revealed more C-O/C=O structures on the surface of the fresh catalyst than the spent one (Table S2). This indicates that the electrophilic carboxylic C from stearic acid was attacked by the nucleophilic O on the surface of the activated carbon, creating a tetrahedral intermediate. Subsequent proton transfer from the O^{+} to the O^{-} and elimination of heptadecane resulted in the formation of hydrogen carbonate, which further decomposed back to activated carbon by releasing CO_2.

$$C_{17}H_{33}COOH \xrightarrow{\text{thermal cracking}} \text{lighter HCs} + CO + CO_2 + H_2$$

$$CO + H_2O \xrightleftharpoons{\text{water gas shift}} CO_2 + H_2$$

$$C_{17}H_{33}COOH + H_2 \xrightarrow{\text{hydrogenation}} C_{17}H_{35}COOH$$
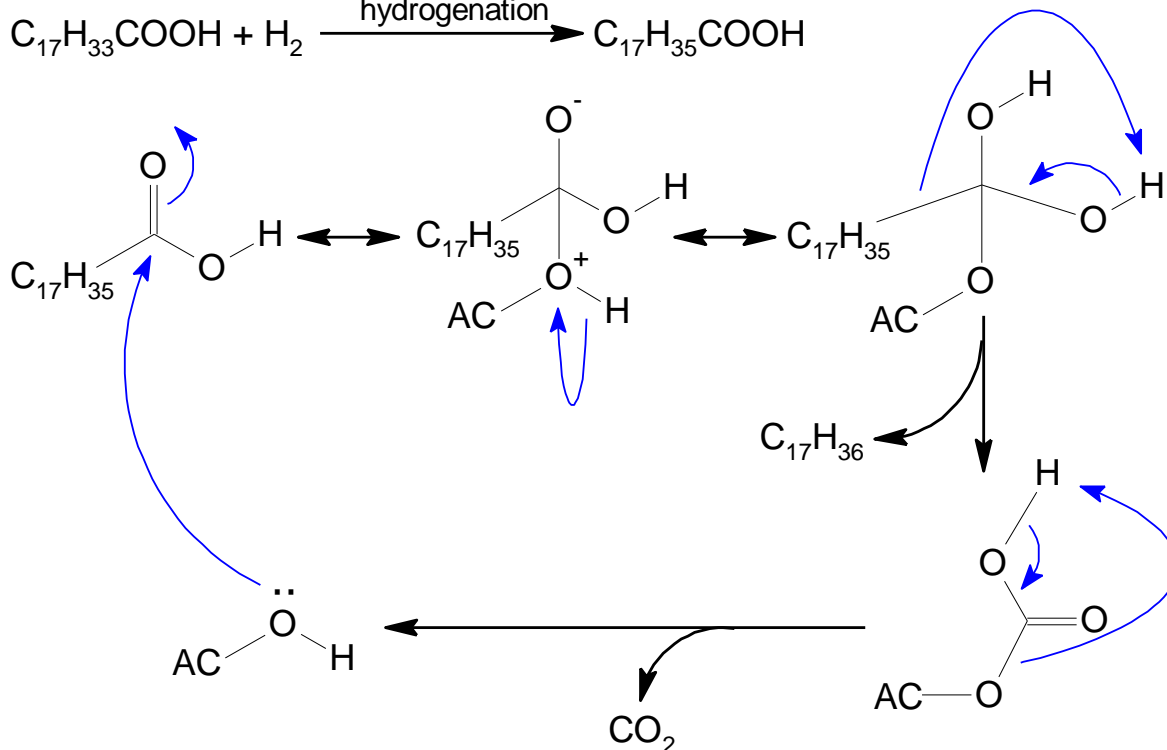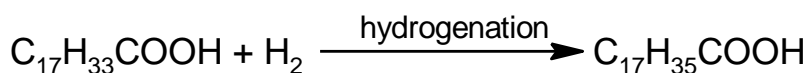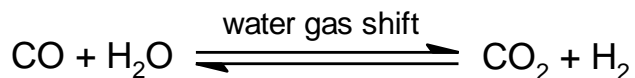
HCs: hydrocarbons; AC: activated carbon (catalyst)

Scheme 3.1. Proposed Reaction Mechanism of Hydrothermal Decarboxylation of Oleic Acid in Subcritical Water on Activated Carbon (AC).

3.4 Catalyst Characterization

3.4.1 BET Surface Area Analysis and Pore Size Distribution

Table 3.4 compares the BET surface areas, pore volumes and pore sizes of fresh and spent catalysts. The results show that the spent activated carbon catalyst loses its activity to a small extent because of its decreased surface area and pore volume. The decrease of the surface area and pore volume of the spent activated carbon might be due to pore blockage by product

molecules that were not completely recovered. The increase of pore size indicates pore breaking during the decarboxylation reaction.

Table 3.4: BET Surface Area, Pore Size and Pore Volume of Fresh and Spent Activated Carbon.

samples	total surface area (m²/g)	total pore volume (cm³/g)	average pore size (nm)
fresh activated carbon	851	0.56	2.6
spent activated carbon	544	0.45	3.6

Figure A4(a) presents the N_2 adsorption-desorption isotherms of fresh and spent activated carbons at -193°C, which exhibit type IV isotherms with a type III hysteresis loop in the relative pressure range from 0.4 to 1.0. This indicates plate-type particles or slit shaped mesopores [38, 39]. Activated carbon has a high BET surface area contributed by mesopores and micropores. The spent catalyst shows a drop in surface area but a similar pore volume and pore size after the decarboxylation reaction.

Figure A4(b) shows the pore size distributions of the activated carbon samples. Both the fresh and spent catalysts exhibit a narrow pore size distributions centered at 4 nm, which is in the mesoporous range (2 - 50 nm).

3.4.2 XRD Analysis

Figure 3.8 shows the XRD patterns of fresh and spent activated carbons. The appearance of broad diffraction peaks in the 2θ ranges of ~15–35° and ~40–50° can be ascribed to randomly arranged amorphous carbon structures containing low contents of crystalline graphite. [40] There is no significant difference between the XRD patterns of the fresh and spent activated carbons except for the shifting of the first peak to slightly lower 2θ values, which might be due to the accumulation of impurities during the decarboxylation reaction.

Coke deposition on a catalyst's surface is quite common upon exposure to high temperatures and will dramatically reduce the catalytic activity and hinder the reusability of the catalyst. As previously reported, deposited coke (graphitic) usually exhibits XRD peaks at 29.84° and 61.92° on the spent catalyst surfaces [41]. However, our XRD pattern of the spent activated

carbon does not show any of these peaks, indicating that no graphitic coke deposition occurred during the decarboxylation of oleic acid in the present study.
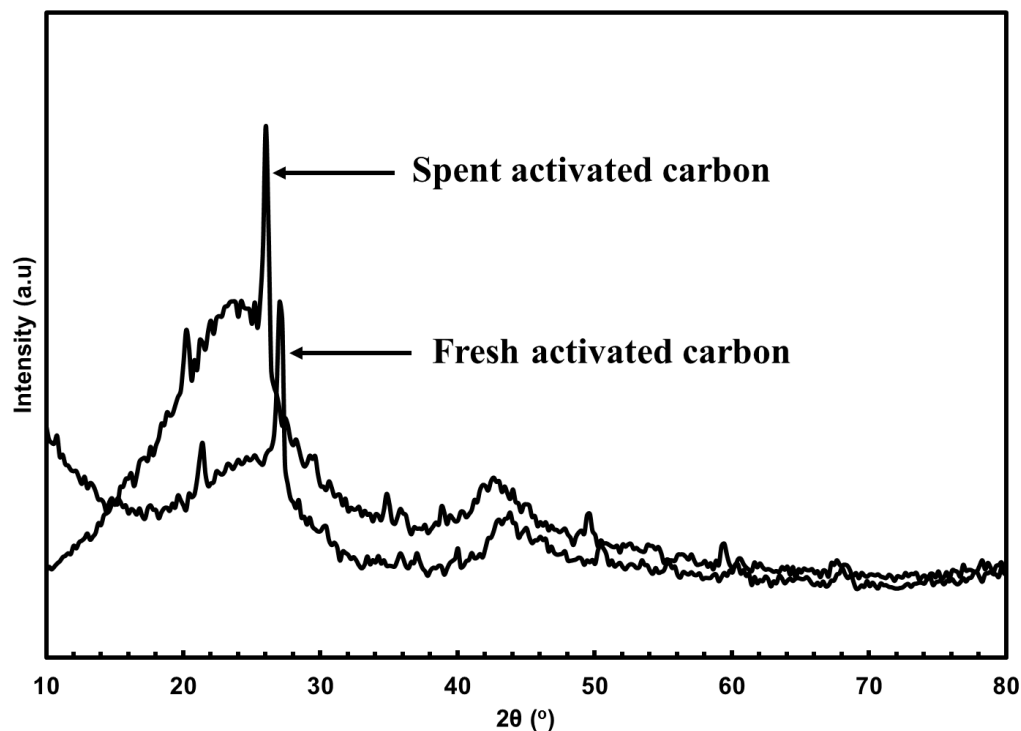
Figure 3.8: XRD patterns of fresh and spent activated carbons.

3.4.3 SEM Analysis

The surface morphologies of the fresh and spent activated carbons were examined by SEM analysis. SEM images of the fresh and spent activated carbons are shown in Figure A5. The SEM image of the fresh catalyst shows a porous structure, whereas that of the spent catalyst indicates a slightly deactivated structure due to agglomeration. The porous structure of the fresh catalyst contributes to the large BET surface, as reported in Table 3.4.

3.4.4 ATR-FTIR and XPS Analysis

Functional groups present on the surface are crucial for activated carbon. Surface functional groups determine the surface properties of the carbon and play a critical role in its catalytic activity [42]. The FTIR spectra of fresh and spent activated carbon samples were found to provide limited information (data not shown), which we attribute to the low concentration of functional groups at the carbon surface. Hence, we further examined the surface chemistry of

the fresh and spent activated carbons by XPS. The survey XPS spectra of the fresh and spent catalysts are shown in Figure A6. The survey spectra of fresh and spent activated carbons show very distinct peaks of C and O and traces of Al, Fe, N, S and Si. The atomic percentages of these elements and the relative contents of the carbon species were calculated and are summarized in Table A1 and Table A2. It was found that the concentrations of Al, Fe, and Si on the surface of the activated carbon increased from 0.3%, 0.1%, and 0.6% to 0.8%, 1.2%, and 1.3%, respectively, after the decarboxylation reaction, suggesting the adsorption of impurities during the reaction.

The surface functional groups present in the activated carbon were identified by high-resolution C 1s XPS spectra, as shown in Figure 3.9. The C 1s spectra of fresh and spent activated carbons contain four peaks corresponding to C-C/C=C (284.5 eV), C-OH and C-O-C (286.5), C=O (287.9) and O-C=O (289.0) [43]. Among all of the carbon peaks, the C-C/C=C peak is predominant for both the fresh and spent catalysts, accounting for 86.4% and 94.2%, respectively, of the carbon species. Moreover, the carbon species of O-C=O, C=O, and C-OH/C-O-C decreased from 4.2%, 2.6%, and 6.8%, respectively to 1.9%, 1.2%, and 2.7%, respectively, after the decarboxylation reaction. These changes can be attributed to the partial deactivation of the catalyst, as evidenced by the lower catalytic performance of the spent activated carbon compared to the fresh one, as discussed above.
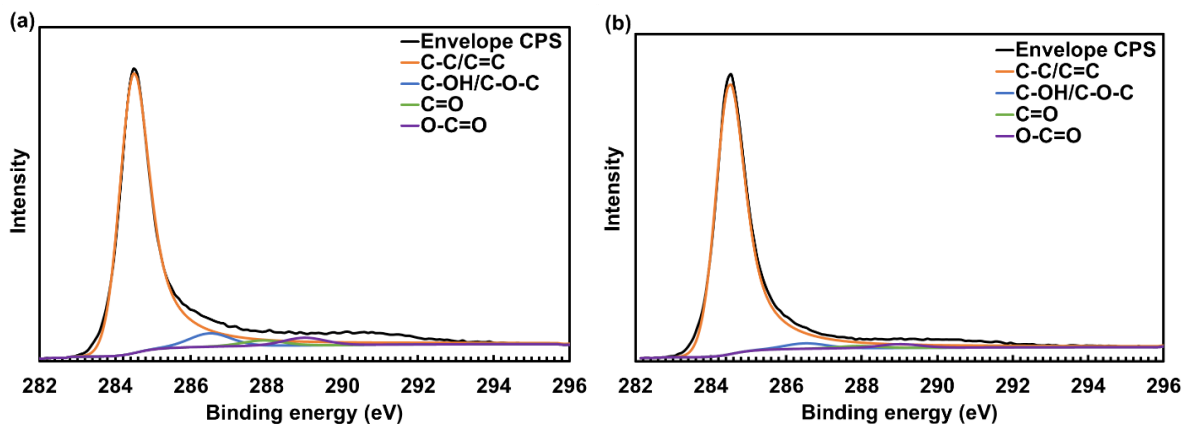
Figure 3.9: High resolution C 1s XPS spectra of (a) fresh and (a) spent activated carbons.

3.4.5 Raman Analysis of the Catalysts

Raman spectroscopy is a powerful nondestructive technique for studying carbonaceous materials. Figure 3.10 compares the Raman spectra of the fresh and spent activated carbons. In the spectrum of the fresh activated carbon, the prominent peak commonly denoted as the G band centered at 1595 cm^{-1} corresponds to the first order scattering of sp^2 hybridized carbon atoms. The D band centered at 1293 cm^{-1} arises from the defect or disordered sites of the sp^3 carbon atoms [44]. Under the same measurement conditions, the intensities of both the D and G bands of the spent activated carbon were much lower than those of the fresh one, suggesting surface contamination by/adsorption of impurities after the decarboxylation reaction. This finding is in good agreement with the XPS results discussed above.
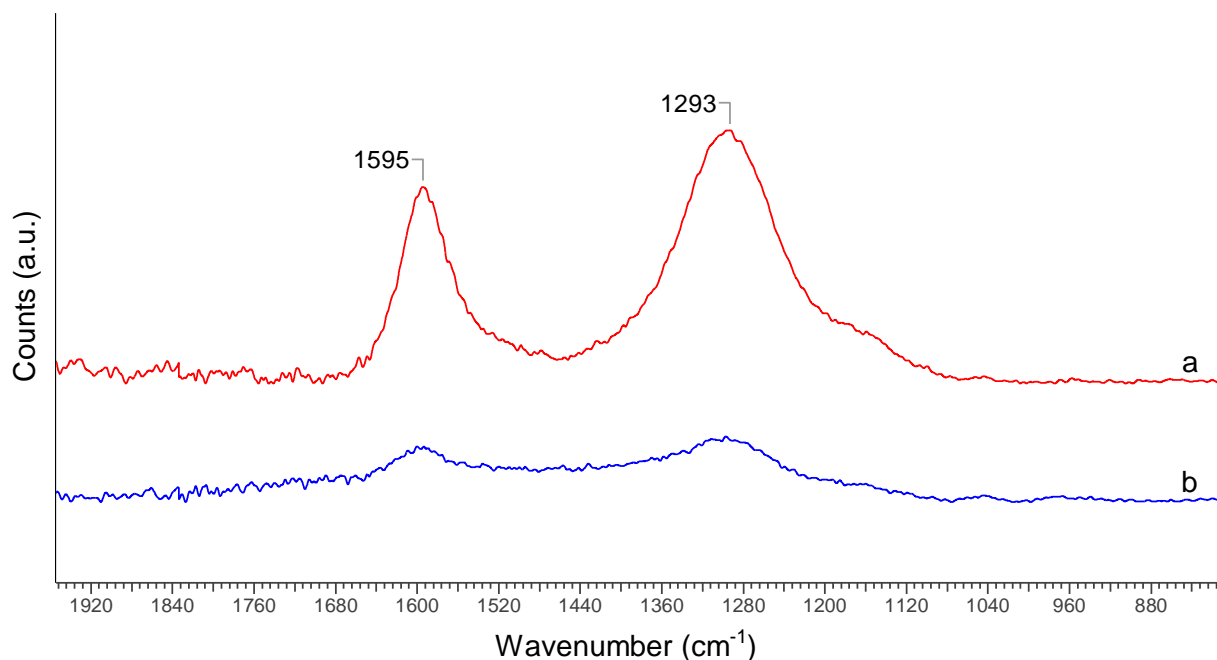
Figure 3.10: Raman spectra of (a) fresh and (b) spent activated carbons.

3.4.6 Thermogravimetric Analysis (TGA)-Differential Thermal Analysis (DTA)

Thermogravimetric analysis (TGA) was further used to compare the fresh and spent catalyst surfaces. Figure 3.11 shows the percentage weight losses (left axis) along with derivative weight loss curves (right axis) as a function of temperature for the fresh and spent catalysts under a N_2 atmosphere. The weight losses observed in the TGA profiles at temperatures of less than 200 ^{o}C are assigned to the removal of adsorbed water or gases from the environment or any easily removable carbonaceous species. The weight loss associated with the fresh catalyst corresponds to the removal of adsorbed water. The weight loss at temperatures of <600 ^{o}C for the spent catalyst corresponds to the easily removable amorphous carbonaceous species that were deposited on the catalyst surface during the decarboxylation reaction. These might be the cause for the observed reduction in catalyst surface area of the spent catalyst.
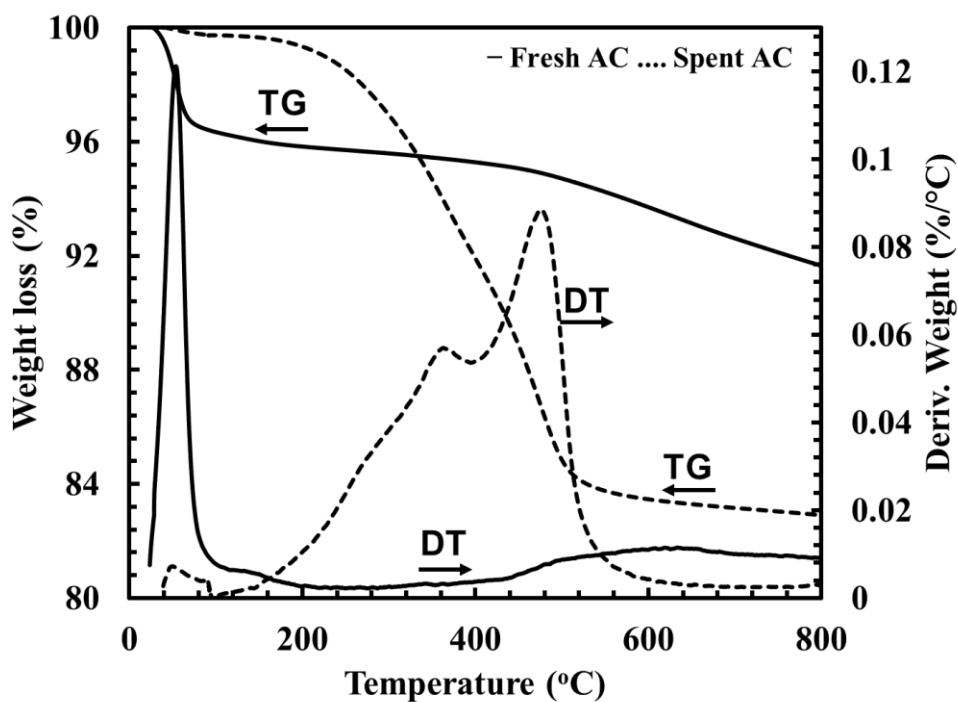
Figure 3.11: TGA (left axis)-DTA (right axis) profiles of fresh and spent activated carbons.

3.5 Kinetics of Oleic Acid Decarboxylation

The decarboxylation kinetics of oleic acid in a batch hydrothermal reactor in the presence of commercial activated carbon was studied under the following experimental conditions:

temperatures in the range from 350 to 400 ºC, reaction times varying from 0.5 to 2.0 h, a reaction pressure of 2200 psi (15.1 MPa), a water-to-oleic acid ratio of 4:1 (v/v), and a catalyst loading for each reaction of 5 g.

Kinetic studies was were performed based on the disappearance of the -COOH peak of oleic acid from ATR-FTIR spectrum. Pseudo-first-order rate constants were calculated from the disappearance of the -COOH peak from oleic acid at different times and temperatures. Figure 3.12(a) clearly shows a linear relationship indicating a pseudo-first-order reaction. The slope can be attributed to the reaction rate constant k which has a dependency on temperature, normally expressed using the Arrhenius equation

$$k = A\exp\left(\frac{-E}{RT}\right)$$
(3.1)

where, A is the pre-exponential factor, E is the activation energy, R is the universal gas constant, and T is the temperature in Kelvin. The activation energy is an important parameter for a chemical reaction as it represents how sensitive the rate of a chemical reaction to temperature. To calculate the activation energy, eqn. 3.1 was transformed into logarithmic form, which is plotted in Figure 3.12 (b).

$$\ln k = \ln A - \frac{E}{RT}$$
(3.2)
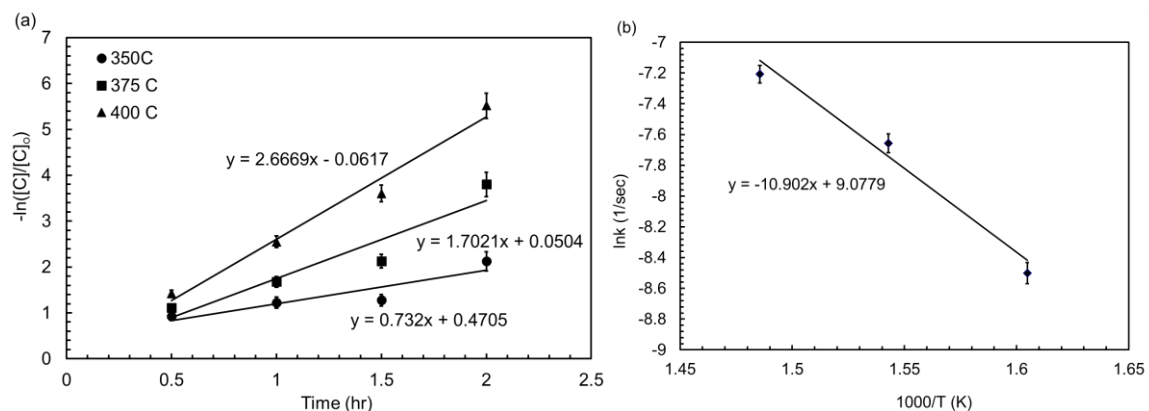
Figure 3.12: (a) Plot of $-\ln([C]/[C]_o)$ vs residence time for –COOH peak disappearance from oleic acid. (b) Effect of temperature on the rate of –COOH disappearance in Arrhenius form.

From the slope of Figure 3.12(b), the activation energy E was calculated to be 90.6 ± 3 kJ/mol. This value is 24.5% lower than the activation energy determined by Popov and Kumar [27] for the rapid hydrothermal deoxygenation of oleic acid over activated carbon in a continuous flow process and 38.8% lower than the activation energy (148 kJ/mol) calculated by Vam [45] who studied continuous deoxygenation of stearic acid diluted in C_{24} solvent in a fixed bed reactor over a Pd/C catalyst with H_2 added. In explanation, continuous stirring during the reaction as utilized in this work enhanced the mass transfer of the reactant molecules and catalyst active sites, enhancing the reaction rate. Because the current study was carried out in a batch hydrothermal stirred reactor, a lower activation energy was observed than in the preceding three studies.

3.6 Conclusions

The scalable hydrothermal decarboxylation of oleic acid under subcritical water conditions was demonstrated and examined in this work. Our study showed that it is possible to remove almost 100% of the carboxylic acid groups from oleic acid simply by heating the precursor with water under subcritical conditions and to produce saturated alkanes without adding any gaseous hydrogen or hydrogen donor solvent. The removal of oxygen from oleic acid as CO_2 was confirmed by ATR-FTIR spectroscopy and GC-FID. The absence of unsaturation in the product was also confirmed by NMR spectroscopy. The decarboxylated product can easily be used to replace conventional fuel because it has properties similar to those of conventional fuel. Our study also avoided using noble metal catalysts and chose activated carbon as a promising and inexpensive material for the hydrothermal decarboxylation of oleic acid. The products observed in this work were mainly alkanes instead of alkenes, with 81% selectivity to heptadecane. The optimum conditions for achieving diesel-like hydrocarbons from oleic acid were found to be 400 °C, reaction time of 2 h and a water-to-OA ratio of 4:1 and a stirring speed of 800 rpm.

The pseudo-first-order rate constant for the activated carbon-catalyzed decarboxylation of oleic acid displayed an Arrhenius activation energy of 90.6 ± 3 kJ/mol, which is lower than the values obtained in similar studies reported in the literature.

References

[1] H. Xin, K. Guo, D. Li, H. Yang, C. Hu, Production of high-grade diesel from palmitic acid over activated carbon-supported nickel phosphide catalysts, Applied Catalysis B: Environmental, 187 (2016) 375-385.

[2] A. Demirbaş, Biodiesel fuels from vegetable oils via catalytic and non-catalytic supercritical alcohol transesterifications and other methods: a survey, Energy conversion and Management, 44 (2003) 2093-2109.

[3] P. Bondioli, The preparation of fatty acid esters by means of catalytic reactions, Topics in Catalysis, 27 (2004) 77-82.

[4] M. Ahmadi, E.E. Macias, J.B. Jasinski, P. Ratnasamy, M.A. Carreon, Decarboxylation and further transformation of oleic acid over bifunctional, Pt/SAPO-11 catalyst and Pt/chloride Al2O3 catalysts, Journal of Molecular Catalysis A: Chemical, 386 (2014) 14-19.

[5] T.M. Yeh, R.L. Hockstad, S. Linic, P.E. Savage, Hydrothermal decarboxylation of unsaturated fatty acids over PtSnx/C catalysts, Fuel, 156 (2015) 219-224.

[6] T. Kalnes, T. Marker, D.R. Shonnard, Green diesel: a second generation biofuel, International Journal of Chemical Reactor Engineering, 5 (2007).

[7] D.Y. Murzin, P. Mäki-Arvela, Catalytic deoxygenation of fatty acids and their derivatives for the production of renewable diesel, in: Thermochemical Conversion of Biomass to Liquid Fuels and Chemicals, 2010, pp. 496-510.

[8] M. Snåre, I. Kubickova, P. Mäki-Arvela, K. Eränen, D.Y. Murzin, Heterogeneous catalytic deoxygenation of stearic acid for production of biodiesel, Industrial & engineering chemistry research, 45 (2006) 5708-5715.

[9] P. Natewong, Y. Murakami, H. Tani, K. Asami, Effect of Support Material on MgO-Based Catalyst for Production of New Hydrocarbon Bio-Diesel, American Scientific Research Journal for Engineering, Technology, and Sciences (ASRJETS), 22 (2016) 153-165.

[10] I. Simakova, O. Simakova, P. Mäki-Arvela, D.Y. Murzin, Decarboxylation of fatty acids over Pd supported on mesoporous carbon, Catalysis Today, 150 (2010) 28-31.

[11] E. Santillan-Jimenez, T. Morgan, J. Lacny, S. Mohapatra, M. Crocker, Catalytic deoxygenation of triglycerides and fatty acids to hydrocarbons over carbon-supported nickel, Fuel, 103 (2013) 1010-1017.

[12] P. Mäki-Arvela, I. Kubickova, M. Snåre, K. Eränen, D.Y. Murzin, Catalytic deoxygenation of fatty acids and their derivatives, Energy & Fuels, 21 (2007) 30-41.

[13] J. Wu, J. Shi, J. Fu, J.A. Leidl, Z. Hou, X. Lu, Catalytic Decarboxylation of Fatty Acids to Aviation Fuels over Nickel Supported on Activated Carbon, Scientific Reports, 6 (2016).

[14] N. Mo, W. Tandar, P.E. Savage, Aromatics from saturated and unsaturated fatty acids via zeolite catalysis in supercritical water, The Journal of Supercritical Fluids, 102 (2015) 73-79.

[15] W. Wagner, A. Pruß, The IAPWS formulation 1995 for the thermodynamic properties of ordinary water substance for general and scientific use, Journal of Physical and Chemical Reference Data, 31 (2002) 387-535.

[16] D.G. Archer, P. Wang, The Dielectric Constant of Water and Debye-Hückel Limiting Law Slopes, Journal of physical and chemical reference data, 19 (1990) 371-411.

[17] M. Watanabe, T. Sato, H. Inomata, R.L. Smith, K. Arai, A. Kruse, E. Dinjus, Chemical reactions of C1 compounds in near-critical and supercritical water, Chemical Reviews, 104 (2004) 5803-5822.

[18] I. Kubičková, M. Snåre, K. Eränen, P. Mäki-Arvela, D.Y. Murzin, Hydrocarbons for diesel fuel via decarboxylation of vegetable oils, Catalysis Today, 106 (2005) 197-200.

[19] M. Snåre, I. Kubičková, P. Mäki-Arvela, K. Eränen, J. Wärnå, D.Y. Murzin, Production of diesel fuel from renewable feeds: kinetics of ethyl stearate decarboxylation, Chemical Engineering Journal, 134 (2007) 29-34.

[20] P. Mäki-Arvela, M. Snåre, K. Eränen, J. Myllyoja, D.Y. Murzin, Continuous decarboxylation of lauric acid over Pd/C catalyst, Fuel, 87 (2008) 3543-3549.

[21] J. Fu, X. Lu, P.E. Savage, Hydrothermal decarboxylation and hydrogenation of fatty acids over Pt/C, ChemSusChem, 4 (2011) 481-486.

[22] J.-G. Na, B.E. Yi, J.K. Han, Y.-K. Oh, J.-H. Park, T.S. Jung, S.S. Han, H.C. Yoon, J.-N. Kim, H. Lee, Deoxygenation of microalgal oil into hydrocarbon with precious metal catalysts: Optimization of reaction conditions and supports, Energy, 47 (2012) 25-30.

[23] P.T. Do, M. Chiappero, L.L. Lobban, D.E. Resasco, Catalytic deoxygenation of methyl-octanoate and methyl-stearate on Pt/Al2O3, Catalysis Letters, 130 (2009) 9-18.

[24] Q. Tian, K. Qiao, F. Zhou, K. Chen, T. Wang, J. Fu, X. Lu, P. Ouyang, Direct Production of Aviation Fuel Range Hydrocarbons and Aromatics from Oleic Acid without an Added Hydrogen Donor, Energy & Fuels, 30 (2016) 7291-7297.

[25] S. Blakey, L. Rye, C.W. Wilson, Aviation gas turbine alternative fuels: A review, Proceedings of the combustion institute, 33 (2011) 2863-2885.

[26] J. Fu, F. Shi, L. Thompson Jr, X. Lu, P.E. Savage, Activated carbons for hydrothermal decarboxylation of fatty acids, ACS Catalysis, 1 (2011) 227-231.

[27] S. Popov, S. Kumar, Rapid hydrothermal deoxygenation of oleic acid over activated carbon in a continuous flow process, Energy & Fuels, 29 (2015) 3377-3384.

[28] E.A. Youssef, G. Nakhla, P.A. Charpentier, Oleic acid gasification over supported metal catalysts in supercritical water: hydrogen production and product distribution, International Journal of Hydrogen Energy, 36 (2011) 4830-4842.

[29] G. Akgül, A. Kruse, Influence of salts on the subcritical water-gas shift reaction, The Journal of Supercritical Fluids, 66 (2012) 207-214.

[30] J. Asomaning, P. Mussone, D.C. Bressler, Thermal deoxygenation and pyrolysis of oleic acid, Journal of Analytical and Applied Pyrolysis, 105 (2014) 1-7.

[31] T.D. Hong, T.H. Soerawidjaja, I.K. Reksowardojo, O. Fujita, Z. Duniani, M.X. Pham, A study on developing aviation biofuel for the Tropics: Production process—Experimental and theoretical evaluation of their blends with fossil kerosene, Chemical Engineering and Processing: Process Intensification, 74 (2013) 124-130.

[32] http://www.engineeringtoolbox.com/fuels-higher-calorific-values-d_169.html (accessed on July 8, 2016).

[33] Jet fuel: ASTM D1655-15d, Diesel: Petro-Canada MSDS (accessed on July 8, 2016).

[34] The Official Site of the National Biodiesel Board: Biodiesel.org (accessed on July 8, 2016).

[35] J.G. Immer, H.H. Lamb, Fed-batch catalytic deoxygenation of free fatty acids, Energy & Fuels, 10 (2010) 5291-5299.

[36] R.O. Idem, S.P. Katikaneni, N.N. Bakhshi, Thermal cracking of canola oil: reaction products in the presence and absence of steam, Energy & Fuels, 10 (1996) 1150-1162.

[37] A.O. Adebanjo, A.K. Dalai, N.N. Bakhshi, Production of diesel-like fuel and other value-added chemicals from pyrolysis of animal fat, Energy & fuels, 19 (2005) 1735-1741.

[38] D.H. Everett, R.A.W. Haul, L. Moscou, R. Pierrotti, J. Rouquerol, T. Siemienieswka, Reporting Physisorption Data for Gas/Solid Systems, Pure Appl. Chem, 57 (1985) 603.

[39] Y.-C. Chiang, P.-C. Chiang, C.-P. Huang, Effects of pore structure and temperature on VOC adsorption on activated carbon, Carbon, 39 (2001) 523-534.

[40] L. Geng, G. Yu, Y. Wang, Y. Zhu, Ph-SO 3 H-modified mesoporous carbon as an efficient catalyst for the esterification of oleic acid, Applied Catalysis A: General, 427 (2012) 137-144.

[41] M.B. Chowdhury, M.M. Hossain, P.A. Charpentier, Effect of supercritical water gasification treatment on Ni/La2O3-Al2O3-based catalysts, Applied Catalysis A: General, 405 (2011) 84-92.

[42] T. Budinova, E. Ekinci, F. Yardim, A. Grimm, E. Björnbom, V. Minkova, M. Goranova, Characterization and application of activated carbon produced by H 3 PO 4 and water vapor activation, Fuel Processing Technology, 87 (2006) 899-905.

[43] M. Seah, The quantitative analysis of surfaces by XPS: a review, Surface and Interface Analysis, 2 (1980) 222-239.

[44] R. Escribano, J. Sloan, N. Siddique, N. Sze, T. Dudev, Raman spectroscopy of carbon-containing particles, Vibrational Spectroscopy, 26 (2001) 179-186.

[45] V. Albert, Kinetics of the Hydro-Deoxygenation of Stearic Acid over Palladium on Carbon Catalyst in Fixed-Bed Reactor for the Production of Renewable Diesel, MS Thesis, University of Dayton, Dayton, OH, (2013).

Chapter 4

Continuous low pressure decarboxylation of fatty acids to fuel-range hydrocarbons with *insitu* hydrogen production[2]

Abstract

Fatty acids are considered as a renewable feedstock for the production of high value products such as fuel-range hydrocarbons. Decarboxylation can produce high quality fuels from fatty acids, although either high pressure or additional hydrogen is required. This study investigated a low pressure (<500 psi) continuous decarboxylation process examining oleic acid in a continuous fixed bed reactor using activated carbon, which gave surprisingly high quality fuel-like hydrocarbons with no external hydrogen. The results showed that activated carbon performed as a catalyst for both decarboxylation and *insitu* hydrogen production. The reaction parameters for maximum degree of decarboxylation (91%) was found to be 400 ºC, 2 h and water-to-oleic acid ratio of 4:1. To determine the degree of decarboxylation and reaction mechanism, the formed liquid products were examined by ATR-FTIR, Raman and GC-FID analysis, respectively. The liquid product was found to consist of mainly saturated hydrocarbons containing heptadecane (89.3% selectivity) as the major compound. The liquid product was found to have a similar density and higher heating value (HHV) to commercial diesel and jet fuel. The mechanism for decarboxylation reaction along with *insitu* hydrogen formation was proposed in this study.

4.1 Introduction

Energy security, sustainability and global climate change concerns resulting from society's energy consumption has increased our need to find renewable energy resources [1]. The large scale substitution of petroleum based fuels and products with those obtained from renewable sources is a major driving force towards sustainable development. Foremost among these concerns is the issue of the release and accumulation in the atmosphere of CO_2 and other climate-changing gases. Transportation fuel derived from renewable resources can be an alternative to reduce CO_2 emissions significantly since the largest source (27% in the Unites States [2]) of greenhouse gas emissions is from the burning of fossil fuels by transportation vehicles. Biodiesel (produced by the transesterification of triglycerides with methanol) is one of the most popular renewable transportation fuels which is currently used either as is, or blended with petroleum feedstocks. The chemical composition and physicochemical properties are very important for identifying the performance and emission characteristics of any fuel. Biodiesel is composed of a significant amount of oxygen containing molecules compared to conventional petroleum fuels [3]. Higher viscosity, cloud point and acid number of biodiesel can cause engine problems which prevent their usability in cold areas such as the northern US and Canada [4]. Biodiesel has much higher kinematic viscosity [5], NO_x emissions, oxidative stability and poor cold flow properties compared to conventional diesel [6, 7].

On the other hand, green diesel, which is essentially free of oxygen, is almost identical to petroleum diesel. Green diesel has higher heating value, higher energy density, and a very high Cetane number (80-90) compared to biodiesel [8, 9]. Fuel properties of biodiesel completely depend on the feedstock source and process configuration. In comparison, green diesel is independent of feedstock and the oxygen free liquid hydrocarbon fuel that is ready to use with conventional diesel fuel. UOP/ENI Ecofining™ process was the first commercial hydrodeoxygenation (HDO) technology to produce green diesel from biologically derived feedstocks [9]. Although HDO technology has been widely used to remove oxygen from various feedstocks to produce hydrocarbon fuels, it consumes expensive hydrogen gas [10, 11]. Additionally, HDO often requires expensive platinum or palladium catalysts [12-14].

As an alternative to HDO to produce oxygen free fuel range hydrocarbons, decarboxylation can be used. Decarboxylation is simply the removal of CO_2 from a fatty acid chain, normally

with the assistance of a catalyst. Depending on the reaction media and type of catalyst used [15-17], decarboxylation can potentially produce *insitu* hydrogen, although the mechanism is unclear. Although decarboxylation has mainly been studied using noble metal catalysts such as Pd or Pt in supercritical water [18-20], no report was available for complete decarboxylation until our previous study [15]. We showed that commercial activated carbon (AC) was an efficient and inexpensive catalyst for complete decarboxylation of oleic acid in a larger 300 mL stirred batch reactor. The final products were mainly straight chain hydrocarbons without an external source of hydrogen. This result motivated us to proceed to investigate this system in a continuous flow reactor, which would be required for commercial implementation.

The goal of the present study was to explore the one-step continuous decarboxylation of oleic acid (OA) into fuel range hydrocarbons in subcritical water using a fixed bed tubular reactor at relatively low operating pressure (<500 psi) with no added hydrogen. This study also investigates the source of *insitu* hydrogen required for carbon saturation. The quality of the liquid fuel products was measured and compared to commercial fuels.

4.2 Experimental section

4.2.1 Materials

90% pure oleic acid, powder activated carbon (AC-DARCO G-60, 100-325 mesh particle size), granular activated carbon (4-14 mesh particle size) and hexanes (ACS Grade) were obtained from Sigma-Aldrich, Oakville, ON, Canada, and are used as received. De-ionized water (18.2 MΩ) was taken from a compact ultrapure water system (EASY pure LF, Mandel Scientific Co., model BDI-D7381).

4.2.2 Experimental set-up

Hydrothermal decarboxylation of OA was conducted using a bench top continuous flow through reactor (BTRS-JR, Autoclave Engineers, Erie, PA) with a maximum operating pressure 2900 psi at 650 $^{\circ}$C. A simplified sketch of the BTRS-JR reaction system is shown in Figure 4.1. The system mainly consists of a fixed bed tubular reactor (I) with a furnace assembly (J), an oven (O) and a gas liquid separator (M). The reactor (316 stainless steel reactor tube with type 316 stainless steel fittings) dimension is 0.312" I.D. x 0.562" O.D. x 11" L. The

reactor was loaded with AC in each catalytic experiment. The reactor is connected to four feed lines i.e a total of four gases or two liquids or combination of both can be entered into the reactor. This study used only three feed lines (two for liquids such as OA and water, one for N_2 gas) which are shown in Figure 4.1. Two Isco 260DM syringe pumps (C) were used to feed OA (A) and water (B) continuously to the reactor. N_2 gas (D) was used only during the heating up the reactor with AC to prevent oxidation of carbon. A minimum flow of N_2 gas was maintained using metering valve because high flow rate of N_2 may blow out the catalyst which can plug the reactor system. N_2 flow was stopped after reaching the desired reaction temperature and kept the outlet valve open for few minutes to release N_2 before feeding the reactants. The feeds next enter the mixer vaporizer (H) where they are homogeneously mixed and vaporized. The furnace was used to heat up the reactor to obtain desired reaction temperature. The reactor with furnace assembly, feed mixture and system tubing and switching valves are all placed in a heated, insulated, stainless steel oven which allows good temperature control via the oven temperature set-point. The maximum operating temperature is 250 ℃. For this study, the oven temperature was maintained at 200 ℃. The gas-liquid separator (150 mL) is located outside the oven. The reactant/product gas enters the gas-liquid separator through a dip tube in the top with the product gas exiting through a tee in the top. The product gas was passed through a mass flow controller with totalizer (Q) (Omega Engineering Inc.) to quantify the amount of gas produced during decarboxylation of OA and stored in an air tight Tedlar gas bag (S) obtained from SKC Inc. (PA, USA) for further analysis. The separator was wrapped with copper coils for water cooling. A metering valve and air operated valve are connected to the bottom of the reactor to drain the liquid to a glass vial (T). After leaving the gas-liquid separator, the reactant/product stream passes through a back pressure regulator (N) to maintain the pressure set-point. System pressure was monitored by an isolated pressure gauge/transducer. System has a pressure sensor (K) at the top which helps for a sudden release of pressure through rupture disc (L) if the operating pressure exceeds the maximum allowable pressure of the system.
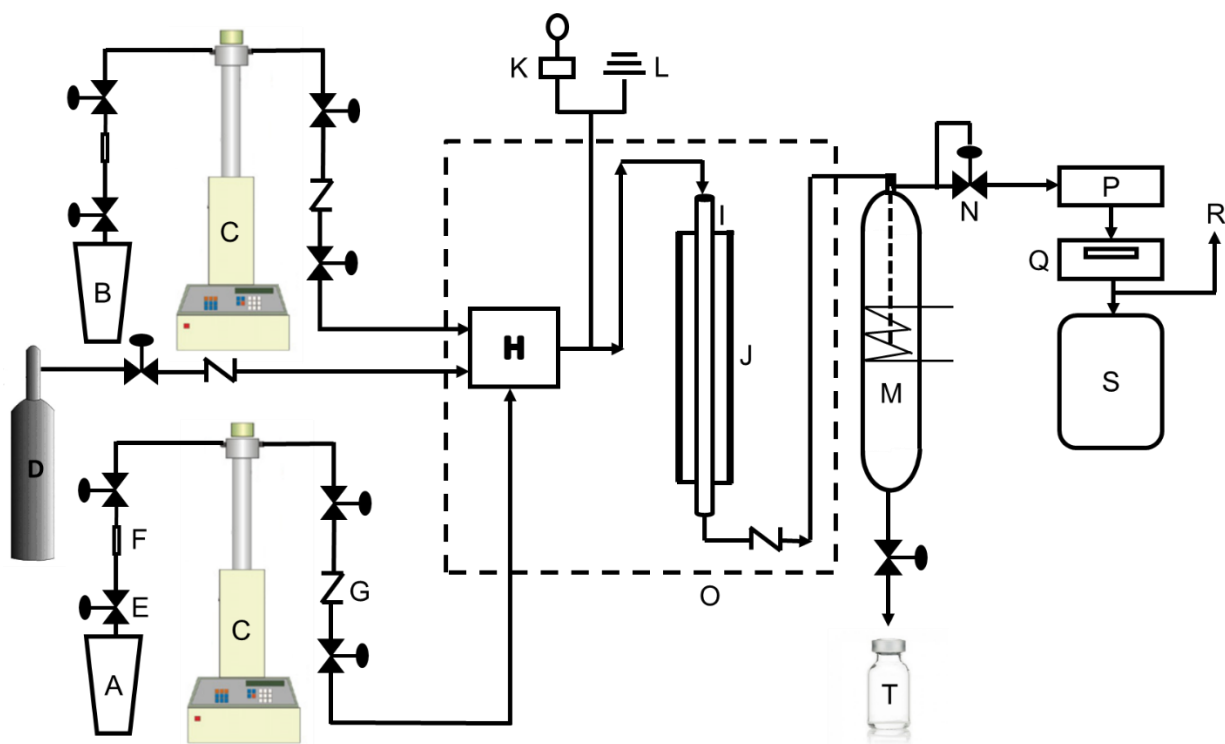
Figure 4.1: Schematic of Continuous Reactor Setup: (A) oleic acid tank, (B) H_2O tank, (C) Isco 260DM syringe pump, (D) N_2 cylinder, (E) gate valve, (F) & (P) filters, (G) check valve, (H) mixer vaporizer, (I) tubular reactor, (J) electric furnace, (K) pressure sensor, (L) rupture disk, (M) gas-liquid separator, (N) back pressure regulator, (O) oven, (Q) mass flow controller, (R) vent, (S) gas bag, (T) glass vial.

Before starting any experiment, the reactor and gas-liquid separator were washed thoroughly by injecting a minimum of 100 mL of hexanes to remove residuals from previous experiment and then purging with N_2 gas for a minimum of 15 min. Before feeding the reactants to the reactor, the outlet valve of the gas-liquid separator was opened several times during reactor heating (with nitrogen) to remove residual hexanes from the system to avoid contamination with the product.

The flow rates of reactants such as OA and water were determined for catalytic experiments by using the tapped density of powder AC (0.4 g/mL), space time (15 min to 2.5 h) and a water-to-OA ratio (v/v) (2:1 to 5:1) during the investigation. The space time is defined as follows:

$$Space\ time\ (\tau) = \frac{Volume\ of\ catalyst\ used\ in\ the\ reactor}{Volumetric\ flow\ rate\ of\ OA\ and\ water} \tag{4.1}$$

93

As for example, the calculated flow rates of H_2O and OA at 400ºC, 2 h of space time and 4:1 ratio of H_2O to OA were 0.0667 and 0.0167 mL/min, respectively. Volume of the reactor was used to calculate the space time for the noncatalytic experiments. AC loading for each of the catalytic experiments was 4g, which is the maximum loading capacity of the fixed bed reactor. Spent catalyst was removed from the reactor after each run and washed with hexanes to extract any produced product. The spent AC was dried in a vacuum oven at 80 ºC overnight.

4.2.3 Liquid and gaseous products analysis

Shimadzu, GC-2014 connected with a flame ionization detector (FID) and a capillary DB WAX column (Agilent Technologies, Santa Clara, CA, USA) (dimension: 30m x 0.250mm x 0.25μm, temperature limit: 20 to 260 ºC) was used to identify and quantify the compounds present in the liquid products by matching the gas chromatograph retention times (retention time is the time for a compound to travel through the chromatography column from injection to detection) with known standards (C8-C20 saturated hydrocarbons, heptadecene, oleic acid and stearic acid) obtained from Sigma-Aldrich, Oakville, ON. 1μL of sample was injected manually into the column with a 10:1 split ratio and was repeated at least 3X to minimize analytical error. Helium, hydrogen and helium-air were used as the carrier gas, flame gas and make-up, respectively. Selectivity of products were calculated as the peak area of an individual compound divided by the total peak area of all compounds of interest present in the liquid product. The GC oven temperature was programmed as follows: 3 min hold at 50 ºC, 10 ºC/min ramp at 250 ºC. The injector and detector temperature were maintained at 200 and 250 ºC, respectively.

ATR-FTIR spectroscope (Nicolet 6700 FTIR, Thermo Scientific) was used to obtain the infrared spectra of OA and liquid products. The spectra were recorded in the range of 600-4000 cm^{-1} with a resolution of 4 cm^{-1} over 64 scans. % removal of -COOH group was calculated from the peak (1707 cm^{-1}) areas of -COOH group in both reactants and liquid products as follows:

$$\% \, removal \, of - COOH \, group \, (Degree \, of \, decarboxylation) =$$
$$\frac{(Initial \, peak \, area \, of - COOH \, group \, in \, OA) - (Peak \, area \, of - COOH \, group \, in \, the \, liquid \, product)}{(Initial \, peak \, area \, of - COOH \, group \, in \, OA)} \, x \, 100 \, (4.2)$$

Raman spectroscopy measurements of OA and liquid products were performed using a Kaiser Optical Systems RXNI-785 with an excitation wavelength of 785 nm. The ATR-FTIR results were confirmed using Raman spectroscopy.

Density of the liquid products were measured using an Eagle Eye SG-Ultra Max Hydrometer (Density meter) (dimension = $5.5''W$ x $5.5''D$ x $1''H$ (outside)). Liquid products higher heating values (HHV) were measured using an IKA C2000 bomb calorimeter.

Gas chromatograph Shimadzu, GC-2014 equipped with a thermal conductivity detector (TCD) and a 120/80 Hayesep D (High purity divinylbenzene) packed column in nickel alloy tubing (3.18 mm ID, 6.2 m L) was used to quantify the gaseous products formed during decarboxylation using standard calibration gases (a mixture of H_2, N_2, O_2, CH_4, CO, CO_2) by injecting 1 mL of gas sample manually. Injection was repeated 3X to minimize any analytical error. SGE gas tight syringe (Model number 008100, Reno, NV USA) was used to inject the gas sample into the GC. Higher hydrocarbon gases (C2 to C4) were determined by subtracting the number of moles of known gas from the total no of moles of gas produced. The GC oven temperature was programmed as follows: 6 min hold at 35 ^{o}C, 25 ^{o}C/min ramp at 200 ^{o}C, 1 min hold at 200 ^{o}C. The injector and detector temperature were maintained at 200 and 250 ^{o}C, respectively with He used as the carrier gas.

4.2.4 Catalyst characterization

Tristar II 3020 (Micromeritics Instrument Corporation) was used to measure the specific surface area, pore diameter and pore volume of the fresh and spent AC using the Brunauer-Emmett-Teller (BET) and Barret-Joyner-Halenda (BJH) methods. A minimum of 80 mg of sample was degassed at 150 °C for 12 h before measurements to remove the moisture and other adsorbed gases from the catalyst surface. The analysis was performed at -193 °C using 99.995% pure N_2 gas obtained from Praxair (Oakville, Canada). A Bruker D2 Phaser powder diffractometer was used to study the crystal structure of the fresh and spent AC using Cu K_α radiation (λ for K_α is equal to 1.54059 Å) over 2θ = 10 - 80 using a scan rate 0.2 ^{o}/min. A TGA/SDT A851 model gravimetric analyzer was used to perform thermogravimetric analysis of catalyst samples with a heating rate of 10 ^{o}C/min from ambient temperature to 1000 ^{o}C in N_2 with a flow rate of 50 mL/min. ATR-FTIR spectroscope (Nicolet 6700 FTIR, Thermo Scientific OMNIC^{TM} software) was used to obtain infrared spectra of the fresh and spent AC.

4.3 Results and discussion

4.3.1 Effect of temperature, space time and water-to-OA ratio on degree of decarboxylation

The % removal of –COOH group is an important measure for green diesel production to determine the degree of decarboxylation. This was determined from the decrease in FTIR peak area of the –COOH group (1707 cm^{-1}) in oleic acid (OA) and from the formed liquid products at different reaction conditions using eqn. 4.2. The decarboxylation process is very sensitive to the reaction parameters including temperature, space time, water-to-OA ratio, and the type and amount of catalyst. To determine the reaction temperature to maximize the degree of decarboxylation and effect of catalyst, initial decarboxylation experiments were conducted at 300-400 °C, water-to-OA ratio of 4:1 and space time of 2 h, respectively. The degree of decarboxylation results are presented in Figure 4.2(a) and the corresponding ATR-FTIR spectra will be found in Fig. S1. The % removal of –COOH group was found to increase with increasing temperature from 300 to 400 °C without catalyst whereas the addition of catalyst greatly enhanced the removal of –COOH group during the reaction. The degree of decarboxylation increased from 18% at 300 °C to 45% at 400 °C for blank experiments whereas the values were 32% and 91% at 300 and 400 °C, respectively in the presence of catalyst. This result indicates that the catalyst plays an important role for increasing the degree of decarboxylation. Higher temperatures (400 °C) were favorable for achieving a higher degree of decarboxylation (91%) for the above mentioned process conditions.
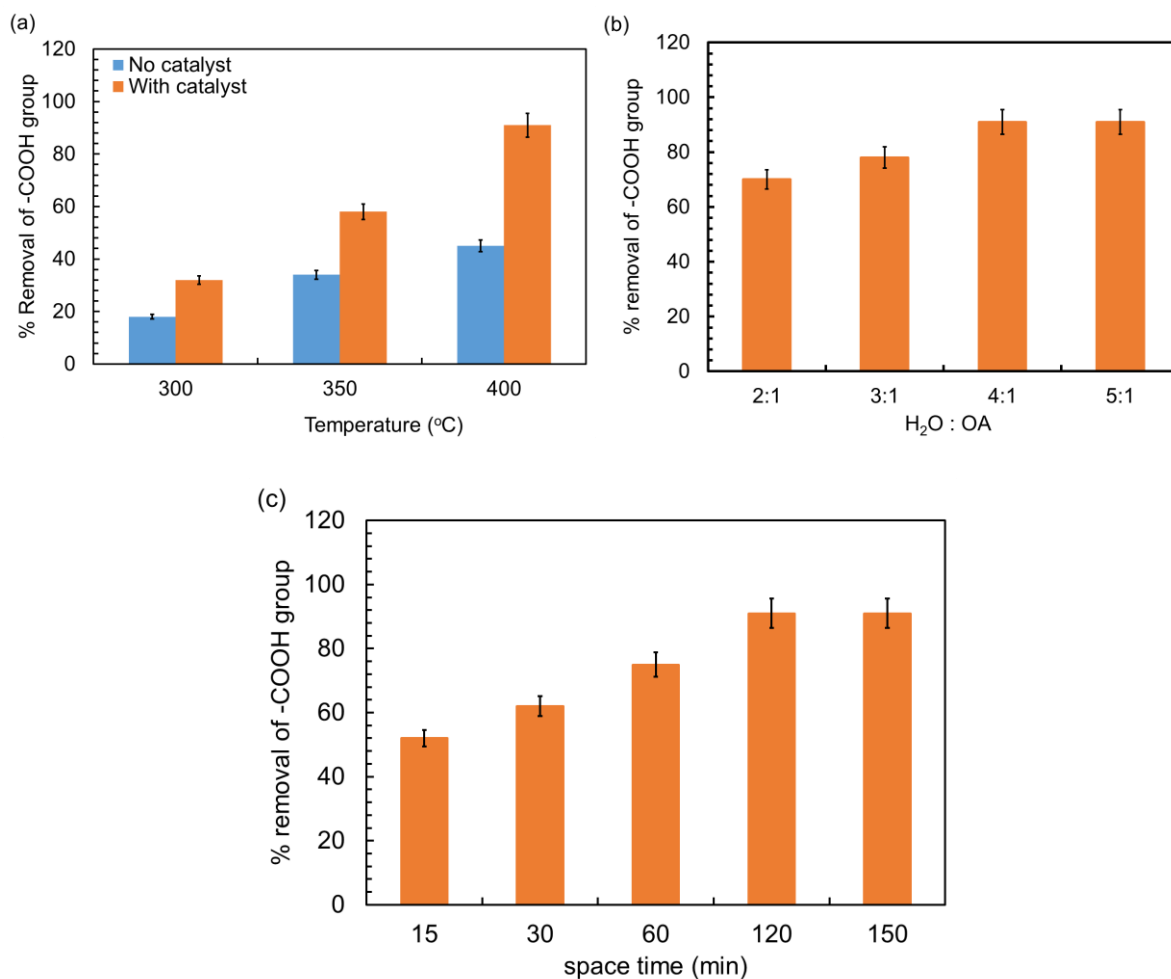
Figure 4.2: Degree of decarboxylation of oleic acid (a) without and with catalyst (b) different water-to-OA ratio at 400 ℃ and 120 min of space time in the presence of AC (c) different space times at 400 ℃ and water-to-OA ratio of 4:1 in the presence of AC.

Water-to-OA ratio and space time were optimized in the continuous fixed bed reactor for maximum removal of the –COOH group from OA by performing the experiments at 400 ℃ in the presence of catalyst. The degree of decarboxylation obtained at different water-to-OA ratios and space times are provided in Figure 4.2(b) & (c) and the corresponding ATR-FTIR spectra are shown in Figure 4.2. The degree of decarboxylation increased from 70 to 91% with increasing water-to-OA ratio from 2:1 to 4:1 at 400 ℃ and space time of 2 h using the catalyst. The decarboxylation increased from 52 to 91% with increasing space time from 15 min (0.25 h) to 2 h using a water-to-OA ratio of 4:1 at 400 ℃. Further increasing the space time from 2 to 2.5 h did not increase the degree of decarboxylation. Also, increasing the water-to-OA ratio

from 4:1 to 5:1 for 2 h space time did not improve the degree of decarboxylation further. Hence, the reaction conditions for maximum degree of decarboxylation of oleic acid in the continuous flow through reactor using catalyst in our study was at 400 °C, 2 h and water-to-OA ratio of 4:1.
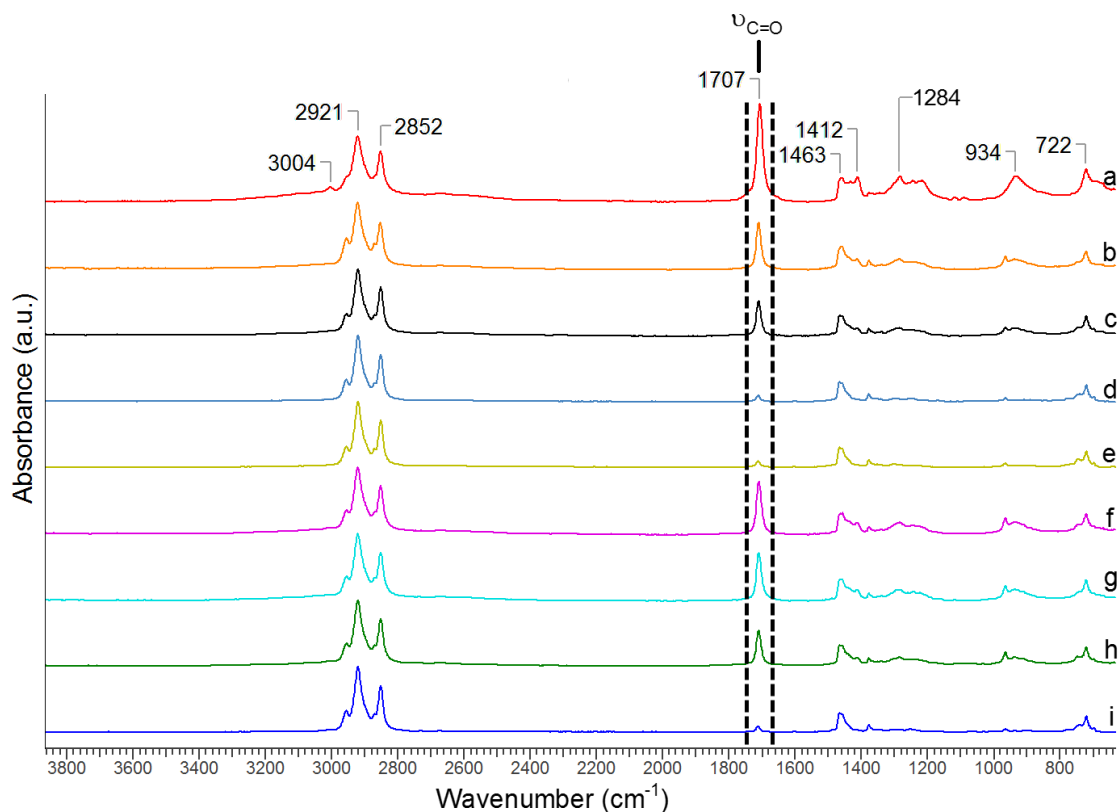
Figure 4.3: ATR-FTIR spectra of (a) oleic acid and the formed products after reactions under different conditions (water-to-OA ratio and space time) at 400 °C using (b) 2:1, 2 h; (c) 3:1, 2 h; (d) 4:1, 2 h; (e) 5:1, 2 h; (f) 4:1, 0.25 h; (g) 4:1, 0.5 h; (h) 4:1, 1 h; and (g) 4:1, 2.5 h.

The presence of alkenyl =CH stretching at 3004 cm^{-1} (Figure B1) for all non-catalytic reactions clearly shows that the reaction requires a catalyst to saturate the C=C bond. The disappearance of alkenyl =CH stretching for all catalytic reactions (Figure 4.3) implies that AC plays a significant role for both hydrogenation of C=C and decarboxylation. The peaks related to C-O stretching (1412 cm^{-1}), combination of C-O stretching and O-H deformation (1412 cm^{-1}) and O-H out of plane bending mode (934 cm^{-1}) also decrease significantly in the formed liquid

products compared to OA during the decarboxylation reaction. This also confirms the decarboxylation of oleic acid in the presence of catalyst.

Raman spectra of oleic acid and the decarboxylated liquid product (at reaction conditions for maximum degree of decarboxylation) were collected and are compared in Figure 4.4. The spectrum of oleic acid Figure 4.4a) shows a few major peaks at 3008, 1655, 1439 and 1302 cm^{-1}. The peaks at 3008 and 1655 cm^{-1} are attributed to the alkenyl =CH stretching and C=C stretching modes, respectively. The peak at 1439 cm^{-1} is assigned to CH_2 scissoring mode while the peak at 1302 cm^{-1} is attributable to CH_2 wagging and the carboxylic C-O stretching mode. After the decarboxylation reaction, the alkenyl peaks almost disappeared while the carboxylic C-O peak at 1302 cm^{-1} decreased significantly in comparison to the CH_2 scissoring peak at 1439 cm^{-1} (Figure 4.4b). These results are in good agreement with the FTIR results, confirming effective decarboxylation and hydrogenation of oleic acid using AC.
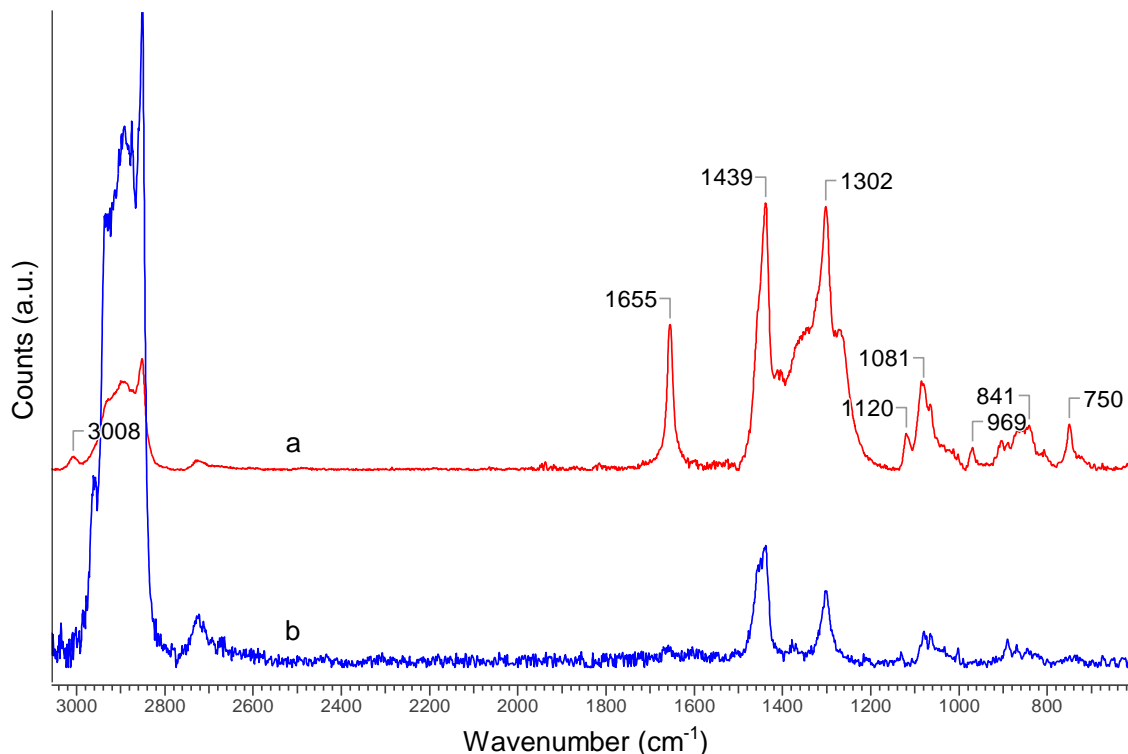
Figure 4.4: Raman Spectra of (a) oleic acid, and (b) the decarboxylated products obtained using AC.

4.3.2 Liquid product(s) quantification

It is very important to know the types of hydrocarbon compounds present in the decarboxylated liquid product for potential fuel use. Figure 4.5 shows the distribution of compounds present in the liquid products at different reaction conditions. Figure 4.5(a) and (b) compares the selectivity of the compounds present in the liquid products with and without catalyst at temperature ranges from 300-400 $^{\circ}$C, water-to-OA ratio of 4:1 and 2 h of space time. Figure 4.5(c) shows the distribution of products varying the ratio of water-to-OA from 2:1 to 4:1 at 400°C and 2 h of space time in the presence of AC. Figure 4.5(d) represents the distribution of compounds at different space times (0- 2 h) at 400°C and water-to-OA ratio of 4:1. The selectivity of heptadecane was found to increase with increasing temperature. A two-fold increase of heptadecane selectivity was observed using catalyst at the maximized reaction conditions when compared to no catalyst. 89.3% selectivity was achieved in the presence of AC at 400 $^{\circ}$C, 2 h of space time and water-to-OA ratio of 4:1 whereas the selectivity of heptadecane is only 44% for the non-catalytic decarboxylation reaction under identical conditions. On the other hand, the non-catalytic reaction was more favorable for higher selectivity of heptadecene instead of heptadecane compared to the catalytic reaction. The selectivity of heptadecene for blank experiments was 88 and 53% at 300 and 400 $^{\circ}$C whereas the values were significantly reduced with the addition of AC in both cases, i.e. 38 and 0.5%, respectively. This result indicates that the C=C group of heptadecene was not saturated due to a lack of hydrogen production without any catalyst. The source of *insitu* hydrogen is discussed in more details in section 4.3.4.
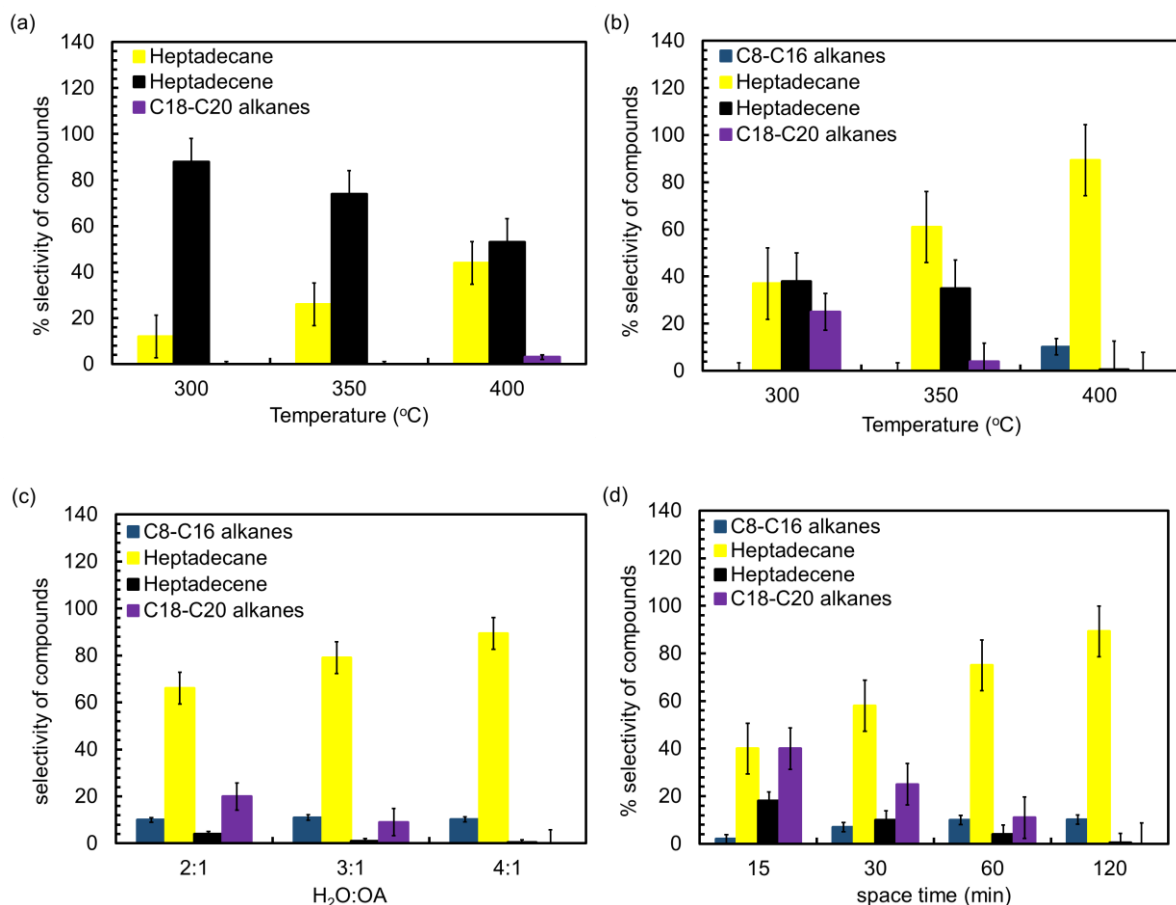
Figure 4.5: Distribution of compounds present in decarboxylated liquid products (a) without catalyst (b) with catalyst (c) at different water-to-OA ratio's at 400°C and 120 min space time in presence of AC (d) at different space times at 400°C and water-to-OA ratio of 4:1 in presence of AC.

Heptadecane selectivity was increased while its selectivity was decreased with increasing water-to-OA ratio and space time in the presence of AC. In the presence of catalyst, the selectivity of heptadecane and heptadecene were 66 % and 4 % respectively for water-to-OA ratio of 2:1 at 400°C and 2 h of space time, whereas the values were 89.3% and 0.5% respectively for water-to-OA ratio of 4:1 at identical conditions. 89.3% selectivity of heptadecane was obtained by increasing the space time from 15 min (40%) to 2 h in the presence of AC. The heptadecene selectivity significantly reduced from 18 to 0.5% by increasing the space time from 15 min to 2 h. The selectivity of C18 to C20 saturated hydrocarbons was found to be 3% at 400 °C without catalyst whereas the values are 25 and 0% at 300 and 400 °C respectively in the presence of AC. Increasing the water-to-OA ratios, the

selectivity of C8 to C16 remains almost constant and that of C18 to C20 decreased. Increasing the space time, the selectivity of C8 to C16 and C18 to C20 increased and decreased respectively using AC. Table 4.1 represents the composition of the hydrocarbons present in the liquid at maximized reaction conditions.

Table 4.1: Selectivity of the hydrocarbons present in the liquid product at maximized reaction conditions using AC.

compounds	Percentage selectivity (composition)
C8-C16 alkanes	10.2
heptadecane	89.3
heptadecene	0.5
C18-C20 alkanes	0.0

Since 91% degree of decarboxylation was achieved at the maximized reaction conditions and AC was hydrogenating OA into stearic acid, no peak was detected in GC-FID analysis for OA. 9.4% unconverted stearic acid was determined from the peak areas (before and after the decarboxylation reaction) of stearic acid in GC-TCD analysis. This result corroborates the ATR-FTIR results.

Table 4.2 compares the selectivity of heptadecane obtained from decarboxylation or deoxygenation of OA using available related literature data. Compared to the literature data, the current study achieved 89.3% selectivity of heptadecane during OA decarboxylation in subcritical water at 400ºC, 2 h of space time and water-to-OA ratio of 4:1. This is the highest selectivity reported in the open source literature without using an external source of hydrogen at moderate pressure. The final product obtained using the maximized conditions is mainly saturated hydrocarbon instead of unsaturated which indicates that H_2 was produced *insitu* during decarboxylation of OA in subcritical water and participated OA hydrogenation. Fu et al. [16] and Hossain et al. [15] previously showed the ability of hydrogenation using AC for hydrothermal decarboxylation of OA. Li et al. [21] found 96.2% selectivity of heptadecane during hydrodecarbonylation of OA in decalin which required hydrogen addition. Yang et al. [22] obtained 90.5±1.3% selectivity of heptadecane using 0.5%Pt/ZIF-67 membrane/Zeolite 5A bead. Pt was found to be a good catalyst for the decarboxylation reaction although it is expensive and is of less interest for industrial scale up. 63.5% liquid product yield was obtained

at the maximized conditions in this study (Figure B2). The mass balance was 100% for this experiment and was found to be 94 to 98% for all other experiments performed.

Table 4.2: Summary of literature data using different catalysts for OA decarboxylation or deoxygenation.

Catalyst	Reaction medium	Mode of operation	T (°C)	t (h)	H$_2$ source added (Yes/No)	Conversion (%)	Heptadecane selectivity (%)	Authors
AC	Subcritical water	Continuous	400	2	No	91	89.3	Current study
AC	Subcritical water	Batch	400	2	No	97	81	Hossain et al. [15]
AC	Near or Supercritical water	Continuous	370±2	0.35	Yes	99.4±0.5	80.6±4	Popov & Kumar [23]
AC	Near or supercritical water	Batch	370	3	No	80±4	7±1	Fu et al. [16]
Pt/C	High temperature water	Batch	330	2.5	No	68.9±8.8	9.2±2.8	Fu et al. [24]
14.8% Pd/carbon bead	Mesitylene	Batch	300	9	Yes	100	70.5	Dragu et al. [25]
14.8% Pd/carbon bead	Mesitylene	Batch	300	9	No	30	7	Dragu et al. [25]
10 wt% Ni/ZnO-Al$_2$O$_3$	Decalin	Batch	300	6	Yes	100	96.2	Li et al. [21]
5wt% Pt-SAPO-34	N/A	Batch	325	2	Yes	~100	66.9	Ahmadi et al. [26]
NiWC/Al-SBA-15	Supercritical water	Batch	400	4	No	30.7	0.72	Al Alwan et al. [27]
NiWC/Al-SBA-15	Subcritical water	Batch	350	4	No	35.8	0.01	Al Alwan et al. [27]
PtSn$_3$/C	Liquid water	Batch	350	2	No	~100	~60	Yeh et al. [28]
0.5%Pt/ZIF-67 membrane/Zeolite 5A bead	N/A	Batch	320	2	No	~100	90.5±1.3	Yang et al. [22]
0.5%Pt/ZIF-67 membrane/Zeolite 5A bead	N/A	Batch	320	2	Yes	~100	80.0±4.3	Yang et al. [22]
Pt/C	N/A	Batch	350	1.33	No	~100	71±2.4	Tian et al. [29]
1wt% Pt/zeolite 5A	N/A	Batch	320	2	No	98.74	72.6±2	Yang et al. [30]
1wt% Pt/ZIF67/zeolite 5A	N/A	Batch	320	2	No	98.74	81.5±3	Yang et al. [30]
5wt% Pt/Ga-MOF	N/A	Batch	320	2	No	91	21.5	Yang et al. [31]
MgO-Al$_2$O$_3$	N/A	Batch	400	3	No	88.1	6.1	Na et al. [32]

4.3.3 Fuel quality

Liquid density is an important characteristic used to provide information concerning composition, concentration, mass flow in fuels, and calorific content. The variation of density with temperature for the decarboxylated products at maximized reaction conditions is shown in Figure 4.6. The density of the decarboxylated products using AC decreased with increasing temperature. The density of some commercials fuels such as kerosene, diesel and jet fuel are 780-820 at 15.6 °C, 780-840 at 15 °C and 800-960 kg/m^3 at 15.6 °C, respectively [33, 34]. Compared to the commercial fuels, the density of decarboxylated product using AC at 15.6 °C was 784.3 kg/m^3 which falls between the kerosene and diesel range.
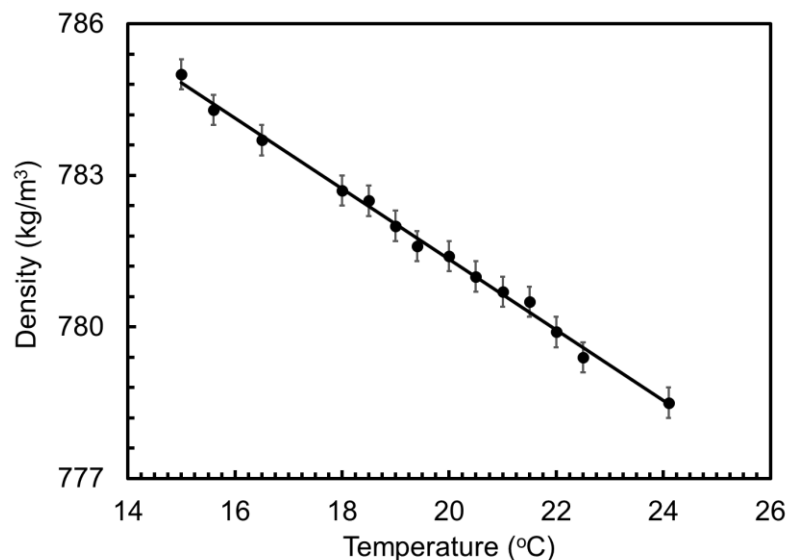
Figure 4.6: Variation of density over temperature for the decarboxylated product.

Higher heating value (HHV) of a liquid fuel is an important consideration when selecting it for a diesel engine. Engine efficiency is typically dependent on the heating values of the fuel. The calculated HHV values of the reactant (OA) and the decraboxylated products at maximized conditions using AC are 39.2 and 45.0 MJ/kg, respectively. The HHV's of several commercial fuels such as jet fuel, kerosene and diesel are 43.5, 46.2 and 44.8 MJ/kg, respectively [33, 35]. Comparing the HHV's of commercial fuels and decarboxylated product (Table 4.3) shows that the decarboxylated product was very close to jet fuel, kerosene and diesel.

Table 4.3: High heating values of feed, products and commercial fuels.

Compound	HHV's (MJ/kg)
Oleic acid	39.2
Decarboxylated product[*]	45.0
Jet fuel	43.5
Kerosene	46.2
Diesel	44.8

[*] maximized reaction conditions

4.3.4 Proposed reaction mechanism

4.3.4.1 Source of hydrogen determination and gaseous products quantification

Hydrogen is required for saturation of the C=C double bond of OA to produce alkanes as the product. Since no extra hydrogen was added in this study and heptadecane was the principal product, the source of *insitu* hydrogen is of interest. Two additional experiments were conducted using only water or OA in the presence of AC at 400°C to confirm the production of *insitu* hydrogen. No hydrogenation occurred in the absence of AC. When water was passed through the catalyst bed of AC, it produced hydrogen (Figure 4.7a). This observation indicates that AC acts as not only a catalyst but also as reactant for hydrogenation. By measuring the weight loss (~ 4.5 wt%) of AC catalyst after the decarboxylation reactions, it was found that only a small amount of AC was consumed as reactant (Figure B2). Water reacts with C to form CO and H_2 and CO further participates in the water gas shift reaction to produce H_2 and CO_2 as shown in Figure 4.7a. A significant amount of CH_4 was also formed in this reaction indicating that *insitu* H_2 participates in the methanation reaction. On the other hand, when OA was passed through the catalyst bed, OA was decomposed into a gaseous product stream containing CO, CO_2, H_2 and lighter hydrocarbons (HC's) (Figure 4.7b). Since water was absent in this reaction, a significant amount of CO was produced but in the decarboxylation reaction, CO may participate in the water gas shift reaction to produce additional H_2. Asomaning et al. [36] also showed H_2 production during pyrolysis of OA.
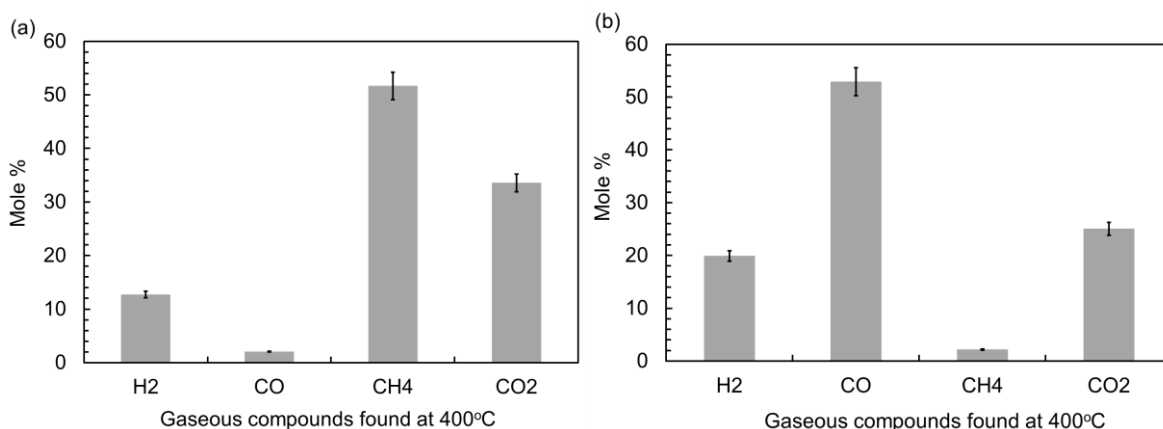
Figure 4.7: Gaseous products formed at 400°C; reaction of (a) H_2O with AC and (b) OA with AC.

Removal of CO_2 from OA via decarboxylation was confirmed by performing gas analysis using GC-TCD. Figure 4.8 depicts the number of moles of CO_2 and CO present in the gases produced at (a) different temperatures for water-to-OA ratio = 4:1 and space time = 2 h; (b) different water-to-OA ratios at 400°C and 2 h space time in presence of AC. The moles of CO_2 increased with increasing temperature and ratio of water-to-OA whereas the moles of CO decreased indicating that decarboxylation is the dominant reaction at 400°C, water-to-OA ratio = 4:1 and space time = 2 h in the presence of AC. The number of moles of CO_2 and CO found at maximixed conditions were 93 and 5 mol % using AC. GC-TCD results are consistent with the ATR-FTIR results. Other gases were also found at significantly lower amounts in the decarboxylation gas stream. Small amounts of H_2 gas were obtained in the gaseous products which may be from the leftover H_2 after the hydrogenation reaction. Lighter fractions of hydrocarbons along with CH_4 were also detected by GC-TCD (data not shown). Mass balance at the maximized reaction conditions showed the amount of individual gases produced during the decarboxylation reaction for this condition (Fig. S2).
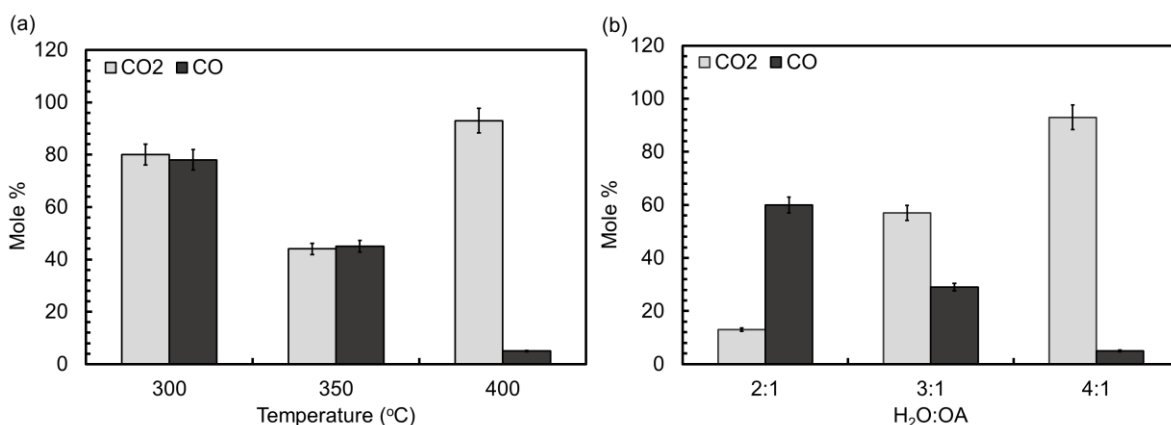
Figure 4.8: Mole percent of CO_2 and CO present in the gas fractions during OA decarboxylation (a) at different temperatures (b) at different ratio's at 400°C.

4.3.4.2 Decarboxylation pathways

A proposed reaction mechanism of hydrothermal decarboxylation of OA is shown in scheme 4.1. Since the final product is mainly saturated hydrocarbon, the hydrogenation and decarboxylation reactions are occurring simultaneously in the presence of AC. Hydrogenation of OA was accomplished by *insitu* hydrogen produced via carbon reforming and thermal

cracking (as described earlier) during decarboxylation reaction over AC. Therefore, H_2 is produced from two parallel sources in sufficient amounts to hydrogenate OA into stearic acid. The intermediate product such as stearic acid was then decarboxylated into straight chain heptadecane.

i. $\quad C + H_2O \longrightarrow CO + H_2$

$$CO + H_2O \underset{\text{water gas shift}}{\rightleftharpoons} CO_2 + H_2$$

$$C_{17}H_{35}COOH \xrightarrow{\text{Thermal cracking}} CO + CO_2 + H_2 + \text{lighter HC's}$$

ii. $\quad C_{17}H_{33}COOH + H_2 \xrightarrow{\text{Hydrogenation}} C_{17}H_{35}COOH$

iii. $\quad C_{17}H_{35}COOH \xrightarrow{\text{Decarboxylation}} C_{17}H_{36} + CO_2$
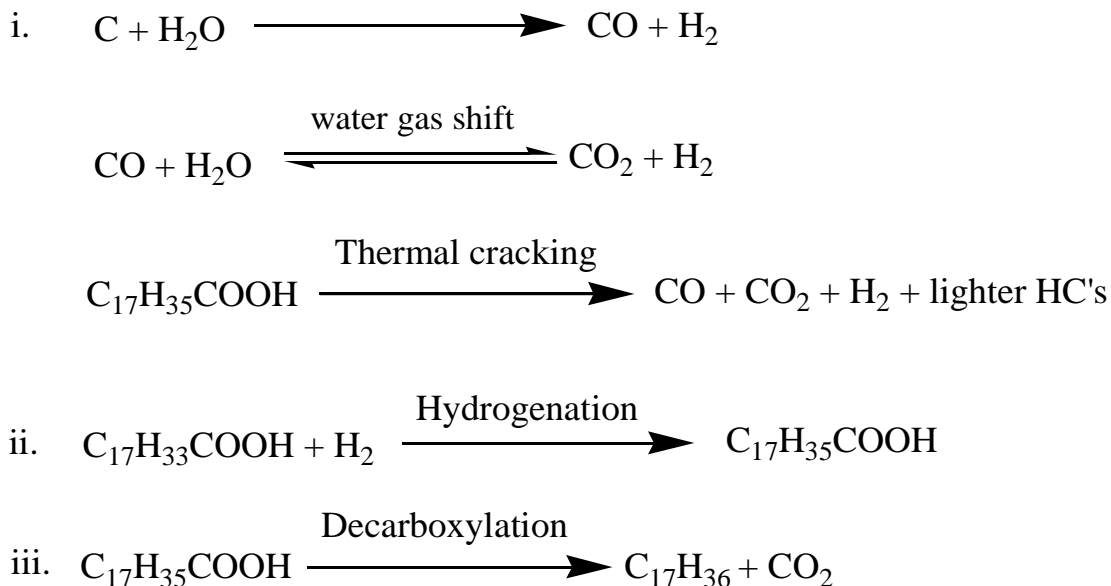
Scheme 4.1. Hydrothermal decarboxylation mechanism of OA over AC.

Using the fixed-bed continuous reactor, the results in this work showed a maximum decarboxylation of 91%, whereas our previous batch results were found to provide 97% removal [15]. This may be due to both the process and reaction dynamics of the system.

4.3.5 Characterizations of fresh and spent catalysts

BET surface area and pore size distribution of any catalyst are crucial to predict its catalytic activity. Higher BET surface area and porosity of the catalyst provides more active sites for a reaction to enhance its catalytic activity. Table 4.4 shows the textural properties of fresh and spent AC, respectively. The results indicate that the spent catalysts lost their surface area and pore volume significantly compared to fresh catalyst, due to the longer reaction time (minimum 24 h). The average pore sizes of all the catalysts are quite similar, indicating that the pores did not collapse during the decarboxylation reaction.

Table 4.4: Textural Properties of AC.

Name of the samples	BET surface area (m^2/g)	Pore volume (cm^3/g)	Average Pore diameter (nm)
Fresh AC	857	0.63	3.5
Spent AC	159	0.20	3.7

Crystallinity of fresh and spent AC were obtained by performing XRD analysis. XRD patterns of the AC samples are shown in Figure 4.9. The XRD pattern of fresh and spent AC indicate their amorphous nature [23]. There was no peak found in the XRD pattern for graphitic coke deposition in the spent AC during decarboxylation of OA, which usually appears at 29.84 and 61.92° [37, 38]. No graphitic coke deposition was obtained as also confirmed by TG-DTA analysis of the spent AC (Figure 4.10). Weight losses observed in the TG-DTA spectra of both fresh and spent AC corresponds to the removal of moisture and adsorbed molecules.
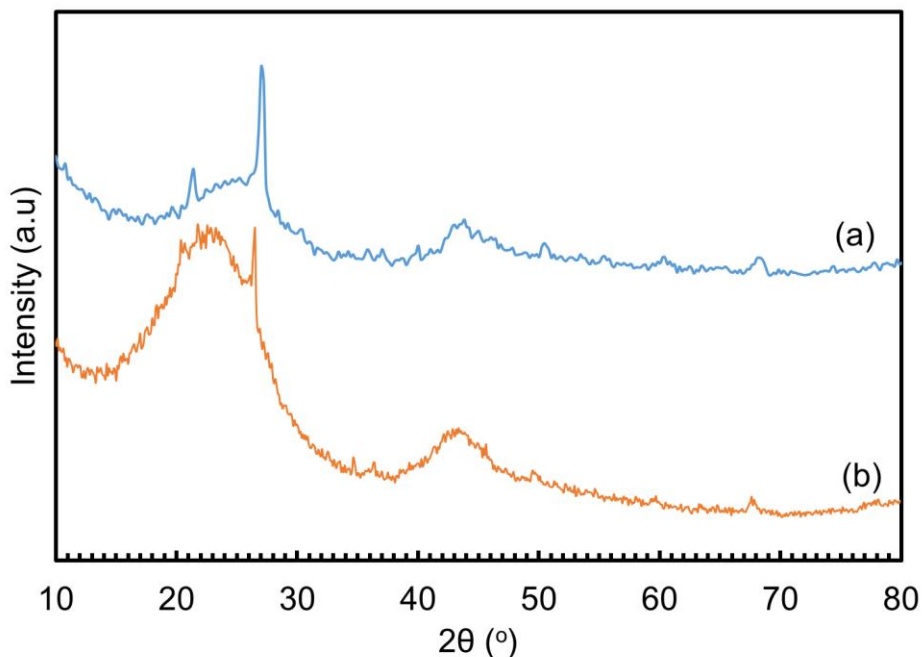
Figure 4.9: XRD patterns of (a) fresh and (b) spent AC.
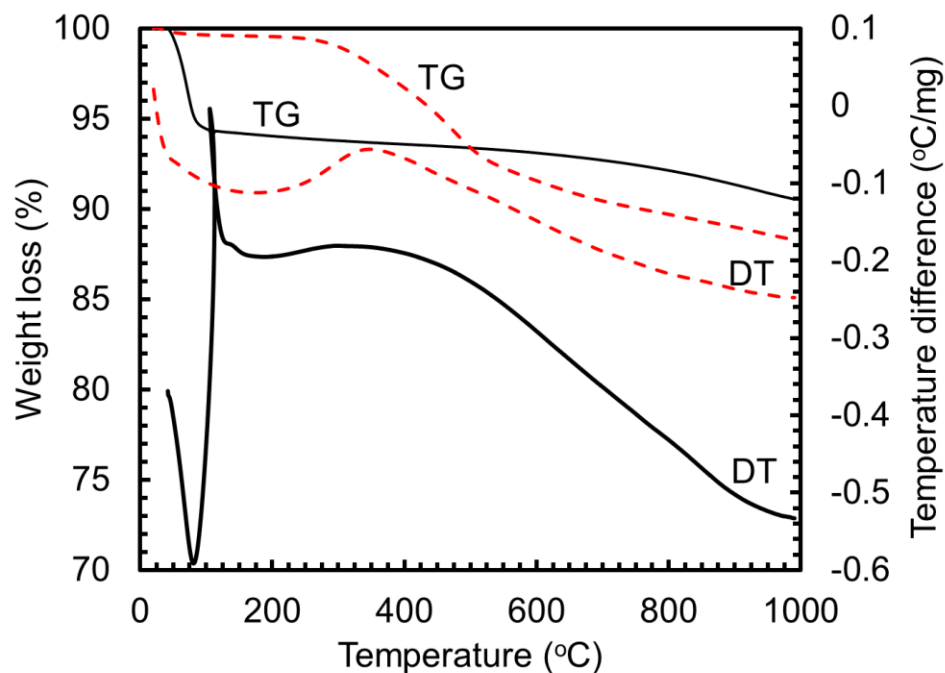
Figure 4.10: TG-DTA analysis of fresh (black line) and spent (red line) AC.

The surface functional groups are sometimes important for catalytic activity of AC which were characterized by ATR-FTIR. Due to the low concentration of functional groups, no significant surface functional groups were found in the spectra of fresh and spent AC (data not shown). The catalytic activity of AC mainly accounts from the large surface area and pore volume.

A preliminary test of the stability of the AC was measured by conducting an additional 45 h time on stream decarboxylation experiment using the maximized conditions. The results indicate that the AC started deactivating after 30 h and was completely deactivated at 45 h time of stream. The degree of decarboxylation dropped from 91 at 10 h to 60% at 40 h whereas the values was 50% after 45 h. Details about the deactivation of AC mechanism and its effect on hydrocarbon selectivity and fuel value will be discussed in Chapter 5.

4.4 Conclusion

Low pressure continuous hydrothermal decarboxylation of oleic acid was investigated in a fixed bed tubular reactor without adding external hydrogen to produce fuel range hydrocarbons

in the presence of activated carbon catalyst. 91% conversion of oleic acid was obtained at the maximized reaction conditions at 400ºC, 2 h of space time and water-to-oleic acid ratio of 4:1. It was found that *insitu* hydrogen was participating for hydrogenation of liquid products in the decarboxylation reaction. The liquid product was found to mainly contain saturated hydrocarbons, especially heptadecane with 89.3% selectivity. Liquid product can easily be replaced/blended with conventional diesel fuel as it has the identical properties of conventional fuels.

References

[1] S. Chu, A. Majumdar, Opportunities and challenges for a sustainable energy future, nature, 488 (2012) 294-303.

[2] United States Environnmental Protection Agency (accessed on 24 April, 2017).

[3] G. Knothe, K.R. Steidley, Kinematic viscosity of biodiesel fuel components and related compounds. Influence of compound structure and comparison to petrodiesel fuel components, Fuel, 84 (2005) 1059-1065.

[4] A. Centeno, E. Laurent, B. Delmon, Influence of the support of CoMo sulfide catalysts and of the addition of potassium and platinum on the catalytic performances for the hydrodeoxygenation of carbonyl, carboxyl, and guaiacol-type molecules, Journal of Catalysis, 154 (1995) 288-298.

[5] A. Demirbas, Biodiesel production via non-catalytic SCF method and biodiesel fuel characteristics, Energy conversion and Management, 47 (2006) 2271-2282.

[6] R. Lin, Y. Zhu, L.L. Tavlarides, Effect of thermal decomposition on biodiesel viscosity and cold flow property, Fuel, 117 (2014) 981-988.

[7] K. Anand, R. Sharma, P. Mehta, Experimental investigations on combustion, performance, and emissions characteristics of a neat biodiesel-fuelled, turbocharged, direct injection diesel engine, Proceedings of the Institution of Mechanical Engineers, Part D: Journal of Automobile Engineering, 224 (2010) 661-679.

[8] T. Kalnes, T. Marker, D.R. Shonnard, Green diesel: a second generation biofuel, International Journal of Chemical Reactor Engineering, 5 (2007).

[9] J. Holmgren, C. Gosling, T. Marker, P. Kokayeff, G. Faraci, C. Perego, E.S. Refining, Green diesel production from vegetable oil, in: 2007 Spring AIChE Conference, 2007.

[10] M. Toba, Y. Abe, H. Kuramochi, M. Osako, T. Mochizuki, Y. Yoshimura, Hydrodeoxygenation of waste vegetable oil over sulfide catalysts, Catalysis Today, 164 (2011) 533-537.

[11] Y. Sugami, E. Minami, S. Saka, Renewable diesel production from rapeseed oil with hydrothermal hydrogenation and subsequent decarboxylation, Fuel, 166 (2016) 376-381.

[12] H. Ohta, H. Kobayashi, K. Hara, A. Fukuoka, Hydrodeoxygenation of phenols as lignin models under acid-free conditions with carbon-supported platinum catalysts, Chemical Communications, 47 (2011) 12209-12211.

[13] L. Faba, E. Díaz, A. Vega, S. Ordóñez, Hydrodeoxygenation of furfural-acetone condensation adducts to tridecane over platinum catalysts, Catalysis Today, 269 (2016) 132-139.

[14] C. Liu, J. Sun, H.M. Brown, O.G. Marin-Flores, J.T. Bays, A.M. Karim, Y. Wang, Aqueous phase hydrodeoxygenation of polyols over Pd/WO 3-ZrO 2: Role of Pd-WO 3 interaction and hydrodeoxygenation pathway, Catalysis Today, 269 (2016) 103-109.

[15] M.Z. Hossain, A.K. Jhawar, M.B. Chowdhury, W.Z. Xu, W. Wu, D. Hiscott, P.A. Charpentier, Using subcritical water for decarboxylation of oleic acid into fuel range hydrocarbons, Energy & Fuels, 31 (2017) 4013-4023.

[16] J. Fu, F. Shi, L. Thompson Jr, X. Lu, P.E. Savage, Activated carbons for hydrothermal decarboxylation of fatty acids, ACS Catalysis, 1 (2011) 227-231.

[17] J. Fu, X. Lu, P.E. Savage, Catalytic hydrothermal deoxygenation of palmitic acid, Energy & Environmental Science, 3 (2010) 311-317.

[18] P. Mäki-Arvela, I. Kubickova, M. Snåre, K. Eränen, D.Y. Murzin, Catalytic deoxygenation of fatty acids and their derivatives, Energy & Fuels, 21 (2007) 30-41.

[19] I. Simakova, O. Simakova, P. Mäki-Arvela, D.Y. Murzin, Decarboxylation of fatty acids over Pd supported on mesoporous carbon, Catalysis Today, 150 (2010) 28-31.

[20] M. Snåre, I. Kubičková, P. Mäki-Arvela, K. Eränen, J. Wärnå, D.Y. Murzin, Production of diesel fuel from renewable feeds: kinetics of ethyl stearate decarboxylation, Chemical Engineering Journal, 134 (2007) 29-34.

[21] G. Li, F. Zhang, L. Chen, C. Zhang, H. Huang, X. Li, Highly Selective Hydrodecarbonylation of Oleic Acid into n-Heptadecane over a Supported Nickel/Zinc Oxide–Alumina Catalyst, ChemCatChem, 7 (2015) 2646-2653.

[22] L. Yang, M.A. Carreon, Effect of reaction parameters on the decarboxylation of oleic acid over Pt/ZIF-67membrane/zeolite 5A bead catalysts, Journal of Chemical Technology and Biotechnology, 92 (2017) 52-58.

[23] S. Popov, S. Kumar, Rapid hydrothermal deoxygenation of oleic acid over activated carbon in a continuous flow process, Energy & Fuels, 29 (2015) 3377-3384.

[24] J. Fu, X. Lu, P.E. Savage, Hydrothermal decarboxylation and hydrogenation of fatty acids over Pt/C, ChemSusChem, 4 (2011) 481-486.

[25] A. Dragu, S. Kinayyigit, E. García-Suárez, M. Florea, E. Stepan, S. Velea, L. Tanase, V. Collière, K. Philippot, P. Granger, Deoxygenation of oleic acid: Influence of the synthesis route of Pd/mesoporous carbon nanocatalysts onto their activity and selectivity, Applied Catalysis A: General, 504 (2015) 81-91.

[26] M. Ahmadi, A. Nambo, J. Jasinski, P. Ratnasamy, M. Carreon, Decarboxylation of oleic acid over Pt catalysts supported on small-pore zeolites and hydrotalcite, Catalysis Science & Technology, 5 (2015) 380-388.

[27] B. Al Alwan, S.O. Salley, K.S. Ng, Biofuels production from hydrothermal decarboxylation of oleic acid and soybean oil over Ni-based transition metal carbides supported on Al-SBA-15, Applied Catalysis A: General, 498 (2015) 32-40.

[28] T.M. Yeh, R.L. Hockstad, S. Linic, P.E. Savage, Hydrothermal decarboxylation of unsaturated fatty acids over PtSnx/C catalysts, Fuel, 156 (2015) 219-224.

[29] Q. Tian, K. Qiao, F. Zhou, K. Chen, T. Wang, J. Fu, X. Lu, P. Ouyang, Direct Production of Aviation Fuel Range Hydrocarbons and Aromatics from Oleic Acid without an Added Hydrogen Donor, Energy & Fuels, 30 (2016) 7291-7297.

[30] L. Yang, K.L. Tate, J.B. Jasinski, M.A. Carreon, Decarboxylation of oleic acid to heptadecane over Pt supported on zeolite 5A beads, ACS Catalysis, 5 (2015) 6497-6502.

[31] L. Yang, G. Ruess, M. Carreon, Cu, Al and Ga based metal organic framework catalysts for the decarboxylation of oleic acid, Catalysis Science & Technology, 5 (2015) 2777-2782.

[32] J.-G. Na, B.E. Yi, J.N. Kim, K.B. Yi, S.-Y. Park, J.-H. Park, J.-N. Kim, C.H. Ko, Hydrocarbon production from decarboxylation of fatty acid without hydrogen, Catalysis Today, 156 (2010) 44-48.

[33] http://www.engineeringtoolbox.com/fuels-higher-calorific-values-d_169.html (accessed on April 19, 2017).

[34] Jet fuel: ASTM D1655-15d, Diesel: Petro-Canada MSDS (accessed on April 19, 2017).

[35] The Official Site of the National Biodiesel Board: Biodiesel.org (accessed on April 19, 2017).

[36] J. Asomaning, P. Mussone, D.C. Bressler, Thermal deoxygenation and pyrolysis of oleic acid, Journal of Analytical and Applied Pyrolysis, 105 (2014) 1-7.

[37] M.B. Chowdhury, M.M. Hossain, P.A. Charpentier, Effect of supercritical water gasification treatment on Ni/La 2 O 3-Al 2 O 3-based catalysts, Applied Catalysis A: General, 405 (2011) 84-92.

[38] M.Z. Hossain, M.B. Chowdhury, Q. Alsharari, A.K. Jhawar, P.A. Charpentier, Effect of mesoporosity of bimetallic Ni-Ru-Al 2 O 3 catalysts for hydrogen production during supercritical water gasification of glucose, Fuel Processing Technology, 159 (2017) 55-66.

Chapter 5

Deactivation and regeneration studies of activated carbon during continuous decarboxylation of oleic acid in subcritical water

Abstract

Activated carbon (AC) is a low cost commercial catalyst which has been found effective for decarboxylation of fatty acids in sub or supercritical water. However, catalyst deactivation and regeneration is a major challenge which has not been addressed. This work investigated for the first time the underlying mechanism of deactivation of AC to provide a deeper understanding of the active sites and catalytic mechanism during hydrothermal decarboxylation of oleic acid. The products obtained from the decarboxylation with AC contained mainly straight chain hydrocarbons with the AC becoming deactivated after 30 h on stream at 400 ^{o}C, water-to-oleic acid ratio of 4:1, space time of 2 h. The thermal regeneration of deactivated AC was also examined using potassium hydroxide (KOH) treatment at 750 ^{o}C which helped to regain the physical properties of fresh AC. Deactivation and regeneration of used AC was confirmed by various physico-chemical techniques such as BET surface area, XRD, ATR-FTIR, Raman, XPS and SEM. The results showed that 87% of BET surface area was reobtained by regeneration using activated carbon under KOH treatment at high temperature, with the re-AC actively decarboxylating oleic acid in hydrothermal media. Deactivation was found to occur due to deposition of impurities during the decarboxylation reaction which blocks the pores of AC. The degrees of decarboxylation of oleic acid using fresh and regenerated activated carbon were 91% and 87%, respectively. On the other hand, the selectivity of heptadecane obtained using fresh and regenerated activated carbon was 89.3% and 81.2%, respectively. Decarboxylated liquid products using fresh and regenerated activated carbon have the similar density and HHV's as commercial fuels.

5.1 Introduction

The increasing number of worldwide transportation vehicles and raising environmental concerns related to conventional fuels has led to the urgent need to find renewable transportation fuels [1]. Transesterification of fats or oils to produce fatty acid methyl esters (FAME) is a well-known process for renewable biodiesel production [2]. However, biodiesel is not suitable for use in cold countries because of its higher cloud point and higher viscosity compared to convention fuels [3]. These poorer properties compared to conventional fuels is primarily due to the difference in molecular structure containing oxygen moieties (e.g. –COOH groups). Removal of oxygen from biodiesel can improve its stability for enhancing its integration into the fuel value chain. The hydrodeoxygenation (HDO) process was used to remove oxygen from lipids but the process consumes excess hydrogen [4]. Decarboxylation is an alternative of HDO which does not require hydrogen [5-7].

The decarboxylation process normally requires catalysts to produce higher selectivity of liquid hydrocarbons. The most efficient decarboxylation catalysts reported in the literature are precious metals such as Pt and Pd [8-10]. However, due to their rarity and high cost, alternatives such as metal catalysts or activated carbon are of interest. Transition metal catalysts have been shown to enhance mainly the cracking reactions instead of the decarboxylation reaction, leading to a lower liquid hydrocarbon yield [11, 12]. Activated carbon (AC) was found to be a very effective low cost catalyst for hydrothermal decarboxylation of fatty acids and their derivatives [5, 7, 13]. Medina et al. [14] reported that the activity of AC depends on its surface area and surface based oxygenated functional groups. Popov and Kumar [13] had similar findings for hydrothermal decarboxylation of oleic acid in a continuous flow process in the presence of AC. Fu et al. [7] and Hossain et al. [5, 15] demonstrated that the activity of AC is associated with its large surface area and narrow pore size distribution. However, very limited information is available in the literature for deactivation and regeneration studies of AC as catalyst. Any catalyst has a limited life time to participate in the reaction effectively which is a major drawback to use it commercially.

Another issue is to dispose the catalyst after use when it is deactivated. To make the process feasible from an economic point of view, it is necessary to regenerate the deactivated catalysts and reuse. AC deactivates during the course of the reaction with a resulting reduction in surface area due to pore blockage and deposition of contaminants from the feed stream and products. Hossain et al. [5] reported that deactivation of AC occurred mainly due to the deposition of impurities after the decarboxylation reaction. Some portion of fatty acids may polymerize which is deposited on the surface of AC to fill the pores. This type of impurities is not able to remove by simply washing with organic solvents. On the other hand, AC is also participating in the steam reforming reaction to produce H_2 during decarboxylation which may cause deactivation [15].

In this study, we examine the regeneration of deactivated (spent) AC from hydrothermal decarboxylation of oleic acid to both optimize this process while providing a better understanding of the catalytic mechanism. Different types of chemical activating agents have been reported in the literature including $ZnCl_2$, H_3PO_4, KOH, K_2CO_3, NaOH etc [16, 17]. There is a growing interest for using alkali hydroxides as activation agents due to their low cost and high activity, with KOH being found to be very promising [18-22]. The KOH regenerated AC was characterized by using BET surface area analysis and BJH pore size distribution, X-ray diffraction analysis (XRD), thermogravimetric-differential thermal analysis (TG-DTA), Attenuated total reflectance-Fourier transform infrared spectroscopy (ATR-FTIR), X-ray photoelectron spectroscopy (XPS), Raman spectroscopy and Scanning electron microscopy (SEM) analysis to compare with fresh and spent catalysts. The decarboxylation results using fresh, spent and regenerated AC were compared.

5.2 Experimental section

5.2.1 Materials

Oleic acid (90%), powder activated carbon (AC-DARCO G-60, 100-325 mesh particle size) and hexanes (ACS Grade) were purchased from Sigma-Aldrich, Oakville, ON, Canada. Potassium hydroxide (97%) and nitric acid (68 to 70%) were purchased from Caledon Laboratories Ltd., Gerogetown, ON, Canada. All the chemicals were used as received. De-

ionized water (18.2 MΩ) was taken from a compact ultrapure water system (EASY pure LF, Mandel Scientific Co., model BDI-D7381).

5.2.2 Regeneration procedure

Spent AC catalyst was removed from the reactor after each run, then washed with hexanes multiple times to extract the products. The spent AC was placed in a vacuum oven at 80°C overnight prior to a second catalytic run and regeneration. Regeneration of the spent catalyst was performed by mixing with KOH (300% on wt. basis) and heated in a tubular furnace (Barnstead Thermolyne, Dubuque, IA) at 750 °C @ 0.5 °C/min under Ar atmosphere. The holding time at 750 °C was 3 h. When the temperature reached RT after regeneration, the sample was removed from the furnace and transferred into a beaker. A dilute solution of HNO_3 was added to the beaker to neutralize the KOH and the mixture was centrifuged to separate the solid from liquid. Excess amount of water was added to the solid to wash out any remaining KOH or HNO_3 with the washing continued until the pH reached ~7.0. The wet solid was placed in a vacuum oven at 80 °C for 12 h with the dried sample called *regenerated AC*. After decarboxylation experiments, the used regenerated catalyst is called *spent regenerated AC*.

5.2.3 Activity tests

Hydrothermal decarboxylation of OA using fresh, spent and regenerated AC was conducted using a bench top continuous flow through reactor (BTRS-JR, Autoclave Engineers, Erie, PA) with a maximum operating pressure of 2900 psi at 650 °C. Decarboxylation experiments using fresh, spent and regenerated AC were performed only at maximized reaction conditions from our previous study where the detailed experimental set-up and reaction procedure was described [15]. All the experiments were repeated minimum two times to replicate the accuracy of the data.

5.2.4 Catalyst characterization

Tristar II 3020 (Micromeritics Instrument Corporation) was used to measure the specific surface area, pore diameter and pore volume of fresh, spent and regenerated AC using the Brunauer-Emmett-Teller (BET) and Barret-Joyner-Halenda (BJH) methods. A minimum of 80 mg of sample was degassed at 150 °C for 12 h before measurements to remove the moisture and other adsorbed gases from the catalyst surface. The analysis was performed at -193 °C

using 99.995% pure N_2 gas obtained from Praxair (Oakville, Canada). A Bruker D2 Phaser powder diffractometer was used to study the crystal structure of the fresh, spent and regenerated AC using Cu K_α radiation (λ for K_α is equal to 1.54059 Å) over $2\theta = 10$ - 80 using a scan rate 0.2 $^\circ$/min. ATR-FTIR spectroscopy (Nicolet 6700 FTIR, Thermo Scientific OMNIC^{TM} software) was used to obtain infrared spectra of the fresh, spent and regenerated AC. A Kratos Axis Ultra spectrometer using a monochromatic AlK (alpha) source (15 mA, 14 kV) was used to perform the X-ray photoelectron spectroscopy (XPS) analysis. A Kaiser Optical System RXNI-785 with an excitation wavelength of 785 nm was used to conduct Raman spectroscopy measurements of all AC samples. A TGA/SDT A851 model gravimetric analyzer was used to perform thermogravimetric analysis of the catalyst samples with a heating rate of 10 $^\circ$C/min from ambient temperature to 1000 $^\circ$C in N_2 with a flow rate of 50 mL/min. Scanning electron microscopy (SEM) (model LEO1530) was used to obtain the surface morphologies of the catalysts.

5.2.5 Liquid and gaseous products analysis

Decarboxylated liquid products were analyzed by Shimadzu, GC-2014 with a flame ionization detector (FID) and a capillary DB WAX column (Agilent Technologies, Santa Clara, CA, USA). The column dimension is 30m length, 0.250 mm inner diameter and 0.25μm film thickness whereas the column operating temperature is 20 to 260 $^\circ$C. The hydrocarbons present in the decarboxylated liquid product were identified and quantified by matching gas chromatograph retention times with known standards (C8-C20 saturated hydrocarbons, heptadecene and oleic acid) obtained from Sigma-Aldrich, Oakville, ON, Canada. 1μL of sample was injected manually into the column with a 10:1 split ratio and was repeated at least 3X to minimize analytical error. Helium, hydrogen and helium-air were used as the carrier gas, flame gas and make-up, respectively. Selectivity of products were calculated as the peak area of an individual compound divided by the total peak area of all compounds of interest present in the liquid product. The GC oven temperature was programmed as follows: 3 min hold at 50 $^\circ$C, 10 $^\circ$C/min ramp at 250 $^\circ$C. The injector and detector temperature were maintained at 200 and 250 $^\circ$C, respectively.

The degree of decarboxylation of OA was confirmed from the decreasing trend of peak area of –COOH group (1707 cm^{-1}) using eqn. 1. ATR-FTIR spectroscopy (Nicolet 6700 FTIR,

Thermo Scientific) was used to obtain the infrared spectra of OA and decarboxylated liquid products. The spectra were recorded in the range of 600-4000 cm^{-1} with a resolution of 4 cm^{-1} over 64 scans.

$$Degree\ of\ decarboxylation\ (\%\ removal\ of - COOH\ group\ ) =$$
$$\frac{(Initial\ peak\ area\ of -COOH\ group\ in\ OA) - (Peak\ area\ of -COOH\ group\ in\ the\ liquid\ product)}{(Initial\ peak\ area\ of -COOH\ group\ in\ OA)}\ x\ 100\ (5.1)$$

Raman spectroscopy was used to confirm saturation of C=C to C-C as C=C stretching is less sensitive in FTIR than in Raman. A Kaiser Optical System RXNI-785 was used to acquire Raman spectra of OA and decarboxylated liquid products with an excitation wavelength of 785 nm.

An Eagle Eye SG-Ultra Max Hydrometer (Density meter) (dimension = 5.5$^{//}$W x 5.5$^{//}$D x 1$^{//}$H (outside)) was used to measure density of the decarboxylated liquid products. Liquid products higher heating values (HHV) were measured using an IKA C2000 bomb calorimeter.

The gaseous products obtained during decarboxylation of OA was analyzed using Shimadzu, GC-2014 with a thermal conductivity detector (TCD) and a nickel packed column (120/80 Hayesep D stainless steel 3.18 mm ID, 6.2 m). Gases were quantified using standard calibration gases (a mixture of H_2, N_2, O_2, CH_4, CO, CO_2) by injecting 1 mL of gas sample manually. Injection was repeated 3X to minimize any analytical error. SGE gas tight syringe (Model number 008100, Reno, NV USA) was used to inject the gas sample into the GC. The GC oven temperature was programmed as follows: 6 min hold at 35 °C, 25 °C/min ramp at 200 °C, 1 min hold at 200 °C. The injector and detector temperature were maintained at 200 and 250 °C, respectively with He used as the carrier gas.

5.3 Results and discussion

5.3.1 Catalytic activity test of AC during decarboxylation of OA

Decarboxylation of OA was conducted at 400°C, water-to-OA ratio of 4:1, space time of 2 h in the presence of AC (5 g) for 45 h time on stream to observe the stability of catalyst. The calculated flow rates of OA and water were 0.0167 and 0.0667 mL/min. Liquid decarboxylated product was separated continuously during the reaction and examined in terms of the degree of decarboxylation. The catalytic activity of AC was measured based on this degree of

119

decarboxylation. Visual images of the liquid decarboxylated products at different times on stream are shown in Figure 5.1. Products collected at 10, 20 and 30 h showed a clear liquid and only one phase is present whereas the product collected at 40 h showed turbidity with two phases. The liquid phase is at the bottom of the vial while the other phase consists of semisolid wax sticking to the vial walls. The product recovered at 45 h is completely foamy. No liquid phase is present in this sample. Since the expected decarboxylated product is clear liquid, this foamy product indicates that the catalyst was significantly deactivated at this stage.

Products at different time intervals
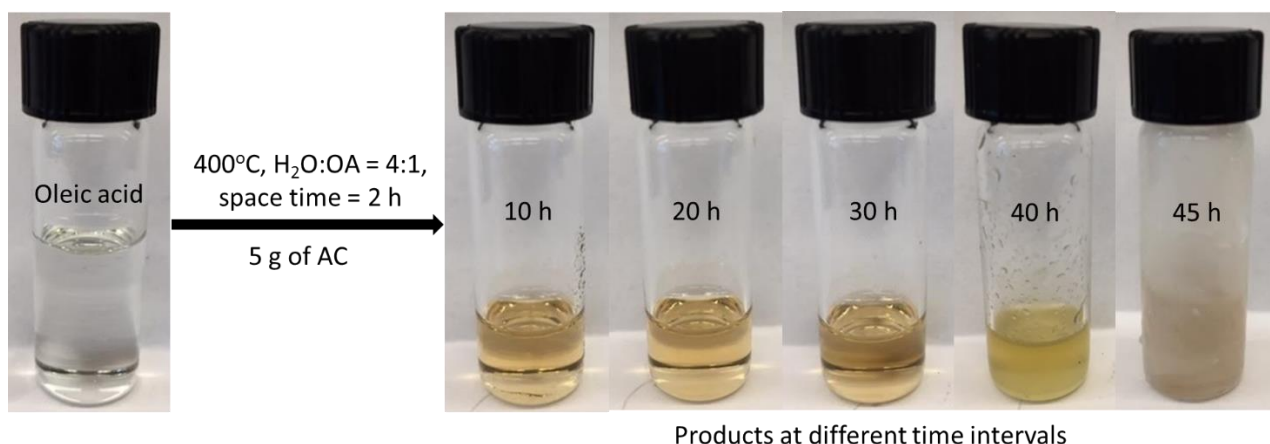
Figure 5.1. Visual images of decarboxylated liquid products obtained after different time intervals.

The ATR-FTIR spectra and corresponding degree of decarboxylation data are shown in Figure 5.2 and Figure C1, respectively. Figure 5.2 shows the ATR-FTIR spectra of the decarboxylated products at different times on stream of the reaction along with OA. Several major peaks were observed in the spectrum of oleic acid at 3004, 2921, 2852, 1707, 1463, 1412, 1284, 934, and 722 cm^{-1}, respectively. The peaks of interest at 3004 and 1707 cm^{-1} are assigned to the C-H stretching of alkenyl group (C=CH) and C=O stretching of carboxylic group. The peak intensity of C=O in the liquid products is considerably lower during the course of reaction until 30 h. There was no significant differences observed for the decarboxylated liquid product obtained after 10, 20 and 30 h. The degree of decarboxylation for these three cases was 91, 90 and 88.9%. The peak intensity of C=O started to increase after 30 h which indicates that the catalyst started to be deactivated. The degree of decarboxylation dropped from 88.9% at 30 h to 60% at 40 h. The degree of decarboxylation of OA decreased to 50% at 45 h. After 45 h, the

condenser was washed with hexanes to remove any residual product. The liquid product was collected after hexane was evaporated. The degree of decarboxylation of this product was found to be 39%. The results suggest that the catalyst performed well for 30 h while demonstrating worsening catalytic activity after 40 h. In addition, the peaks at 1412, 1284, and 934 cm^{-1} which are assigned to combination of C-O stretching and O-H deformation, C-O stretching, and OH out of plane bending modes, respectively, decrease significantly compared to OA during the decarboxylation reaction. This indicates that the decarboxylation reaction occurred in the presence of AC. The alkenyl =CH stretching disappeared after catalytic decarboxylation of OA for all cases, indicating effective hydrogenation of C=C to C-C in the presence of AC.
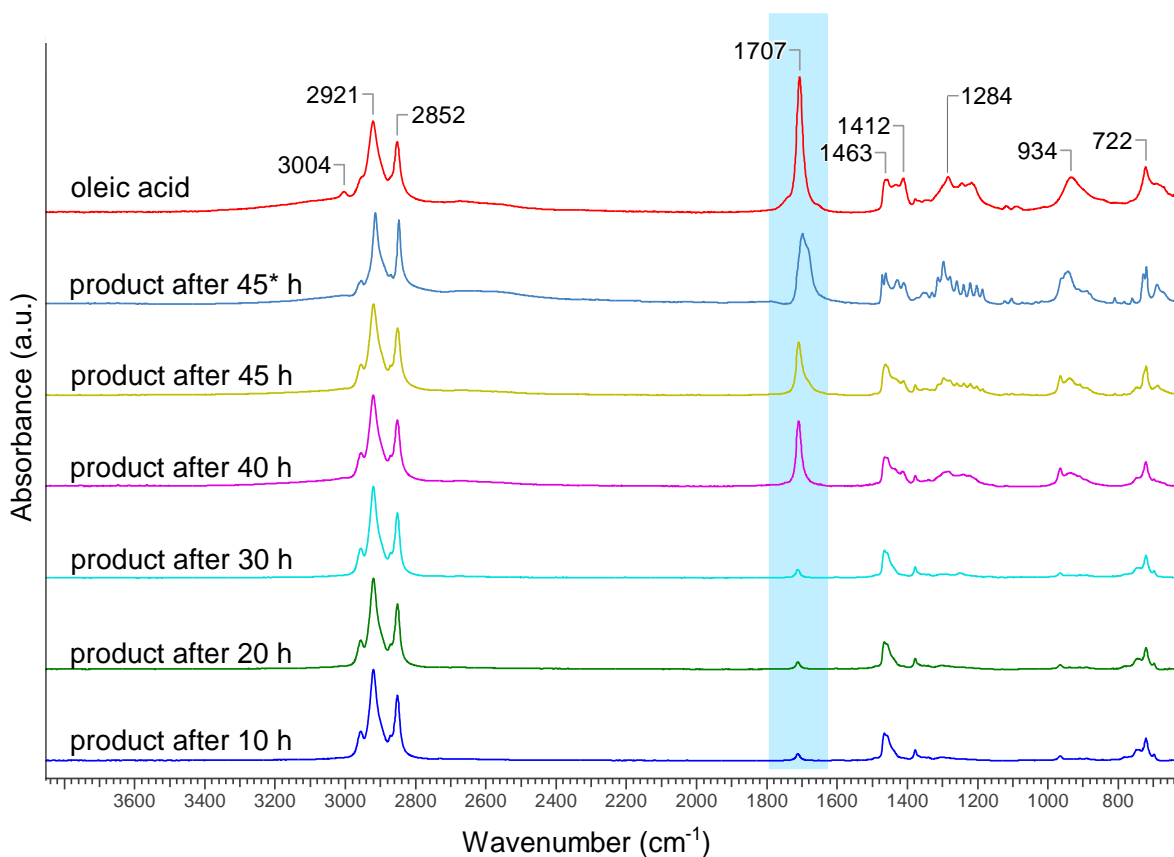
Figure 5.2. ATR-FTIR spectra of decarboxylated liquid products obtained after different times on stream (*product after reactor washed at the end of 45 h reaction).

Hydrocarbons present in the liquid decarboxylated products collected at different time intervals were measured using GC-FID. Figure 5.3 shows the distribution of C8 to C20 alkanes and

heptadecane present in the liquid products. Selectivity of C8 to C16 alkanes slightly increased from 10.2% to 13.4% while the selectivity of heptadecane slightly decreased from 89.3 to 86% from 10 h to 30 h. Negligible amounts of heptadecene was observed during the 10 h to 30 h intervals. The selectivity of heptadecane dropped from 86% to 34% when the duration of reaction time reached from 30 h to 45 h. Even lower amounts of heptadecane was found in the product obtained from reactor washing (16%). The selectivity of C8 to C16 and C18 to C20 alkanes increased after 30 h whereas the significant increase of heptadecene was observed at the same time. 30% selectivity of heptadecene was found in the liquid product obtained from the reactor wash. The results indicate that the catalyst was less active after 30 h resulting in incomplete hydrogenation of oleic acid into straight chain saturated hydrocarbons.
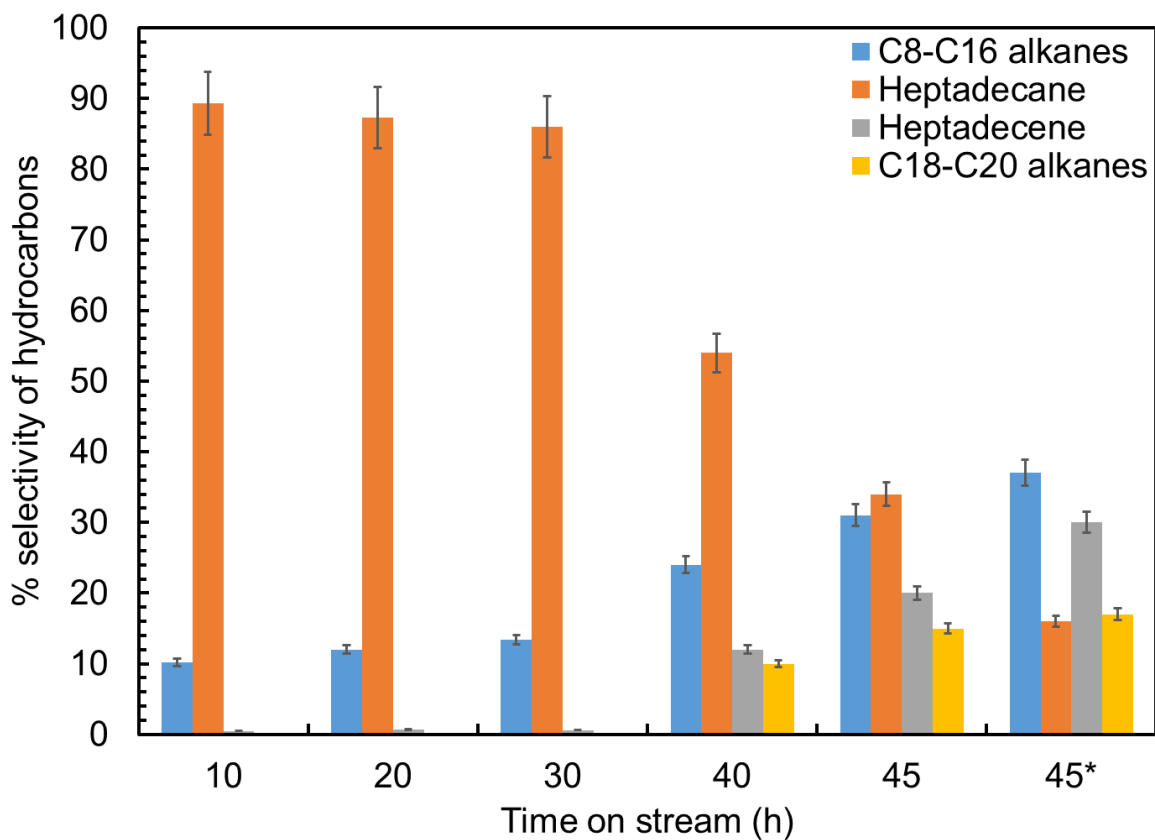
Figure 5.3. Distribution of hydrocarbons in the liquid product at different time on stream (*product after reactor washed at the end of 45 h reaction).

In addition to the FTIR results, decarboxylation was confirmed during the course of the reaction using GC-TCD analysis of gaseous products at different time intervals. The mole

percentage of CO_2 and CO are presented in Figure 5.4. The mole concentration of CO_2 decreased with increasing duration of reaction time whereas the mole concentration of CO increased with increasing reaction time intervals. These results indicate that decarboxylation is the dominating chemical reaction up to 30 h and oleic acid was decarbonylated to liquid hydrocarbons afterwards.
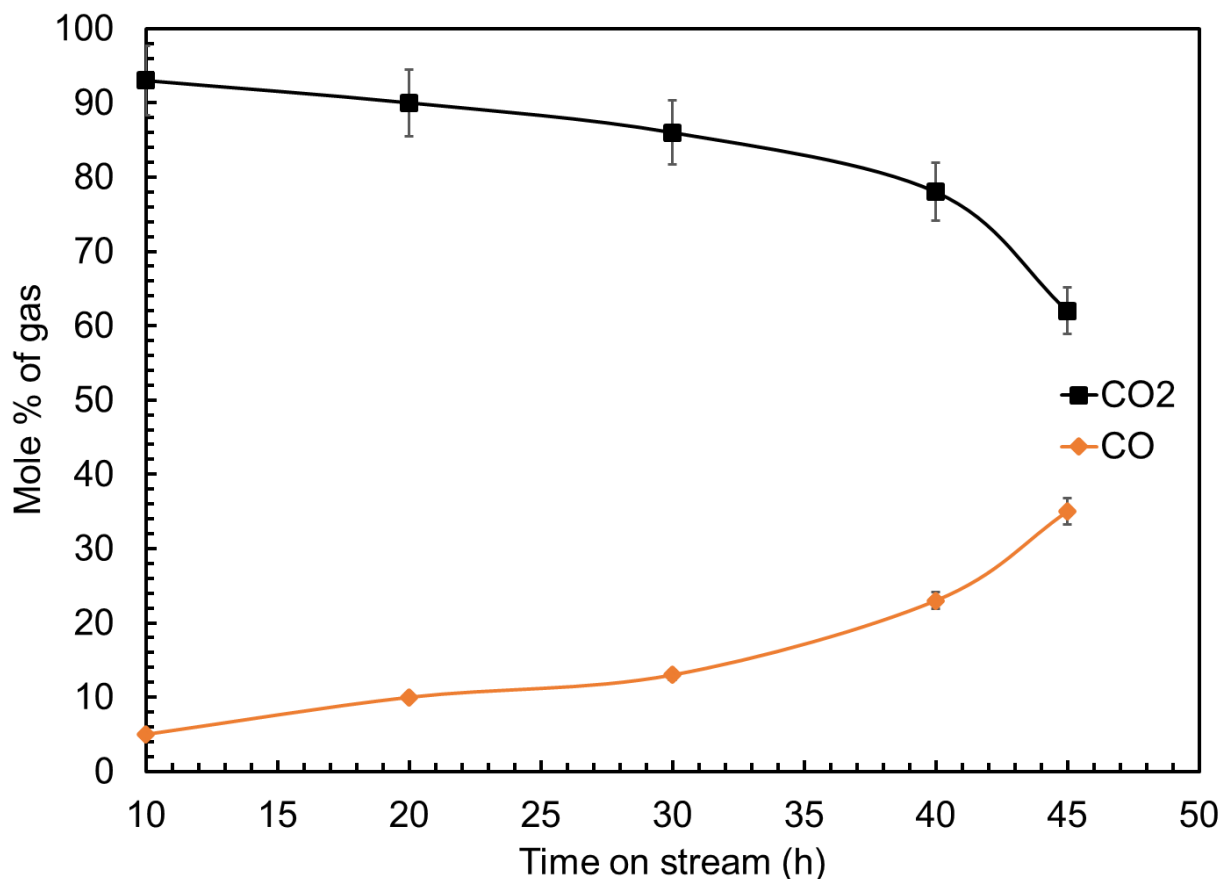
Figure 5.4. Mole percentage of CO_2 and CO present in the gas fraction collected at different time intervals.

HHV's of the decarboxylated liquid products over 45 h time on stream were measured and presented in Table 5.1. The data shows that the HHV of the reactant oleic acid was 39.2 MJ/kg. These HHV values increased by over 10% for the liquid products collected with the catalyst used for 10-30 h on stream whereas the values started decreasing afterwards. The results indicate that catalyst started to lose its activity after 30 h.

Table 5.1. HHV's of the decarboxylated products obtained at different time intervals

Time intervals (h)	HHV's (MJ/kg)
0	39.2
10	45.2
20	45.0
30	44.8
40	43.2
45	41.1
45*	39.5

5.3.2 Analysis of products using regenerated AC

Experiments using spent AC under the conditions of 400°C, water to OA ratio = 4:1 and space time = 2 h with the same catalyst loading were conducted revealing the poor decarboxylation performance of the spent catalyst, i.e. 31% (Figure 5.5b). To make the decarboxylation process more profitable and more responsible for environmental protection, it is necessary to recycle/regenerate the spent AC instead of discarding it to the environment. Figure 5.5 compares the catalytic performance of fresh, spent and regenerated AC in terms of the degree of decarboxylation of OA whereas Figure C2 shows the visual images of decarboxylated products obtained using the fresh and regenerated catalyst. There was no significant differences observed in the liquid products with both providing a clear liquid single phase. The degree of decarboxylation using fresh and regenerated AC was 91 and 87%. These results revealed that the KOH treatment of spent AC was very efficient, significantly improved the removal of − COOH group after regenerating the spent catalyst.
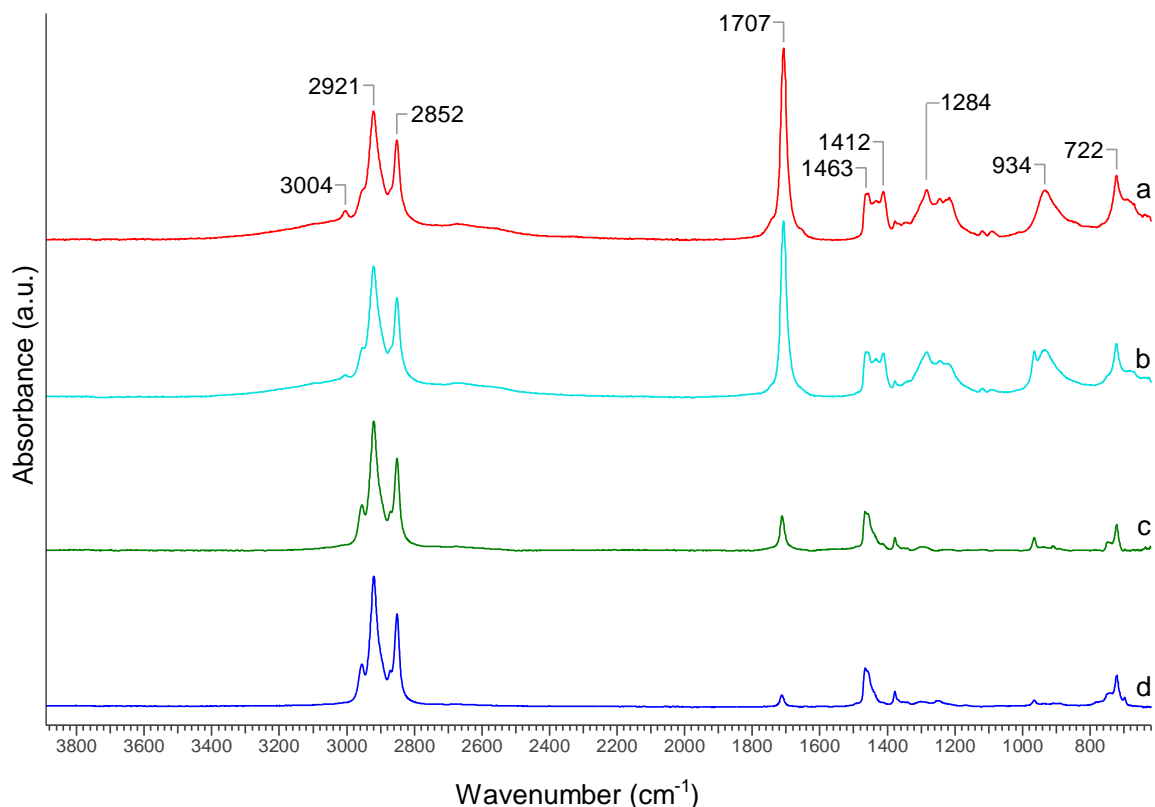
Figure 5.5. ATR-FTIR spectra of (a) oleic acid and the formed products after reactions using (b) spent, (c) regenerated, and (d) fresh AC.

Raman spectra of oleic acid and the decarboxylated products obtained by using fresh and regenerated AC were collected and are presented in . The spectrum of oleic acid shows a few major peaks at 3008, 1655, 1439 and 1302 cm^{-1}. The peaks at 3008 and 1655 cm^{-1} are attributed to the alkenyl =CH stretching and C=C stretching modes, respectively. The peak at 1439 cm^{-1} is assigned to CH$_2$ scissoring mode while the peak at 1302 cm^{-1} is attributable to CH$_2$ wagging and the carboxylic C-O stretching mode. After the decarboxylation reaction, the alkenyl peaks almost disappeared while the carboxylic C-O peak at 1302 cm^{-1} decreased significantly in comparison to the CH$_2$ scissoring peak at 1439 cm^{-1}. These results are in good agreement with the FTIR results, confirming effective Figure 5.6 and hydrogenation of oleic acid using the fresh and regenerated AC.
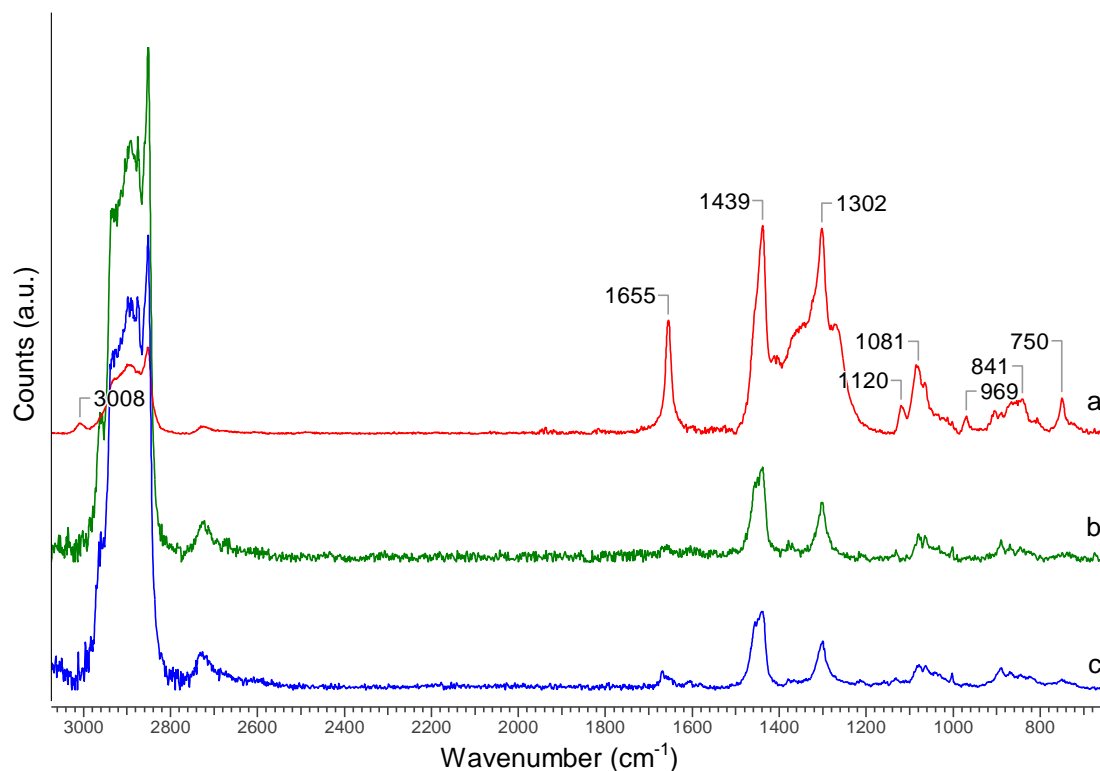
Figure 5.6. Raman Spectra of (a) oleic acid and the decarboxylated products obtained using (b) fresh and (c) regenerated AC.

In addition, ^{1}H NMR spectra of oleic acid and the decarboxylated products obtained by using fresh and regenerated AC were collected and are presented in Figure 5.7. The spectrum of oleic acid (Fig. 7c) shows a few major peaks at 5.36, 2.36 (t), 2.02, 1.64 (quin), 1.30, and 0.89 (t) ppm. The peak at 5.36 ppm is assigned to the alkenyl =CH protons (10 and 11) while the peak at 2.02 ppm is assigned to the methylene protons (9 and 12) next to the alkenyl group. The triplet at 2.36 ppm and the quintet at 1.64 ppm are assigned to the methylene protons (3 and 4) near the carboxylic acid group, respectively. The peak at 0.89 ppm is assigned to the end methyl protons (19) while the broad peak at 1.30 ppm is attributed to other methylene protons (5-8, and 13-18). The carboxylic proton –COOH (1) was evident by a broad peak at 10.74 ppm which is not shown in Figure 5.7. After the decarboxylation process, both the alkenyl related peaks (9-12) and the carboxylic related peaks (1, 3-4) almost disappeared (Figure 5.7a-b), indicating high conversion of alkenyl and carboxylic groups. The negligible difference between Figure 5.7a and Figure 5.7b confirms similar efficiency of decarboxylation and

126

hydrogenation of oleic acid using fresh AC to that using the regenerated AC. These results also corroborate the FTIR and Raman results as discussed above.
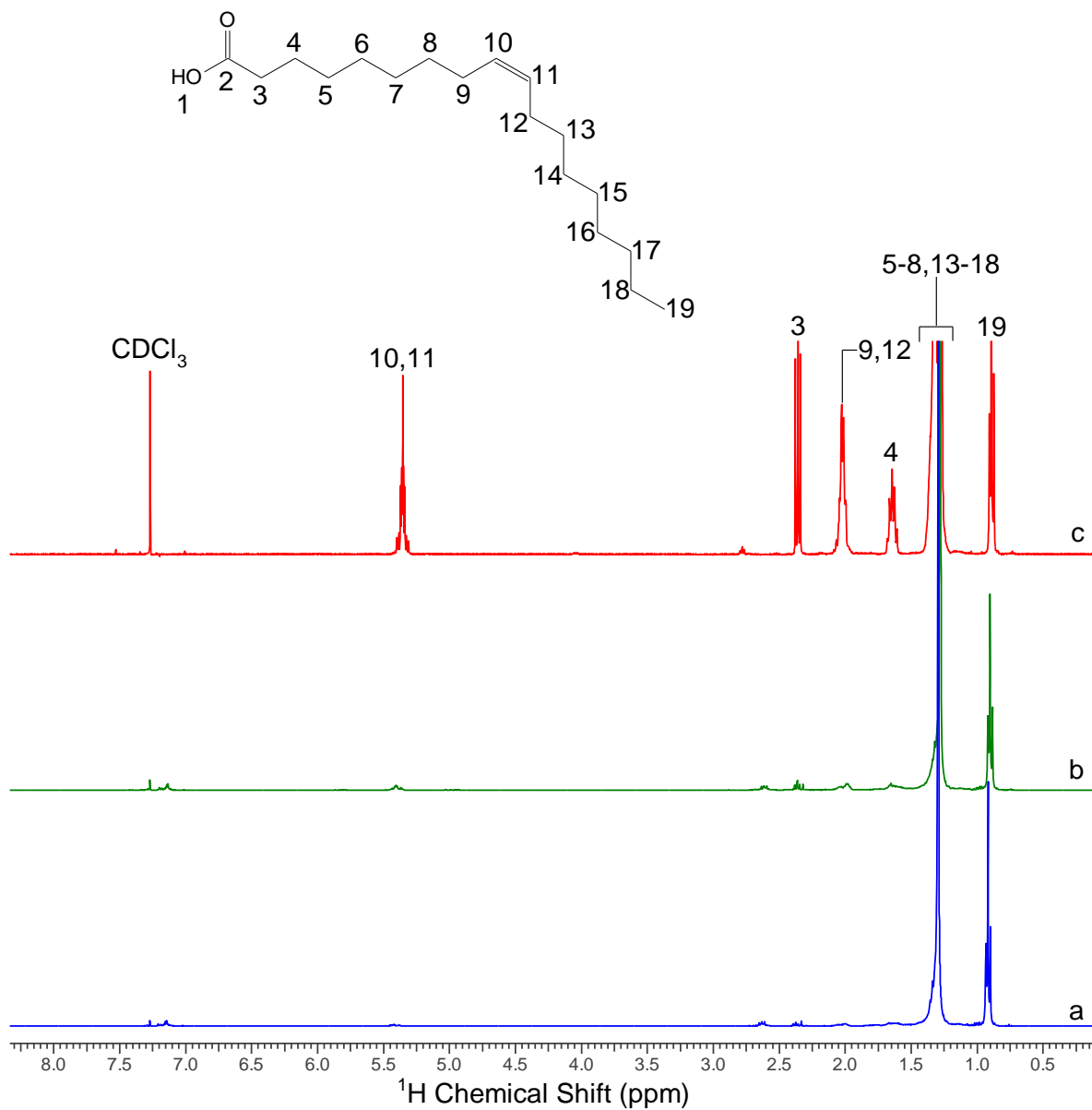
Figure 5.7. ^{1}H NMR spectra of decarboxylated products from oleic acid using (a) fresh AC and (b) regenerated AC, and (c) oleic acid in CDCl$_3$.

Hydrocarbons quantified by GC-FID analysis in the decarboxylated products using fresh and regenerated AC are shown in Table 5.2. The results indicate that there is no significant

difference observed for the selectivity of hydrocarbons present in both liquid products. The selectivity of heptadecane found in the liquid products using fresh and regenerated AC is 89.3 and 81.2%, respectively.

Table 5.2. Selectivity of the compounds present in the liquid product at maximized reaction conditions

compounds	percentage selectivity (composition)	
	fresh AC	regenerated AC
C8-C16 alkanes	10.2	14.8
heptadecane	89.3	81.2
heptadecene	0.5	1.9
C18-C20 alkanes	0.0	2.1

Decarboxylation of OA using fresh and regenerated AC was confirmed by GC-TCD analysis of gaseous products formed during the reaction. The mole percentage of CO and CO_2 obtained using fresh and regenerated AC at optimum conditions was 93% and 5% & 90% and 13%, respectively. This result is consistent with ATR-FTIR and Raman results.

Variation of density and HHV's of liquid decarboxylated products using fresh and spent AC is presented in Figure 5.8 and Table 5.3. The density of decarboxylated product decreases with increasing measurement temperature. The densities of decarboxylated liquid products using fresh and regenerated AC are 0.784 and 0.786 g/mL, respectively, at 15.6 °C. By comparing our experimental results with conventional fuels including Kerosene [23], Jet fuel [24] and Diesel [23], our experimental decarboxylated liquid products fall within typical Kerosene and Jet fuel range. HHV's of the decarboxylated liquid products using fresh and regenerated AC are 45.0 and 45.5 MJ/kg, respectively. Compared with the commercial fuels, the decarboxylated products fall among the Kerosene, Jet fuel and diesel range.
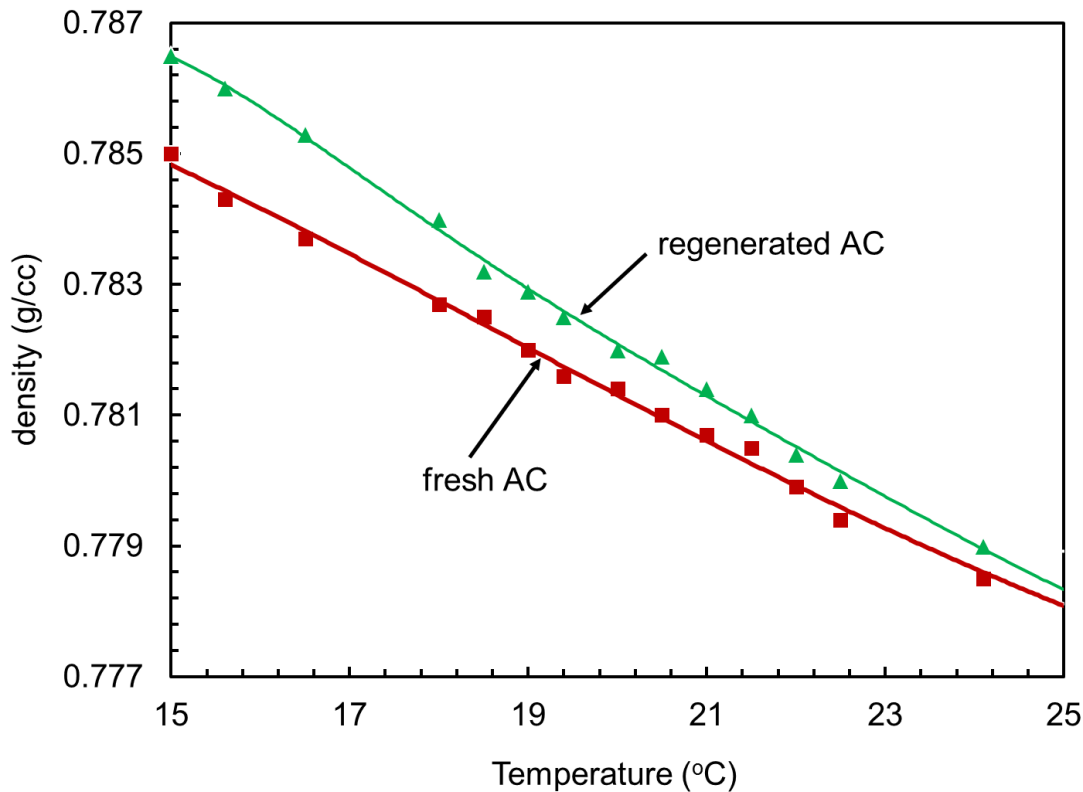
Figure 5.8. Variation of density of decarboxylated products with temperature.

Table 5.3. High heating values of feed, products and commercial fuels

Compound	HHV's (MJ/kg)
Oleic acid	39.2
Decarboxylated products [*]	45.0 (using fresh AC)
	45.5 (using regenerated AC)
Jet fuel [25]	43.5
Kerosene [23]	46.2
Diesel [23]	44.8

[*] produced under maximized conditions

5.3.3 Catalyst characterizations

Textural properties (surface area, pore volume and pore size) are important parameters to measure the catalytic activity of a catalyst. Larger BET surface area and pore volume of a

catalyst imply that it has more active sites which can be exposed for reaction. Table 5.4 compares the surface area, pore volume and average pore size of fresh, spent, and regenerated AC, respectively. The results confirm that the regenerated AC regained surface area (746 m^2/g) and pore volume (0.56 cm^3/g) approaching the fresh AC (857 m^2/g and 0.63 cm^3/g) after activation with KOH. The spent catalysts have smaller surface area and pore volume compared to the fresh and regenerated ones indicating that AC lost its catalytic activities during the course of reaction. All the catalyst samples have a narrow pore size distribution centered at ~ 3.6 nm, indicating that the pores did not break (sinter) during the decarboxylation reaction.

Table 5.4. Textural properties of AC

Name of the samples	BET surface area (m^2/g)	Pore volume (cm^3/g)	Average Pore diameter (nm)
Fresh AC	857	0.63	3.5
Spent AC	114	0.20	3.7
Regenerated AC	746	0.56	3.6
Spent regenerated AC	138	0.18	3.7

Figure 5.9 displays the N$_2$ adsorption-desorption isotherms and pore size distributions of the fresh, regenerated and spent catalysts. Fresh, regenerated and spent AC displayed type IV isotherm (IUPAC system) which confirms the existence of mesopores in the structure [26, 27] and H1-type hysteresis loop is ascribed to a mesoporous network caused by nearly spherical agglomerates [28]. The spent regenerated AC displayed type II isotherm indicating the poor porous structure but H4 hysteresis loop at p/p^o = 0.85 to 0.95 indicates the existence of typical mesopores in the structure. Shifting the hysteresis loops to the higher relative pressure also indicates some pore blockage during the decarboxylation reaction. Reducing the area of hysteresis loops confirms the deceased volume of mesopores. Average pore diameter of all the catalysts indicate the mesoporous structure with pore diameter range between 3 to 4 nm.
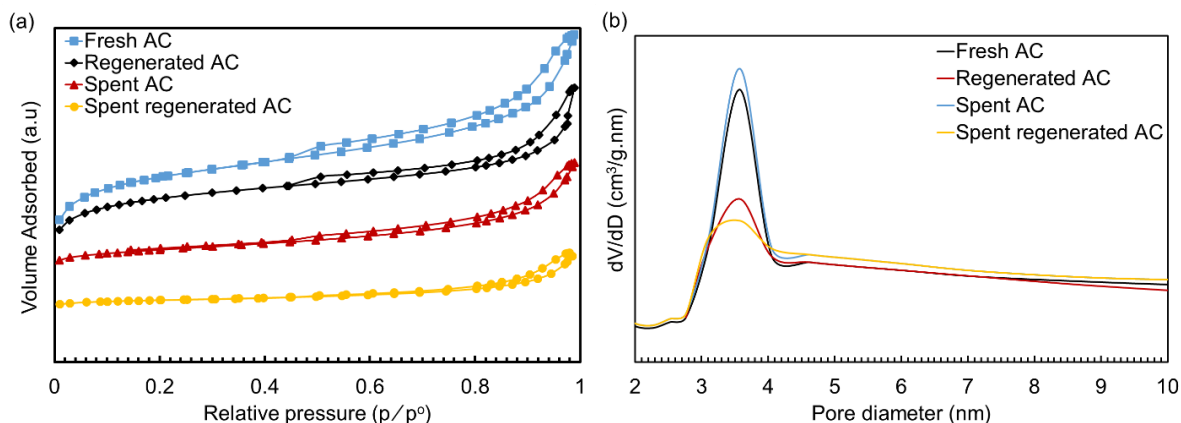
Figure 5.9. (a) N_2 adsorption-desorption isotherms (b) pore size distributions.

Crystallinity of all catalyst samples were measured by XRD analysis, which is presented in Figure S3. The XRD patterns of all the samples show amorphous behaviour [13]. No peak for graphitic coke deposition was detected in the XRD patterns of both spent and spent regenerated AC (Figure S3b and d) during decarboxylation of OA (usually appears at 29.84 and 61.92° [29, 30]). TG-DTA analysis of the spent and spent regenerated AC also confirmed no graphitic coke or amorphous carbon deposition, respectively. The weight loss in TG-DTA profiles of all AC samples resembles to the moisture removal from their surfaces (data not shown).

The surface functional groups of these AC catalysts play an important but poorly understood role in their catalytic activity. The presence of surface functional groups of AC were measured by several spectroscopic techniques. ATR-FTIR spectra of fresh, regenerated and spent AC are presented in Figure C4. No significant surface functional groups were observed in the spectra of fresh and spent AC, which may be due to their low concentrations. However, the spectra of regenerated AC showed a major peak at 1044 cm^{-1}, which is attributable to alcoholic C-O stretching. More C-OH groups (3677 cm^{-1}) were generated by treating spent AC with KOH. This might be the reason for regenerated AC performing actively as fresh AC for decarboxylation of OA. The spectra of spent regenerated AC is very similar to the regenerated one, implying the existence of surface functional groups in the spent regenerated AC.

Raman spectroscopy analysis is very important to characterize the carbonaceous materials, especially molecular morphology and defect density. This technique is able to measure even a slight changes in the surface of the structure. Figure 5.10 compares the Raman spectra of fresh,

131

regenerated, spent, and spent regenerated AC. All of these Raman spectra show two broad overlapping peaks at around 1297 (D-band) and 1595 cm^{-1} (G-band) respectively. D-band corresponds to the presence of defects and G-band represents ideal graphitic sp^2 hybridized carbon atoms [31]. By deconvoluting these peaks, the ratios of D/G were calculated, which are 3.08, 2.45, 2.20, and 2.29 corresponding to fresh, regenerated, spent, and spent regenerated AC samples, respectively. In addition to the highest D/G ratio (3.08) of fresh AC, the regeneration process increased the D/G ratio from 2.20 to 2.45, while the catalytic process generally decreased the D/G ratios. Combining the catalytic performance discussed above, surface defects of AC were found to play a crucial role in the catalytic activity. By comparing Figure 5.10a and c, the peak intensity of the spent AC is much lower than that of the fresh AC, indicating deposition of impurities on the spent AC during decarboxylation of OA which was removed after KOH treatment in the regenerated AC sample. Raman profile of the spent regenerated AC is quite similar to that of the fresh and regenerated AC, indicating lower deposition of impurities on the spent regenerated AC compared to the spent AC.
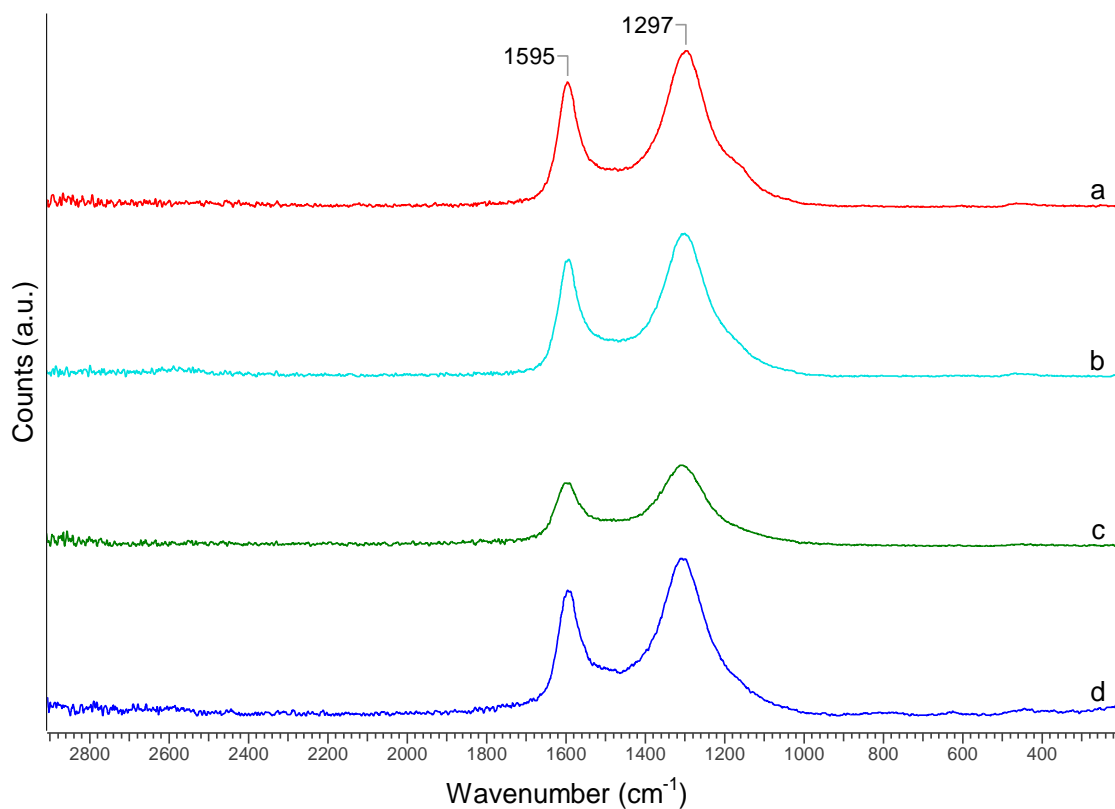
Figure 5.10. Raman spectra of (a) fresh (b) regenerated (c) spent (d) spent regenerated AC.

For a more detailed investigation of the surface properties, the catalyst samples were examined by XPS analysis. The survey XPS spectra of the fresh, regenerated and spent catalysts is shown in Figure 5.11. The survey spectra shows that fresh and spent AC have more elemental peaks compared to regenerated and spent regenerated AC. C, O, Al, Fe, S, N, Si, Na are present in fresh and spent AC whereas regenerated and spent regenerated AC contains only C, O and Si. Elemental compositions and relative contents of oxygenated carbon species are shown in Table C1 and Table C2. The main elements present in all the catalyst samples are C and O. The fresh and spent AC samples contain 89.4% & 87.4% C and 3.4% & 7.4% O, respectively, whereas the regenerated and spent regenerated AC samples contain 63.1% & 69.2% C and 36.8% and 29.8% O, respectively. These results indicate that the regenerated and spent regenerated AC contain lower % C and higher % of O compared to the fresh and spent ones. KOH treatment provides more oxygen functional groups on the surface of the spent AC, which help to regain the catalytic activity for decarboxylation. These results are consistent with the FTIR and BET results. In addition, the fresh and spent AC samples also contain a significant amount of Si (4.0% and 3.9%) compared to the regenerated and spent regenerated AC samples.
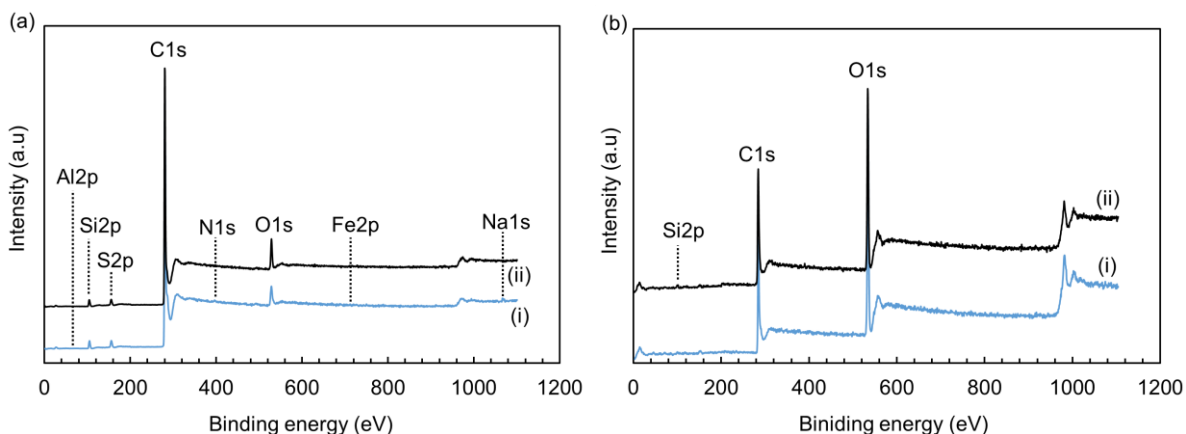
Figure 5.11. XPS survey spectra of a(i) fresh, a(ii) spent, b(i) regenerated, b(ii) spent regenerated AC.

High resolution XPS C1s spectra (Figure 5.12) shows the oxygenated functional groups present in the surface of the fresh, regenerated and spent catalysts. All the catalyst samples contain four peaks corresponding to C-C/C=C (284.5 eV), C-OH and C-O-C (286.5), C=O (287.9) and O-C=O (289.0) [32]. Amongst all the peaks, the C-C/C=C peak is major for all the catalysts,

which accounts for 87.6%, 81.4%, 90.6% and 70.3% of the carbon species in the fresh, regenerated, spent, and spent regenerated AC, respectively. The carbon species of O-C=O, C=O, and C-OH/C-O-C increased from 3.6%, 2.5%, and 6.3% to 3.9%, 4.5%, and 10.1%, respectively after KOH treatment of spent AC to produce regenerated AC. The percentage of O-C=O, C=O, and C-OH/C-O-C decreased in the spent AC compared to fresh one which resulted in the deactivation of the catalyst after first run. But the percentage of C=O and C-OH/C-O-C increased in spent regenerated AC compared to fresh and regenerated AC which might be due to oxidation of catalyst in subcritical water media.
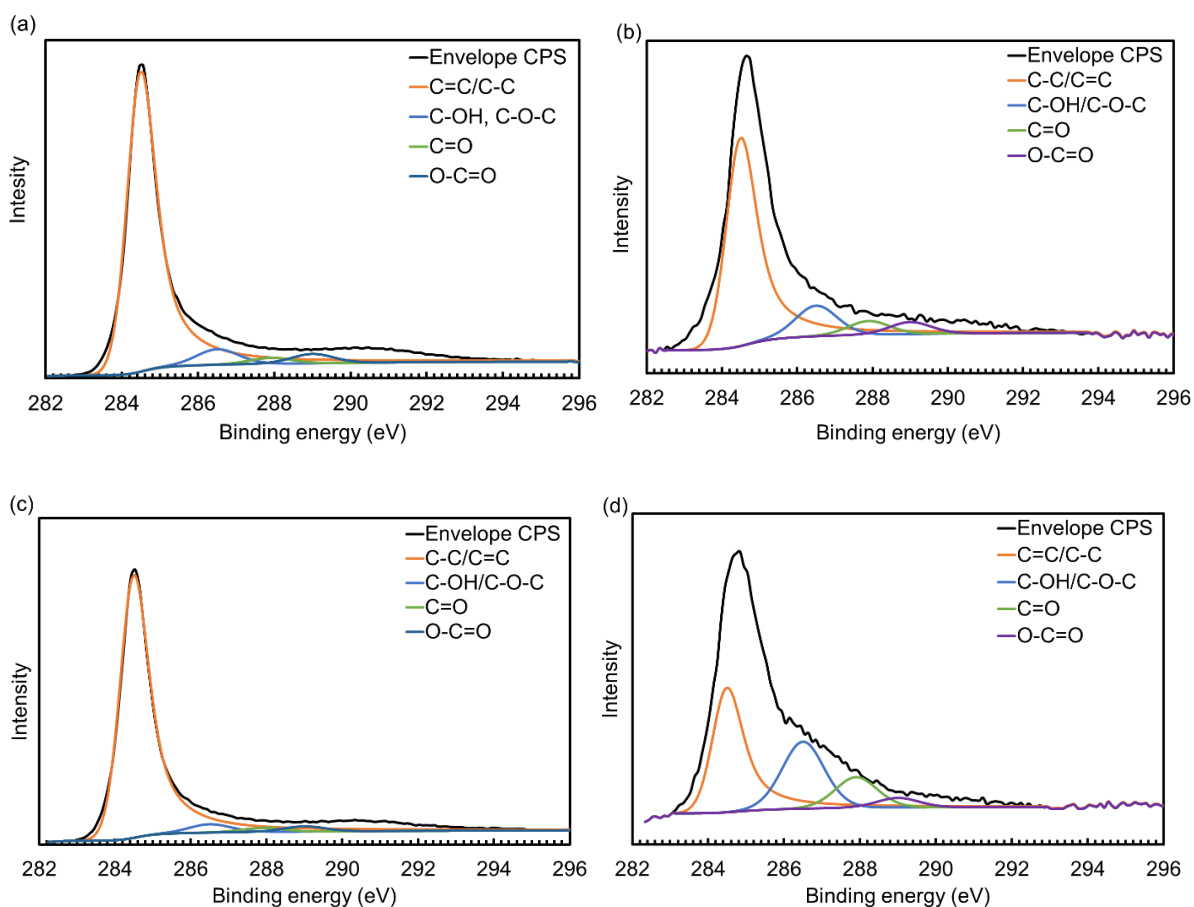
Figure 5.12. High resolution XPS C1s spectra of (a) fresh (b) regenerated (c) spent (d) spent regenerated AC.

The morphologies of the fresh, spent and regenerated AC was imaged by SEM (Figure C5) to compare the catalysts' surfaces during the decarboxylation reaction and the regeneration process. Figure C5(a) and (c) reveal that the fresh and regenerated AC samples had almost the

same morphologies, indicating that the regeneration of spent AC helped to restructure the surface of AC from the decarboxylation process. Figure C5(b) and (d) showed the agglomerated and deactivated structure of AC after decarboxylation reaction.

5.3.4 Regeneration mechanism

According to Jimenez et al. [33], the reduction of KOH on the catalyst surface during regeneration produce K, H_2 and K_2CO_3. Another parallel reaction between KOH and C may occur, although this is not feasible thermodynamically [34]. The formed CO_2 then reacts with KOH.

$$6KOH + 2C \leftrightarrow 2K + 3H_2 + 2K_2CO_3 \tag{5.2}$$

$$4KOH + C \leftrightarrow 4K + CO_2 + 2H_2O \tag{5.3}$$

$$4KOH + 2CO_2 \leftrightarrow K_2CO_3 + 2H_2O \tag{5.4}$$

The K and K_2CO_3 could be continuously eliminated from reaction system with Ar flow during the regeneration process. K, K_2CO_3, and unreacted KOH are completely separated after regeneration by adding HNO_3 solution. Removing K, K_2CO_3, and KOH open up new pores which help to regain porous structure of AC.

5.4 Conclusion

Stability test of AC showed that catalyst was stable until 30 h time on stream in terms of degree of decarboxylation and started deactivating afterwards. AC was completely deactivated at 45 h time on stream. The degree of decarboxylation was dropped from 91% at 10 h to 50% at 45 h whereas the selectivity of heptadecane was decreased from 89.3% to 34%. Deactivated (spent) AC was regenerated using thermal treatment with KOH and the results showed that 87% BET surface area was regained after regeneration. Surface properties of regenerated AC was characterized by ATR-FTIR, Raman, XPS and SEM. It was found that the surface properties of both fresh and regenerated AC are quite similar. Especially, the D/G ratio of fresh (3.08) and regenerated AC (2.45) was found very close. On the other hand, decarboxylation results using regenerated AC showed that the degree of decarboxylation (87%) is closer to that of using fresh AC (91%). The selectivity of heptadecane obtained using fresh and regenerated AC was 89.3 and 81.2%. This observations indicate that thermal treatment of deactivated AC

with KOH is a beneficial approach for regeneration of carbonaceous materials. Liquid decarboxylated products using fresh and regenerated AC have the similar density and HHV's as of commercial fuels.

References

[1] R. Luque, L. Herrero-Davila, J.M. Campelo, J.H. Clark, J.M. Hidalgo, D. Luna, J.M. Marinas, A.A. Romero, Biofuels: a technological perspective, Energy & Environmental Science, 1 (2008) 542-564.

[2] U. Rashid, F. Anwar, Production of biodiesel through optimized alkaline-catalyzed transesterification of rapeseed oil, Fuel, 87 (2008) 265-273.

[3] G. Knothe, Dependence of biodiesel fuel properties on the structure of fatty acid alkyl esters, Fuel Processing Technology, 86 (2005) 1059-1070.

[4] J.-G. Na, B.E. Yi, J.N. Kim, K.B. Yi, S.-Y. Park, J.-H. Park, J.-N. Kim, C.H. Ko, Hydrocarbon production from decarboxylation of fatty acid without hydrogen, Catalysis Today, 156 (2010) 44-48.

[5] M.Z. Hossain, A.K. Jhawar, M.B. Chowdhury, W.Z. Xu, W. Wu, D.V. Hiscott, P.A. Charpentier, Using Subcritical Water for Decarboxylation of Oleic Acid into Fuel-Range Hydrocarbons, Energy & Fuels, 31 (2017) 4013-4023.

[6] J. Fu, C. Yang, J. Wu, J. Zhuang, Z. Hou, X. Lu, Direct production of aviation fuels from microalgae lipids in water, Fuel, 139 (2015) 678-683.

[7] J. Fu, F. Shi, L. Thompson Jr, X. Lu, P.E. Savage, Activated carbons for hydrothermal decarboxylation of fatty acids, ACS Catalysis, 1 (2011) 227-231.

[8] A.K. Sinha, M. Anand, S.A. Farooqui, R. Kumar, R.K. Joshi, R. Kumar, K. Tasleem, A. Parvez, G.S. Malayil, Pt/Pd Sodalite Caged Catalyst Combination with Sulfided Base Metal Catalyst for the Improved Catalytic Hydroprocessing of Feedstock, in, Google Patents, 2016.

[9] J.-G. Na, B.E. Yi, J.K. Han, Y.-K. Oh, J.-H. Park, T.S. Jung, S.S. Han, H.C. Yoon, J.-N. Kim, H. Lee, Deoxygenation of microalgal oil into hydrocarbon with precious metal catalysts: Optimization of reaction conditions and supports, Energy, 47 (2012) 25-30.

[10] L. Yang, M.A. Carreon, Effect of reaction parameters on the decarboxylation of oleic acid over Pt/ZIF-67membrane/zeolite 5A bead catalysts, Journal of Chemical Technology and Biotechnology, 92 (2017) 52-58.

[11] J. Wu, J. Shi, J. Fu, J.A. Leidl, Z. Hou, X. Lu, Catalytic Decarboxylation of Fatty Acids to Aviation Fuels over Nickel Supported on Activated Carbon, Scientific Reports, 6 (2016).

[12] T. Morgan, D. Grubb, E. Santillan-Jimenez, M. Crocker, Conversion of triglycerides to hydrocarbons over supported metal catalysts, Topics in Catalysis, 53 (2010) 820-829.

[13] S. Popov, S. Kumar, Rapid hydrothermal deoxygenation of oleic acid over activated carbon in a continuous flow process, Energy & Fuels, 29 (2015) 3377-3384.

[14] F.A. Medina, J.W. Larsen, H.H. Schobert, Carbon as catalyst for organic electron-transfer reactions, Fuel Chem. Div. Prepr. , 48 (2003) 28.

[15] M.Z. Hossain, M.B.I. Chowdhury, A.K. Jhawar, W.Z. Xu, P. Charpentier, Continuous low pressure decarboxylation of fatty acids to fuel-range hydrocarbons with insitu hydrogen production, Fuel, 212 (2018) 470-478.

[16] L.-Y. Hsu, H. Teng, Influence of different chemical reagents on the preparation of activated carbons from bituminous coal, Fuel Processing Technology, 64 (2000) 155-166.

[17] Y. Sudaryanto, S. Hartono, W. Irawaty, H. Hindarso, S. Ismadji, High surface area activated carbon prepared from cassava peel by chemical activation, Bioresource Technology, 97 (2006) 734-739.

[18] M. Evans, E. Halliop, J. MacDonald, The production of chemically-activated carbon, Carbon, 37 (1999) 269-274.

[19] A. Ahmadpour, B.A. King, D.D. Do, Comparison of equilibria and kinetics of high surface area activated carbon produced from different precursors and by different chemical treatments, Industrial & engineering chemistry research, 37 (1998) 1329-1334.

[20] M. Afdhol, R. Amiliana, A. Hanafi, B. Rachmanda, Preparation of Activated Carbon from Palm Shells using KOH and ZnCl2 as the Activating Agent, in: IOP Conference Series: Materials Science and Engineering, IOP Publishing, 2017, pp. 012282.

[21] S. Li, K. Han, J. Li, M. Li, C. Lu, Preparation and characterization of super activated carbon produced from gulfweed by KOH activation, Microporous and Mesoporous Materials, 243 (2017) 291-300.

[22] V. Barranco, M. Lillo-Rodenas, A. Linares-Solano, A. Oya, F. Pico, J. Ibanez, F. Agullo-Rueda, J. Amarilla, J. Rojo, Amorphous carbon nanofibers and their activated carbon nanofibers as supercapacitor electrodes, The Journal of Physical Chemistry C, 114 (2010) 10302-10307.

[23]   http://www.engineeringtoolbox.com/fuels-higher-calorific-values-d_169.html (accessed on April 19, 2017).

[24] Jet fuel: ASTM D1655-15d, Diesel: Petro-Canada MSDS (accessed on April 19, 2017).

[25] The Official Site of the National Biodiesel Board: Biodiesel.org (accessed on April 19, 2017).

[26] A. Benhouria, M.A. Islam, H. Zaghouane-Boudiaf, M. Boutahala, B. Hameed, Calcium alginate–bentonite–activated carbon composite beads as highly effective adsorbent for methylene blue, Chemical Engineering Journal, 270 (2015) 621-630.

[27] K. Sing, Reporting physisorption data for gas/solid systems with special reference to the determination of surface area and porosity (Provisional), Pure and applied chemistry, 54 (1982) 2201-2218.

[28] K.S. Sing, D.H. Everett, R. Haul, L. Moscou, R.A. Pierotti, J. Rouquerol, T. Siemieniewska, Reporting physisorption data for gas/solid systems, Handbook of Heterogeneous Catalysis, (2008).

[29] M.B. Chowdhury, M.M. Hossain, P.A. Charpentier, Effect of supercritical water gasification treatment on Ni/La2O3-Al2O3-based catalysts, Applied Catalysis A: General, 405 (2011) 84-92.

[30] M.Z. Hossain, M.B. Chowdhury, Q. Alsharari, A.K. Jhawar, P.A. Charpentier, Effect of mesoporosity of bimetallic Ni-Ru-Al2O3 catalysts for hydrogen production during supercritical water gasification of glucose, Fuel Processing Technology, 159 (2017) 55-66.

[31] R. Escribano, J. Sloan, N. Siddique, N. Sze, T. Dudev, Raman spectroscopy of carbon-containing particles, Vibrational Spectroscopy, 26 (2001) 179-186.

[32] M. Seah, The quantitative analysis of surfaces by XPS: a review, Surface and Interface Analysis, 2 (1980) 222-239.

[33] V. Jiménez, J.A. Díaz, P. Sánchez, J.L. Valverde, A. Romero, Influence of the activation conditions on the porosity development of herringbone carbon nanofibers, Chemical Engineering Journal, 155 (2009) 931-940.

[34] M. Lillo-Ródenas, D. Cazorla-Amorós, A. Linares-Solano, Understanding chemical reactions between carbons and NaOH and KOH: an insight into the chemical activation mechanism, Carbon, 41 (2003) 267-275.

Chapter 6

Continuous decarboxylation of fatty acids and their derivatives into liquid hydrocarbons using Mo/Al$_2$O$_3$ catalysts

Abstract

In this study, we report the single step continuous production of oxygen free straight chain liquid hydrocarbons from oleic acid and other fatty acid derivatives of interest including castor oil, frying oil and palm oil using Mo, MgO and Ni on Al$_2$O$_3$ as catalysts in subcritical water. It was found that the Mo-Al$_2$O$_3$ catalyst exhibited higher decarboxylation activity (91%) and liquid yield (71%) compared to the other two catalysts. Straight chain hydrocarbons were obtained via decarboxylation and hydrogenation without adding any external source of hydrogen. The reaction conditions including temperature, water-to-feed ratio and space time were maximized for the Mo-Al$_2$O$_3$ catalyst. The liquid product obtained at the optimized conditions has a similar density and HHV as commercial fuels. Characterization of catalysts showed that an insignificant amount of amorphous carbon deposited on the spent Mo-Al$_2$O$_3$ catalyst could be removed by simple carbon burning in air.

6.1 Introduction

Renewable resources are required to produce fuel range hydrocarbons, especially liquid transportation fuels due to the depletion of fossil fuel reserves. Fats and oil (which mainly contain triglycerides and fatty acids) have been used as renewable feedstocks for producing transportation fuels such as biodiesel [1-4] or green diesel [5-8]. Non-edible resources (jatropha oil, algae, waste cooking oil, animal fats, tallow etc.) are preferred as feedstocks over edible resources to avoid the food vs fuel issue. But higher oxygen content and acidity of these feedstocks prevent them from being used directly as fuel because of their corrosive properties and higher viscosity compared to fossil fuels [9]. Deoxygenation is an efficient upgrading pathway to produce diesel range liquid hydrocarbons to improve the fuel properties of these feedstocks as well as minimize any engine compatibility issues. Liquid hydrocarbons produced via the deoxygenation process sometimes obtain larger Cetane numbers (85 to 99) compared to petroleum diesel (45-55) [10].

The deoxygenation process can occur via three different pathways, i.e. decarbonylation, decarboxylation and hydrodeoxygenation (Scheme 6.1). Hydrodeoxygenation requires hydrogen to produce the liquid hydrocarbons whereas decarbonylation or decarboxylation require less/no hydrogen which makes the process less expensive compared to hydrodeoxygenation. Decarbonylation and decarboxylation are parallel reactions whereas decarboxylation sometimes play a dominant role based on the reaction parameters.

$$R = C_{15}H_{29} \text{ for oleic acid}$$
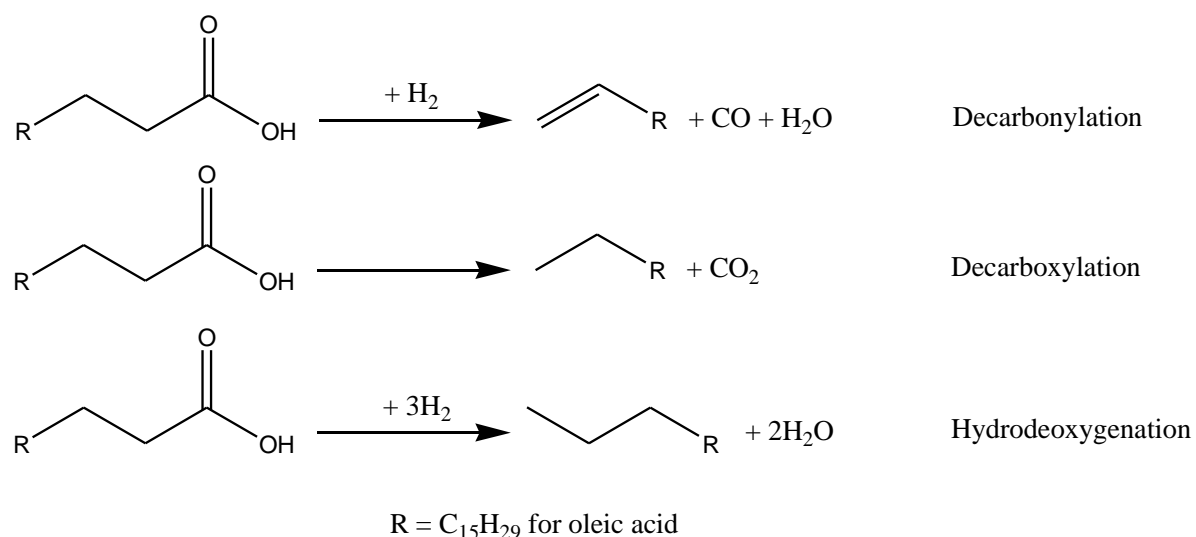
Scheme 6.1. Different pathways of deoxygenation of fatty acids.

140

The decarboxylation process requires a catalyst to produce higher selectivity of liquid hydrocarbons. Decarboxylation catalysts can be divided into two broad classes. The first category is called hydrodesulfurization (HDS) catalysts (e.g., sulfided CoMo or NiMo oxides) which are mainly used for hydrodeoxygenation [11, 12]. The second category of catalysts is group 10 metal catalysts such as Pd, Pt etc. which are selective to decarbonylation or decarboxylation [4, 6, 13, 14]. The main shortcoming of noble metal catalysts is their limited availability and high cost. Sulfide catalysts are comparatively cheaper than noble metal catalysts but leaching of sulfur may deactivate the catalytic activity and contaminate the products which require an additional step for sulfur recovery.

Decarboxylation of fatty acids was reported either in batch or continuous system using different types of metal supported catalysts. Wu et al. [15] conducted decarboxylation of stearic acid using Ni/C catalysts (in 1.67 mL micro-batch reactor) and obtained 80% selectivity of heptadecane. Miao et al. [16] performed hydrothermal decarboxylation of palmitic acid using Ni/ZrO_2 catalysts (in 10 mL batch mini-batch reactor) and showed 64.2 C% selectivity and paraffin yield reached 38.6 C%. Na et al. [17] obtained fuel range hydrocarbons from oleic acid decarboxylaton using MgO-hydrotalcites catalysts. Hollak et al. [9] performed hydrodeoxygenation of oleic acid using tungsten and molebdenum carbide catalysts and showed that moledenum based catalysts have increased activity and catalyst stability to obtain paraffins as the desired product compared to tungsten based catalyst. Hancsok et al. [18] obtained bioparaffin from sunflower and rapeseed oil using reduced $CoMo/Al_2O_3$, $NiMo/Al_2O_3$ and NiW/Al_2O_3 catalysts. The highest liquid yield (75–85%) was obtained using $CoMo/Al_2O_3$ catalyst with high Cetane numbers (490) and good blending properties. Harnos et al. [19] compared the activity between sulfided and nonsulfided catalysts (Pd/AC, Pd/Al_2O_3, Ni/Al_2O_3 and $NiMo/Al_2O_3$) at 340ºC and 21 bars H_2 pressure and showed that the obtained product distribution, i.e., the C17/C18 ratio, was greatly influenced by the type of catalyst used. The non-sulfided catalysts exhibited higher catalytic activity compared to the sulfided catalysts.

Most catalytic hydrothermal processes for decarboxylation use high pressure and external sources of hydrogen. Low-cost stable catalysts for continuous decarboxylation are required to be developed for potential commercialization. Moreover, the effect on the catalyst due to the exposure of a harsh environment like sub or near supercritical water is poorly reported. The

scope of this work is focused on the continuous hydrothermal decarboxylation of oleic acid and some other fatty acid derivatives such as castor oil, frying oil and palm oil using low cost catalysts without any external source of hydrogen.

In this work, we synthesize sulfur free molebdenum (Mo), MgO and Ni loaded alumina (γ-Al_2O_3) catalyst and investigate them for decarboxylation of oleic acid (OA). The best catalyst has been chosen among these three catalysts based on the degree of decarboxylation of OA. The effects of reaction parameters including temperature, space time, and water-to-OA ratio are studied in subcritical water using a continuous fixed bed catalytic reactor. The catalytic activities for decarboxylation of several fatty acid derivatives including castor oil, waste cooking oil, palm oil have been investigated. To understand the effect of the SCW process on catalyst activity, the fresh and spent catalysts were characterized using N_2-physisorption (BET surface area and pore size distribution), X-ray diffraction (XRD), temperature programmed reduction (TPR), scanning electron microscopy (SEM), energy-dispersive X-ray spectroscopy (EDX) and X-ray photoelectron spectroscopy (XPS).

6.2 Experimental

6.2.1 Materials

Oleic acid (90%), castor oil, hexanes (ACS Grade), ammonium molebdate tetrahydrate [$(NH4)_6Mo_7O_{24}.4H_2O$], Nickel nitrate hexahydrate [$Ni(NO_3)_2.6H_2O$], magnesium sulfate heptahydrate [$MgSO_4.7H_2O$] were purchased from Sigma-Aldrich, Canada, and are used as received. Alumina (γ-Al_2O_3) powder was obtained from SASOL (Catalox SSCa 5/200). Waste cooking oil was obtained from home and filtered to remove solid particles before use. De-ionized water (18.2 MΩ) was taken from a compact ultrapure water system (EASY pure LF, Mandel Scientific Co., model BDI-D7381).

6.2.2 Catalyst synthesis

Ni, Mo and MgO supported on γ-Al_2O_3 catalyst was synthesized using an incipient impregnation method [20, 21]. For a typical synthesis, the desired amount of metal precursor for 10 wt% loading was dissolved in deionised water equivalent to 120vol% of pore volume of alumina (0.50 cm^3/gm). For example, 1g 10 wt% Ni-Al_2O_3 catalyst requires 0.50g of

Ni(NO3)$_2$.6H$_2$O and 0.9g of Al$_2$O$_3$, 1g 10wt% Mo catalyst requires 0.18g of (NH4)$_6$Mo$_7$O$_{24}$.4H$_2$O and 0.9 g of Al$_2$O$_3$, 1g of 10 wt% MgO requires 0.64g of MgSO$_4$.7H$_2$O and 0.9 g of Al$_2$O$_3$, respectively. All alumina was immersed into the metal solution at once for better dispersion. The wet catalyst was placed into a vacuum oven at 80°C overnight. The dry powder was then calcined into a muffle furnace at 600 ^{o}C @ 5 ^{o}C/min for 4 h. Hydrogen reduction with 5 vol% H$_2$ balanced with N$_2$ at 950 °C @ 3 ^{o}C/min for 2 h was performed afterwards for Ni and Mo catalysts only. The actual metal loadings were confirmed by EDX and XPS analysis.

6.2.3 Catalyst testing

Decarboxylation of OA and its derivatives was performed in a bench top reaction system (BTRS-JR, Autoclave Engineers, Erie, PA) with a maximum operating pressure of 2900 psi at 650°C. The experimental set-up is shown in Figure 6.1. The system has a 10 mL tubular reactor (316 stainless steel reactor tube with type 316 stainless steel fittings) assembled with a furnace to heat up the reactor to the desired reaction temperature. The reactor is connected with four feed lines. Either four gases or two gases and two liquids feed can be used. All the feeds are mixed into a mixer vaporizer where they are uniformly mixed and vaporized. The feed stream then passed through the reactor. The mixer is placed into an oven to preheat the feed mixture whereas the maximum oven temperature is 250°C. A gas-liquid separator is located outside the oven after the reactor. The separator is surrounded by cooling arrangement connected with a chiller whereas the chiller temperature was maintained at 6°C during the reaction to separate the gas and liquid phases.

Before starting any experiment, the reactor was washed thoroughly with soapy water, clean water then hexanes to remove any residuals from previous experiments. Air was passed through the reactor to remove any water or hexane sticking on the walls. 5 g of catalyst was loaded for each experiment into the reactor and enough quartz wool was placed at the top and bottom of the reactor to maintain the catalyst inside. All the fittings were attached to the reactor and the reactor placed into the furnace. The oven door was closed afterwards to start the reaction. The main power of the system was turned on and set the oven temperature set to 200 ^{o}C and the desired reaction temperature, respectively. The reaction temperature was varied from 325 to 375 ^{o}C according to the experimental methodology explained below. The furnace and the oven switch was turned on and waited for 30-40 min to reach the desired temperature.

During the reactor heating, N_2 gas was flowed through the reactor to make the reactor air free. N_2 flow was stopped and the reactor outlet was opened to get remove any N_2 from the system. Two reactants (OA/ its derivatives) and water were then fed to the reactor continuously. Each experiment was run for a minimum of 24 h. The space time (τ) was calculated from the volume of the catalyst divided by the reactant flow rate. Volume of catalyst was calculated from the amount of catalyst used divided by the density of catalyst (1 g/mL). The liquid and gaseous products were collected and analyzed continuously from the gas-liquid separator until the catalyst started deactivation. Liquid product was stored in glass vials and the gaseous product was collected into an air tight Tedler gas bag (SKC Inc., PA) for further analysis. Spent catalyst was removed from the reactor after each run and washed with hexanes to extract the liquid products. The spent catalyst was dried in a vacuum oven at 80 ^{o}C overnight.
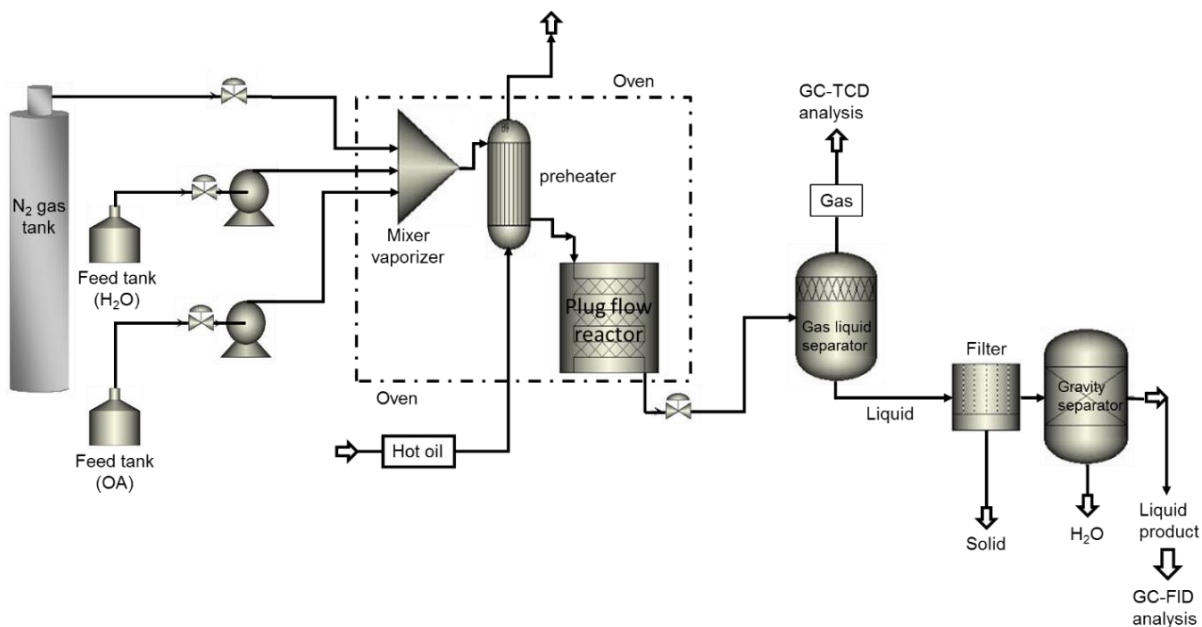
Figure 6.1: Schematic of Continuous Reactor Setup.

6.2.4 Product analysis

Quantification of the hydrocarbon compounds present in the liquid product was performed by using a Shimadzu, GC-2014 connected with a flame ionization detector (FID) and a capillary DB WAX column (Agilent Technologies, Santa Clara, CA, USA) (dimension: 30m x 0.250mm x 0.25μm, temperature limit: 20 to 260 ^{o}C). The hydrocarbon molecules were identified using

known standards (C8-C20 saturated hydrocarbons, heptadecene) obtained from Sigma-Aldrich, Oakville, ON by matching the gas chromatograph retention times. 1µL of sample was injected manually into the column with a 10:1 split ratio and was repeated at least 3X to minimize analytical error. Helium, hydrogen and helium-air were used as the carrier gas, flame gas and make-up, respectively. Selectivity of products were calculated as the peak area of an individual compound divided by the total peak area of all compounds of interest present in the liquid product. The GC oven temperature was programmed as follows: 3 min hold at 50 $^{\circ}$C, 10 $^{\circ}$C/min ramp at 250 $^{\circ}$C. The injector and detector temperature were maintained at 200 and 250 $^{\circ}$C, respectively.

An ATR-FTIR spectroscope (Nicolet 6700 FTIR, Thermo Scientific) was used to obtain the infrared spectra of OA and liquid products. The spectra were recorded in the range of 600-4000 cm^{-1} with a resolution of 4 cm^{-1} over 64 scans. Percentage removal of -COOH group or degree of decarboxylation was calculated from the peak (1707 cm^{-1}) areas of -COOH group in both reactants and liquid products as follows:

$$\% \ removal \ of - COOH \ group \ (Degree \ of \ decarboxylation) =$$
$$\frac{(Initial \ peak \ area \ of -COOH \ group \ in \ OA) \ -(Peak \ area \ of -COOH \ group \ in \ the \ liquid \ product)}{(Initial \ peak \ area \ of -COOH \ group \ in \ OA)} \ x \ 100 \ (6.1)$$

Density of the liquid products were measured using an Eagle Eye SG-Ultra Max Hydrometer (Density meter) (dimension = 5.5$^{//}$W x 5.5$^{//}$D x 1$^{//}$H (outside)). Liquid products higher heating values (HHV) were measured using an IKA C2000 bomb calorimeter.

Gas chromatograph Shimadzu, GC-2014 equipped with a thermal conductivity detector (TCD) and a nickel packed column (120/80 Hayesep D stainless steel 3.18 mm ID, 6.2 m L) was used to quantify the gaseous products formed during decarboxylation using standard calibration gases (a mixture of H_2, N_2, O_2, CH_4, CO, CO_2), by injecting 1 mL of gas sample manually. Injection was repeated 3X to minimize any analytical error. SGE gas tight syringe (Model number 008100, Reno, NV USA) was used to inject the gas sample into the GC. Higher hydrocarbon gases (C2 to C4) were determined by subtracting the number of moles of known gas from the total no of moles of gas produced. The GC oven temperature was programmed as follows: 6 min hold at 35 $^{\circ}$C, 25 $^{\circ}$C/min ramp at 200 $^{\circ}$C, 1 min hold at 200 $^{\circ}$C. The injector and

detector temperature were maintained at 200 and 250 $^{\circ}$C, respectively with He used as the carrier gas.

6.2.5 Catalyst characterization

6.2.5.1 N₂-physisorption

Brunauer−Emmett−Teller (BET) surface area and Barrett-Joyner-Halend (BJH) pore size distributions of fresh and spent catalysts were measured using BET and BJH method, respectively. Tristar II 3020 (Micromeritics Instrument Corporation) was used to measure the specific surface area, pore diameter and pore volume of fresh, and spent catalysts. A minimum of 80 mg of sample was degassed at 150 °C for 12 h before measurements to remove the moisture and other adsorbed gases from the catalyst surface. The analysis was performed at -193 °C using 99.995% pure N_2 gas obtained from Praxair (Oakville, Canada). Adsorption isotherms were obtained in the relative pressure range of 0.04−1.

6.2.5.2 X-ray diffraction (XRD) analysis

A Bruker D2 Phaser powder diffractometer was used to study the crystal structure of the fresh and spent catalyst using Cu K_α radiation (λ for K_α is equal to 1.54059 Å) over 2θ = 10 - 80 using a scan rate 0.1 $^{\circ}$/min.

6.2.5.3 Temperature programmed reduction (TPR)

Micromeritics Autochem II 2920 analyzer was used to obtain the TPR profiles of fresh catalysts. A minimum 140−150 mg catalyst sample was used for each analysis. The TPR analysis was performed by circulating a stream of gas containing 10 % H_2 balanced Ar at a rate of 50 mL/min. The temperature was raised from ambient to 1100°C at a rate of 10°C/min. A thermal conductivity detector (TCD) was used to record the change of hydrogen concentration of the gas stream passing through the catalyst sample for calculating the amount of hydrogen consumed during the reduction process. The amount of H_2 uptake by the sample could be calculated via numerical integration of the TPR area.

6.2.5.4 Scanning electron microscopy (SEM) imaging

The morphologies of both the fresh and spent catalysts were obtained from SEM imaging (LEO 1530). Samples for SEM imaging were prepared by applying the powder directly to aluminium stubs on carbon adhesion tape.

6.2.5.5 Energy dispersive X-ray (EDX) analysis

Elemental composition of fresh and spent catalyst was confirmed and quantified by using the EDX feature of the SEM.

6.2.5.6 X-ray photoelectron spectroscopy (XPS) analysis

A Kratos Axis Ultra spectrometer using a monochromatic AlK (alpha) source (15 mA, 14 kV) was used to perform the X-ray photoelectron spectroscopy (XPS) analysis.

6.3 Results and Discussion

6.3.1 Screening of decarboxylation catalyst

The first set of experiments compared the catalytic activities for the decarboxylation of oleic acid in a continuous flow thorough reactor using 10 wt% loading of Ni, Mo and MgO on γ-Al_2O_3 at 375°C, space time of 4 h and water-to-OA ratio of 5:1 using 5 g of catalyst. Figure 6.2 depicts the ATR-FTIR spectra of decarboxylated liquid products along with the starting materials. The results show that the degree of decarboxylation of OA varied strongly using the investigated catalysts being 67, 65 and 92% using a 10 wt% MgO-Al_2O_3, 10 wt% Ni-Al_2O_3 and 10 wt% Mo-Al_2O_3 catalyst respectively. On the other hand, the liquid and gaseous product yields using these three catalysts are 65 and 35, 30 and 70, 71 and 29, respectively. The liquid and gaseous product yields clearly indicate that the 10 wt% Ni-Al_2O_3 catalyst is primarily a gasification catalyst, consistent with our previous work on supercritical water gasification [22-25].
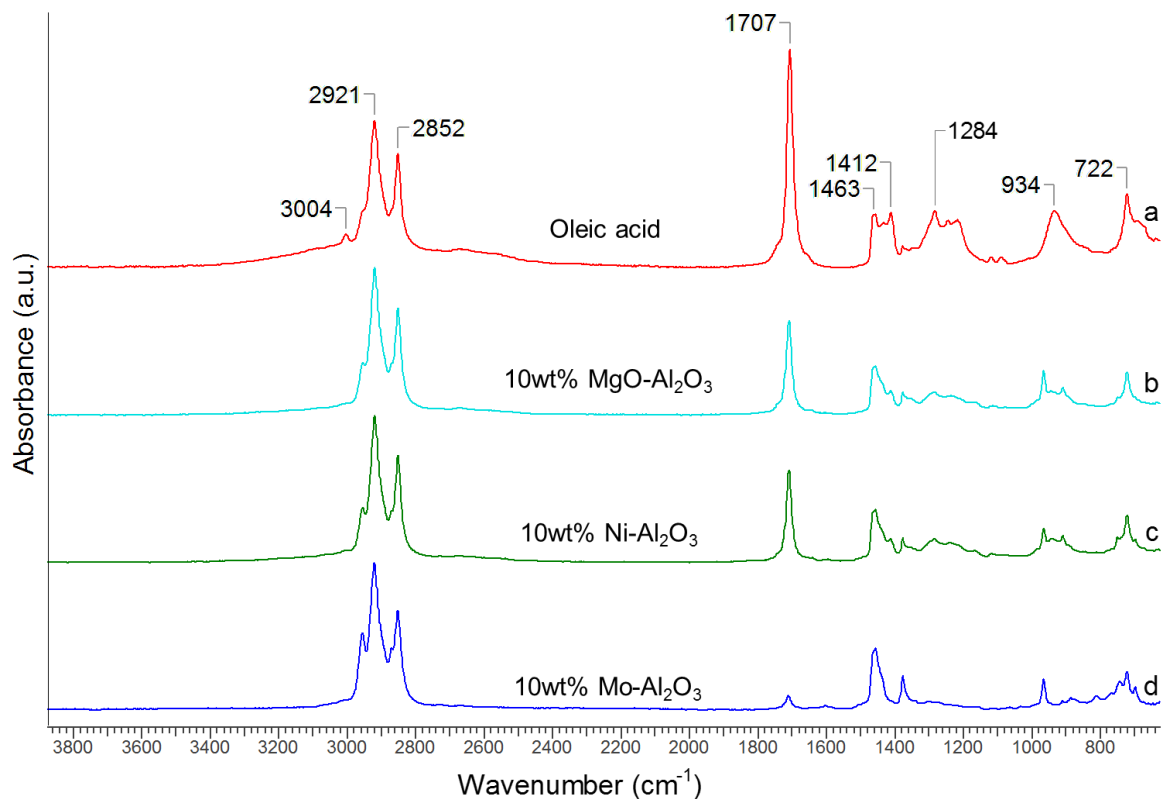
Figure 6.2: ATR-FTIR spectra of oleic acid and the formed products using different catalysts.

The gaseous products CO and CO_2 found in the product streams are compared in Figure 6.3. The 10 wt% $Ni\text{-}Al_2O_3$ and 10 wt% $MgO\text{-}Al_2O_3$ catalysts provided a higher yield of CO compared to CO_2 while the 10 wt% $Mo\text{-}Al_2O_3$ catalyst provided a higher yield of CO_2 compared to CO. This indicates that the Mo based catalyst dominates the decarboxylation of OA under the chosen reaction conditions. Significant amounts of H_2, CH_4 and lighter factions of hydrocarbons (C_2 to C_4) were found using 10 wt% $Ni\text{-}Al_2O_3$ catalyst (data not shown). Based on these initial ATR-FTIR and GC-TCD results, the 10 wt% $Mo\text{-}Al_2O_3$ catalyst was chosen for the subsequent parametric study.
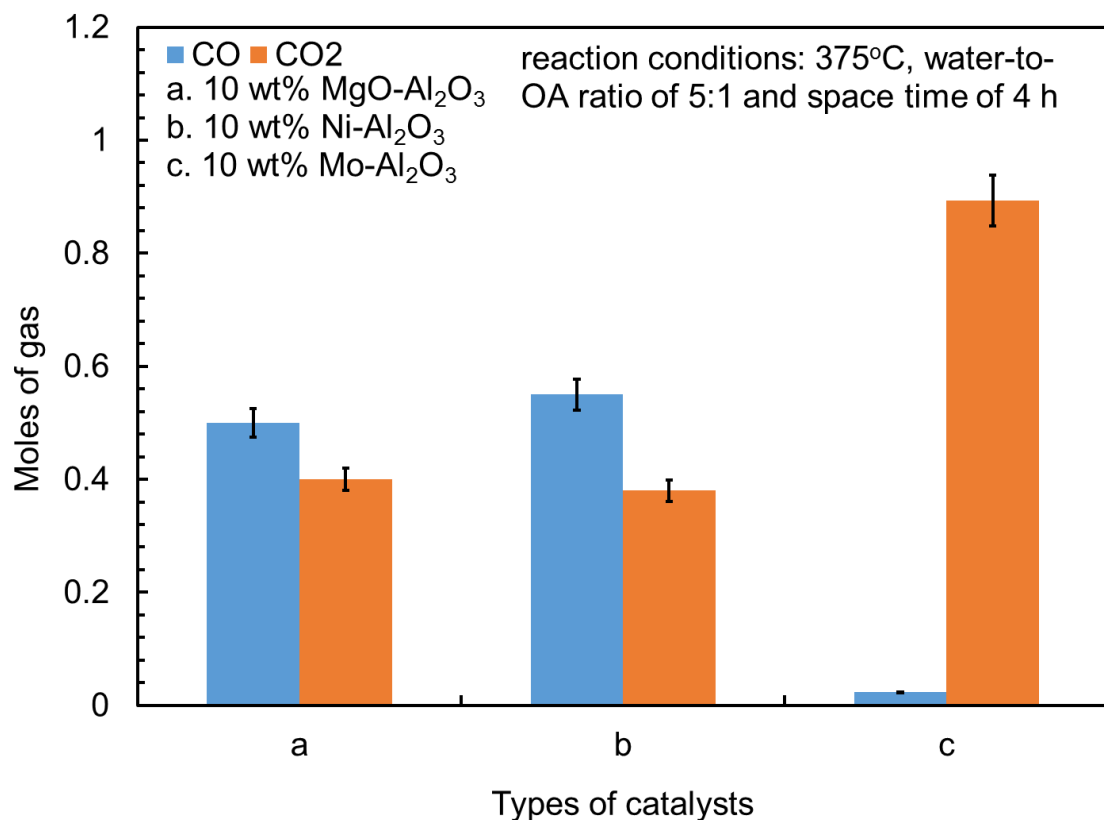
Figure 6.3: GC-TCD analysis of product gases using different catalysts.

6.3.2 Decarboxylation of OA

6.3.2.1 Effect of reaction parameters on degree of decarboxylation

Reaction temperature, water-to-OA ratio and space time (τ) are three of the most important parameters for the hydrothermal decarboxylation of oleic acid, as described in the previous chapters of this dissertation. The degree of decarboxylation results obtained at different experimental conditions (T = 325 to 400°C, water to OA ratio = 2:1 to 5:1 and space time = 0.5 to 4 h) using 5 g of the 10 wt% Mo-Al$_2$O$_3$ catalyst are presented in Figure 6.4 while Figure D1 shows the corresponding ATR-FTIR diagram. The results show that the degree of decarboxylation increased (from 55 to 92%) with increasing temperature from 325 to 375°C (Figure 6.4a). Further increasing temperature form 375 to 400°C improved the degree of decarboxylation by only 0.3%. The results show that the degree of decarboxylation of OA is less sensitive to temperature above 375°C. Therefore, the maximized temperature chosen for this study was 375°C.
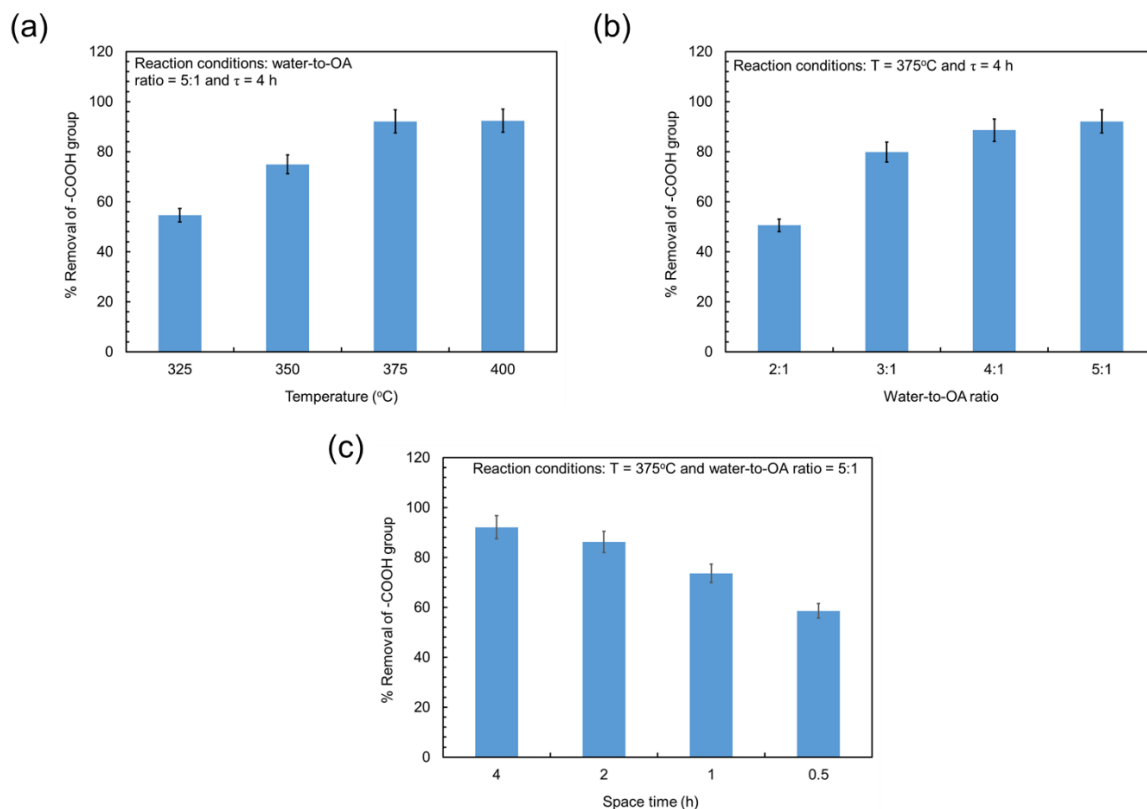
Figure 6.4: Percentage removal of –COOH group at different (a) temperatures (b) water-to-OA ratio's (c) space times.

The effect of water-to-OA ratio and space time on the degree of decarboxylation are presented in Figure 6.4b and c, respectively. Figure D2 shows their corresponding ATR-FTIR spectra. The results indicate that the degree of decarboxylation increased with increasing water-to-OA ratio from 2:1 to 5:1 and increasing space time from 0.5 to 4 h. The maximum degree of decarboxylation obtained at 375°C, water-to-OA ratio of 5:1 and space time of 4 h was 92%. Based on these results, the maximum degree of decarboxylation using the 10wt% Mo-Al$_2$O$_3$ catalyst for the current study was 375°C, water-to-OA ratio of 5:1 and space time of 4 h.

The disappearance of alkenyl =CH stretching at 3004 cm^{-1} (Figure D1 and Figure D2) for all catalytic experiments clearly shows the 10wt% Mo-Al$_2$O$_3$ catalyst plays a dual role for both hydrogenation of C=C and decarboxylation. The peaks assigned to C-O stretching (1412 cm^{-1}), combination of C-O stretching and O-H deformation (1412 cm^{-1}) and O-H out of plane bending mode (934 cm^{-1}) also decrease significantly in the formed liquid products compared

to OA during the decarboxylation reaction. This confirms the decarboxylation of oleic acid in the presence of the 10wt% Mo-Al$_2$O$_3$ catalyst.

6.3.2.2 GC-FID analysis of liquid products

Use of liquid products as commercial fuel largely depends on an understanding of controlling the molecular fingerprint. Figure 6.5 shows the distribution of hydrocarbons present in the liquid decarboxylated products at different experimental conditions using 5 g of 10 wt% Mo-Al$_2$O$_3$ catalyst. Selectivity of hydrocarbon varies with temperature which is presented in Figure 6.5a. The selectivity of tetradecane increased from 0 to 34.8% whereas pentadecane selectivity decreased from 49.3 to 24% when the temperature was increased from 325 to 375 ^{o}C. At the same time, the selectivity of hexadecane decreased from 39 to 22.9% and the selectivity of hetadecane slightly increased from 10.7 to 18.3%. Lower heptadecane and higher tetradecane selectivities at 375°C indicates that the Mo based catalyst cracks OA into smaller hydrocarbons.

Selectivities of hydrocarbon compounds vary with the ratio of water-to-OA and space times. Figure 6.5b and c shows the effect of water-to-OA and space time on the distribution of hydrocarbon compounds in the liquid decarboxylated products. The selectivity of tetradecane increased (from 34.8 to 77%) with decreasing water-to-OA ratio from 5:1 to 2:1 and decreased (from 34.8 to 14.5) with decreasing space time from 4 to 0.5 h. The selectivity of pentadecane increased (from 7.2 to 24% and 9.2 to 24%) with increasing ratio from 2:1 to 5:1 and space time from 0.5 to 4 h, respectively. The selectivity of hexadecane slightly increased with increasing water-to-OA ratio and space time. The selectivity of heptadecane increased with increasing ratio and decreased with increasing space time. The results conclude that higher temperature, lower water-to-OA ratio and space time favors higher selectivity of hepatadecane (73.6%) whereas higher temperature, water-to-OA ratio and space time provides higher tetradecane selectivity (34.8%). Lower selectivity of hetadecene at all catalytic experiments indicate that the higher degree of saturation of C=C to C-C. This result is consistent with ATR-FTIR results.
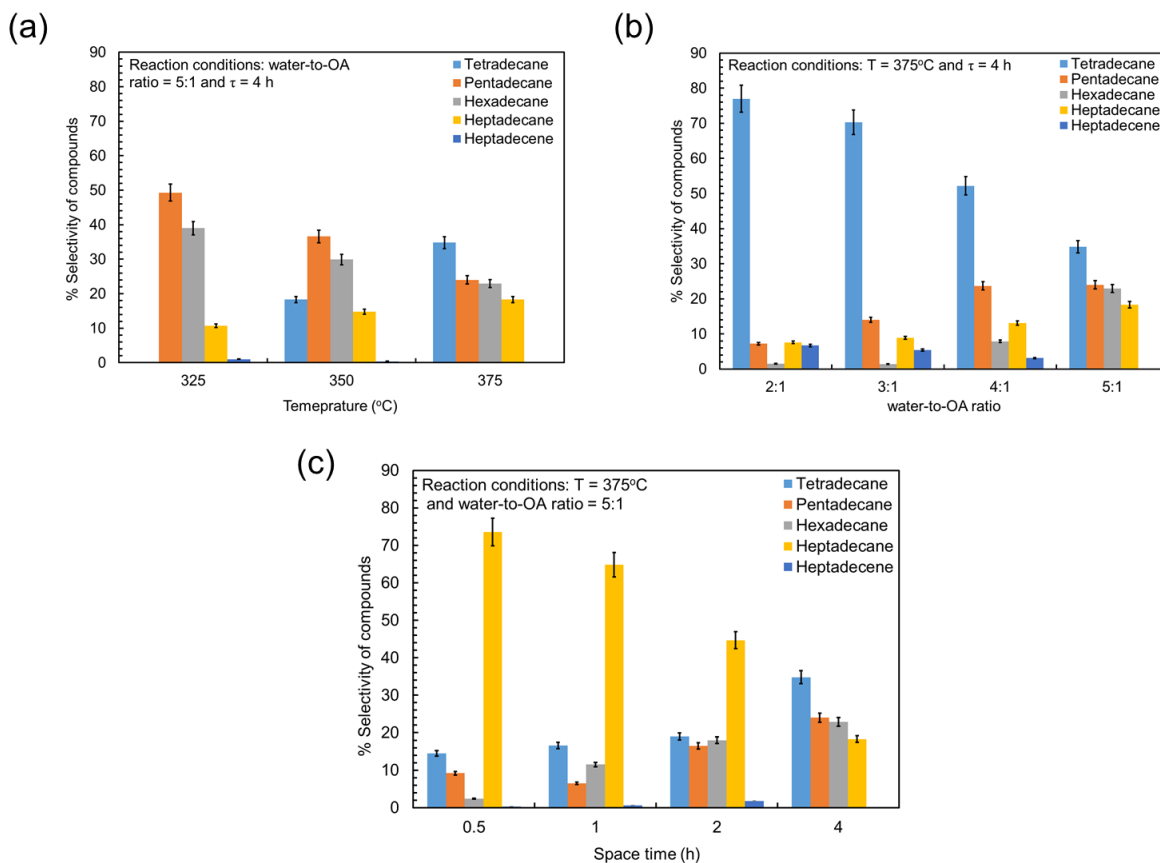
Figure 6.5. Hydrocarbons present in the liquid products at different (a) temperatures (b) water-to-OA ratio's (c) space times.

6.3.2.3 Fuel quality

Density is an important physical characteristic of liquid fuel which determines whether it can be used as diesel, kerosene or jet fuel. For liquids, temperature is an important factor that can affect a liquids density with density being expressed at a given temperature for comparison purposes. The values of density of the decarboxylated product at different temperatures and of some commercial fuels are listed in Table 6.1. Comparing the experimental data with conventional fuels indicates that the decarboxylated product falls within the typical diesel range.

Table 6.1: Density of decarboxylated product and some commercial fuels.

Compounds	Temperature ($^{\circ}$C)	Density (kg/m^3)
decarboxylated product[*]	15.6	0.85
	21.6	0.85
	25	0.85
	40	0.84
kerosene [26]	15.6	0.78-0.82
jet fuel [27]	15	0.78-0.84
diesel [26]	15.6	0.80-0.96

* maximized conditions

High heating value (HHV) is the most important parameter for any fuel which determines the economics of the fuel usage. The higher the HHV, the lesser the amount of fuel required. If any fuel has higher HHV it will have a tendency to produce more power in the engine. The fuels with less HHV tend to burn inefficiently thus causing lots of exhaust and air-pollution [28]. Table 6.2 shows the HHV values of the decarboxylated product with some commercial fuels. The results indicate that the HHV of the decarboxylated product is similar to jet fuel, kerosene and diesel.

Table 6.2: High heating values of feed, product and commercial fuels.

Compounds	HHVs (MJ/kg)
Oleic acid	39.2
Decarboxylated product[*]	44.7
Jet fuel [29]	43.5
Kerosene [26]	46.2
Diesel [26]	44.8

*maximized conditions

6.2.2.4 GC-TCD analysis of gaseous products

Decarboxylation of OA was confirmed by analyzing the gaseous products using GC-TCD. The results obtained at different reaction temperatures are presented in Figure 6.6. The number of moles of CO and CO_2 were decreased and increased, respectively with increasing reaction temperature from 325 to 375°C. This result indicates that the decarboxylation is the dominating

153

reaction at 375°C, although 10 wt% Mo-Al$_2$O$_3$ catalyst slightly cracks the reactant molecules into smaller hydrocarbons. The GC-TCD results help confirm the ATR-FTIR results. A small amount of lighter fraction of hydrocarbons (C$_2$ to C$_4$) was identified in the gaseous products (data not shown).
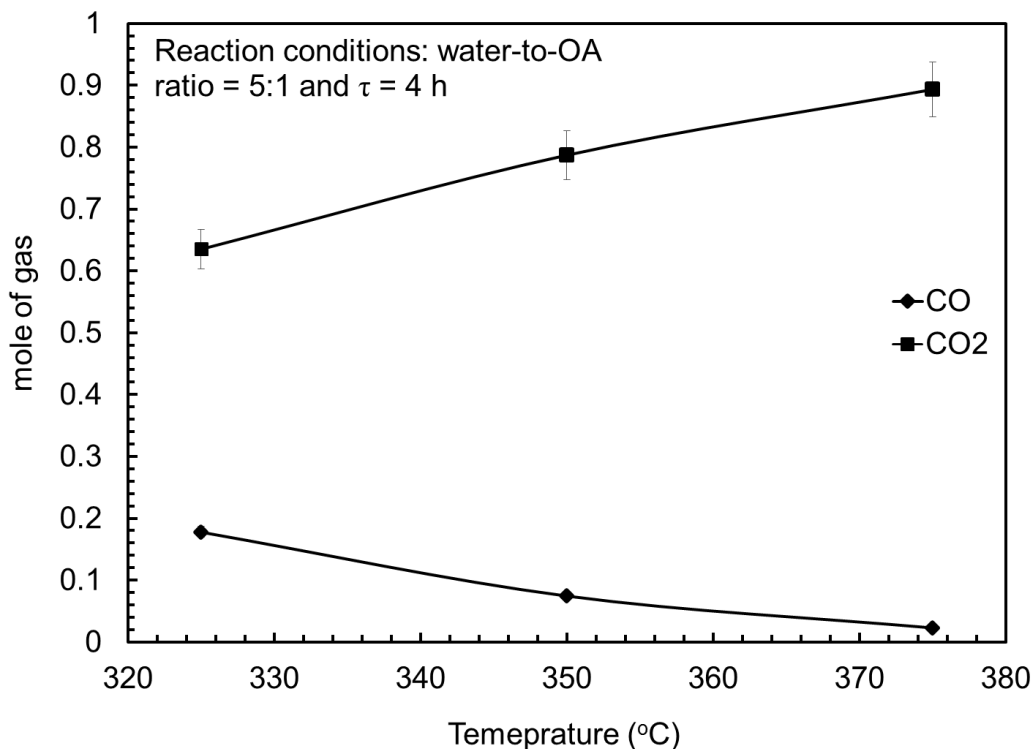
Figure 6.6: Number of moles of CO and CO$_2$ present in the gas product.

6.3.3 Decarboxylation of fatty acid derivatives

Hydrothermal decarboxylation of three non-edible feedstocks including castor oil, palm oil and frying oil was performed at the maximized conditions achieved for OA decarboxylation. The maximized conditions are: T = 375°C, water-to-oil ratio = 5:1, space time = 4 h and amount of catalyst = 5 g (10wt% Mo-Al$_2$O$_3$). The ATR-FTIR results of the formed products from castor oil, palm oil and frying oil are presented in Figure 6.7.
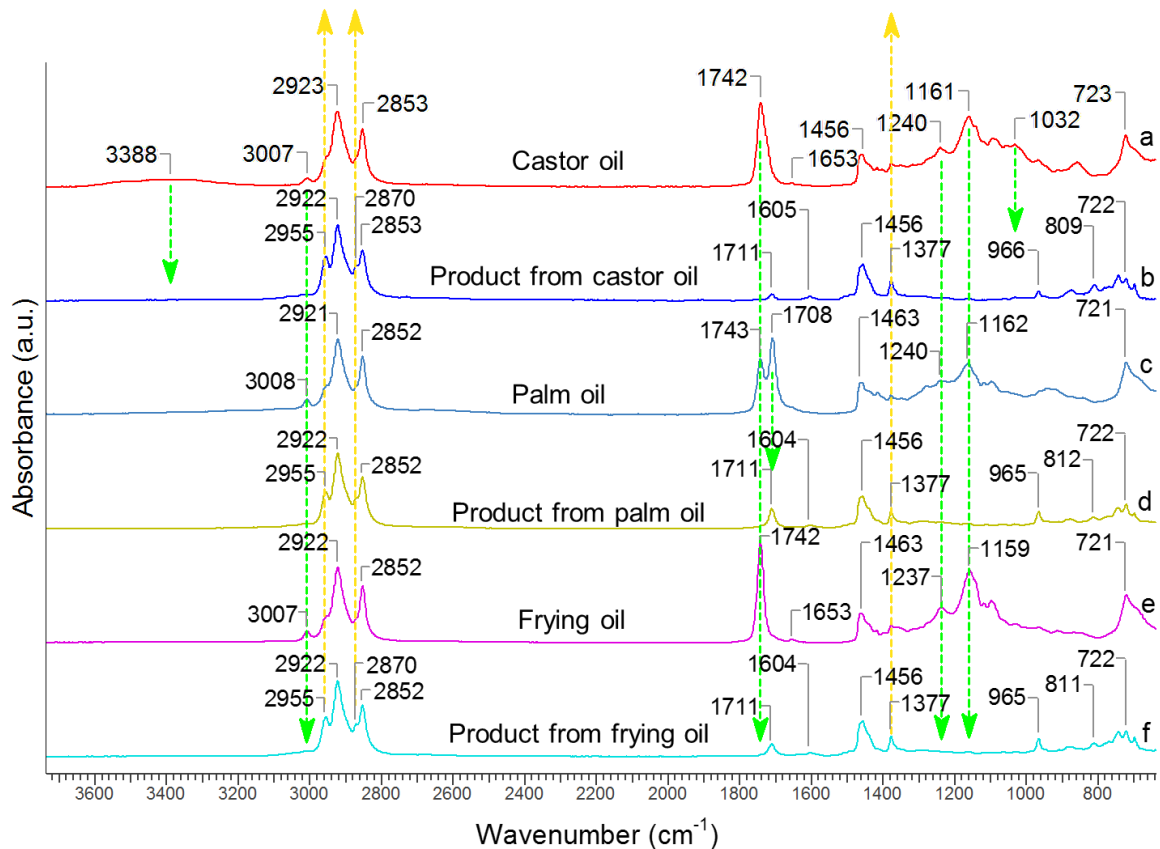
Figure 6.7: ATR-FTIR spectra of different fatty acid derivatives and formed products.

Figure 6.7 compares the ATR-FTIR spectra of the corresponding products with the starting oils, i.e., castor oil, palm oil, and frying oil. In the spectrum of castor oil (Figure 6.7a), there are several absorbance peaks at 3388, 3007, 2923, 2853, 1742, 1653, 1456, 1240, 1161, 1032, and 723 cm^{-1} resulting from hydroxyl, alkenyl, methylene, and carboxylic ester groups of ricinoleic acid contained in castor oil. The peaks at 3388 and 1032 cm^{-1} are assigned to alcoholic O-H and C-O stretching modes, respectively, while the peaks at 3007 and 1653 cm^{-1} are ascribed to alkenyl =C-H and C=C stretching modes, respectively. The peaks at 2923, 2853, and 723 cm^{-1} are attributed to methylene C-H asymmetric stretching, symmetric stretching, and rocking modes, respectively. The peak at 1456 cm^{-1} is assigned to methylene C-H scissoring and methyl C-H asymmetric bending modes. The peaks at 1742, 1240, and 1161 cm^{-1} are attributable to carboxylic ester C=O stretching and C-O stretching modes of the glycerol ester, respectively. After the decarboxylation reaction, all the peaks related to C=O,

155

C-O, O-H, C=C, =C-H vibrations disappear while a few new peaks appear at 2955, 2870, 1711, 1605, 1377, 966, and 809 cm^{-1} (Figure 6.7b). The peaks at 2955, 2870, and 1377 cm^{-1} are attributed to methyl C-H asymmetric stretching, symmetric stretching, and umbrella modes, respectively. The peak at 1711 cm^{-1} is ascribed to carboxylic C=O stretching mode. The peaks at 1605, 966, and 809 cm^{-1} are attributable to aromatic C=C stretching and C-H out-of-plane bending modes, respectively. These results confirm conversion of carboxylic ester (C(=O)-O), alcoholic OH, and alkenyl (C=C) groups and formation of methyl (CH$_3$), and small amount of carboxylic acid (-COOH) and aromatic compounds.

In the spectrum of palm oil (Figure 6.7c), there are several absorbance peaks at 3008, 2921, 2852, 1743, 1708, 1463, 1240, 1162, and 721 cm^{-1} resulting from alkenyl, methylene, and carboxylic ester, carboxylic acid groups contained in palm oil. The peak at 3007 cm^{-1} is ascribed to alkenyl =C-H stretching mode while the peak at 1708 cm^{-1} is assigned to the C=O stretching mode of palmitic acid and oleic acid contained in palm oil. The peaks at 2921, 2852, and 721 cm^{-1} are attributed to methylene C-H asymmetric stretching, symmetric stretching, and rocking modes, respectively. The peak at 1463 cm^{-1} is assigned to methylene C-H scissoring mode. The peaks at 1743, 1240, and 1162 cm^{-1} are attributable to carboxylic ester C=O stretching and C-O stretching modes of the glycerol ester, respectively. After the decarboxylation reaction, all the peaks related to C=O, C-O, C=C, =C-H vibrations disappear while a few new peaks appear at 2955, 1711, 1604, 1377, 965, and 812 cm^{-1} (Figure 6.7d). The peaks at 2955 and 1377 cm^{-1} are attributed to methyl C-H asymmetric stretching and umbrella modes, respectively. The peak at 1711 cm^{-1} is ascribed to carboxylic acid C=O stretching mode. The peaks at 1604, 965, and 812 cm^{-1} are attributable to aromatic C=C stretching and C-H out-of-plane bending modes, respectively. These results confirm conversion of carboxylic ester (C(=O)-O), and alkenyl (C=C) groups and formation of methyl (CH$_3$), and small amount of carboxylic acid (-COOH) and aromatic compounds.

In the spectrum of frying oil (Figure 6.7e), there are several absorbance peaks at 3007, 2922, 2852, 1742, 1653, 1463, 1237, 1159, and 721 cm^{-1} resulting from alkenyl, methylene, and carboxylic ester groups contained in frying oil. The peaks at 3007 and 1653 cm^{-1} are ascribed to alkenyl =C-H and C=C stretching modes, respectively. The peaks at 2922, 2852, and 721 cm^{-1} are attributed to methylene C-H asymmetric stretching, symmetric stretching, and rocking modes, respectively. The peak at 1463 cm^{-1} is assigned to methylene C-H scissoring mode.

The peaks at 1742, 1237, and 1159 cm^{-1} are attributable to carboxylic ester C=O stretching and C-O stretching modes of the glycerol ester, respectively. After the decarboxylation reaction, all the peaks related to C=O, C-O, C=C, =C-H vibrations disappear while a few new peaks appear at 2955, 2870, 1711, 1604, 1377, 965, and 811 cm^{-1} (Figure 6.7f). The peaks at 2955, 2870, and 1377 cm^{-1} are attributed to methyl C-H asymmetric stretching, symmetric stretching, and umbrella modes, respectively. The peaks at 1711 cm^{-1} is ascribed to carboxylic C=O stretching mode. The peaks at 1604, 965, and 811 cm^{-1} are attributable to aromatic C=C stretching and C-H out-of-plane bending modes, respectively. These results confirm conversion of carboxylic ester (C(=O)-O) and alkenyl (C=C) groups and formation of methyl (CH_3), and small amount of carboxylic acid (-COOH) and aromatic compounds.

Decarboxylation of castor, palm and frying oil was further confirmed by GC-TCD analysis of gaseous products formed during the reaction. Figure 6.8 shows the number of moles of CO or CO_2 present in the gaseous products. The amount of CO_2 was found to be 0.88, 0.86 and 0.77 moles in the gaseous products formed during the decarboxylation of castor, frying and palm oil. On the other hand, the quantity of CO was found to be 0.05, 0.13 and 0.23, respectively. Although complete decarboxylation was not achieved for the above three non-edible feedstocks, our hydrothermal decarboxylation process shows feasibility to decarboxylate any fatty acid or its derivatives without adding any external hydrogen source or hydrogen donor solvent. These results are attractive to implement the process for commercial production of liquid hydrocarbons from various feed sources, which can help lower our dependency on fossil fuels.
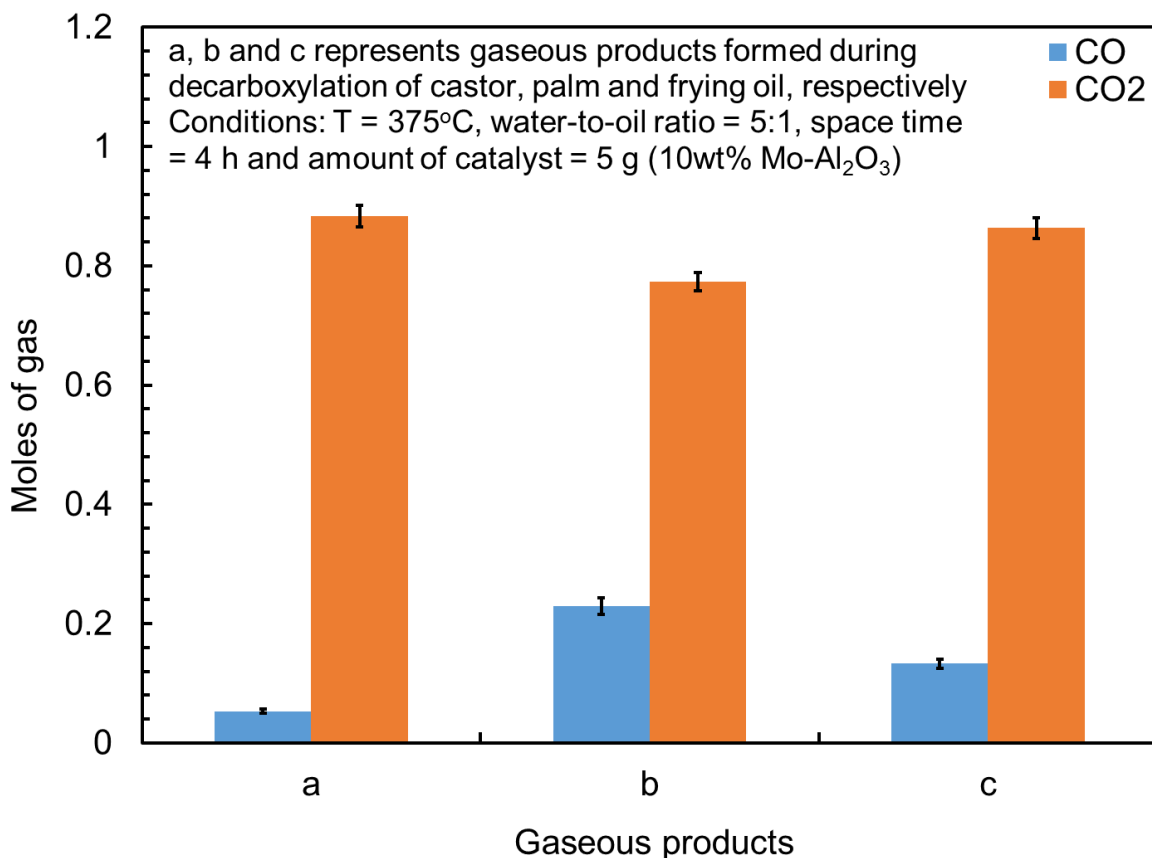
Figure 6.8: Identification of CO and CO_2 in the gaseous products formed during decarboxylation of castor, palm and frying oil.

6.3.4 Catalyst Characterization

6.3.4.1 Characterization of fresh catalysts

To determine the actual loading of metal on Al_2O_3, EDX analysis was performed and the results are shown in Figure 6.9. The actual loading of Mo and Ni was found to be 10.13 and 9.96 wt%, respectively. Os and C were detected during EDX analysis from sample holder not from sample. The wt% of Mo (9.86%) was also confirmed by XPS analysis. Since, EDX cannot determine the oxide state of any metal, the actual loading of MgO was calculated form the weight difference between the catalyst sample after reduction and before loading. The loading of MgO was found to be 9.76 wt%.
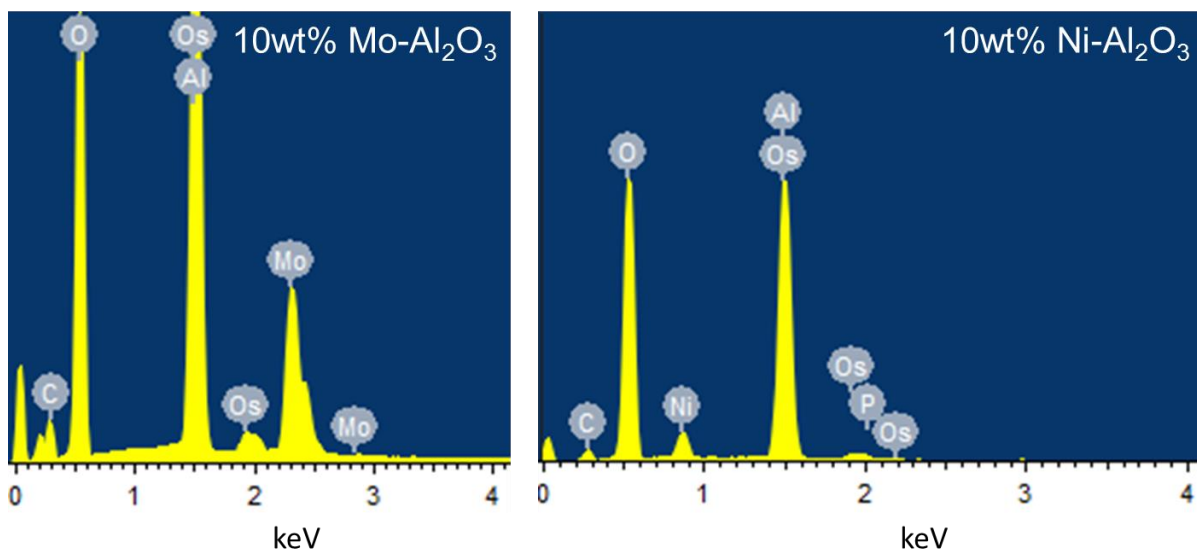
Figure 6.9: EDX analysis of fresh catalysts.

Textural properties of any catalyst are important parameters to measure its catalytic activity. N_2 adsorption-desorption isotherm and pore size distributions are shown in Figure 6.10 and their corresponding pore properties are shown in Table 6.3. The isotherms of Al_2O_3 Figure 6.10(i)a, 10 wt% Mo-Al_2O_3 in Figure 6.10(i)b, 10 wt% MgO-Al_2O_3 in Figure 6.10(i)c and 10 wt% Ni-Al_2O_3 in Figure 6.10(i)d showed typical type IV isotherms with the H1-type hysteresis loop. This indicates that all the fresh catalysts possessed a mesoporous structure [30, 31]. Mesoporosity of the prepared catalysts were confirmed by pore size distributions in Figure 6.10(ii). As presented in Table 6.3, the BET surface area and pore volume of all the fresh catalysts are lower than that of the support, indicating that Mo, MgO and Ni loadings partially blocked Al_2O_3 pores during the catalyst preparation step (impregnation method). BET surface area and pore volume of the three synthesized catalysts are slightly different from each other which follows the order: 10 wt% MgO-Al_2O_3 > 10 wt% Mo-Al_2O_3 > 10 wt% Ni-Al_2O_3. The average pore size of all the catalysts are close to each other and slightly lower than the Al_2O_3 support. However, these differences are insignificant due to the catalytic activity.

159

Table 6.3: Summary of BET surface area, pore volume and pore size of fresh and spent catalysts.

Name of the sample	Fresh/Spent	BET surface area (m^2/g)	Pore volume (cm^3/g)	Average pore size (nm)
Al$_2$O$_3$	Fresh	179	0.50	11.1
10 wt% Mo-Al$_2$O$_3$	Fresh	160	0.44	9.6
	Spent	78	0.23	10.2
10 wt% MgO-Al$_2$O$_3$	Fresh	163	0.45	10.5
	Spent	99	0.22	18.4
10 wt% Ni-Al$_2$O$_3$	Fresh	158	0.45	10.5
	Spent	111	0.28	10.0
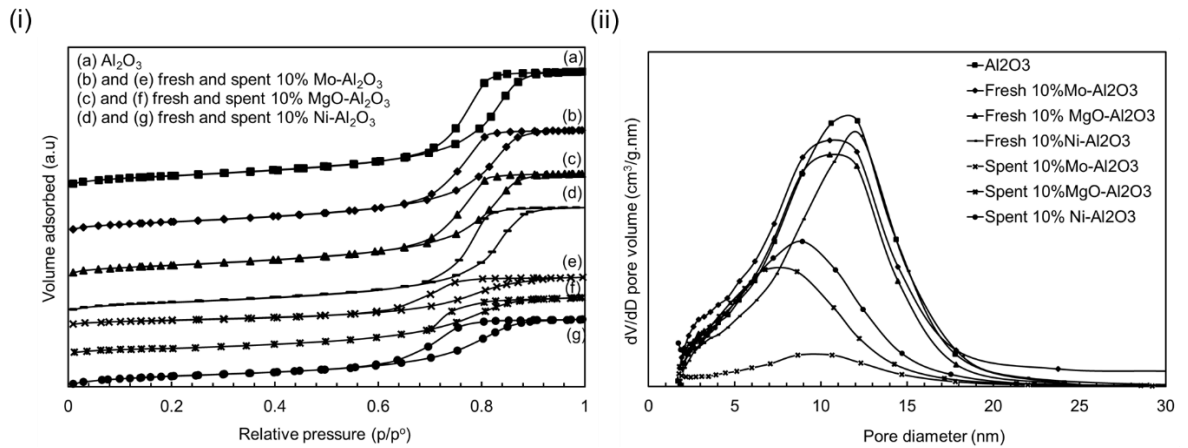
Figure 6.10: (i) N$_2$ adsorption-desorption isotherms and (ii) pore size distributions of fresh and spent catalysts

Crystallinity of a catalyst greatly enhances its catalytic activity which is usually measured by XRD. XRD pattern of fresh catalysts and support are shown in Figure 6.11. Figure 6.11a shows the pure γ-Al$_2$O$_3$ phase at 2θ = 35.2, 47.2 and 67.6° [32]. Mo, MoAl$_2$O$_4$ and Al$_2$O$_3$ phases were found in the XRD pattern of fresh 10 wt% Mo-Al$_2$O$_3$ catalyst (Figure 6.11b). Most of the Mo particles were found as spinel MoAl$_2$O$_4$ phase in the catalyst surface which shows the strong diffraction peak at 2θ = 27, 38 and 54°. Very weak reflections of pure Mo are seen at 2θ = 42 and 61°. Fresh 10 wt% MgO-Al$_2$O$_3$ and 10 wt% Ni-Al$_2$O$_3$ catalysts shows mainly MgAl$_2$O$_4$ and NiAl$_2$O$_4$ phases which indicates that all the MgO and Ni particle reacts with Al$_2$O$_3$ to form MgAl$_2$O$_4$ and NiAl$_2$O$_4$, respectively (Figure 6.11d and f). Spinel MgAl$_2$O$_4$ phase was found at

$2\theta = 19.2, 31.5, 37.1, 45.3$ and $66.1°$. Spinel $NiAl_2O_4$ phase was found at $2\theta = 19, 37, 45$ and $66°$. No diffraction peaks of MgO and Ni were found in the XRD pattern of fresh catalysts, which may be due to the overlapping by reflections of $MgAl_2O_4$ and $NiAl_2O_4$ peaks or due to the better dispersion of MgO or Ni species on the catalyst surface [32, 33]. The formation of $MoAl_2O_4$, $MgAl_2O_4$ and $NiAl_2O_4$ is due to the high reduction or calcination temperature [34]. The sharp peak intensity of fresh 10 wt% $Ni-Al_2O_3$ catalyst compared to fresh 10 wt% MgO-Al_2O_3 and 10 wt% $Ni-Al_2O_3$ catalysts indicate the smaller particle phases present on the surface. Moreover, no reflections for $\theta-Al_2O_3$ (25.6 and 43.3°) or $\alpha-Al_2O_3$ (31.2 and 36.6°) were observed on the calcined/reduced catalysts, indicating that transformation of Al_2O_3 was not enhanced by the chosen reduction/calcination temperature.
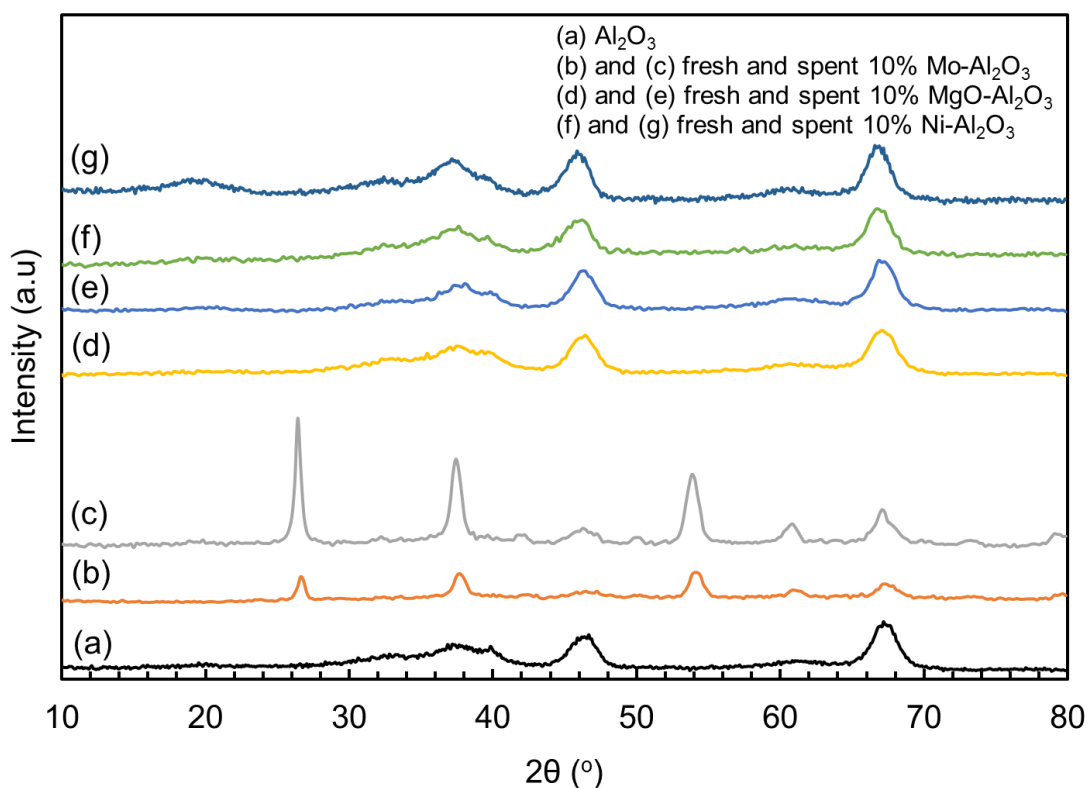
Figure 6.11: XRD patterns of fresh and spent catalysts.

In order to determine the reducibility as well as the optimum reduction temperature for the investigated catalysts for decarboxylation in subcritical water, TPR-H_2 experiments were undertaken. In conjunction with the XRD data, it was also useful to determine the type of

161

species present in the calcined/reduced catalysts. H_2-TPR profiles of fresh catalysts are shown in Figure 6.12. There are four reduction peaks observed in the TPR profile of fresh 10 wt% Mo-Al_2O_3 at 475, 666, 925 and 1065 $^{\circ}$C, respectively. It has been reported that the reduction of Mo species is a two-step process such as MoO_3 to MoO_2 and then MoO_2 to Mo [35]. Different reduction temperatures obtained in the TPR profile indicate the formation of different Mo species. It was previously found that the reduction of the Mo-Al_2O_3 catalyst produced four different forms of Mo phases. Ma et al. [36] reported two kinds of Mo species. One was polynuclear, either in the octahedral-coordinated MoO_3 crystallite form or in the MoO_x form with a square–pyramidal coordination, and located on the external surface of the support. The second one was related to Al atoms in the lattice channel of support. The reduction peak at 475 $^{\circ}$C of fresh 10 wt% Mo-Al_2O_3 is ascribed to the reduction of MoO_3 to MoO_2 [37]. The strong peak assigned to 1065 $^{\circ}$C indicates further reduction of MoO_2 to form metallic Mo [38]. The reduction peaks at 666 and 925 $^{\circ}$C may be ascribed to the initial and the further reduction of the aggregative MoO_3 species [35].
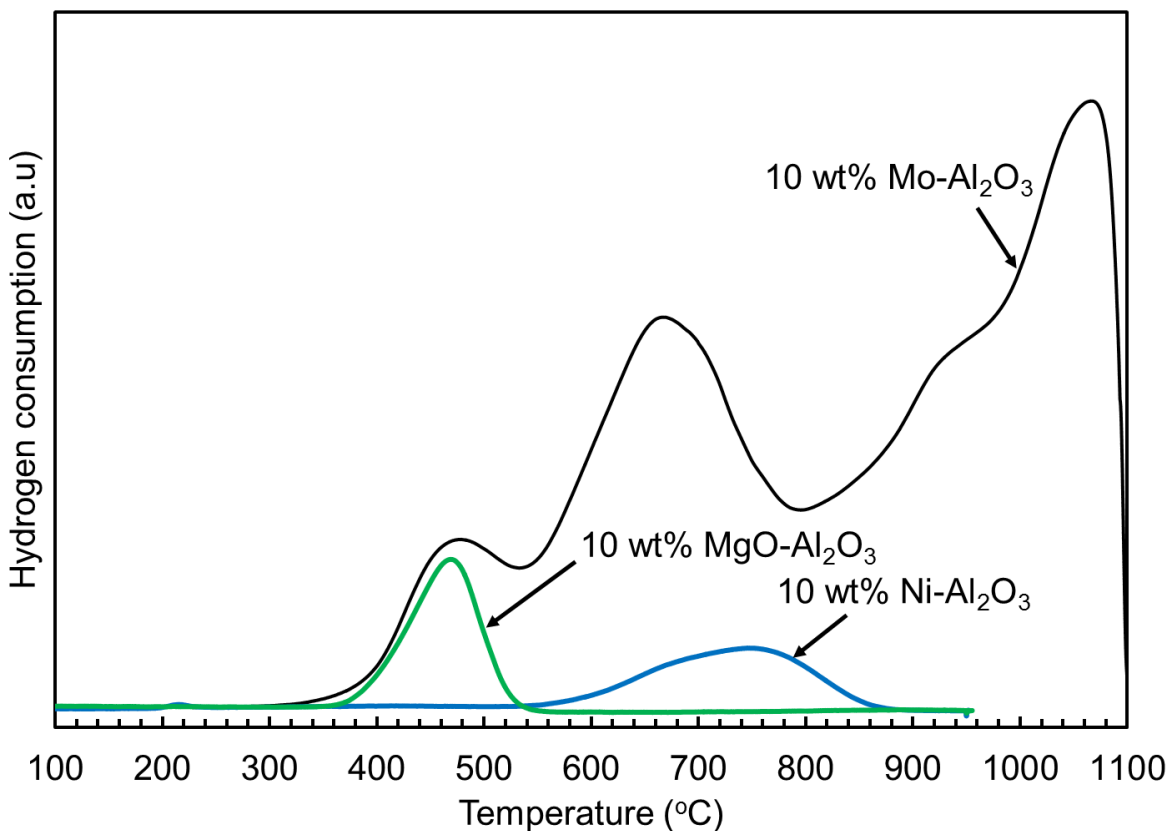
Figure 6.12: TPR profiles of fresh catalysts.

Fresh 10 wt% MgO-Al$_2$O$_3$ catalyst shows its only reduction peak at 475°C, which represents the reduction of MgAl$_2$O$_4$. Usually Ni-Al$_2$O$_3$ catalyst shows two major reduction peaks at 250-350°C and 600 to 850°C which correspond to the easily reducible NiO and hard to reduce NiO, respectively [39]. Since there is no peak observed around 250-350°C in this study, all the NiO reacts with Al$_2$O$_3$ to form NiAl$_2$O$_4$. The reduction peak of NiAl$_2$O$_4$ observed at 750°C for the fresh 10 wt% Ni-Al$_2$O$_3$. Reducibility of nickel catalysts largely depends on the nickel loading, calcination or reduction temperature and the interaction of nickel oxide and alumina [40]. Calcination or reduction at high temperature increases the metal-support interaction and the formation of NiAl$_2$O$_4$, which results in greater difficulty of nickel catalysts in reduction.

The reduction temperature and peak width measured by TPR are indications of the ease of reduction and the degree of interaction between different metallic species, respectively. A high reduction temperature indicates difficulty in reduction whereas wide peaks indicate a higher degree of interaction between the species and the support. It is seen from the TPR-H$_2$ profile that both fresh 10wt% Mo-Al$_2$O$_3$ and 10 wt% Ni-Al$_2$O$_3$ reduced at higher temperature compared to fresh 10 wt% MgO-Al$_2$O$_3$ catalyst. Comparing the fresh Mo and Ni based catalysts, the Mo catalyst was reduced at higher temperatures. However, the TPR-H$_2$ peaks for the MgO catalyst is comparatively narrower than those for the other two catalysts implying a lower degree of interaction of MgO with Al$_2$O$_3$. H$_2$-TPR results are consistent with the XRD results.

For a more detailed investigation of the surface structure, XPS spectra of fresh and spent 10wt% Mo-Al$_2$O$_3$ is presented in Figure 6.13. The Mo catalyst shows the characteristic doublet of Mo^{6+}, Mo^{5+}, Mo^{4+}, Mo^o at 234, 231.5, 229.7 and 229.4 eV, respectively [41, 42]. This result is supported by the TPR investigation of the Mo catalyst.
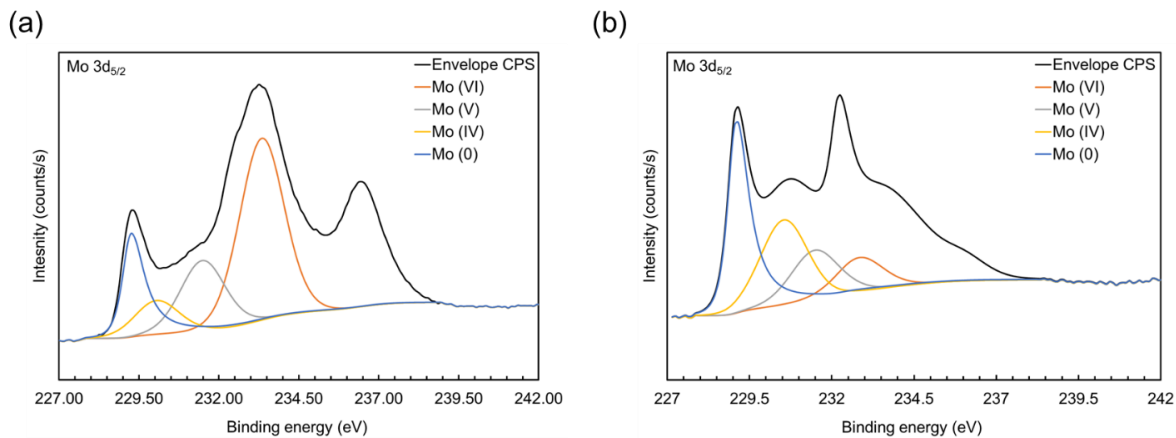
Figure 6.13: XPS analysis of 10wt% Mo-Al$_2$O$_3$ catalyst (a) fresh and (b) spent.

6.3.4.2 Catalysts deactivation studies

Metal supported catalyst has a tendency for deactivation when it is exposed to harsh (high temperature or pressure) environment. Deactivation of a metal catalyst can occur from several factors including: adsorption of impurities from the feed/product streams, coke deposition on the catalyst surface, oxidation of metal, metallic surface area reduction from sintering/ leaching, and a drop in surface area from pore blockage. [43]. XRD analysis was performed on all three spent catalysts (Figure 6.11). Metal supported spent catalysts usually show the peaks for graphitic coke formation at $2\theta = 62^o$ and atomic coke formation at $2\theta = 30^o$, respectively [5, 22]. From the XRD pattern, no such peak was found for all three catalysts (Figure 6.11c, e and g). There was no significant differences observed in the XRD patterns for fresh and spent 10wt% MgO-Al$_2$O$_3$ and 10wt% Ni-Al$_2$O$_3$ catalysts. On the other hand, peak intensities for the spent 10wt% Mo-Al$_2$O$_3$ catalyst were found to be larger than its fresh one, indicating catalyst agglomeration from the decarboxylation reaction. Agglomeration of Mo particles may be the main reason for the observed reduction of BET surface area of spent Mo catalyst compared to the spent MgO and Ni catalysts (Table 6.3 and Figure 6.10i). The lower BET surface area observed for the spent Mo catalyst may be due to pore blockage by produced hydrocarbon molecules which did not wash out with hexanes or catalyst drying step. Although all the spent catalysts have lower BET surface areas than their fresh ones, they still maintain the mesoporous pore size distributions (Figure 6.10ii).

The surface morphology of the synthesized catalysts were examined by SEM imaging both before and after the decarboxylation reaction (Figure 6.14). All the fresh catalysts showed uniform metal/metal oxide particles distribution on the surface of the catalysts, indicating better catalytic properties. Although the Ni catalyst has a similar morphology to the Mo and MgO catalyst, the Ni catalyst was found to gasify the feedstock at the chosen reaction conditions instead of decarboxylation (explained earlier). Agglomerated structure of the spent 10wt% Mo-Al_2O_3 catalyst was confirmed from the SEM images. There was no morphological differences observed for the fresh and spent 10wt% MgO-Al_2O_3 and 10wt% Ni-Al_2O_3 catalysts. These results are consistent with the XRD and BET results.
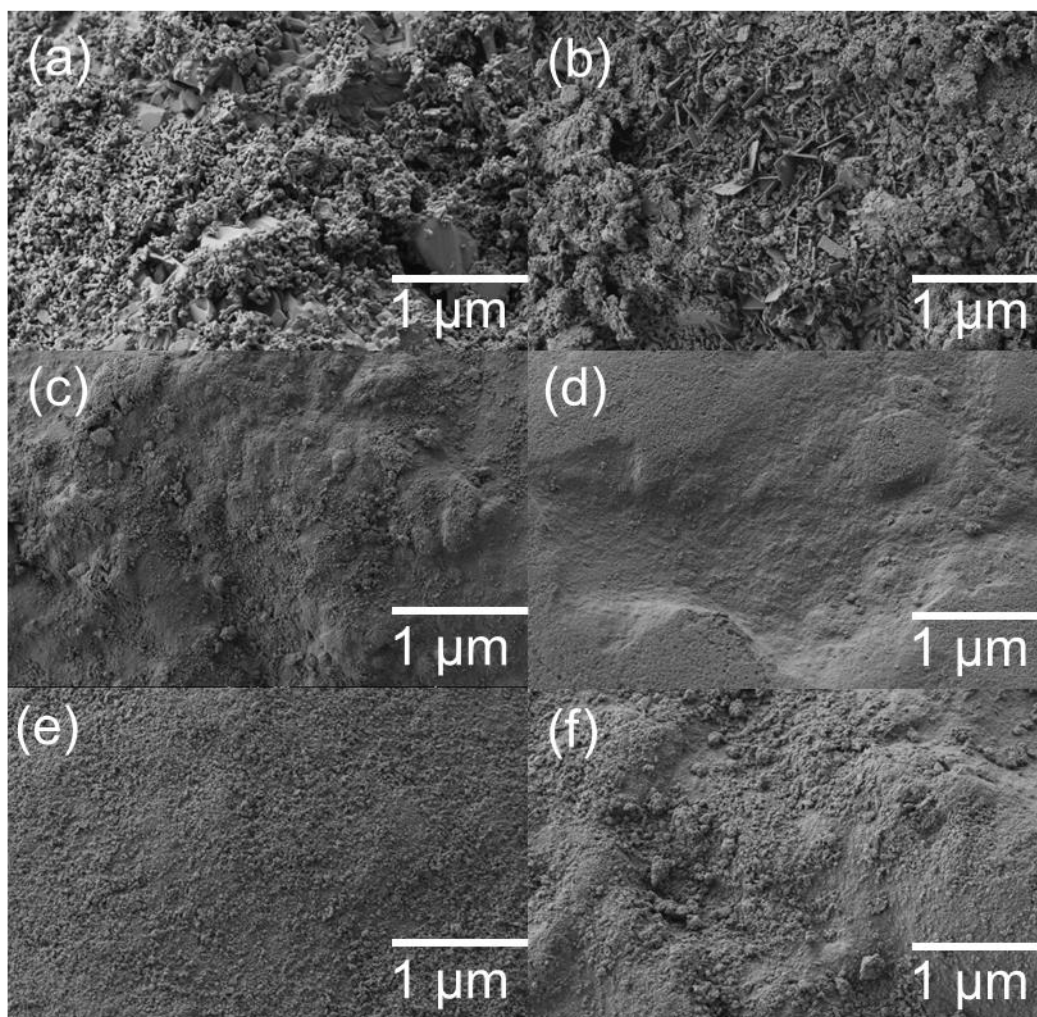
Figure 6.14: SEM images of fresh and spent catalysts: (a) and (b) 10wt% Mo-Al_2O_3; (c) and (d) 10wt% MgO-Al_2O_3; (e) and (f) 10wt% Ni-Al_2O_3.

Elemental analysis was performed for all three spent catalysts to see the composition differences between their fresh and spent states (Figure 6.15). As mentioned earlier, C found on the fresh catalysts originates from the sample holder. But the peak intensities of C in all three spent catalysts are significantly larger than the fresh ones, indicating that the catalysts have carbon deposition from the decarboxylation reaction. Since the XRD did not detect any crystalline carbon (atomic or coke), the carbon identified by EDX analysis is likely amorphous carbon. Amorphous carbon can be simply removed by calcining the catalyst above the reaction temperature under an inert atmosphere.
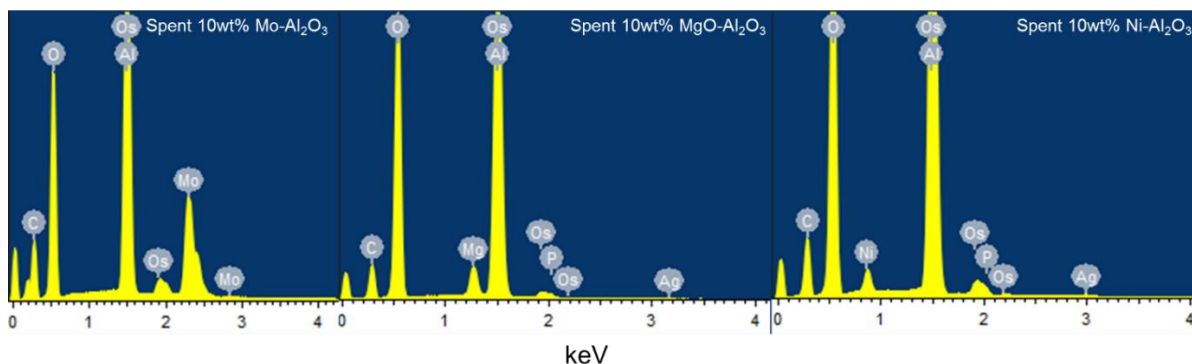
Figure 6.15: EDX analysis of spent catalysts.

XPS survey spectra of fresh and spent 10wt%Mo-Al$_2$O$_3$ catalyst was obtained to provide insight into the Mo catalyst deactivation process (Figure 6.16). Carbon in the fresh 10wt%Mo-Al$_2$O$_3$ catalyst corresponds to adventitious carbon which is typically detected in samples that have been exposed to the atmosphere or generated during the analysis. The relative content of C in the fresh catalyst is 16.5%, whereas the amount in the spent catalyst was 43.6%. Thus large increase in C on the spent catalyst indicates deposition from the decarboxylation reaction. This C potentially may be bound with multiple Mo ions which is hard to remove by simple hexane washing or vacuum drying [44]. The different states of Mo ions were confirmed in the spent 10wt%Mo-Al$_2$O$_3$ catalyst using high resolution XPS spectra (Figure 6.13b).
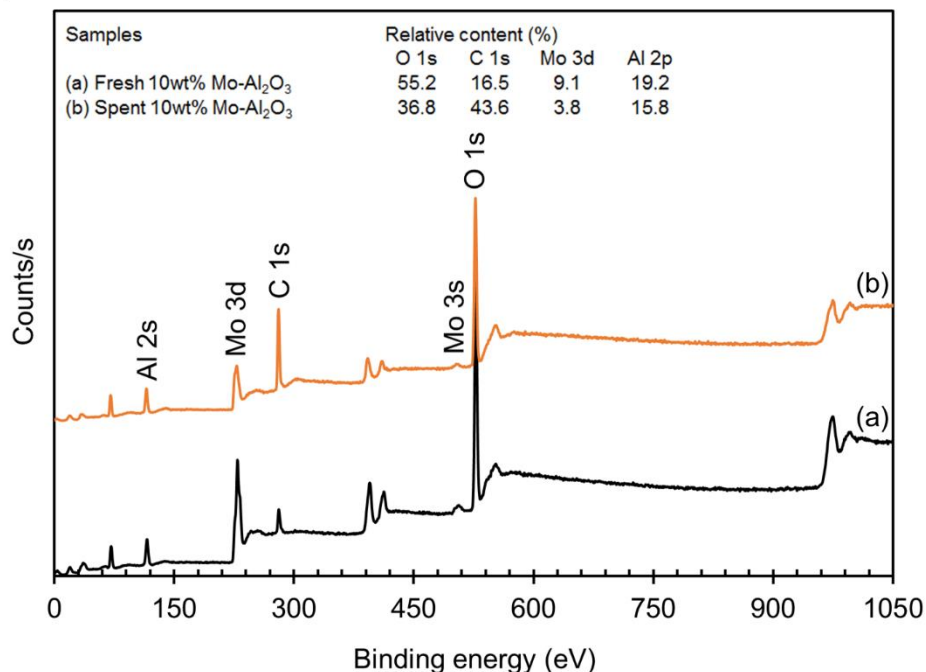
Figure 6.16: XPS survey spectra of fresh and spent Mo-Al$_2$O$_3$ catalyst.

6.4 Conclusion

This work investigated three different catalysts including 10wt% Mo-Al$_2$O$_3$, 10wt% MgO-Al$_2$O$_3$ and 10wt% Ni-Al$_2$O$_3$ catalysts and showed that the Mo catalyst is an efficient catalyst for decarboxylation of oleic acid and their derivatives in subcritical water. The reaction conditions for maximum degree of decarboxylation of oleic acid (92%) and liquid yield (71%) was found to be 375°C, water-to-OA ratio of 5:1 and space time of 4 h using 5 g of 10wt% Mo-Al$_2$O$_3$ catalyst. The Mo catalyst was found to crack the oleic acid into smaller hydrocarbon molecules. The selectivity's of hydrocarbons obtained at maximized reaction conditions were: 34.8% tetradecane, 24% pentadecane, 22.9% hexadecane and 18.3% heptadecane. The Mo catalyst was found to hydrogenate C=C bond to C-C without adding any external source of hydrogen. The deactivation studies of catalysts showed that the Mo catalyst was slightly agglomerated compared to Ni and MgO catalyst. No graphitic coke was found in the three evaluated catalysts but amorphous coke was detected in the Mo catalyst surface. Amorphous coke is easy to remove by simply calcination and catalyst can be reused.

167

References

[1] A. Demirbaş, Biodiesel fuels from vegetable oils via catalytic and non-catalytic supercritical alcohol transesterifications and other methods: a survey, Energy conversion and Management, 44 (2003) 2093-2109.

[2] M.J. Ramos, C.M. Fernández, A. Casas, L. Rodríguez, Á. Pérez, Influence of fatty acid composition of raw materials on biodiesel properties, Bioresource Technology, 100 (2009) 261-268.

[3] A. Sivasamy, K.Y. Cheah, P. Fornasiero, F. Kemausuor, S. Zinoviev, S. Miertus, Catalytic applications in the production of biodiesel from vegetable oils, ChemSusChem, 2 (2009) 278-300.

[4] M. Snåre, I. Kubickova, P. Mäki-Arvela, K. Eränen, D.Y. Murzin, Heterogeneous catalytic deoxygenation of stearic acid for production of biodiesel, Industrial & engineering chemistry research, 45 (2006) 5708-5715.

[5] M.Z. Hossain, A.K. Jhawar, M.B. Chowdhury, W.Z. Xu, W. Wu, D. Hiscott, P.A. Charpentier, Using subcritical water for decarboxylation of oleic acid into fuel range hydrocarbons, Energy & Fuels, 31 (2017) 4013-4023.

[6] J. Fu, X. Lu, P.E. Savage, Hydrothermal decarboxylation and hydrogenation of fatty acids over Pt/C, ChemSusChem, 4 (2011) 481-486.

[7] J. Fu, F. Shi, L. Thompson Jr, X. Lu, P.E. Savage, Activated carbons for hydrothermal decarboxylation of fatty acids, ACS Catalysis, 1 (2011) 227-231.

[8] J. Fu, X. Lu, P.E. Savage, Catalytic hydrothermal deoxygenation of palmitic acid, Energy & Environmental Science, 3 (2010) 311-317.

[9] S.A. Hollak, R.W. Gosselink, D.S. van Es, J.H. Bitter, Comparison of tungsten and molybdenum carbide catalysts for the hydrodeoxygenation of oleic acid, ACS Catalysis, 3 (2013) 2837-2844.

[10] M. Snåre, P. Mäki-Arvela, I. Simakova, J. Myllyoja, D.Y. Murzin, Overview of catalytic methods for production of next generation biodiesel from natural oils and fats, Russian Journal of Physical Chemistry B, 3 (2009) 1035-1043.

[11] L. Boda, G. Onyestyák, H. Solt, F. Lónyi, J. Valyon, A. Thernesz, Catalytic hydroconversion of tricaprylin and caprylic acid as model reaction for biofuel production from triglycerides, Applied Catalysis A: General, 374 (2010) 158-169.

[12] R. Tiwari, B.S. Rana, R. Kumar, D. Verma, R. Kumar, R.K. Joshi, M.O. Garg, A.K. Sinha, Hydrotreating and hydrocracking catalysts for processing of waste soya-oil and refinery-oil mixtures, Catalysis Communications, 12 (2011) 559-562.

[13] T.M. Yeh, R.L. Hockstad, S. Linic, P.E. Savage, Hydrothermal decarboxylation of unsaturated fatty acids over PtSnx/C catalysts, Fuel, 156 (2015) 219-224.

[14] R. Sotelo-Boyas, Y. Liu, T. Minowa, Renewable diesel production from the hydrotreating of rapeseed oil with Pt/Zeolite and NiMo/Al2O3 catalysts, Industrial & Engineering Chemistry Research, 50 (2010) 2791-2799.

[15] J. Wu, J. Shi, J. Fu, J.A. Leidl, Z. Hou, X. Lu, Catalytic Decarboxylation of Fatty Acids to Aviation Fuels over Nickel Supported on Activated Carbon, Scientific Reports, 6 (2016).

[16] C. Miao, O. Marin-Flores, S.D. Davidson, T. Li, T. Dong, D. Gao, Y. Wang, M. Garcia-Pérez, S. Chen, Hydrothermal catalytic deoxygenation of palmitic acid over nickel catalyst, Fuel, 166 (2016) 302-308.

[17] J.-G. Na, B.E. Yi, J.N. Kim, K.B. Yi, S.-Y. Park, J.-H. Park, J.-N. Kim, C.H. Ko, Hydrocarbon production from decarboxylation of fatty acid without hydrogen, Catalysis Today, 156 (2010) 44-48.

[18] J. Hancsók, T. Kasza, S. Kovács, P. Solymosi, A. Holló, Production of bioparaffins by the catalytic hydrogenation of natural triglycerides, Journal of Cleaner Production, 34 (2012) 76-81.

[19] J. Duan, J. Han, H. Sun, P. Chen, H. Lou, X. Zheng, Diesel-like hydrocarbons obtained by direct hydrodeoxygenation of sunflower oil over Pd/Al-SBA-15 catalysts, Catalysis Communications, 17 (2012) 76-80.

[20] M.B.I. Choudhury, S. Ahmed, M.A. Shalabi, T. Inui, Preferential methanation of CO in a syngas involving CO2 at lower temperature range, Applied Catalysis A: General, 314 (2006) 47-53.

[21] M.B.I. Chowdhury, M.M. Hossain, P. A. Charpentier, Effect of supercritical water gasification treatment on Ni/La2O3-Al2O3-based catalysts Appl. Catal A, 405 (2011) 84-92.

[22] M.Z. Hossain, M.B. Chowdhury, Q. Alsharari, A.K. Jhawar, P.A. Charpentier, Effect of mesoporosity of bimetallic Ni-Ru-Al 2 O 3 catalysts for hydrogen production during supercritical water gasification of glucose, Fuel Processing Technology, 159 (2017) 55-66.

[23] M.Z. Hossain, M.B. Chowdhury, A.K. Jhawar, P.A. Charpentier, Supercritical water gasification of glucose using bimetallic aerogel Ru-Ni-Al 2 O 3 catalyst for H 2 production, Biomass and Bioenergy, 107 (2017) 39-51.

[24] E.A. Youssef, M.B. Chowdhury, G. Nakhla, P. Charpentier, Effect of nickel loading on hydrogen production and chemical oxygen demand (COD) destruction from glucose oxidation and gasification in supercritical water, international journal of hydrogen energy, 35 (2010) 5034-5042.

[25] M.B. Chowdhury, M.M. Hossain, P.A. Charpentier, Effect of supercritical water gasification treatment on Ni/La 2 O 3-Al 2 O 3-based catalysts, Applied Catalysis A: General, 405 (2011) 84-92.

[26] http://www.engineeringtoolbox.com/fuels-higher-calorific-values-d_169.html (accessed on April 19, 2017).

[27] Jet fuel: ASTM D1655-15d, Diesel: Petro-Canada MSDS (accessed on April 19, 2017).

[28] P. McKendry, Energy production from biomass (part 1): overview of biomass, Bioresource technology, 83 (2002) 37-46.

[29] The Official Site of the National Biodiesel Board: Biodiesel.org (accessed on April 19, 2017).

[30] S.M. Morris, P.F. Fulvio, M. Jaroniec, Ordered mesoporous alumina-supported metal oxides, Journal of the American Chemical Society, 130 (2008) 15210-15216.

[31] B. Xu, T. Xiao, Z. Yan, X. Sun, J. Sloan, S.L. González-Cortés, F. Alshahrani, M.L. Green, Synthesis of mesoporous alumina with highly thermal stability using glucose template in aqueous system, Microporous and Mesoporous Materials, 91 (2006) 293-295.

[32] N. Charisiou, A. Baklavaridis, V. Papadakis, M. Goula, Synthesis Gas Production via the Biogas Reforming Reaction Over Ni/MgO–Al2O3 and Ni/CaO–Al2O3 Catalysts, Waste and Biomass Valorization, 7 (2016) 725-736.

[33] A. Iriondo, V. Barrio, J. Cambra, P. Arias, M. Guemez, M. Sanchez-Sanchez, R. Navarro, J. Fierro, Glycerol steam reforming over Ni catalysts supported on ceria and ceria-promoted alumina, international journal of hydrogen energy, 35 (2010) 11622-11633.

[34] B. Dou, C. Wang, Y. Song, H. Chen, Y. Xu, Activity of Ni–Cu–Al based catalyst for renewable hydrogen production from steam reforming of glycerol, Energy Conversion and Management, 78 (2014) 253-259.

[35] X. Ma, K. Cui, W. Hao, R. Ma, Y. Tian, Y. Li, Alumina supported molybdenum catalyst for lignin valorization: effect of reduction temperature, Bioresource technology, 192 (2015) 17-22.

[36] D. Ma, Y. Shu, X. Bao, Y. Xu, Methane dehydro-aromatization under nonoxidative conditions over Mo/HZSM-5 catalysts: EPR study of the Mo species on/in the HZSM-5 zeolite, Journal of Catalysis, 189 (2000) 314-325.

[37] V. Benitez, C. Querini, N. Fıgoli, Characterization of WO x/Al 2 O 3 and MoO x/Al 2 O 3 catalysts and their activity and deactivation during skeletal isomerization of 1-butene, Applied Catalysis A: General, 252 (2003) 427-436.

[38] R.L. Cordero, F.G. Llambias, A.L. Agudo, Temperature-programmed reduction and zeta potential studies of the structure ofMo/O3Al2O3 andMo/O3SiO2 catalysts effect of the impregnation pH and molybdenum loading, Applied Catalysis, 74 (1991) 125-136.

[39] S. Wang, G. Lu, Reforming of methane with carbon dioxide over Ni/Al 2 O 3 catalysts: effect of nickel precursor, Applied Catalysis A: General, 169 (1998) 271-280.

[40] Y.-g. Chen, J. Ren, Conversion of methane and carbon dioxide into synthesis gas over alumina-supported nickel catalysts. Effect of Ni-Al 2 O 3 interactions, Catalysis Letters, 29 (1994) 39-48.

[41] F. Barath, M. Turki, V. Keller, G. Maire, Catalytic Activity of Reduced MoO3/α-Al2O3 for Hexanes Reforming: I. preparation, characterization, and x-ray photoelectron spectroscopy studies, Journal of Catalysis, 185 (1999) 1-11.

[42] E. Mannei, F. Ayari, C. Petitto, E. Asedegbega–Nieto, A.R. Guerrero–Ruiz, G. Delahay, M. Mhamdi, A. Ghorbel, Light hydrocarbons ammoxidation into acetonitrile over Mo–ZSM-5 catalysts: Effect of molybdenum precursor, Microporous and Mesoporous Materials, 241 (2017) 246-257.

[43] E. Santillan-Jimenez, M. Crocker, Catalytic deoxygenation of fatty acids and their derivatives to hydrocarbon fuels via decarboxylation/decarbonylation, Journal of Chemical Technology and Biotechnology, 87 (2012) 1041-1050.

[44] X. Huang, J. Liu, J. Chen, Y. Xu, W. Shen, Mechanistic study of selective oxidation of dimethyl ether to formaldehyde over alumina-supported molybdenum oxide catalyst, Catalysis letters, 108 (2006) 79-86.

Chapter 7

Green Diesel Production from Corn Distillers Oil through Hydrothermal Decarboxylation

Abstract

Catalytic hydrothermal conversion of non-edible corn distillers oil (CDO), a low value by-product of ethanol industries, into so called green diesel (high value fuel grade hydrocarbons) was investigated in near supercritical water. The decarboxylation experiments were conducted using activated carbon in a 300 mL batch stirred tank reactor at reaction temperatures 300-400°C with pressure ranges from 2200-2500 psi, water-to-CDO ratio from 2:1 to 4:1 and reaction time from 0.5 to 4 h at constant stirring speed (800 rpm). For the first time, complete removal of the -COO- group from CDO was achieved at 400°C with 4 h of reaction time and a water-to-CDO ratio of 4:1. The liquid products obtained were a mixture of saturated hydrocarbons, mainly C_8 to C_{16} (selectivity 49.7%) and heptadecane (48.9%) which have similar specific gravity, higher heating value (HHV), cloud and pour points to those of commercial fuels. The reaction mechanism was found to follow pseudo first order kinetics with an activation energy 66.1±3 kJ/mol, which is much lower than similar reported literature values for the decarboxylation process.

KEYWORDS: Near supercritical water, corn distillers oil (CDO), hydrothermal decarboxylation, biofuel, kinetics, activation energy.

7.1 Introduction

Due to the depleting reserves of fossil fuels, and the significant environmental issues associated with greenhouse gas emissions, economic, social and environmental requirements have motivated research converging on carbon neutral sources such as renewable feedstocks. Research efforts have concentrated on the progress of advanced biofuel technologies i.e. 2nd generation biofuels in order to reduce the environmental effect of biofuel production. Lower greenhouse gas (GHG) emissions compared to current biofuels and non-food renewable feedstocks are two main features of 2nd generation biofuels [1].

Approximately 2.7 billion pounds per year of non-edible corn distillers oil (CDO) is produced across North America by ethanol producers [2]. The CDO has a high lipid content (85%), in particular a variety of long-chain esters including linoleate, palmoleate, oleate and high free fatty acids. CDO is a transparent, light reddish-orange coloured liquid that displays the general physical characteristics of common corn oil with no rancid odour. CDO is clear and has suspended free-fatty acids (FFA) at room temperature, but it is free from any other suspended material [3]. Current technologies for producing biodiesel have largely focused on fatty acid methyl esters (FAME) production during transesterification of oils with methanol [4]. However, the products have a lower higher heating value (LHHV) compared to petroleum diesel due to the presence of oxygen. Only 5% of biodiesel can be blended with petroleum diesel due to its poor storage stability, marginal cold flow properties, and limited compatibility with conventional diesel engines, excessive solvency and use of high quality food feedstocks [5]. In addition, the biodiesel market has become saturated with very low margins and blenders do not utilize this product in the winter. Biodiesel's high cloud point in comparison to petroleum diesel is a major problem in cold winters from northern climates. This requires the biodiesel to have additional processing or the addition of expensive additives to improve its low temperature properties before blending into diesel, further reducing margins [6].

Apart from the quality issues of biodiesel, life cycle analysis of the raw materials utilized for biodiesel production shows that petroleum derived diesel is still more energy efficient [5]. Due to the problems associated with biodiesel usage, efforts are provided to develop alternative biofuel production processes to produce hydrocarbons that are drop-in replacements for traditional petroleum-derived fuels. Removal of oxygen via decarboxylation or

decarbonylation represents an alternative and direct pathway to produce hydrocarbon fractions that have almost similar properties to commercial fuels and can be used directly in existing infrastructure without any alterations [7-9].

Decarboxylation of fatty acids was conducted previously in organic solvents such as dodecane [10, 11]. Recently, water has been shown as a green reaction medium for the decarboxylation reaction instead of organic solvents [12, 13]. There are several advantages for using water as the reaction medium including: (i) water is an eco-friendly and low cost solvent, (ii) water can easily hydrolyze triglycerides to provide aqueous stream of fatty acids, and (iii) water properties are tunable by changing T and P. Near supercritical water as a reaction media can quickly dissolve triglycerides and then hydrolyze them into free fatty acids and glycerol [14]. Glycerol has been reported as an *in situ* hydrogen donor in hydrothermal media by aqueous phase reforming (APR) [15-18]. Utilizing glycerol APR for *in situ* hydrogen production can reduce the cost of the process by avoiding high pressure hydrogen. Hydrogen is required to hydrogenate unsaturated fatty acids to straight chain alkanes. A continuous hydrogen supply can be obtained by the APR of glycerol released from triglyceride hydrolysis.

Decarboxylation of fatty acids or their derivatives provides low hydrocarbon yield at moderate temperatures (<400 ^{o}C), which indicates the need for a catalyst for this reaction [19]. In the published literature, decarboxylation reaction chemistry has mostly been reported using noble metal catalysts such as Pd [20-22] or Pt [7, 12, 23]. Popov & Kumar [24] and Fu et al. [13] reported that activated carbon could be an alternative to the expensive noble metal catalysts for decarboxylation of fatty acids in sub- and supercritical water.

To the best of our knowledge, there has been no open source literature available until date about the hydrothermal decarboxylation of CDO over commercial activated carbon as catalyst. Commercial activated carbon could be a suitable low cost catalyst compared to noble metal catalysts for the hydrothermal decarboxylation of CDO. In the present work, we demonstrate the complete removal of -COO- from CDO using activated carbon during hydrothermal decarboxylation in near supercritical water to produce so called green diesel without adding hydrogen. Green diesel is expected as the second generation diesel fuel which fits the next generation diesel engine due to its physicochemical properties which are very similar to conventional diesel and show an excellent low temperature fluidity which enables its use in cold weather.

7.2 Experiments

7.2.1 Materials

Corn distillers oil (CDO) was received from Green Field Specialty Alcohols (GFSA) and used without further purification. Powder activated carbon (DARCO G-60, 100-325 mesh particle size) and hexane (ACS grade) were purchased from Sigma-Aldrich, Oakville, ON and used as received. De-ionized water (18 MΩ) was obtained from a compact ultrapure water system (EASY pure LF, Mandel Scientific Co., model BDI-D7381).

7.2.2 Catalyst Characterization

Tristar II 3020 (Micromeritics Instrument Corporation) was used to measure the Brunauer-Emmett-Teller (BET) surface area, pore diameter and pore volume of both fresh and spent activated carbon at −193 °C using 99.99% pure N_2 gas (Praxair, Oakville, Canada). The samples were degassed at 150°C for 12 h before measurements to remove the moisture and other adsorbed gases from the catalyst surface.

X-ray diffraction (XRD) was used to study the crystal structure of fresh and spent activated carbon. The analysis was done in a Bruker D2 Phaser powder diffractometer using Cu Kα radiation (λ for Kα is equal to 1.54059 Å) over 2θ = 10º – 80º using a scan rate 0.2º per min.

TGA/SDT A851 model gravimetric analyzer was used to identify the deposited coke on the spent catalyst surface. Approximately 10 mg of sample was loaded into an alumina crucible with a reference (an empty alumina crucible) and heated from ambient temperature to 1000 ºC @ 10 ºC/min under N_2 (50 mL/min) atmosphere.

7.2.3 Reaction procedure

The catalytic hydrothermal decarboxylation of CDO was conducted in a 300 mL stainless steel stirred semi-batch reactor (Autoclave Engineers, Erie, PA) with an operating pressure of 5500 psi rating at 340 ºC. The reactor was heated with a 1.2 kW electric furnace (Industrial Heater Corp., Cheshire, CT). The experimental setup is shown in Figure 7.1. The reactor was washed with soapy water, clean water and hexane to remove any residuals from previous experiments. The reactor was placed in an oven after cleaning for 15-20 min to remove any water and hexane. After removing the reactor from the oven and cooling down, 5 g of activated carbon and the required amount of water was loaded into the reactor. The amount of water used for

each reaction depends on the desired water-to-CDO ratio. The reactor lid was closed and the bolts tightened with a torque wrench. N_2 gas was flowed for 10-15 min to remove any air. The reactor outlet was then closed and the furnace started to heat up the reactor to the desired temperature. The pressure ranges for all the parametric studies was 2000-2500 psi (near-supercritical conditions). When the desired reaction temperature was obtained, the reactor was left for 5 min to stabilize the temperature. The required amount of CDO was filled and pressurized (above the reactor pressure) using a syringe pump (Isco 100 DM, Lincoln, NE) from the beginning of the reaction. The CDO feed was injected and the reaction time initiated using a stopwatch. When the desired reaction time was completed, the electric furnace was removed from the reactor body with the body quenched using an ice bath. When the reactor temperature was less than 30°C, the solid, liquid and gaseous products were separated through a filter and gas-liquid separator. The solid catalyst was washed with hexane to remove any liquid products with the catalyst placed in a vacuum oven at 90°C overnight. Hexane was evaporated from the hexane-liquid product mixture to obtain pure product. The liquid product was mainly collected from the gas-liquid separator. The product collected from the separator was combined with the product recovered from the catalyst to calculate the total liquid product yield. Collected liquid product was analyzed using a GC-MS and GC-FID, respectively. Obtained gases were stored in Tedlar gas bags (SKC Inc., Pittsburgh, PA) for subsequent GC-TCD analysis.
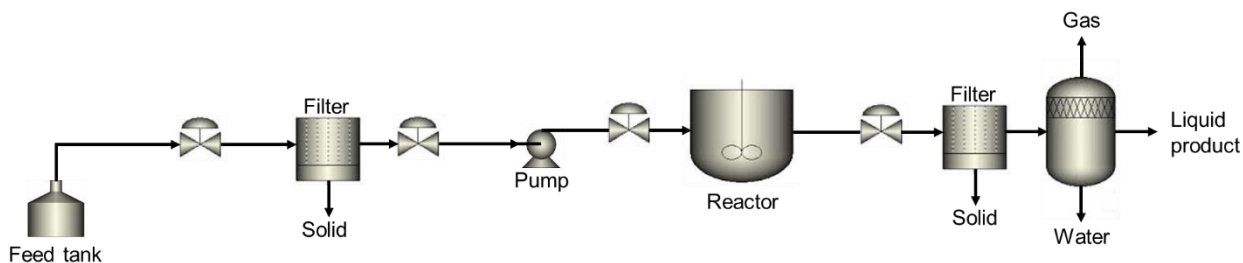
Figure 7.1: Hydrothermal semi-batch reactor system.

7.2.4 Feed and Product analysis

Infrared analysis of reactant and product samples was performed using an ATR-FTIR spectroscope (Nicolet 6700 FTIR, Thermo Scientific). The spectra were recorded in the range

of 600-4000 cm^{-1} with a resolution of 4 cm^{-1} over 32 scans. Percent removal of -COO- groups was obtained from peak areas using the following equation:

$$\% \; removal \; of - COO - groups = \frac{[initial \; peak \; area \; of -COO-group \; in \; CDO]-[peak \; area \; of -COO-group \; in \; the \; product]}{[initial \; peak \; area \; of -COO-group \; in \; CDO]} x100 \quad (7.1)$$

[1]H and ^{13}C nuclear magnetic resonance (NMR) spectra of the reactant and product samples were recorded using a Varian Inova 400 spectroscope. Samples were dissolved in CDCl$_3$ and the chemical shifts were referenced to tetramethylsilane (0.0 ppm). Based on the NMR data, the CDO produced by GFSA and other EtOH producers contains free fatty acids (FFA) and a variety of lipid-based materials, in particular a variety of long-chain esters including linoleate, palmoleate and oleate as shown in Figure 7.2. The relative content of different types of esters in CDO are provided in Table E1.
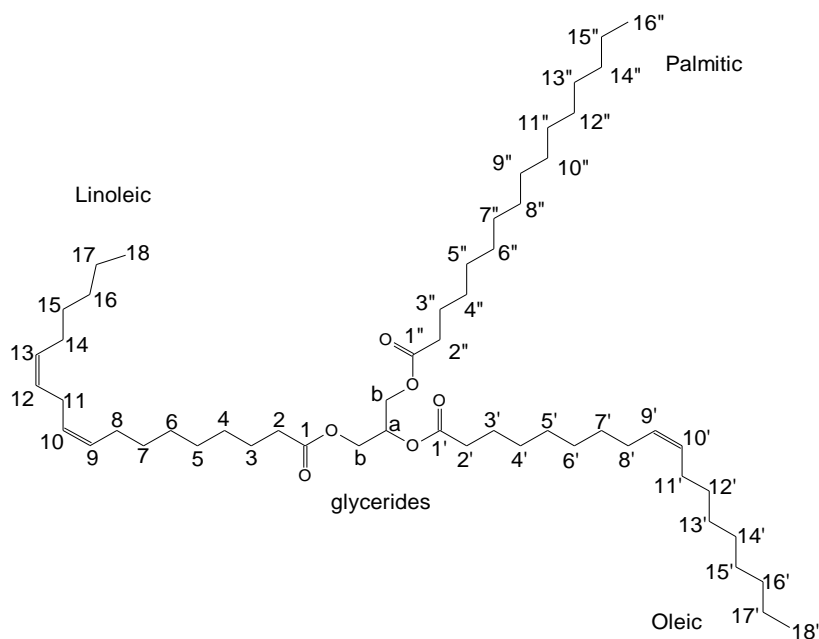
Figure 7.2: Proposed chemical structure of corn oil.

Qualitative analysis of liquid products was performed using a high resolution mass spectrometer (GCMS-QP2010) coupled with a Finnigan MAT8400 ion-trap detector and a DB-5 capillary column (dimension: 30m x 0.32mm x 0.25µm) using a Tri Plus RSH auto sampler. The GC-MS oven temperature was programmed as follows: 45 ºC (hold for 3 min) and raised

at 320 ºC @ 5 ºC/min (hold for 5 min). The sample injector and detector were maintained at 250 ºC. Compounds were identified by matching the derived ion mass spectra to spectral libraries using HP chemstation software. The similarity indexes (SI) of the compounds reported were greater than 75%.

Quantitative analysis of liquid products were also performed using a gas chromatograph (Shimadzu, GC-2014) equipped with flame ionization detector (FID) and a capillary DB WAX column (Agilent Technologies, Santa Clara, CA, USA) (dimension: 30m x 0.250mm x 0.25μm, temperature limit: 20 to 260 ºC). The GC oven temperature was programmed as follows: 3 min hold at 50 ºC, 10 ºC/min ramp at 250 ºC. The injector and detector temperature were maintained at 200 and 250 ºC, respectively. Samples (1μL) were injected manually into the column with a 10:1 split ratio. The injection of liquid sample into the GC was repeated for minimum three times and the results averaged to minimize analytical error. Helium, hydrogen and helium-air were used as the carrier gas, flame gas and make-up, respectively. The reaction products were determined by matching the gas chromatograph retention times with known standards from Sigma-Aldrich, Oakville, ON. Quantitative measurements (calculating selectivity of products) were performed as follows: the total areas of the detected peaks count as 100% and obtained the relative percentage (area of peak/total area of peaks) of individual product.

Density of the products were measured using an Eagle Eye SG-Ultra Max Hydrometer (Density meter) [dimension = 5.5"W x 5.5"D x 1"H (outside)] using the oscillating U-tube technology. Measuring density range for this density meter is 0 to 3 gm/cc and operating temperature ranges from -10 to 50 ºC.

Higher heating values (HHV) of the liquid product, also called gross calorific values, were measured using an IKA C2000 bomb calorimeter. Cloud and pour points of the decarboxylated liquid product were obtained from InnoTech Alberta, Edmondon, Canada.

The gaseous products were analyzed using the same gas chromatograph (Shimadzu, GC-2014) equipped with a thermal conductivity detector (TCD) and 120/80 Hayesep D stainless steel 3.18 mm ID, 6.2 m nickel packed column. The GC oven temperature was programmed as follows: 6 min hold at 35 ºC, 25 ºC/min ramp at 200 ºC, 1 min hold at 200 ºC. The injector and detector temperature were maintained at 200 and 250 ºC, respectively. Helium was used as the

carrier gas. The gas chromatograph was calibrated using a standard gas mixture of known composition. The analysis was performed manually using 1 mL SGE gas tight syringe (Model number 008100, Reno, NV USA) by collecting the sample from the gas bag. The injection of sample gas into the GC was repeated for minimum three times and the results were averaged to minimize analytical error.

7.3 Results and Discussion

7.3.1 Effect of reaction conditions on decarboxylated products

The effect of reaction conditions on the decarboxylated liquid products was investigated by GC-FID analysis. Non catalytic hydrothermal decarboxylation reactions were performed to compare the selectivity of the hydrocarbons with catalytic experiments. Figure 7.3 shows the selectivity of the hydrocarbons in the liquid product at different temperatures (300-400 $^{\circ}$C) without and with catalyst, water-to-CDO ratio and reaction times, respectively. Figure 7.3(a) and (b) compares the selectivity of hydrocarbons at different temperatures (300-400 $^{\circ}$C), water to CDO ratio of 4:1, 4 h reaction time and 800 rpm with and without catalyst. Figure 7.3(c) shows the effect of different water to CDO ratio in the presence of catalyst on the product distribution at 400 $^{\circ}$C, 4 h of reaction time and 800 rpm, respectively. Figure 7.3(d) shows the effect of different reaction times (0.5 to 4 h) in the presence of catalyst at 400 $^{\circ}$C, water-to-CDO ratio = 4:1 and 800 rpm, respectively.
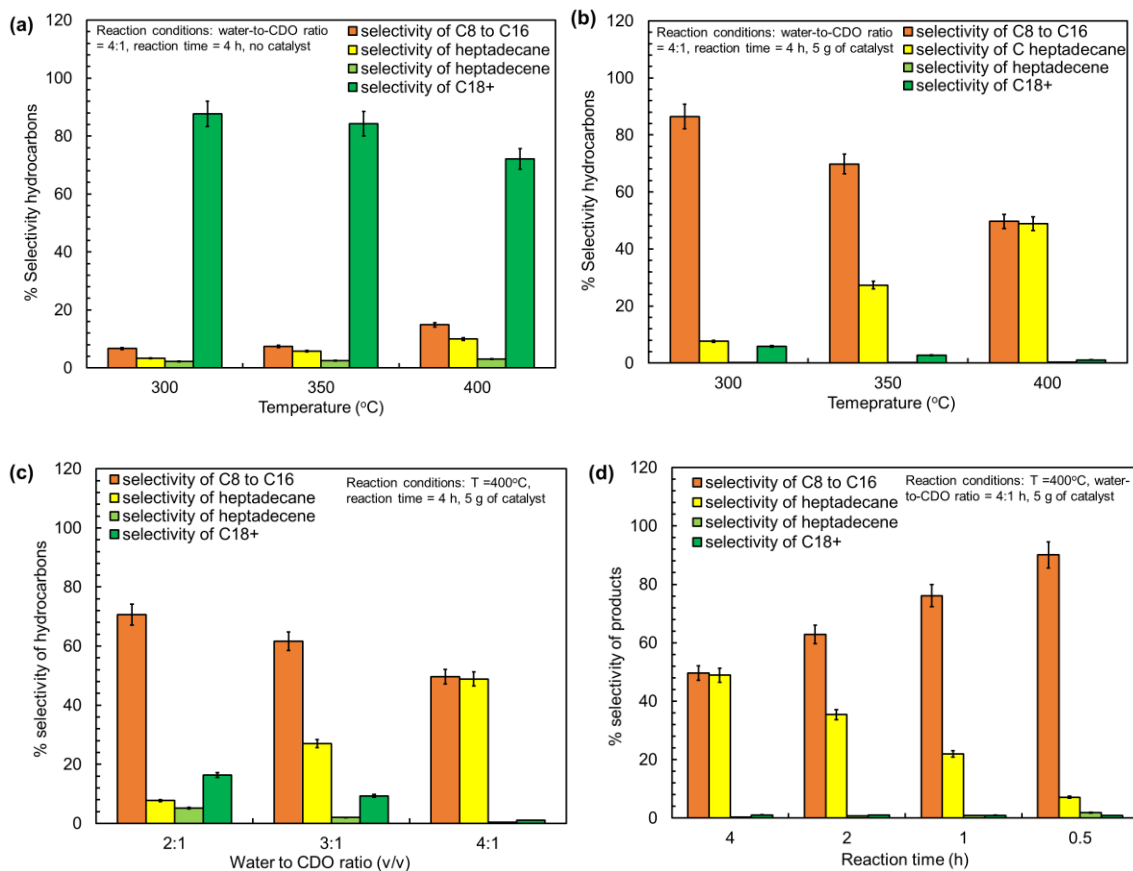
Figure 7.3: Product distributions (a) without (b) with catalyst (c) for different water to CDO ratio (d) different reaction times.

Selectivity of C_8 to C_{16} alkanes, heptadecane and heptadecene increases with increasing temperature with no added catalyst, whereas the selectivity of $C_{18}+$ alkanes decreases with increasing temperature at identical conditions as shown in Figure 7.3(a). As shown in Figure 7.3(b), the selectivity of $C_{18}+$ alkanes decreases with increasing temperature in the presence of catalyst. It is also seen that the selectivity of C_8 to C_{16} hydrocarbons increases with increasing temperature which indicates that the catalyst helps breaking down the larger hydrocarbon molecules into smaller molecules. For instance, the selectivity of $C_{18}+$ alkanes was 72.1% without catalyst in comparison to 1.1% with catalyst at 400 °C. On the other hand, the selectivity of heptadecane was 10% without catalyst whereas the selectivity of heptadecane was 48.9% with catalyst at 400 °C. The selectivity of C_8 to C_{16} with catalyst improved to 86.4% at 300 °C from only 6.7% for the noncatalytic reaction. The selectivity of heptadecene from

180

the noncatalytic reaction at 400 °C was only 3.1%, which was further lowered to 0.4% with catalyst, indicating hydrogen was produced *in situ* from glycerol by the APR reaction [15, 18]. The selectivity of C_8 to C_{16} alkanes, heptadecene, $C_{18}+$ decreases with increasing water to CDO ratio (from 2:1 to 4:1) whereas the selectivity of heptadecane increases (from 7.7% to 48.9%) with increasing water-to-CDO ratio. The selectivity of C_8 to C_{16} decreases and the selectivity of heptadecane and $C_{18}+$ increases with increasing reaction time (from 0.5 h to 4 h) whereas the selectivity for heptadecene decreases with increasing reaction time. The optimum conditions for complete removal of -COO- groups from CDO (shown later in Figure 7.5) and higher heptadecane yield was found to be 400 °C, water to CDO ratio of 4:1, 4 h of reaction time and 800 rpm in the presence of catalyst, respectively. 65% liquid and 35% gaseous yield were obtained under these optimum conditions (see Figure E1). The calculated mass balance was around 94% or higher in all cases.

A typical hydrocarbon distribution is shown in Table 7.1 for the optimum reaction conditions (400 °C, water to CDO ratio of 4:1, 4 h of reaction time and 800 rpm in the presence of catalyst). Products identified by GC-MS are shown in Table E2.

Table 7.1: Product distribution of CDO decarboxylation at optimum reaction conditions.

Compound	% selectivity
C_8 to C_{16} alkanes	49.7
n-Heptadecane	48.9
Heptadecene	0.40
C_{18+} alkanes	1.10

Although the optimum conditions for complete removal of -COO- group and higher heptadecane yield was found to be 400 °C, water-to-CDO ratio of 4:1, 4 h of reaction time and 800 rpm in the presence of catalyst, the reaction at 400 °C, water to CDO ratio of 5:1, 2 h of reaction time and 800 rpm in the presence of catalyst also provides full removal of -COO- groups (Fig. S2) and almost similar product distribution (Table S3). This result indicates that the increasing water to CDO ratio is favorable for decarboxylation at shorter residence times which can significantly reduce the cost of the process.

7.3.2 Fuel Quality

7.3.2.1 Specific gravity measurement

Liquid density is an important parameter used to obtain information regarding concentration, composition, mass flow in fuels, caloric content etc. Density is expressed as mass per unit volume but is often expressed in terms of specific gravity (SG), which is the ratio of the liquid density to the density of water, both taken at the same T,P.

$$SG = \frac{\rho_{liq}}{\rho_{water}}$$ (7.2)

Table 7.2 shows the specific gravity of the decarboxylated product and commercial fuels at different temperatures.

Table 7.2: Specific gravity of decarboxylated product and commercial fuels.

Compounds	Temperature (°C)	Specific gravity
Decarboxylated product*	15.6	0.801
	21.6	0.801
	25	0.793
	40	0.782
Kerosene [25]	15.6	0.78-0.82
Jet fuel [26]	15	0.78-0.84
Diesel [25]	15.6	0.80-0.96

* Product at optimum reaction conditions

The petroleum industry frequently uses the specific gravity 60/60, which means that the densities of liquid product and water were measured at 60 °F ($\rho_{water}|_{60^oF} = 0.999041 \ g/cc$) and atmospheric pressure. The petroleum industry uses another measure, degree API gravity, based on oil specific gravity at 60/60:

$$^o_{API} = \frac{141.5}{SG_{60/60}} - 131.5$$ (7.3)

Note that the lighter the fluid, the higher the API gravity. API gravity is one factor that determines the price of oil per barrel [27].

Table 7.2 clearly shows that the product is in the range of kerosene, jet fuel and diesel. The calculated °API gravity value for the decarboxylated product is 45°. Oil with API gravity between 40 and 45° commands the highest prices. Above 45°, the molecular chains become shorter and less valuable to refineries [27].

7.3.2.2 Higher heating value measurement

The heating value of a fuel is the amount of heat released during the combustion of a specified amount, which is characteristic for each fuel. Table 7.3 shows the HHV values of the feed, product, and commercial fuels, where it is found that the HHV of the decarboxylated product is comparable with that of commercial fuels such as jet fuel, kerosene and diesel.

Table 7.3: High heating values of feed, product and commercial fuels.

Compounds	HHVs (MJ/kg)
Corn oil	39.2
Decarboxylated product[*]	44.3
Jet fuel [28]	43.5
Kerosene [25]	46.2
Diesel [25]	44.8

*product at optimum reaction conditions

7.3.2.3 Cloud and pour point measurement

Cloud point and pour point are two important physical properties of any liquid fuel. Cloud point is the temperature at which a cloud of wax crystals first appear in a liquid fuel when it is cooled under special testing conditions. The cloud point of any petroleum product is an indicator of how well the fuel will perform under cold weather conditions. Pour point refers to the lowest temperature at which movement of oil is observed and the fuel can be pumped easily. The cloud and pour points of the decarboxylated product at optimum reaction conditions were obtained as per ASTM D5773 and ASTM D5949 (3 °C testing interval) standards to be -35.6 °C and -45 °C, respectively.

7.3.3 Reaction Mechanism

7.3.3.1 ATR-FTIR analysis of liquid products

To examine the decarboxylation of CDO at different temperatures without using catalyst, ATR-FTIR spectra of CDO and the formed products were measured and are compared in Figure 7.4. The spectrum of CDO (Figure 7.4a) shows several major peaks at 3007, 2922, 2852, 1742, 1457, 1160, and 721 cm^{-1}. The peak at 3004 cm^{-1} is ascribed to the alkene CH stretching mode. The peaks at 2922, 2852, and 721 cm^{-1} are ascribed to asymmetric stretching,

symmetric stretching, and rocking modes of CH$_2$, respectively. The peak at 1457 cm^{-1} is assigned to CH$_2$ scissoring and CH$_3$ asymmetric bending modes. The peak at 1742 and 1160 cm^{-1} are attributable to C=O stretching, and C-O stretching of the ester groups, respectively. After the reactions in the absence of catalyst, the ester peaks disappeared while new peaks appeared at 1707, 1412, 1283, and 934 cm^{-1} (Figure 7.4b-d). These new peaks are attributable to C=O stretching, combination of C-O stretching and O-H deformation, C-O stretching, and OH out of plane bending modes, respectively as a result of the formation of carboxylic acids by hydrolysis. In addition, the peak at 3007 cm^{-1} decreased after reaction at 300 ^{o}C (Figure 7.4b) and almost disappeared at higher temperatures such as 350 ^{o}C or 400 ^{o}C (Figure 7.4c-d).
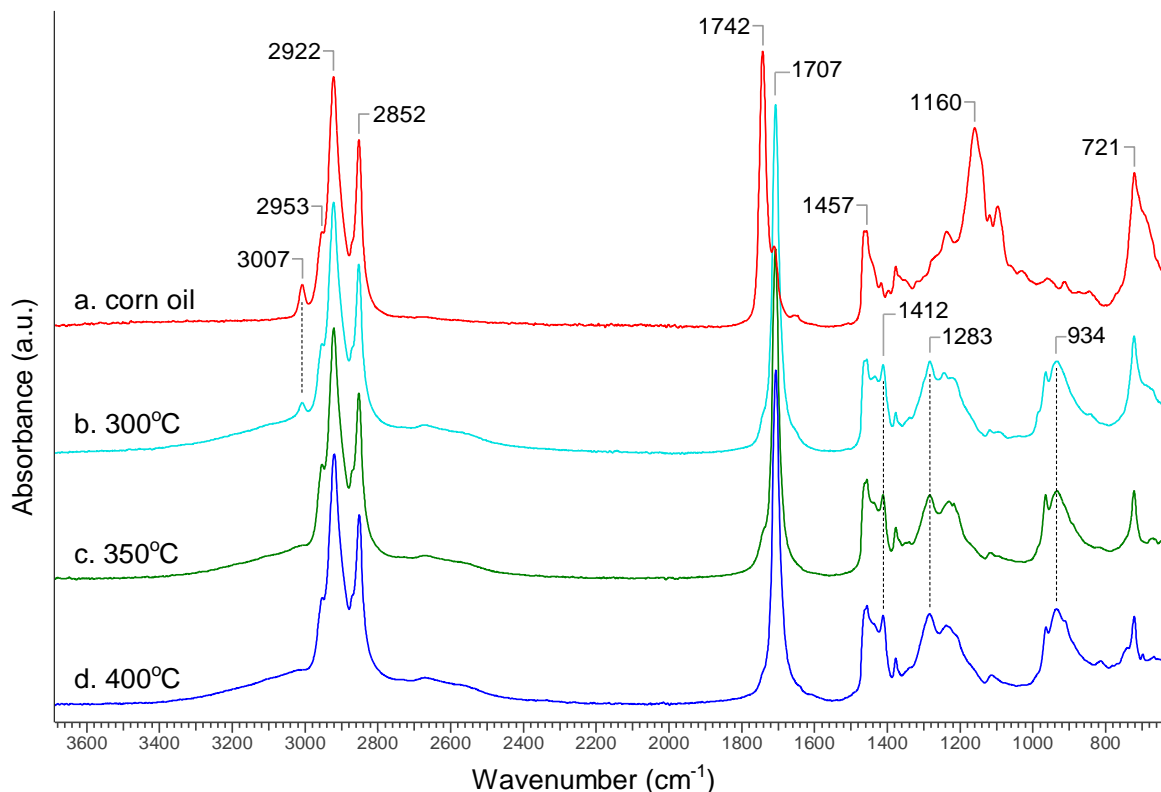
Figure 7.4: ATR-FTIR spectra of (a) CDO and products obtained from reactions at different temperatures (b. 300 ^{o}C; c. 350 ^{o}C; and d. 400 ^{o}C) without catalyst.

ATR-FTIR spectra of the decarboxylated products formed under different reaction conditions were collected and are compared in Figure 7.5 whereas Figure 7.6 shows the visual effect of residence time on the product quality. By comparing Figure 7.5a, b and h, it is seen that the

degree of decarboxylation increased (from 80 to 100%) with increasing water to corn oil ratio from 2:1 to 4:1 at 400 °C for 4h reaction, as evidenced by the significant decrease in the carboxylic acid peaks at 1707, 1412, 1283, and 934 cm^{-1}. By comparing Figure 7.5c, d, e and h, it is found that the degree of decarboxylation increased (from 71.6 to 100%) with increasing reaction time from 0.5 h to 4 h at 400 °C with water to corn oil ratio of 4:1. By comparing Figure 7.5f, 5g and 5h, it is observed that the degree of decarboxylation increased (from 75.9 to 100%) with increasing reaction temperature from 300 °C to 400 °C with reaction time of 4 h and water to corn oil ratio of 4:1. Moreover, the carboxylic acid peaks disappeared completely after a reaction at 400 °C for 4 h with water to CDO ratio of 4:1 (Figure 7.5h), which is considered as the optimum reaction conditions in the present study. In addition, the peak at 3007 cm^{-1} which is assigned to the alkenyl CH stretching vibration also disappeared in all these hydrothermal reactions, confirming complete conversion of the alkenyl group.
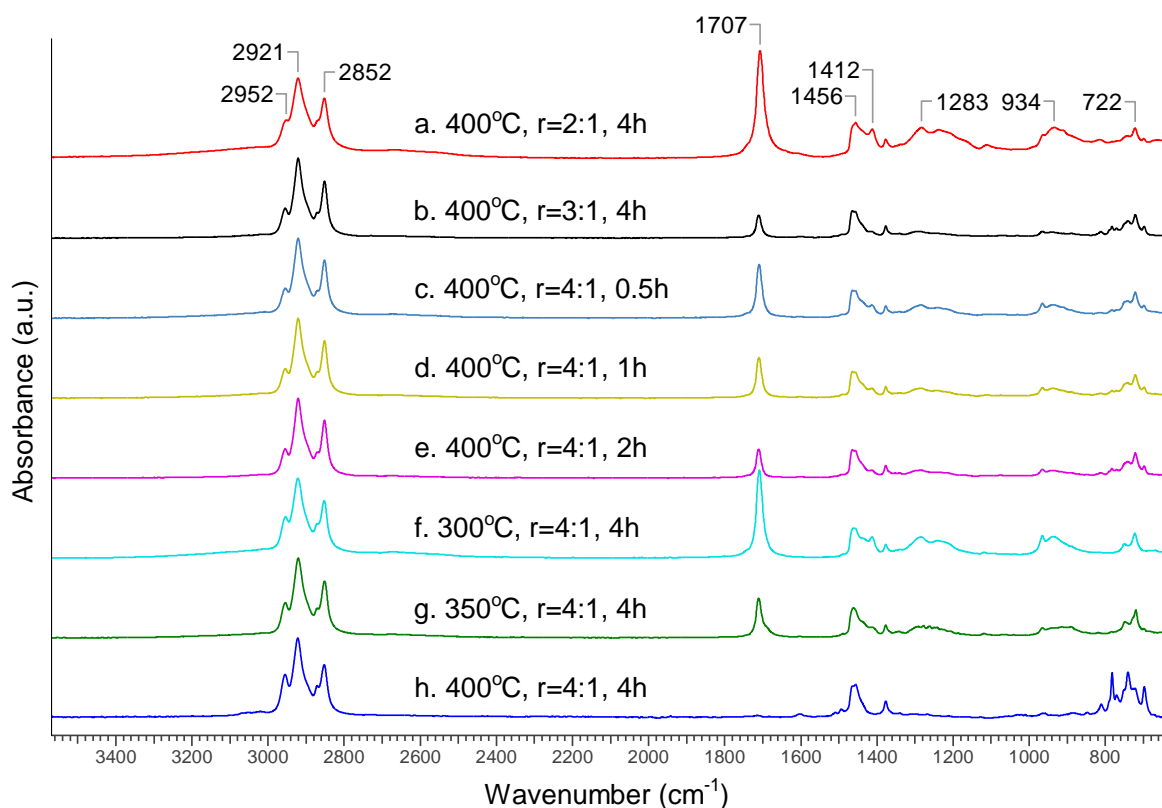
Figure 7.5: ATR-FTIR spectra of the decarboxylated products obtained from reactions under different reaction conditions [temperature, water-to-CDO (v/v) ratio, and residence time] with 5 g of activated carbon loading.
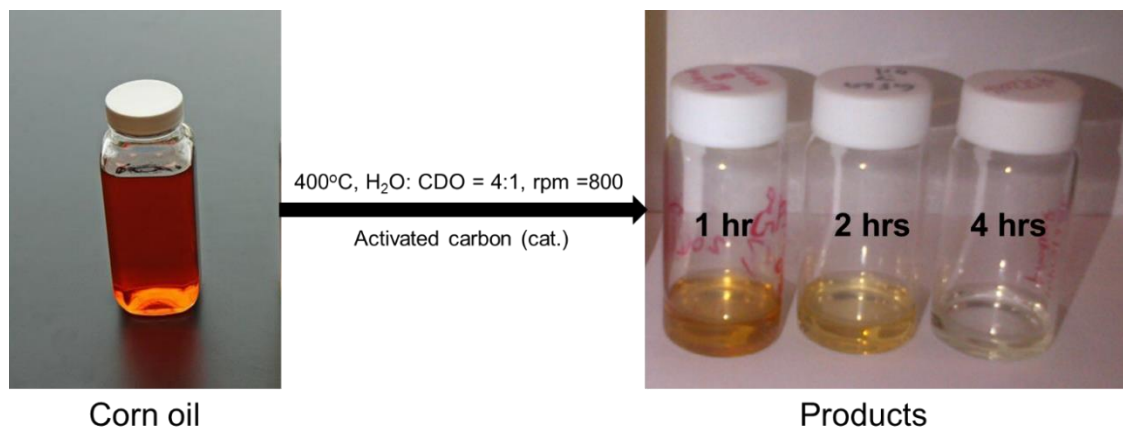
Figure 7.6: Effect of residence time on product quality.

7.3.3.2 NMR analysis of liquid products

To further confirm the decarboxylation reaction mechanism, NMR analysis of CDO and the decarboxylated product was conducted. Figure 7.7 and Figure 7.8 shows ^{1}H-NMR and ^{13}C-NMR spectrum of CDO (top) and decarboxylated product at optimum reaction conditions, respectively.

In the ^{1}H-NMR spectrum of the decarboxylated product, ester peaks of a, b, 2-3, 2′-3′and 2″-3″and the alkenyl peaks of 8-14 and 8′-11′disappeared. In the ^{13}C-NMR spectrum of decarboxylated product, ester peaks of a, b, 1-3, 1′-3′ , 1″-3″and the alkenyl peaks of 8, 11, 14 and 8′, 11′ disappeared after the hydrothermal reaction. The disappearance of the above mentioned peaks indicate the removal of -COO- group and conversion of C=C into C-C, respectively. The peaks between 7.0 and 8.0 ppm in the ^{1}H-NMR spectrum and 125 and 130 ppm in ^{13}C-NMR spectrum of the product may be ascribed to the formed aromatic rings during the hydrothermal reaction. Therefore, the ATR-FTIR and NMR results are consistent and confirm the removal of the carbonyl carbon peaks (carboxylic acids and esters) from CDO during hydrothermal decarboxylation reaction. The conversion of C=C into C-C confirms that glycerol produced by hydrolysis of triglycerides donate hydrogen by APR reaction [15, 18].
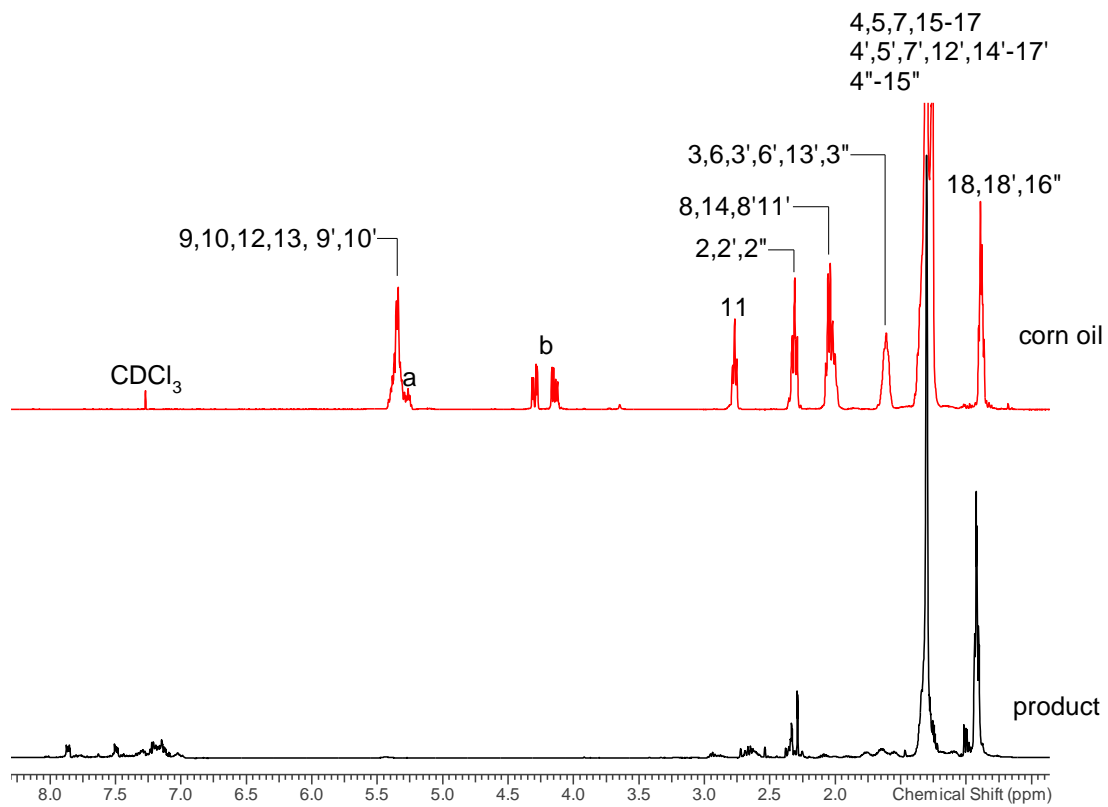
Figure 7.7: ^{1}H NMR spectra of (top) CDO and (bottom) the formed product.
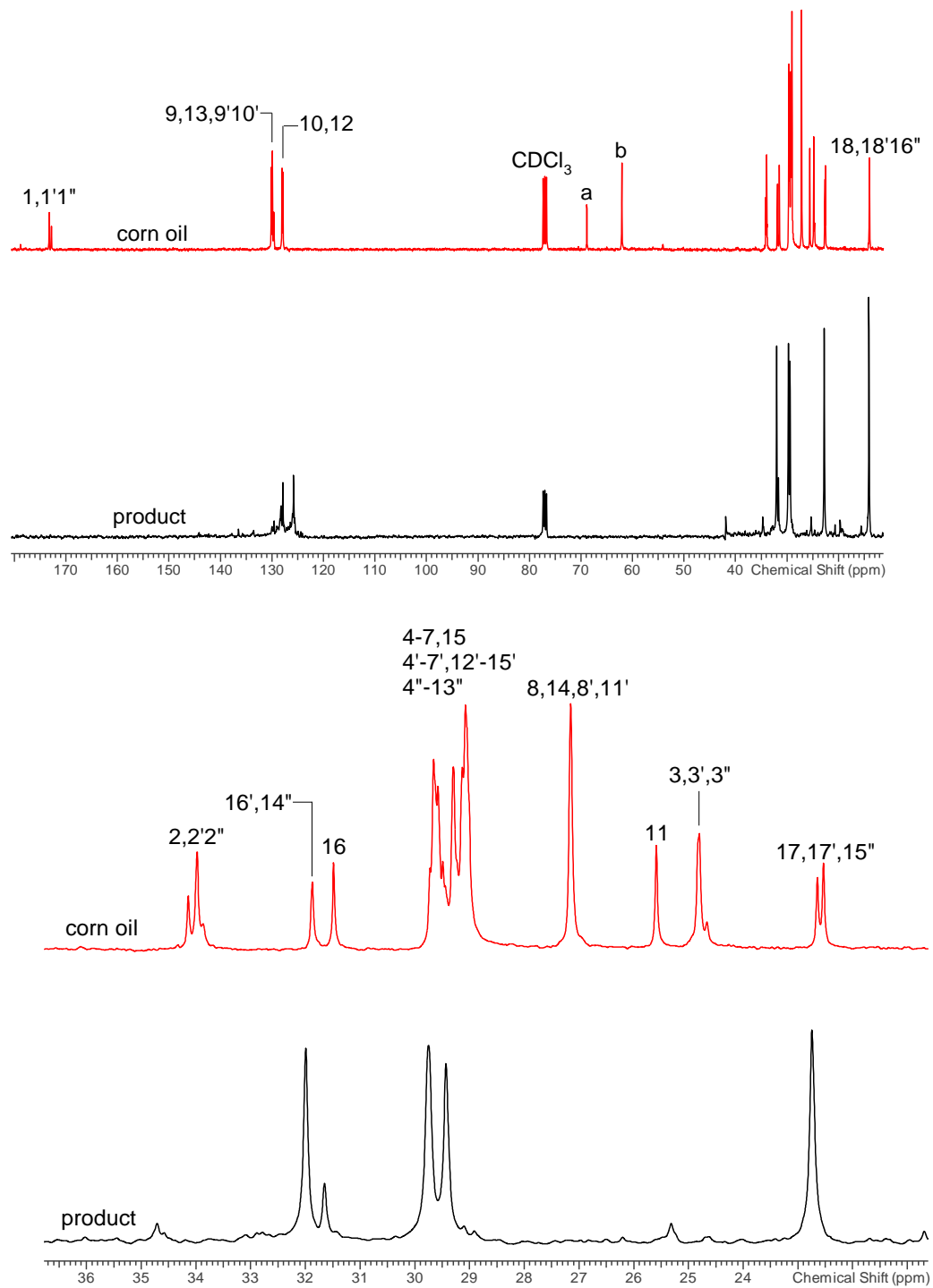
Figure 7.8: ^{13}C NMR spectra of (top) Corn oil and (bottom) the formed product.

7.3.3.3 GC-TCD analysis of gaseous products

A significant portion of gaseous products were also formed along with liquid products during the hydrothermal decarboxylation of CDO in near-supercritical water. GC TCD analysis was conducted to identify the gases present in the gaseous mixtures. Gases identified by GC TCD were H_2, CO, CO_2, CH_4 and higher hydrocarbon gases (ethane, ethene, propane, propene, butane, butene). Since this study focuses on the decarboxylation of CDO, only the results of CO and CO_2 are presented here.

Figure 7.9 shows the mole fraction of CO and CO_2 present in the gaseous mixture. The concentration of CO decreases with increasing water to CDO ratio whereas the concentration of CO_2 increases with increasing water to CDO ratio. At 400 ^oC, with a water to CDO ratio = 4:1, reaction time 4 h and rpm = 800, concertation of CO_2 was achieved ~100 mole% with almost zero concentration of CO in the gaseous mixture. This indicates the complete removal of -COO- from CDO during hydrothermal treatment of CDO in near-supercritical water at the optimum experimental conditions. This result is consistent with the ATR-FTIR and NMR results.
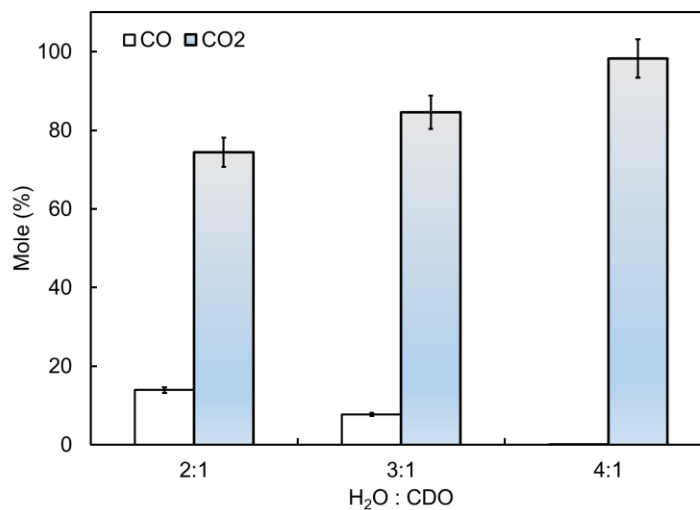
Figure 7.9: Percentage of CO and CO_2 in the gas fraction of CDO decarboxylated products.

7.3.3.4 Proposed mechanism

A proposed reaction mechanism of hydrothermal decarboxylation of CDO in near supercritical water based on the experimental results is shown below. CDO was first hydrolyzed into

glycerol, linoleic acid, oleic acid and palmitic acid. This reaction is confirmed by the FTIR spectra of the products obtained without catalyst. Since the products obtained in this study are mainly saturated hydrocarbons without adding any external H_2, H_2 must be produced *in situ* during the decarboxylation reaction. It is well established that during hydrothermal decarboxylation of oleic acid, H_2 was produced *in situ* during simultaneous gasification of oleic acid [12, 29]. Since fatty acids are produced during hydrolysis of CDO, H_2 may also be produced *in situ* during the gasification of fatty acids. There are also some other sources reported in the literature for producing H_2 *in situ* during hydrothermal decarboxylation of triglycerides. Aqueous phase reforming (APR) of glycerol is a good source for producing H_2 *in situ* [15, 18]. Our study also indicates that the chosen reaction temperature is favorable for glycerol decomposition in hydrothermal media in the presence of activated carbon as catalyst, producing mainly H_2, CO and CO_2 along with insignificant quantities of lighter fractions of hydrocarbon. Since decarbonylation is a parallel reaction with decarboxylation, CO may also participate in the water gas shift reaction to produce H_2 [30]. The produced H_2 can then participate in the hydrogenation of unsaturated linoleic and oleic acids into stearic acid. Decarboxylation and decarbonylation of stearic acid and palmitic acid produces saturated heptadecane and pentadecane, respectively. The higher hydrocarbon molecules may further combine into larger hydrocarbon, aromatics and cyclic compounds or break down into smaller hydrocarbon fractions.

Step 1: Hydrolysis of triglyceride into linoleic, oleic and palmitic acid, respectively.
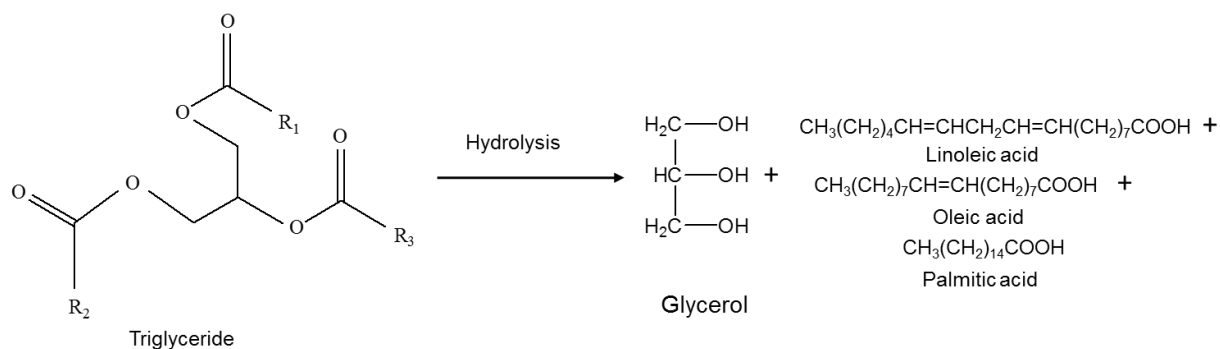
where, R_1, R_2 and R_3 represent the hydrocarbon chain of linoleate or oleate or palmitoleate.

Step 2: *In situ* hydrogen production via gasification of fatty acids or APR or decomposition of glycerol or during water gas shift reaction, respectively.

$$CH_3(CH_2)_4CH=CHCH_2CH=CH(CH_2)_7COOH$$

(i) $\quad CH_3(CH_2)_7CH=CH(CH_2)_7COOH \qquad \xrightarrow{\text{Gasification}} \qquad H_2 + CO_2 + CO$

$$CH_3(CH_2)_{14}COOH$$

(ii)

$$
\begin{array}{l}
H_2C\!-\!OH \\
| \\
HC\!-\!OH \\
| \\
H_2C\!-\!OH
\end{array}
\quad
\begin{cases}
\xrightarrow{\text{Aqueous phase reforming}} H_2 + CO_2 \\
\\
\xrightarrow[\text{Decomposition}]{} H_2 + CO_2 + CO
\end{cases}
$$

(iii) $CO + H_2O \xrightarrow{\text{Water gas shift reaction}} CO_2 + H_2$
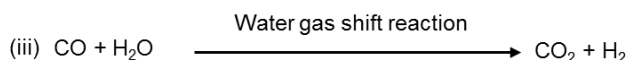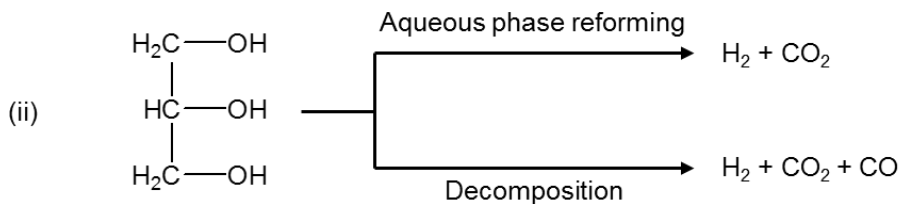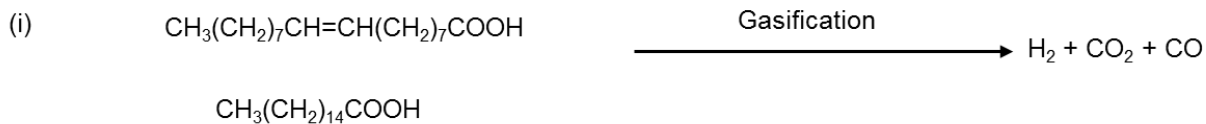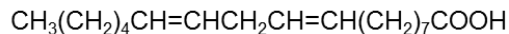
Step 3: Hydrogenation of unsaturated fatty acids into saturated fatty acid

$$CH_3(CH_2)_4CH=CHCH_2CH=CH(CH_2)_7COOH$$

$$+ H_2 \xrightarrow{\text{Hydrogenation}} CH_3(CH_2)_{16}COOH$$

$$CH_3(CH_2)_7CH=CH(CH_2)_7COOH$$
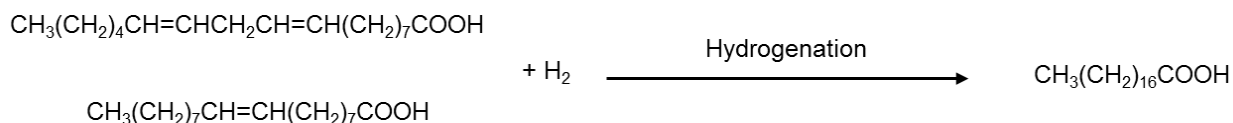
Step 4: Decarboxylation/Decarbonylation of saturated fatty acids into straight chain hydrocarbons

$$CH_3(CH_2)_{16}COOH
\begin{cases}
\xrightarrow{\text{Decarboxylation}} C_{17}H_{36} + CO_2 \\
\\
\xrightarrow{\text{Decarbonylation}} C_{17}H_{36} + CO + H_2O
\end{cases}
$$

$$CH_3(CH_2)_{14}COOH
\begin{cases}
\xrightarrow{\text{Decarboxylation}} C_{15}H_{32} + CO_2 \\
\\
\xrightarrow{\text{Decarbonylation}} C_{15}H_{32} + CO + H_2O
\end{cases}
$$
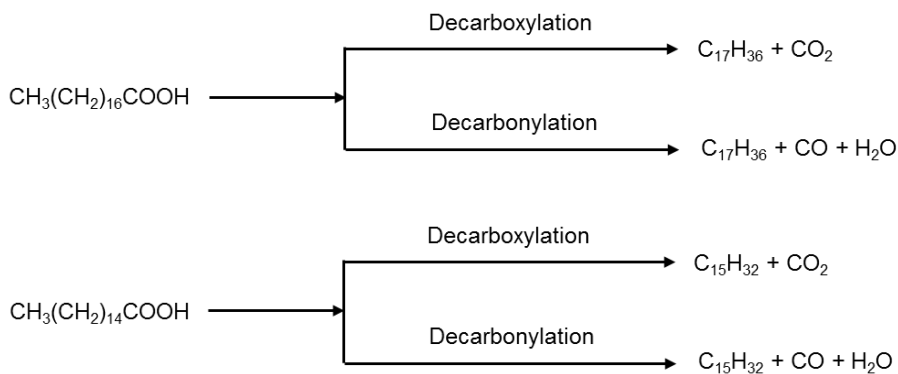
7.3.4 Kinetics of CDO decarboxylation

Kinetics of CDO decarboxylation in near-supercritical water in the presence of activated carbon as catalyst were performed to determine the activation energy based on the disappearance of the -COO- group from CDO (as measured by FTIR) at different temperature (300-400 °C) and reaction time (0.5 to 4 h). The amount of catalyst and volume ratio of water

to CDO used for each experiment was 5gm and 4:1, respectively. The activation energy is defined as the minimum energy required for a chemical system with potential reactants to result in a chemical reaction. Good contact between the reactant molecules and catalyst active sites is very important for lowering the activation energy for a chemical reaction.

A pseudo first order rate constant has been calculated from the disappearance of the –COO– peak from CDO at different reaction times and temperatures. Figure 7.10(left) clearly shows a linear relationship for a pseudo first order reaction. The slope can be attributed to the reaction rate constant k which has a dependency on temperature, normally expressed using the Arrhenius equation:

$$k = A exp\left(\frac{-E}{RT}\right) \tag{7.4}$$

where A is the pre-exponential factor, E the activation energy, R the universal gas constant, and T is the temperature in Kelvin.

To calculate the activation energy, equation 1 was transformed into the logarithmic form, which is plotted in Figure 7.10(right).

$$\ln k = \ln A - \frac{E}{RT} \tag{7.5}$$
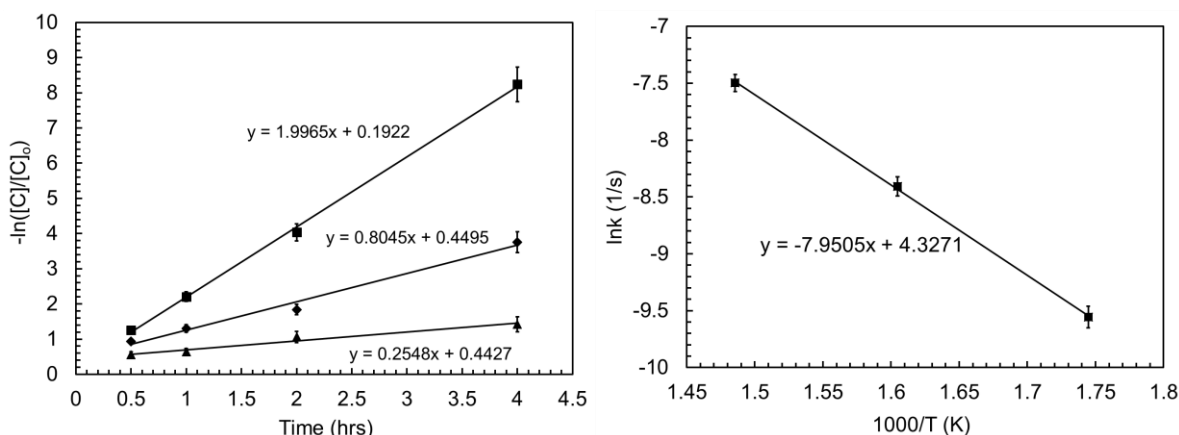
Figure 7.10: (Left) Plot of $-\ln([C]/[C]_o)$ vs residence time for -COO- peak disappearance from corn oil, (Right) effect of temperature on the rate of -COO- disappearance in Arrhenius form.

Plotting ln k vs 1000/T yields a straight line with a slop of $-E/R$, as shown in Figure 7.10 (right). The slop of the line is -7.95. Multiplying the slop by ($-R$) yields $E = 66.1\pm3$ kJ/mol.

Fu et al. [13] calculated the activation energy (125±3 kJ/mol) for palmitic acid decarboxylation in the presence of activated carbon in a batch reactor. The activation energy for palmitic acid decarboxylation using Pt/C catalyst was calculated by the same research group which was about 79±5 kJ/mol [31]. Popov and Kumar [24] evaluated the activation energy for oleic acid deoxygenation in the presence of activated carbon in a continuous flow process and the value was about 120±5 kJ/mol. Vam [32] evaluated the activation energy (148 kJ/mol) for the deoxygenation in the presence of Pd/C catalyst and H_2 in a fixed bed reactor. The activation energy calculated in this study is lower compared to these studies, which were performed either in a non-stirred small reactor in a fluidized bath or a fixed catalytic bed. This work used a stirred tank reactor which will help provide better mixing and minimize the mass transfer limitations helping reduce the activation energy of the process. Li et al. [33] calculated the activation energy (112.1 kJ/mol) for the deoxygenation of fatty acids in the presence of Ni(OAc)$_2$. Kumar et al. [34] performed kinetics of stearic acid hydrodeoxygenation in the presence of supported nickel catalysts and estimated the activation energy value to be 205.2 kJ/mol. Although these two studies were conducted under continuous stirring but the activation energy is still higher than the current study. Catalyst and reaction environment may play an important role for lowering the activation energy in the current study.

7.3.5 Catalyst characterization

7.3.5.1 BET surface area analysis

Table 7.1 shows the BET surface area, pore volume and pore size of fresh and spent catalysts. A significant reduction in surface area and pore volume was observed for activated carbon once it was exposed to the hydrothermal media. Lower surface area and pore volume of spent activated carbon may be due to the harsh environment of the hydrothermal media. The increase of pore size indicates the breaking down of pore during the decarboxylation reaction.

Table 7.4: BET surface area, pore size and pore volume of fresh and spent catalysts.

Sample	Total surface area (m^2/gm)	Pore volume (cm^3/gm)	Average pore size (nm)
Fresh Activated Carbon	851	0.56	0.26
Spent Activated Carbon	343	0.30	0.35

7.3.5.2 XRD analysis

Figure 7.11 shows the XRD patterns of fresh and spent activated carbon. The appearance of broad diffraction peaks in the range of 2θ ~15–35° and ~40–50° ascribes the randomly arranged amorphous carbon structures containing low content of crystalline graphite [35]. There is no significant difference in the XRD patterns between fresh and spent activated carbon except the peak intensities. Lower peak intensity of spent activated carbon may be due to deactivation of catalyst during decarboxylation reaction.

Almost all catalysts have a tendency for coke deposition on their surface when exposed to high temperatures. Deposited coke significantly reduces the activity and prevents reusability of the catalyst. XRD peaks at 29.84° and 61.92° on the spent activated carbon catalyst could be assigned to various types of coke that can be formed on the catalyst surface [36]. Since these two peaks are not present in the XRD pattern of the spent activated carbon, no graphitic coke deposition occurred during decarboxylation of CDO.
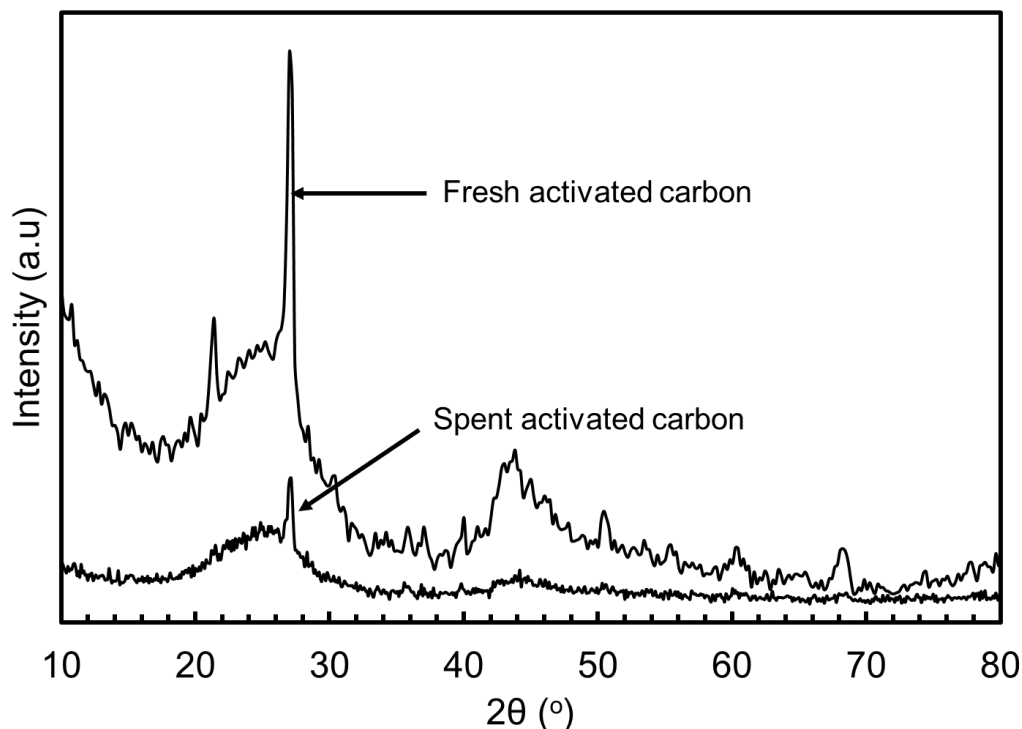
Figure 7.11. XRD patterns of fresh and spent activated carbon.

7.3.5.3 TGA

Thermo-gravimetric analysis (TGA) was further performed to compare the fresh and spent catalyst surface. Figure 7.12 shows the % weight loss along with temperature difference curves as a function of temperature for fresh and spent catalyst under N_2 atmosphere. Weight loss observed in TGA profile before 200 ºC are assigned to the removal of adsorbed water or gases from the environment or any easily removable carbonaceous species. The weight loss associated with fresh catalyst belongs to the removal of adsorbed water. The weight loss at <600 ºC in the spent catalyst corresponds to the easily removable carbonaceous species which were deposited on the catalyst surface during the decarboxylation reaction. There is no such a peak observed in the TGA profiles of spent activated carbon.
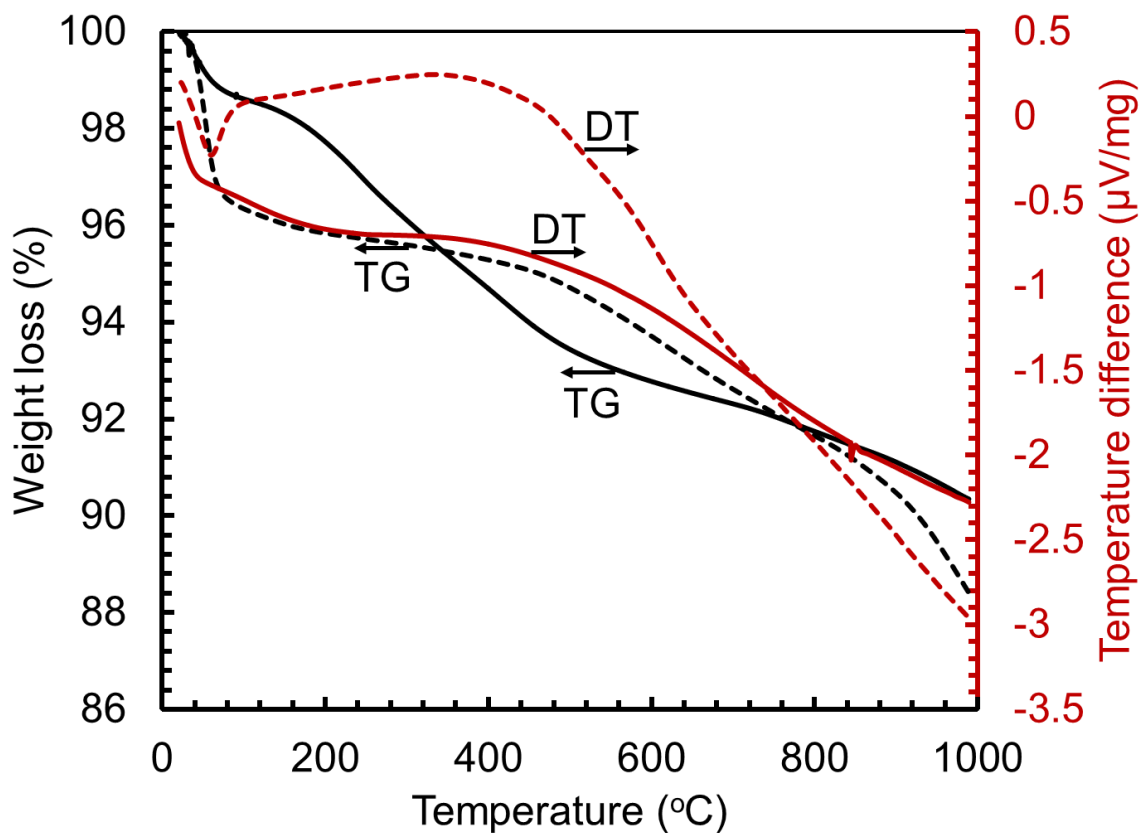
Figure 7.12: TGA profiles of fresh and spent activated carbon (solid line-fresh & dashed line-spent catalyst).

7.4 Conclusion

Complete decarboxylation of CDO into so called green diesel was successfully accomplished over activated carbon as a catalyst under near-supercritical water with no added hydrogen. Pseudo first order kinetics study demonstrated that the disappearance of -COO- groups from CDO follows Arrhenius behaviour and the activation energy calculated for this process to be 66.1 ± 3 kJ/mol. The study demonstrates that glycerol produced during APR reaction donates hydrogen and provide the complete hydrogenation of unsaturated hydrocarbons. The commercially available, cheap and efficient activated carbon was found to be an excellent catalyst alternative to noble metal catalysts for green diesel production in hydrothermal media. The products obtained in this study were mainly saturated alkanes rages from C_8 to C_{20}. The composition of the product at the optimum conditions is as follows: 48.08% of C_8 to C_{14}, 1.57% of pentadecane and hexadecane, 48.89% of heptadecane, 1.09% $C_{18}+$ and a trace amount of heptadecene. C_8 to C_{14} and heptadecane were the major decarboxylated products, respectively. The products can replace petroleum fuels since it has the similar physical properties to conventional fuels. This study provides an alternative way for the production of transportation fuels characterized by low cost, high activity and stability of the catalyst. The processing of CDO in near-supercritical water is an efficient and environmentally benign method that can utilize any feedstocks.

References

[1] D. Kubička, M. Bejblová, J. Vlk, Conversion of vegetable oils into hydrocarbons over CoMo/MCM-41 catalysts, Topics in Catalysis, 53 (2010) 168-178.

[2] B. Dinneen, Ethanol Industry Outlook, in, 2016.

[3] http://www.gfsa.com/.

[4] A. Radich, Biodiesel Performance, Costs and Use, Energy Information Administration, in, 2004.

[5] R. Edwards, V. Mahieu, J.-C. Griesemann, J.-F. Larivé, D.J. Rickeard, Well-to-wheels analysis of future automotive fuels and powertrains in the European context, in, SAE Technical Paper, 2004.

[6] M. Ahmadi, E.E. Macias, J.B. Jasinski, P. Ratnasamy, M.A. Carreon, Decarboxylation and further transformation of oleic acid over bifunctional, Pt/SAPO-11 catalyst and Pt/chloride Al 2 O 3 catalysts, Journal of Molecular Catalysis A: Chemical, 386 (2014) 14-19.

[7] T.M. Yeh, R.L. Hockstad, S. Linic, P.E. Savage, Hydrothermal decarboxylation of unsaturated fatty acids over PtSnx/C catalysts, Fuel, 156 (2015) 219-224.

[8] R. Sotelo-Boyas, Y. Liu, T. Minowa, Renewable diesel production from the hydrotreating of rapeseed oil with Pt/Zeolite and NiMo/Al2O3 catalysts, Industrial & Engineering Chemistry Research, 50 (2010) 2791-2799.

[9] J. Gusmao, D. Brodzki, G. Djéga-Mariadassou, R. Frety, Utilization of vegetable oils as an alternative source for diesel-type fuel: hydrocracking on reduced Ni/SiO 2 and sulphided Ni-Mo/γ-Al 2 O 3, Catalysis Today, 5 (1989) 533-544.

[10] S. Lestari, P. Mäki-Arvela, K. Eränen, J. Beltramini, G.M. Lu, D.Y. Murzin, Diesel-like hydrocarbons from catalytic deoxygenation of stearic acid over supported Pd nanoparticles on SBA-15 catalysts, Catalysis Letters, 134 (2010) 250-257.

[11] I. Simakova, O. Simakova, P. Mäki-Arvela, A. Simakov, M. Estrada, D.Y. Murzin, Deoxygenation of palmitic and stearic acid over supported Pd catalysts: effect of metal dispersion, Applied Catalysis A: General, 355 (2009) 100-108.

[12] J. Fu, X. Lu, P.E. Savage, Hydrothermal decarboxylation and hydrogenation of fatty acids over Pt/C, ChemSusChem, 4 (2011) 481-486.

[13] J. Fu, F. Shi, L. Thompson Jr, X. Lu, P.E. Savage, Activated carbons for hydrothermal decarboxylation of fatty acids, ACS Catalysis, 1 (2011) 227-231.

[14] D.R. Vardon, B.K. Sharma, H. Jaramillo, D. Kim, J.K. Choe, P.N. Ciesielski, T.J. Strathmann, Hydrothermal catalytic processing of saturated and unsaturated fatty acids to hydrocarbons with glycerol for in situ hydrogen production, Green Chemistry, 16 (2014) 1507-1520.

[15] R.D. Cortright, R. Davda, J.A. Dumesic, Hydrogen from catalytic reforming of biomass-derived hydrocarbons in liquid water, Nature, 418 (2002) 964-967.

[16] D.L. King, L. Zhang, G. Xia, A.M. Karim, D.J. Heldebrant, X. Wang, T. Peterson, Y. Wang, Aqueous phase reforming of glycerol for hydrogen production over Pt–Re supported on carbon, Applied Catalysis B: Environmental, 99 (2010) 206-213.

[17] L. Zhang, A.M. Karim, M.H. Engelhard, Z. Wei, D.L. King, Y. Wang, Correlation of Pt–Re surface properties with reaction pathways for the aqueous-phase reforming of glycerol, Journal of Catalysis, 287 (2012) 37-43.

[18] B. Al Alwan, S.O. Salley, K.S. Ng, Biofuels production from hydrothermal decarboxylation of oleic acid and soybean oil over Ni-based transition metal carbides supported on Al-SBA-15, Applied Catalysis A: General, 498 (2015) 32-40.

[19] P. Mäki-Arvela, I. Kubickova, M. Snåre, K. Eränen, D.Y. Murzin, Catalytic deoxygenation of fatty acids and their derivatives, Energy & Fuels, 21 (2007) 30-41.

[20] I. Kubičková, M. Snåre, K. Eränen, P. Mäki-Arvela, D.Y. Murzin, Hydrocarbons for diesel fuel via decarboxylation of vegetable oils, Catalysis Today, 106 (2005) 197-200.

[21] P. Mäki-Arvela, M. Snåre, K. Eränen, J. Myllyoja, D.Y. Murzin, Continuous decarboxylation of lauric acid over Pd/C catalyst, Fuel, 87 (2008) 3543-3549.

[22] R. Raut, V.V. Banakar, S. Darbha, Catalytic decarboxylation of non-edible oils over three-dimensional, mesoporous silica-supported Pd, Journal of Molecular Catalysis A: Chemical, 417 (2016) 126-134.

[23] C. Yang, R. Nie, J. Fu, Z. Hou, X. Lu, Production of aviation fuel via catalytic hydrothermal decarboxylation of fatty acids in microalgae oil, Bioresource Technology, 146 (2013) 569-573.

[24] S. Popov, S. Kumar, Rapid hydrothermal deoxygenation of oleic acid over activated carbon in a continuous flow process, Energy & Fuels, 29 (2015) 3377-3384.

[25] http://www.engineeringtoolbox.com/fuels-higher-calorific-values-d_169.html (accessed on April 19, 2017).

[26] Jet fuel: ASTM D1655-15d, Diesel: Petro-Canada MSDS (accessed on April 19, 2017).

[27] A. Demirbas, H. Alidrisi, M. Balubaid, API Gravity, Sulfur Content, and Desulfurization of Crude Oil, Petroleum Science and Technology, 33 (2015) 93-101.

[28] The Official Site of the National Biodiesel Board: Biodiesel.org (accessed on April 19, 2017).

[29] E.A. Youssef, G. Nakhla, P.A. Charpentier, Oleic acid gasification over supported metal catalysts in supercritical water: hydrogen production and product distribution, International Journal of Hydrogen Energy, 36 (2011) 4830-4842.

[30] R.L. Holliday, J.W. King, G.R. List, Hydrolysis of vegetable oils in sub-and supercritical water, Industrial & Engineering Chemistry Research, 36 (1997) 932-935.

[31] J. Fu, X. Lu, P.E. Savage, Catalytic hydrothermal deoxygenation of palmitic acid, Energy & Environmental Science, 3 (2010) 311-317.

[32] A. Vam, Kinetics of the Hydro-Deoxygenation of Stearic Acid over Palladium on Carbon Catalyst in Fixed-Bed Reactor for the Production of Renewable Diesel, in, University of Dayton, 2013.

[33] W. Li, Y. Gao, S. Yao, D. Ma, N. Yan, Effective deoxygenation of fatty acids over Ni (OAc) 2 in the absence of H 2 and solvent, Green Chemistry, 17 (2015) 4198-4205.

[34] P. Kumar, S.R. Yenumala, S.K. Maity, D. Shee, Kinetics of hydrodeoxygenation of stearic acid using supported nickel catalysts: Effects of supports, Applied Catalysis A: General, 471 (2014) 28-38.

[35] L. Geng, G. Yu, Y. Wang, Y. Zhu, Ph-SO 3 H-modified mesoporous carbon as an efficient catalyst for the esterification of oleic acid, Applied Catalysis A: General, 427 (2012) 137-144.

[36] M.B. Chowdhury, M.M. Hossain, P.A. Charpentier, Effect of supercritical water gasification treatment on Ni/La 2 O 3-Al 2 O 3-based catalysts, Applied Catalysis A: General, 405 (2011) 84-92.

Chapter 8

Conclusions and Recommendations

8.1 General conclusions

Almost 100% removal of oxygen with 81% selectivity to heptadecane was achieved during batch hydrothermal decarboxylation of oleic acid in the presence of activated carbon as catalyst. The same study was conducted into a scalable continuous reactor system for oleic acid decarboxylation and results showed that 91% removal of oxygen with 89.3% selectivity to heptadecane was obtained at the maximized reaction conditions. It was found that the reaction was sensitive to process parameters such as temperature, water-to-oleic acid ratio and reaction time. The different results obtained from batch and continuous reactor system may be due to the process and reaction dynamics of the system.

The stability test of activated carbon was performed into the continuous reactor system and it was found that activated carbon was started deactivating after 30 h and completely deactivated at 45 h time on stream. Regeneration of deactivated (spent) activated carbon was performed using thermal treatment with KOH and decarboxylation of oleic acid using regenerated activated carbon showed the similar results obtained using fresh activated carbon.

The decarboxylated liquid products obtained from both batch and continuous reactor system using activated carbon as catalyst have the similar density and HHV's as commercial fuels (diesel, kerosene and jet fuel).

Laboratory prepared molybdenum supported alumina catalyst was used for decarboxylation of oleic acid in continuous reactor system and the results showed that 92% decarboxylation activity with 18.3% selectivity to heptadecane was obtained at the maximized conditions. Lower selectivity of heptadcane indicates that molybdenum catalyst slightly enhanced cracking reactions.

Decarboxylation of real feedstocks such as castor oil, frying oil, palm oil and corn distiller's oil using activated carbon and molybdenum supported alumina catalyst was conducted in both batch and continuous reactor systems. Decarboxylation of castor oil, frying oil and palm oil using molybdenum catalyst into continuous reactor system showed that > 90% removal of

oxygen was achieved in all cases. Decarboxylation of corn distillers oil in batch reactor system using activated carbon as catalyst showed that the decarboxylated product at the optimum reactions conditions have the similar density, HHV's, cloud and pour point as commercial fuels.

8.2 Recommendation and future works

The following recommendations can be make based on this dissertation:

Catalyst deactivation during the course of the reaction is a major challenge for the decarboxylation process. A long term stable catalyst needs to be developed for commercializing this process. This dissertation utilized a commercial catalyst (AC) and few metal based homemade catalysts including Ni, Mo and MgO supported on commercial γ-Al_2O_3. The homemade catalyst was prepared using incipient wetness impregnation method. Catalyst preparation is an important factor to enhance their catalytic activities significantly. Controlling the metal particle size and structure of the support materials using different methods may help to improve the catalyst life. Sol-gel synthesis method using anionic, cataionic or non-ionic templates improve the porosity of the support which can help the uniform distribution of metals over the support. Sol-gel preparation with $scCO_2$ drying for catalyst synthesis will prevent the collapse of 3D structure of catalysts which can effectively participate the decarboxylation reaction and somewhat prevent deactivation.

Coke and salt deposition on the catalyst are always vital factors for deactivating catalyst. For example, coke/metal particles can attach themselves to the catalyst and/or to the unit internals like the reactor wall/agitator, cooling coil, diptubes, etc. This can be minimized by preprocessing of feedstocks. Preprocessing of feedstocks can be done by washing with concentrated acid and then water. This will help to remove the impurities from the feedstocks which might cause the catalyst deactivation.

65 to 72% liquid yield was obtained in all the cases. Optimization of catalyst is necessary to increase the liquid yield. The current study was conducted in the presence of water where water participates in the decarboxylation reaction as vapor. Increasing system pressure and decreasing the reaction temperature will help to keep water in the reaction media as liquid

phase. Liquid phase reaction can enhance the reaction kinetics as well as higher liquid yield. Decarboxylation reaction in liquid phase can prevent the catalyst deactivation and increase the catalyst life. High pressure helps to prevent all types of carbon (atomic, amorphous and graphitic) deposition on the catalyst surface which is the main reason for catalyst deactivation.

Although water was used as a green reaction media, the used water after decarboxylation reaction needs to thoroughly analyze by measuring TOC, COD and other parameters to determine if there is any organic compounds present before discarding to the municipal system.

A detailed parametric study for decarboxylation of castor oil, frying oil and palm oil is required to produce fuel range hydrocarbons. Some other feedstocks such as tallow, lard and algae oil can be used as decarboxylation feedstocks. Batch reactor system may be an ideal system for solid feedstocks.

Appendix A
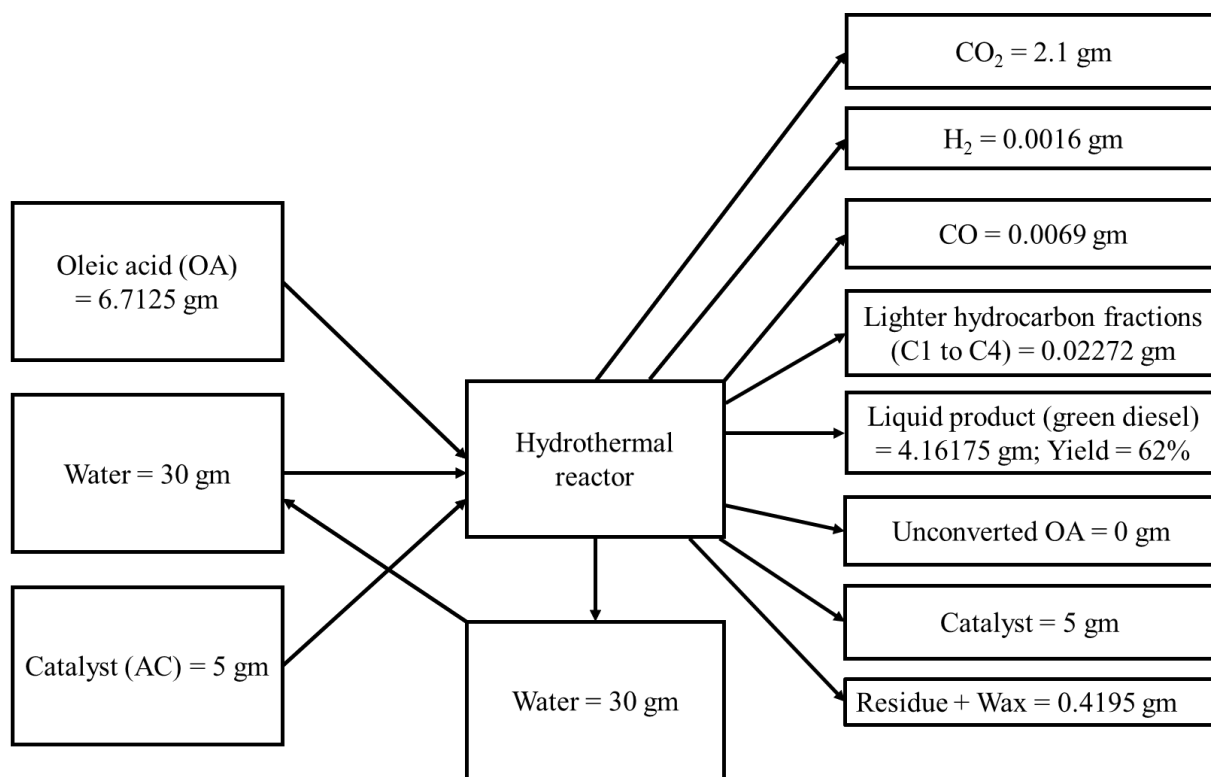
Figure A1: Mass balance at optimum reaction conditions.
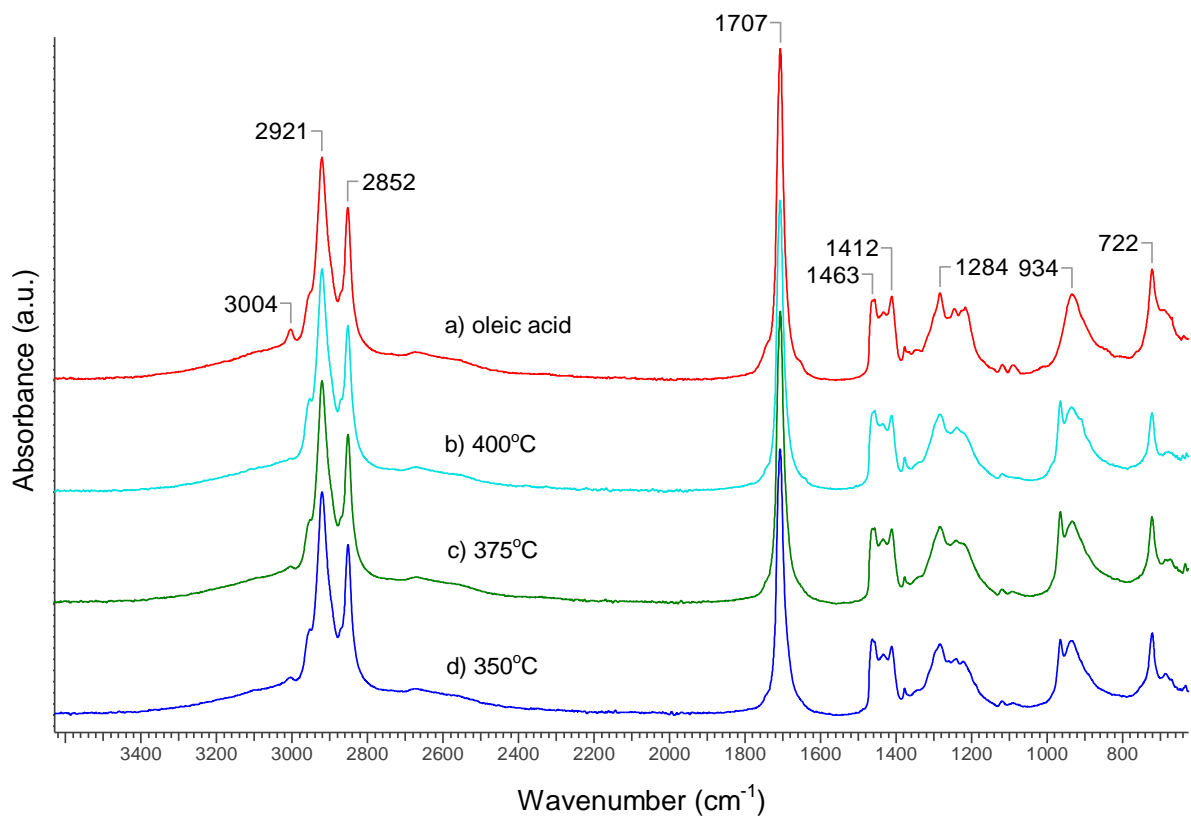
Figure A2: FTIR spectra of (a) oleic acid and the products formed after reactions without using a catalyst at different temperature [(b) 400 ºC, (c) 375 ºC, and (d) 350 ºC], water to OA ratio = 4:1 and reaction time = 2 h.
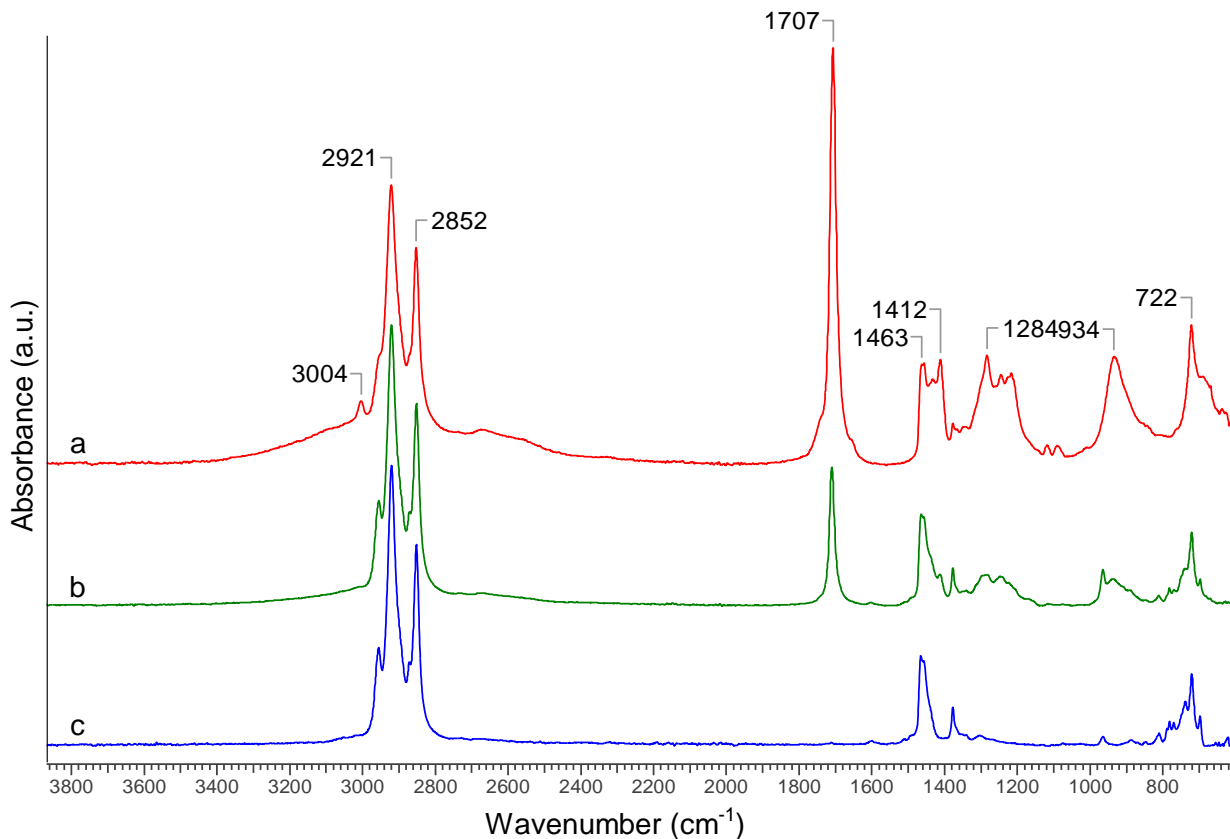
Figure A3: ATR-FTIR spectra of (a) oleic acid and the formed products after reaction at 400 °C for 2 h with water to OA ratio 4:1 by using (b) spent activated carbon and (c) fresh activated carbon.
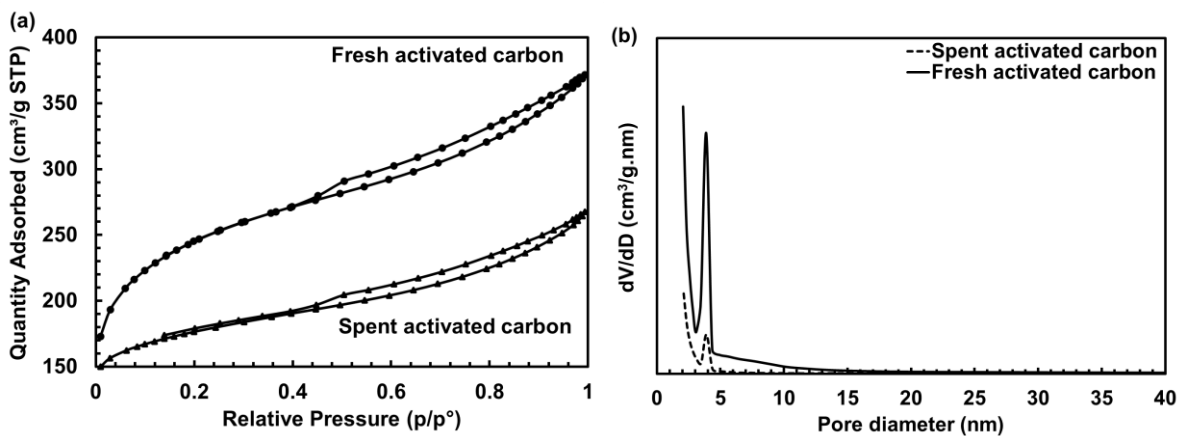
Figure A4: (a) N_2 adsorption-desorption isotherms (b) Pore size distributions.
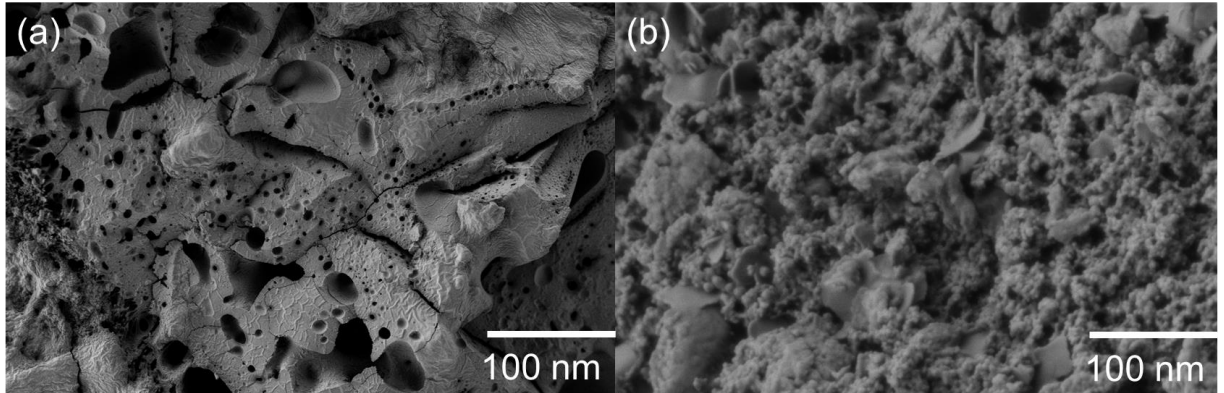
Figure A5: SEM images of fresh (a) and spent (b) activated carbons.
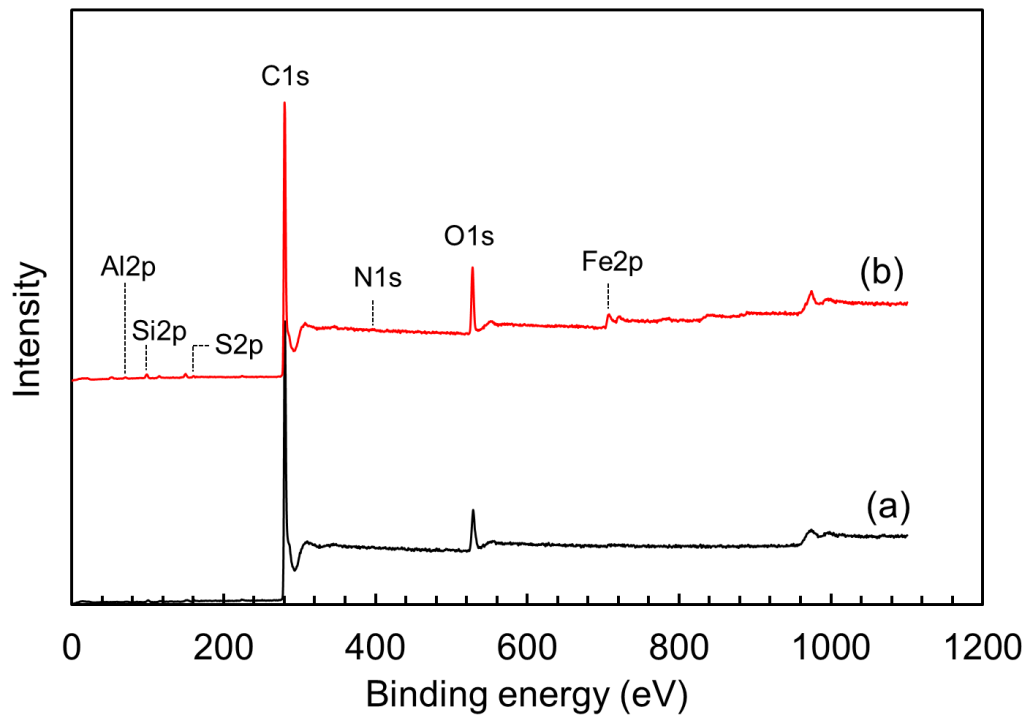
Figure A6: XPS survey spectra of (a) fresh and (b) spent activated carbons.

Table A1: Atomic percentage of the elements present in catalyst surface based on XPS spectra.

Samples	atomic percentage						
	C	O	Al	Fe	N	S	Si
fresh activated carbon	92.1	6.4	0.3	0.1	0.2	0.3	0.6
spent activated carbon	88.3	8.3	0.8	1.2	0.0	0.2	1.3

Table A2: Relative content of carbon species based on XPS spectra.

Samples	Relative content percent			
	O-C=O	C=O	C-OH C-O-C	C-C C=C
fresh activated carbon	4.2	2.6	6.8	86.4
spent activated carbon	1.9	1.2	2.7	94.2

Appendix B
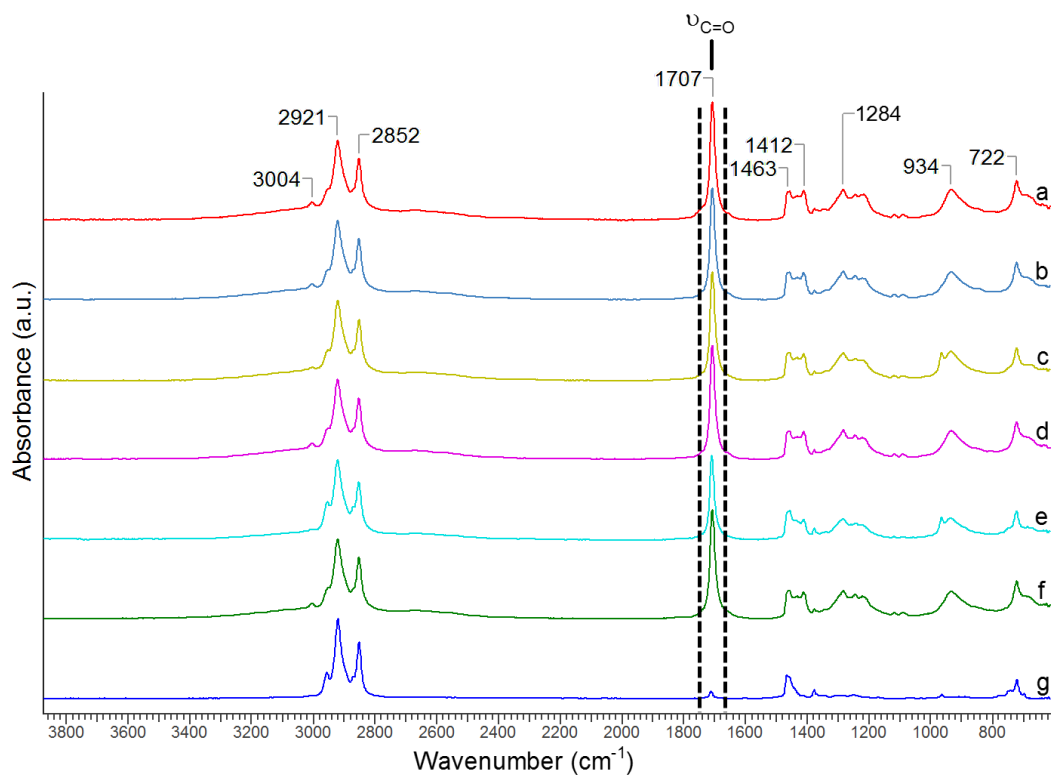
Figure B1: ATR-FTIR spectra of (a) oleic acid and the formed products after 2 h of space time using water-to-OA ratio of 4:1 without and with AC: (b) and (c) at 300 $^{\circ}$C; (d) and (e) at 350 $^{\circ}$C; (f) and (g) at 400 $^{\circ}$C.
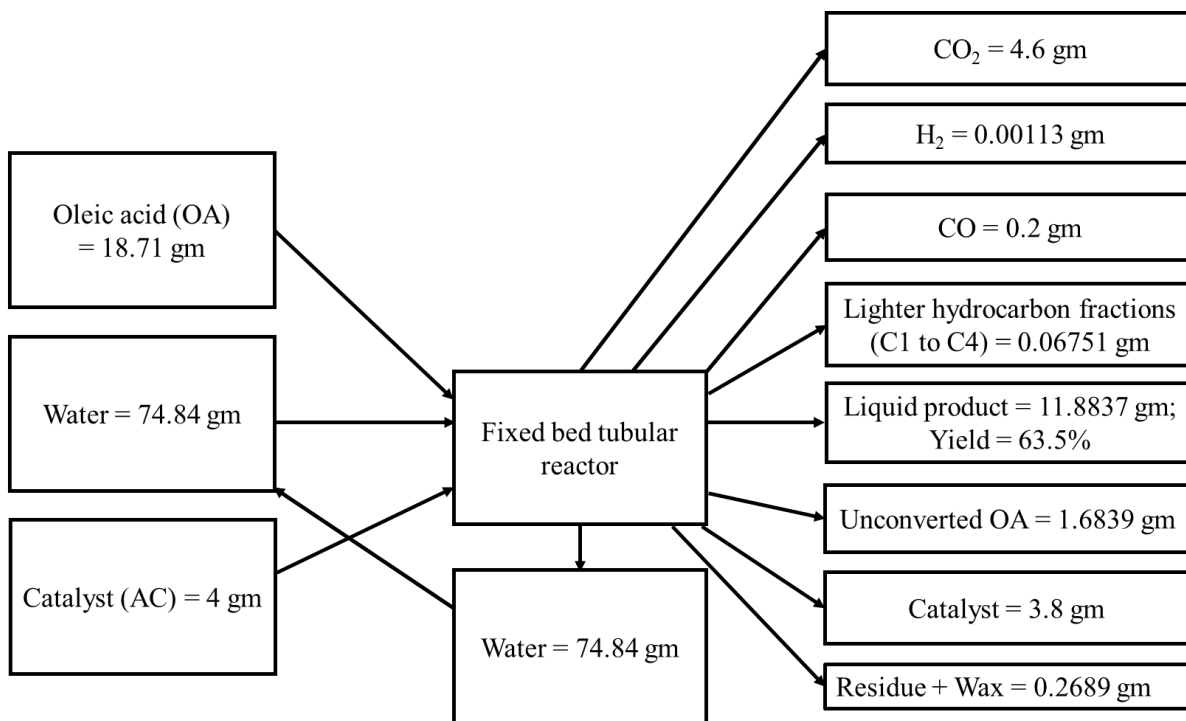
Figure B2: Mass balance at optimum reaction conditions.

Appendix C
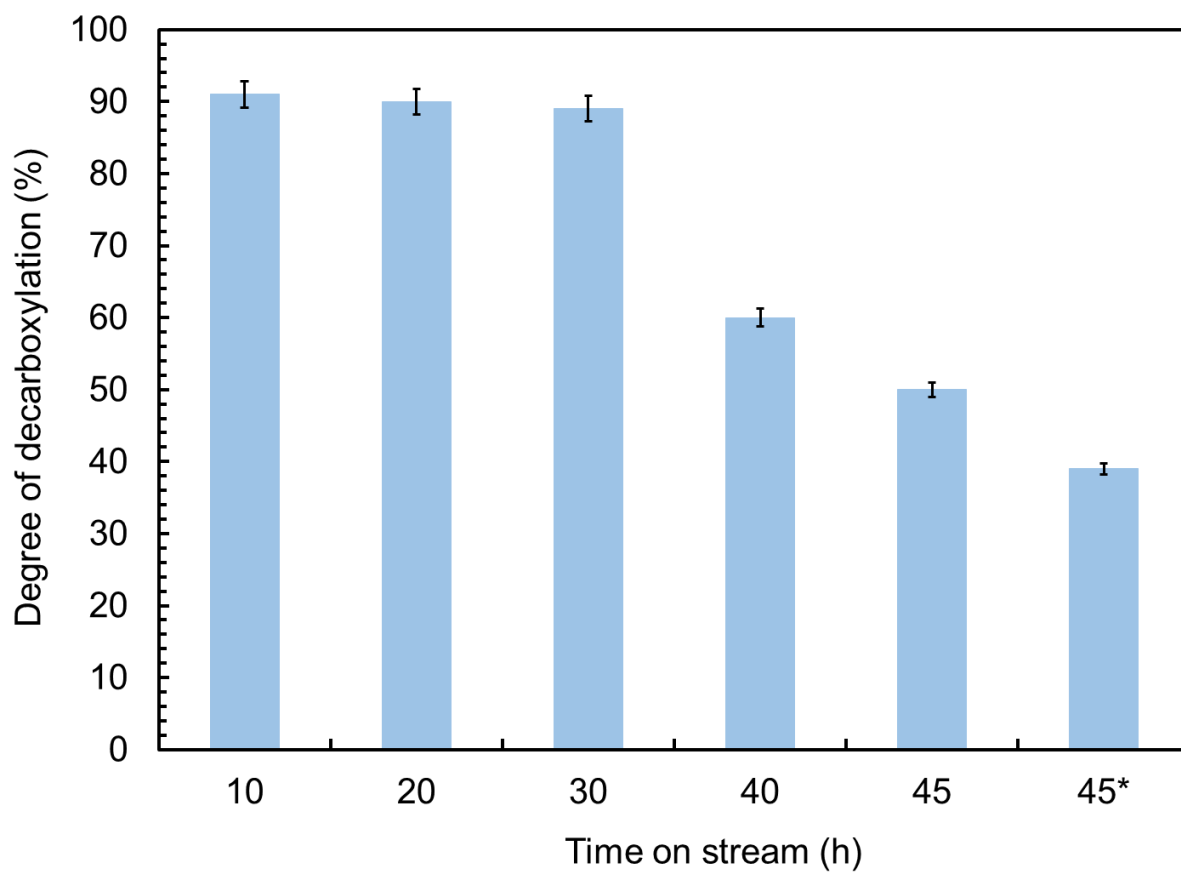
Figure C1. Degree of decarboxylation obtained during 45 h time on stream.
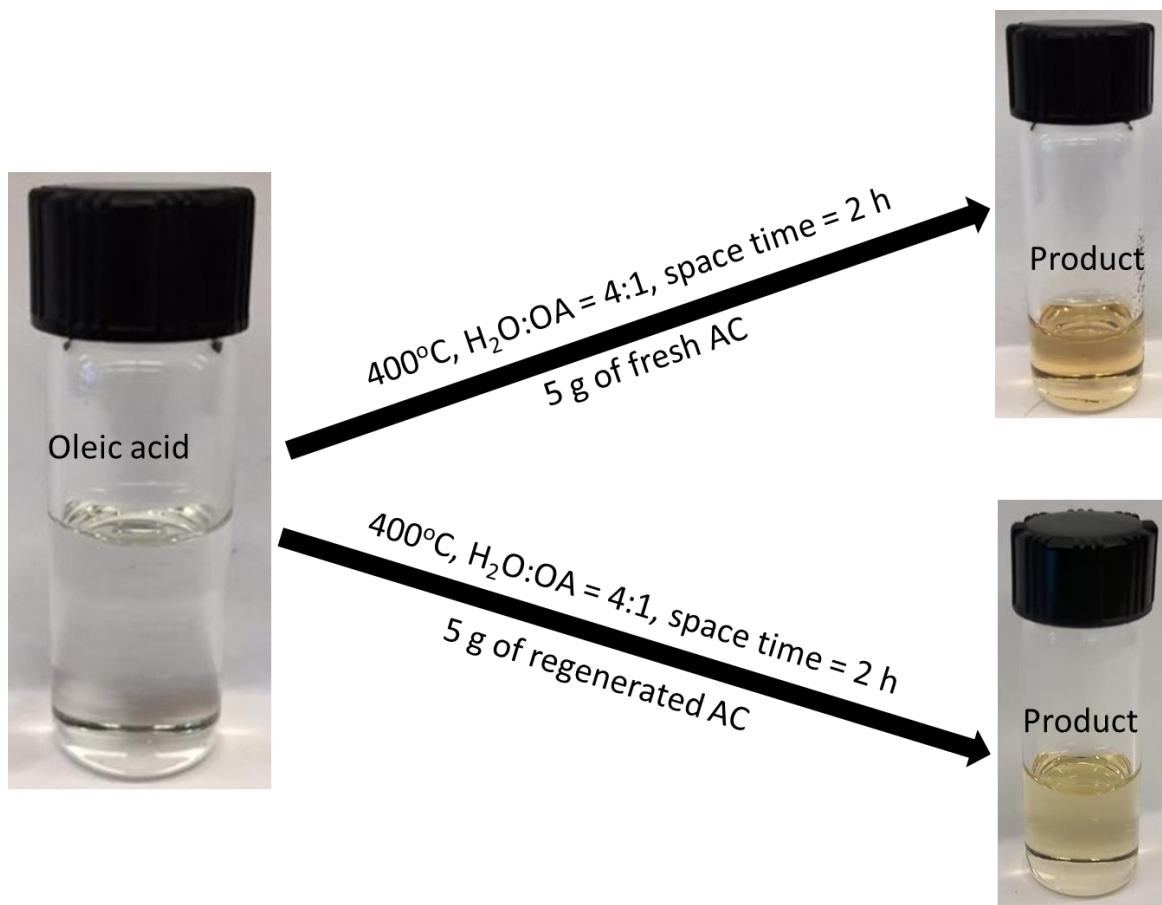
Figure C2. Visual observations of product obtained using fresh and regenerated AC.
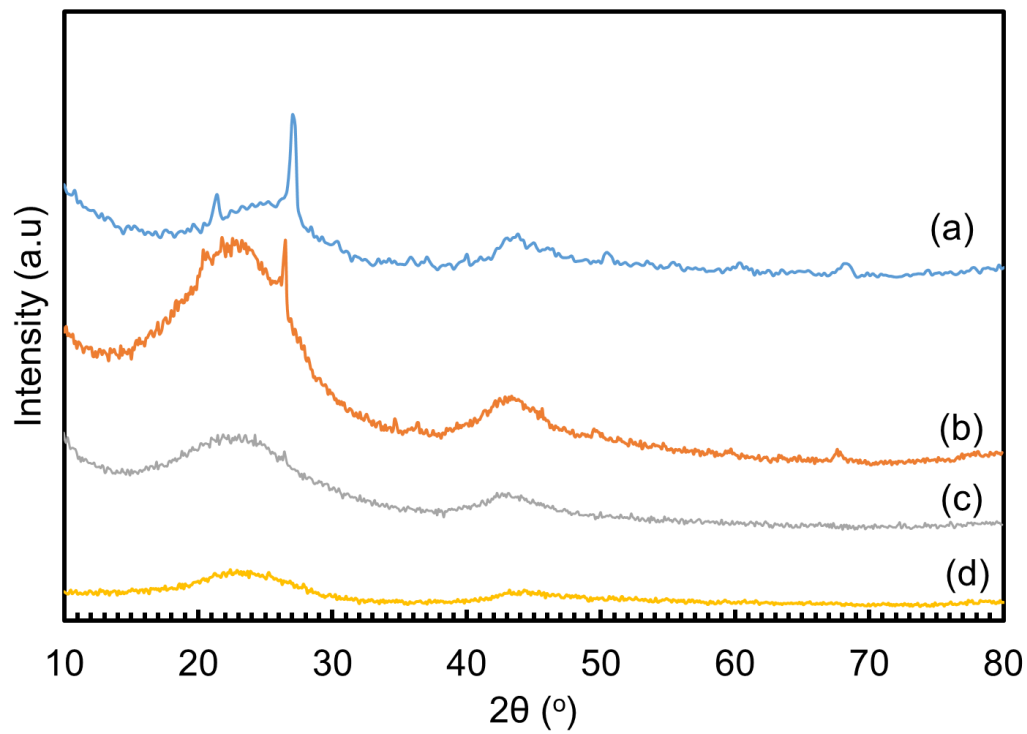
Figure C3. XRD patterns of (a) fresh (b) spent (c) regenerated (d) spent regenerated AC.
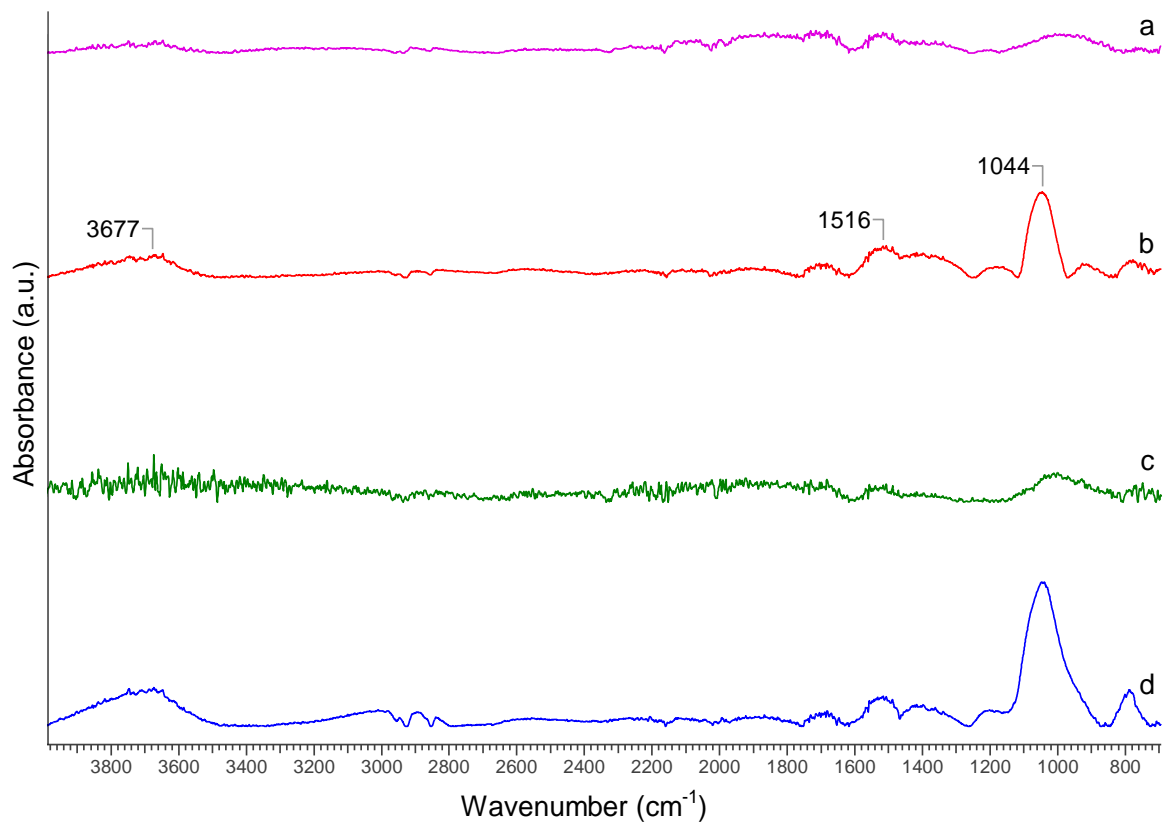
Figure C4. ATR-FTIR Spectra of (a) fresh AC, (b) regenerated AC, (c) spent AC, and (d) spent regenerated AC.
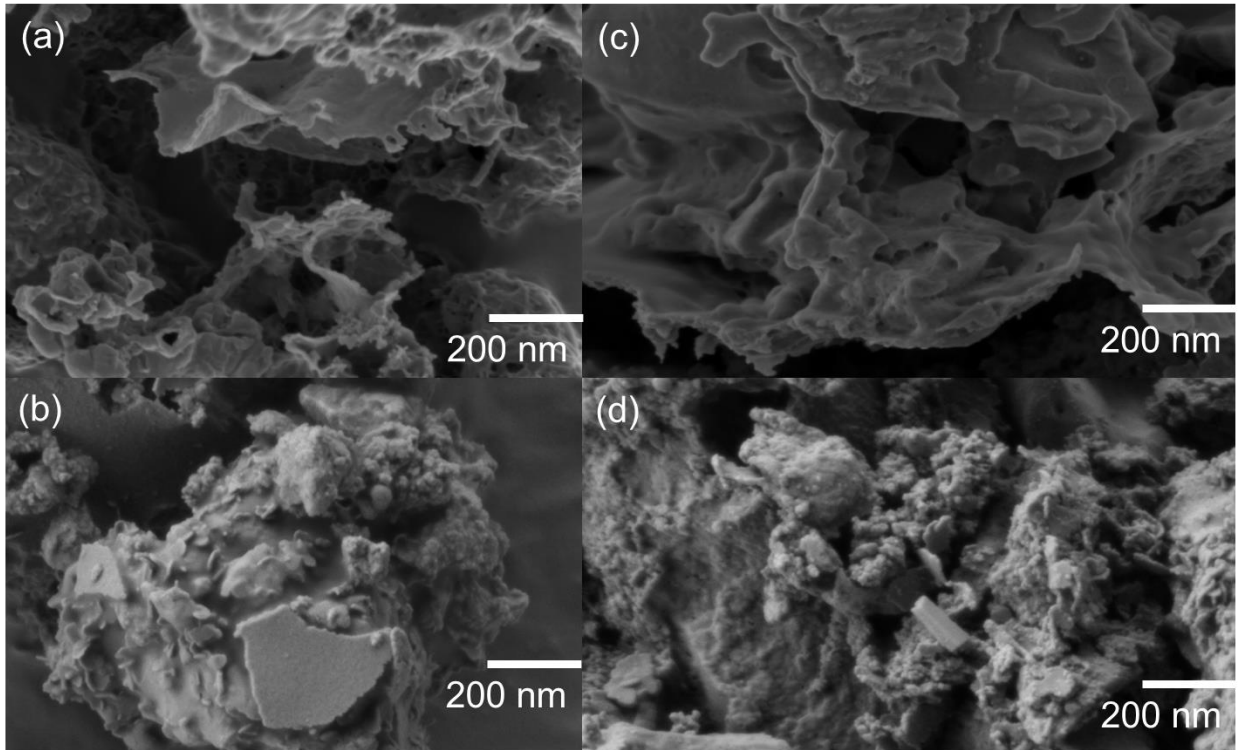
Figure C5. SEM images of (a) fresh (b) spent (c) regenerated (d) spent regenerated AC.

Table C1. Elemental compositions of fresh and spent catalysts based on XPS spectra

Samples	Atomic %							
	C	O	Al	Fe	N	S	Si	Na
Fresh AC	89.4	3.4	0.5	1.0	0.4	1.0	4.0	0.3
Regenerated AC	63.1	36.8	0.0	0.0	0.0	0.0	0.1	0.0
Spent AC	87.4	7.4	0.6	0.4	0.0	0.2	3.9	0.1
Spent regenerated AC	69.2	29.8	0.0	0.0	0.0	0.0	1.0	0.0

Table C2. Relative content of carbon species based on XPS spectra

Samples	Relative content %			
	O-C=O	C=O	C-OH C-O-C	C-C C=C
Fresh AC	3.6	2.5	6.3	87.6
Regenerated AC	3.9	4.5	10.1	81.4
Spent AC	2.8	2.2	4.4	90.6
Spent regenerated AC	2.6	8.5	18.5	70.3

Appendix D
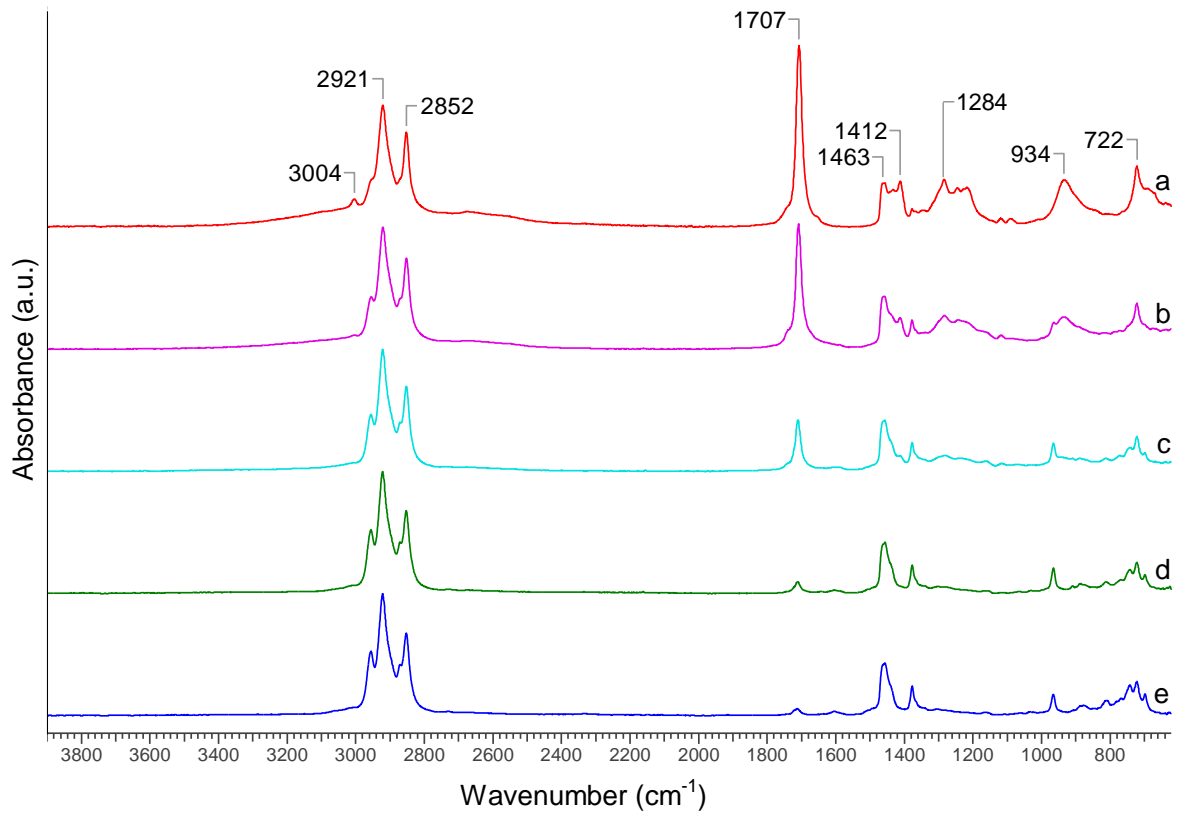
Figure D1: ATR-FTIR spectra of (a) oleic acid and the products formed using water-to-OA ratio of 5:1 and 4 h of reaction time at (b) 325 ^{o}C; (c) 350 ^{o}C; (d) 375 ^{o}C; and (e) 400 ^{o}C.
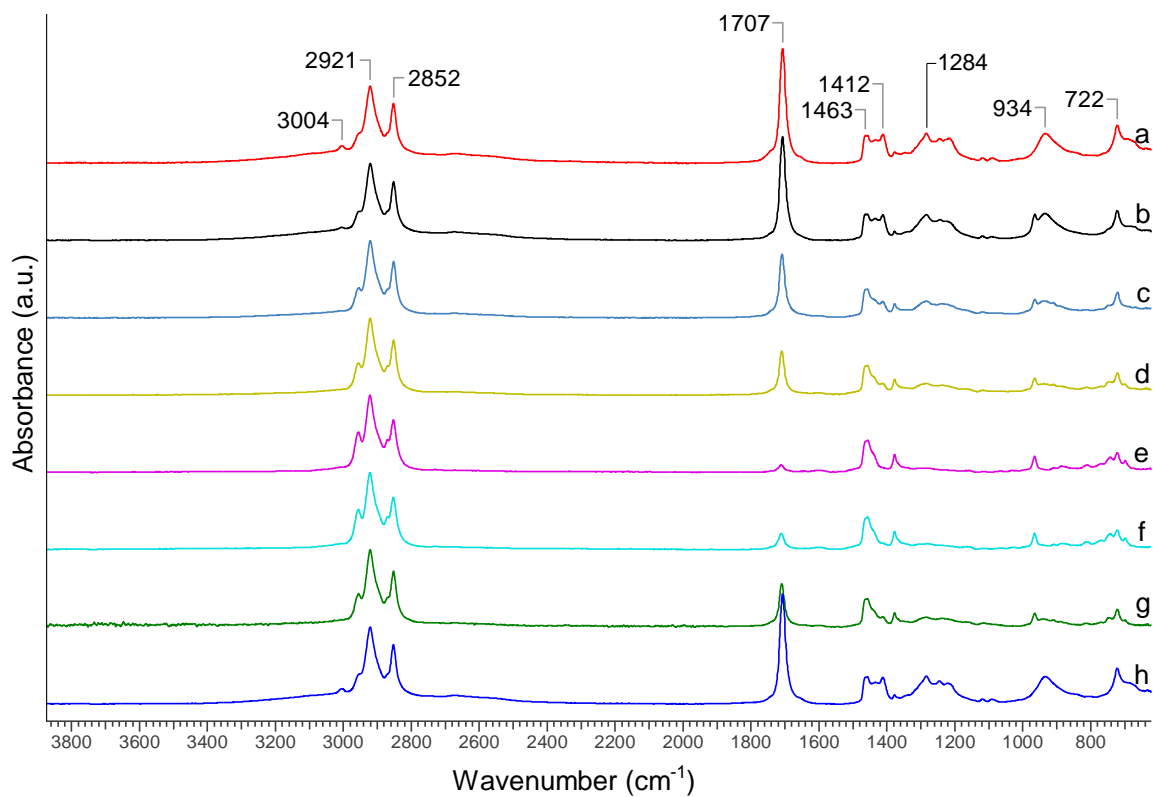
Figure D2: ATR-FTIR spectra of (a) oleic acid and the products formed at 375 °C for different reaction times using different ratios of water-to-OA (b) 0.5 h and ratio of 5:1; (c) 1 h and ratio of 5:1; (d) 2 h and ratio of 5:1; (e) 4 h and ratio of 5:1; (f) 4 h and ratio of 4:1; (g) 4 h and ratio of 3:1; (h) 4 h and ratio of 2:1.

Appendix E
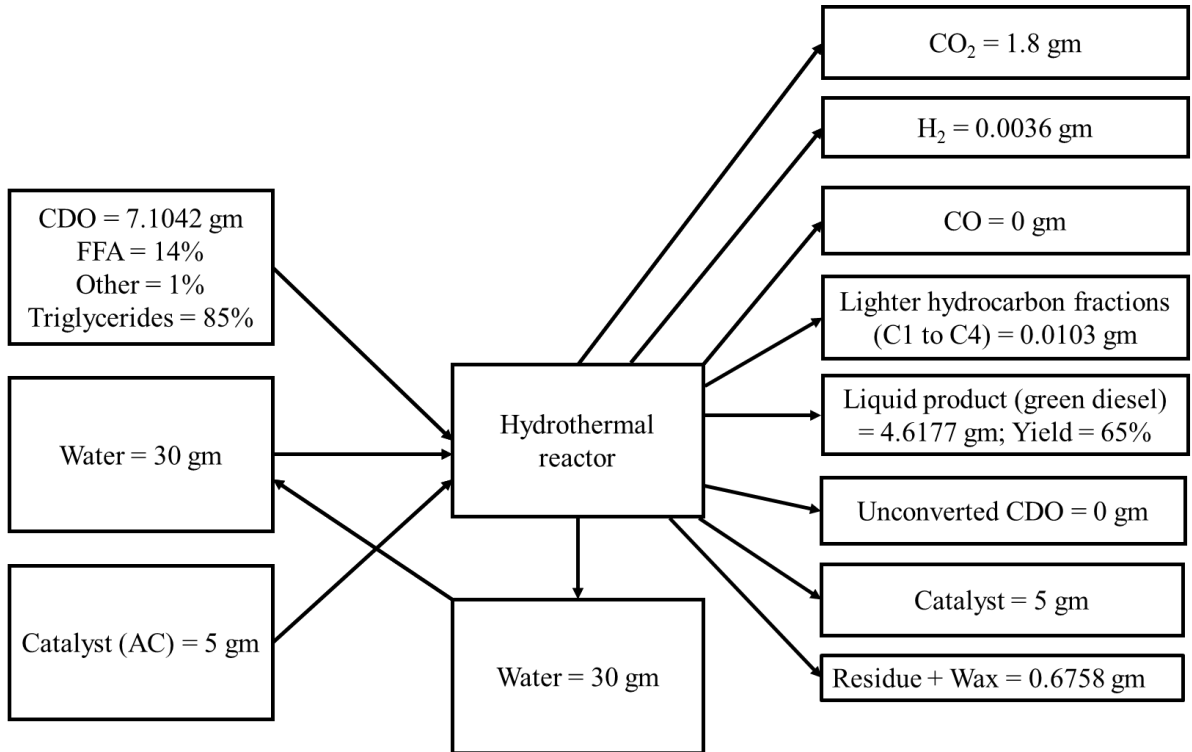
Figure E1. Mass balance of the process at optimum operating conditions.
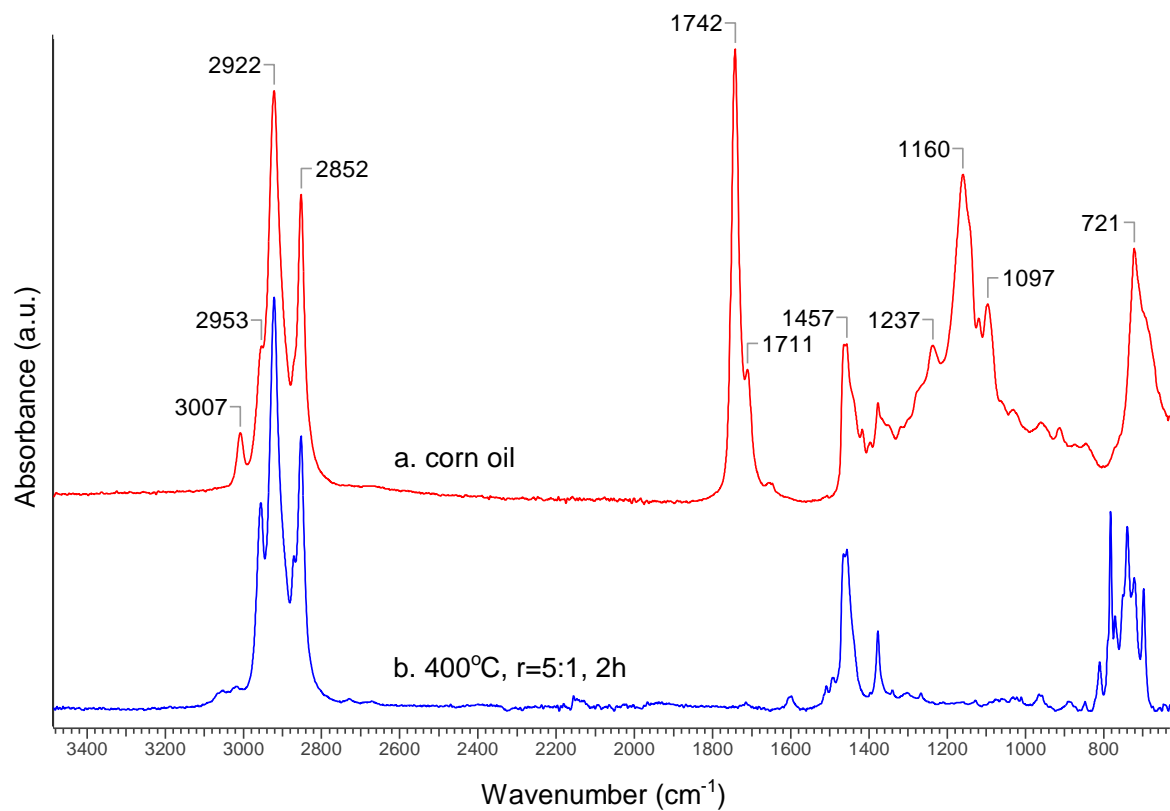
Figure E2. ATR-FTIR spectra of (a) corn distillers oil (CDO) and (b) the decarboxylated product obtained from reactions at 400°C, water to corn oil (v/v) ratio = 5:1, 2 h of reaction time.

Table E1: Typical compositions of corn distillers oil.

Compounds	Relative content (%)
FFA	14
Triglycerides	85
Other	1

Palmitate (C16:0)	12
Oleate (C18:1)	29
Linoleate (C18:2)	56
Linolenate (C18:3)	1
Stearate (C18:0)	2

Table E2: List of the compounds identified by GC MS (ratio of water to CDO = 4:1) in the presence of catalyst.

Compounds	Temperature / Reaction time					
	300ºC/4 h	350ºC/4 h	400ºC/4 h	400ºC/2 h	400ºC/1h	400ºC/0.5 h
Octane(C_8H_{18})	X	X	√	X	X	X
Nonane(C_9H_{20})	X	X	√	X	X	X
Decane($C_{10}H_{22}$)	X	X	√	X	X	X
Undecane($C_{11}H_{24}$)	X	X	√	√	√	X
Dodecane ($C_{12}H_{26}$)	X	X	√	√	√	X
Tridecane ($C_{13}H_{28}$)	X	√	√	√	√	√
Tetradecane ($C_{14}H_{30}$)	√	√	√	√	√	√
Pentadecane ($C_{15}H_{32}$)	√	√	√	√	√	√
Hexadecane($C_{16}H_{34}$)	√	√	√	√	√	√
N-Heptadecane($C_{17}H_{36}$)	√	√	√	√	√	√
Heptadecene	√	√	√	√	√	√
Octadecane($C_{18}H_{38}$)	√	√	√	√	√	√
Nonadecane($C_{19}H_{40}$)	√	√	√	√	X	X
Icosane ($C_{20}H_{42}$)	√	√	√	X	X	X
1,2,3,4,5,8-Hexahydronaphthalene	X	X	√	√	√	√
1-Methyl 2-Propyl Benzene	X	X	√	√	√	√
Methylcyclopropane	X	X	√	√	√	√
(1,1-Dimethylpropyl)Benzene	X	√	√	√	√	√
Pentyl Benzene	√	X	√	√	√	√
(1-Methyl 1 Butenyl) Benzene	√	√	√	√	√	√
(1-Ethyl 1-Propenyl) Benzene	√	√	√	√	√	√
Hexyl Benzene	X	X	√	√	√	√
4,7 Dimethyl Undecane	√	√	√	√	√	√
Butyl Cyclopentane	X	X	√	√	√	√
Heptyl Benzne	X	X	√	√	√	√
2 Methyl Decane	√	√	√	√	√	√
1,5,9-Cyclododecatriyne	X	X	√	√	√	√
Octyl Benzene	X	X	√	√	√	√
Dibenzocycloheptene	X	X	√	√	√	√
Nonyl benzene	X	X	X	√	√	√
1,4-Didecyl Benzene	√	X	X	√	√	√
1-Methyethyl Cylcopentane	√	X	X	√	√	√
1-Methylethyl cyclohexane	X	√	X	√	√	√

√ identified

X not identified

Table E3: Product distribution of CDO decarboxylation at 400ºC, water to CDO ratio = 5:1, 2 h reaction time and 800 rpm in presence of catalyst.

Compound	% Selectivity
C_8 to C_{16} alkanes	47.0
n-Heptadecane	53.0
Heptadecene	0
C_{18+} alkanes	0

Appendix F (Copyright releases)

F-1

Md Zakir Hossain , Anil Kumar Jhawar, Muhammad B. I. Chowdhury, William Z. Xu, Wei Wu, David V. Hiscott, and Paul A. Charpentier, Using Subcritical Water for Decarboxylation of Oleic Acid into Fuel-Range Hydrocarbons, *Energy Fuels*, 2017, *31* (4), pp 4013–4023

DOI: 10.1021/acs.energyfuels.6b03418

Copyright Clearance Center   RightsLink®   Home   Account Info   Help
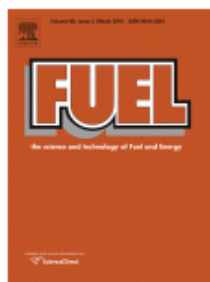
ACS Publications
Most Trusted. Most Cited. Most Read.

Title: Using Subcritical Water for Decarboxylation of Oleic Acid into Fuel-Range Hydrocarbons

Author: Md Zakir Hossain, Anil Kumar Jhawar, Muhammad B. I. Chowdhury, et al

Publication: Energy & Fuels

Publisher: American Chemical Society

Date: Apr 1, 2017

Copyright © 2017, American Chemical Society

Logged in as:
Md Zakir Hossain
Account #:
3000820927
LOGOUT

F-2

Md. Zakir Hossain, Muhammad B.I. Chowdhury, Anil Kumar Jhawar, William Z. Xu, Paul A. Charpentier, Continuous low pressure decarboxylation of fatty acids to fuel-range hydrocarbons with *in situ* hydrogen production, *Fuel* 2018, 212, pp 470-478

DOI. 10.1016/j.fuel.2017.09.092

F-3

Permission for Figure 2.14-2.16

F-4

Permission for Figure 2.17 and 2.18

This Agreement between Md Zakir Hossain ("You") and Elsevier ("Elsevier") consists of your license details and the terms and conditions provided by Elsevier and Copyright Clearance Center.

Print Copy

License Number	4203780156679
License date	Oct 07, 2017
Licensed Content Publisher	Elsevier
Licensed Content Publication	Energy Conversion and Management
Licensed Content Title	Decomposition of a long chain saturated fatty acid with some additives in hot compressed water
Licensed Content Author	Masaru Watanabe,Toru Iida,Hiroshi Inomata
Licensed Content Date	Nov 1, 2006
Licensed Content Volume	47
Licensed Content Issue	18-19
Licensed Content Pages	7
Type of Use	reuse in a thesis/dissertation
Portion	figures/tables/illustrations
Number of figures/tables/illustrations	2
Format	both print and electronic
Are you the author of this Elsevier article?	No
Will you be translating?	No
Original figure numbers	Figure 3 and 4
Title of your thesis/dissertation	Hydrothermal decarboxylation of fatty acids and their derivatives for liquid transportation fuels
Expected completion date	Dec 2017
Estimated size (number of pages)	250
Requestor Location	Md Zakir Hossain Dept. of CBE Faculty of Engg, Western University London, ON N6A5B9 Canada Attn: Md Zakir Hossain
Total	0.00 USD

F-5

Permission for Table 2.1

Curriculum Vitae

Name	Md Zakir Hossain
Post-secondary education and degrees	The University of Western Ontario London, ON, Canada May 2013 - December 2018, PhD Chemical and Biochemical Engineering The University of Western Ontario London, ON, Canada September 2009 – July 2011, MESc Chemical and Biochemical Engineering Shahjalal University of Science and Technology Sylhet, Bangladesh Chemical Engineering and Polymer Science, B.Sc
Related work experience	Graduate Research Assistant Laboratory of Alternative Solvents and Advanced Materials The University of Western Ontario May 2013 - December 2018 Graduate Research Assistant Laboratory of Alternative Solvents and Advanced Materials The University of Western Ontario September 2009 – July 2011 Faculty Chemical Engineering and Polymer Science Shahjalal University of Science and Technology, Bangladesh Feb. 2006 - Aug. 2009 and April 2012 to April 2013

Publications

1. **MZ Hossain**, MBI Chowdhury, AK Jhawar, PA Charpentier, Continuous low pressure decarboxylation of fatty acids to fuel-range hydrocarbons with *insitu* hydrogen production, Fuel 2018, 212, 470-478.

2. **MZ Hossain**, MBI Chowdhury, AK Jhawar, PA Charpentier, Supercritical water gasification of glucose using bimetallic aerogel Ru-Ni-Al_2O_3 catalyst for H_2 production, Biomass and Bioenergy 2017, 107, 39-51.

3. **MZ Hossain**, MBI Chowdhury, Q Alsharari, AK Jhawar, PA Charpentier, Effect of mesoporosity of bimetallic Ni-Ru-Al$_2$O$_3$ catalysts for hydrogen production during supercritical water gasification of glucose, Fuel Processing Technology 2017, 159, 55-66.

4. **MZ Hossain**, AK Jhawar, MBI Chowdhury, WZ Xu, W Wu, DV Hiscott, PA Charpentier,Using Subcritical Water for Decarboxylation of Oleic Acid into Fuel-Range Hydrocarbons, Energy & Fuels 2017, 31 (4), 4013-4023.

5. **MZ Hossain**, PA Charpentier, Hydrogen production by gasification of biomass and opportunity fuels, Compendium of Hydrogen Energy: Hydrogen Production and Purification, 2015, 137.

6. P Saha, **MZ Hossain**, M Mozumder, MT Uddin, MA Islam, J Hoinkis, Shamim A Deowan, Enrico Drioli, Alberto Figoli, MBR technology for textile wastewater treatment: First experience in Bangladesh, Membr. Water Treat. Int. J 2014, 5 (3), 197-205.

7. MA Mumin, KF Akhter, MZ Abedin, **MZ Hossain**, Determination and characterization of caffeine in tea, coffee and soft drinks by solid phase extraction and high performance liquid chromatography (SPE–HPLC), Malaysian Journal of Chemistry 2006, 8 (1), 045-051.